University of Birmingham

School of Biosciences

AN INVESTIGATION INTO THE LOCALISATION AND POSSIBLE PROTEIN PARTNERS OF THE BASE EXCISION REPAIR PROTEIN OGG1

And

THE ROLE OF SRC-LIKE ADAPTOR PROTEINS IN REGULATING GPVI SIGNALLING

A research project report submitted by

Sarah Akbar

as part of the requirement for the
degree of MRes in Molecular and Cellular Biology

This project was carried out at: The University of Birmingham

Under the supervision of: Dr N J Hodges
Dr M G Tomlinson

August 2012

Abstract

A common theme among the two research projects is the dichotomy of biological molecules or pathways contributing to both physiological and pathophysiological processes *in vivo.* Reactive oxygen species (ROS) are involved in redox signalling and phagocytosis, however when present in excess ROS attack cellular structures contributing to the progression of a number of degenerative pathologies such as Alzheimer's and cardiovascular disease. Project 1 investigates the DNA repair protein OGG1 which counteracts the reactive species damage by repairing oxidised DNA base lesions. The DNA glycosylase OGG1 acts via the base excision repair (BER) pathway to mediate the nucleophilic excision of oxidised guanine residues 7,8-dihydro-8-oxoguanine (8-oxoG). The localisation of OGG1 is investigated in the cellular contexts of oxidative stress, apoptosis and mitosis. The protein partners of OGG1 were identified and compared to that of the single-nucleotide polymorphism variant Ser326Cys-OGG1to determine whether reduced repair capacity of the variant is due to impaired protein interactions.

Platelets mediate the physiological process of haemostasis and the pathophysiological process of thrombosis. GPVI is a glycoprotein platelet receptor integral to stable collagen binding at sites of vascular damage to activate haemostasis. As GPVI shares considerable homology to ITAM-receptors, it was hypothesised that GPVI is regulated by Src-like adaptor proteins (SLAP) which are the key negative regulators of ITAM-containing receptors of B cells and T cells. Project 2 investigates the regulation of GPVI by SLAP1 and SLAP2 in a DT40 cell line model using the NFAT/AP1-luciferase assay. Furthermore the contribution of each SLAP2 domain was investigated to elucidate a potential mechanism of SLAP2 mediated inhibition. SLAP1 and SLAP2 significantly inhibit collagen-stimulated GPVI signalling without altering GPVI expression levels indicating

intrinsic inhibition of GPVI signalling. As SLAP proteins are expressed in platelets these are potential regulators of GPVI signalling *in vivo.* Elucidation of GPVI regulation could have implications in the development of anti-thrombosis therapy.

Acknowledgements

I would like to especially thank Dr Nik Hodges and Dr Mike Tomlinson for their support and patience. I would also like to thank the 4th floor and the 8th floor for the great time I have had during laboratory work. I would like to thank Dr Dafforn and Dr Lodge for the continuous support throughout this course.

I would like to thank the various friends who have helped me maintain some sanity during this course. I thank my parents for their encouragement and provision of tea, and I would also like to thank my siblings for supporting me and letting me feel clever every now and then.

Contents

Project 2. THE ROLE OF SRC-LIKE ADAPTOR PROTEINS IN REGULATING GPVI SIGNALLING……100

University of Birmingham

School of Biosciences

Project 1

AN INVESTIGATION INTO THE LOCALISATION AND POSSIBLE PROTEIN PARTNERS OF THE BASE EXCISION REPAIR PROTEIN OGG1

A research project report submitted by

Sarah Akbar

as part of the requirement for the
degree of MRes in Molecular and Cellular Biology

This project was carried out at: The University of Birmingham

Under the supervision of: Dr Nik J. Hodges Date: March 2012

Summary

Reactive oxygen species have several targets within the cell; the most destructive to cellular survival is DNA due to the irreplaceability of DNA. The most common oxidative DNA damage is formation of the single-base modification 7, 8-dihydro-8-oxoguanine (8-oxoG) due to the high susceptibility of guanine to oxidation. The mutagenicity of 8-oxoG is a result of its ability to mimic thymine residues, thus an adenine is incorporated in the opposite strand during transcription. These GC: TA transversion mutations reduce the integrity of the DNA. OGG1 is a DNA glycosylase involved in the excision 8-oxoG via the Base Excision Repair (BER) pathway. OGG1 has been shown to reduce the number of GC:TA transversion mutations in mouse and *E.coli* models. Several single nucleotide polymorphisms (SNP) of OGG1 have been found in the population, the most common is Ser-326-Cys SNP found predominantly in Japanese populations. *In vivo* and *in vitro* studies have demonstrated the reduced enzymatic activity of the variant. Furthermore the Cys-326 genotype has been associated with a number of cancers, notably lung adenocarcinomas. BER characteristically involves the crosstalk and synergy between several proteins; this study aims to identify protein partners associated with OGG1. This study also investigates whether reduced repair activity of the Cys-326 variant is due to different complement of interactions compared to the variant. Furthermore the localisation of the variant and wild-type are compared in normal conditions and oxidative stress conditions to investigate whether delayed response of the variant is due to delayed relocalisation.

Contents

List of Figures

List of Tables

Abbreviations

8-oxoG	7,8-dihydro-8oxoguanine
A	Adenine
APE1	AP endonuclease 1
Arg	Arginine
Asn	Asparagine
Asp	Asparagine
BER	Base Excision Repair
C	Cytosine
C’	Carbon
cDNA	Complementary Deoxyribonucleic acid
CSB	Cockayne Syndrome B
Cys	Cysteine
DMEM	Dulbecco’s Modified Eagle Medium
DNA	Deoxyribonucleic acid
DSS	Disuccinimidyl suberate
ECL	Enhanced chemiluminescence
FapyG	2,6-diamino-4-hydroxy- 5-formamidopyrimidine
FEN	Flap endonuclease 1
FISH	Fluorescence In situ Hybridisation
G	Guanine
GFP	Green Fluorescent Protein
Gln	Glutamine
Gly	Glycine
H	Hydrogen
HCL	Hydrochloric Acid
His	Histidine
K	Lysine
MMR	Mismatch Repair
mRNA	Messenger Ribonucleic acid
MSH2	Mutator gene S homolog 2
MTT	3-[4,5-Dimethylthiazol-2-yl]-2,5-diphenyl tetrazolium bromide
MutM	Mutator gene M
MutT	Mutator gene Y
MutY	Mutator gene T
N	Asparagine
N’	Nitrogen
NEH1	Nei homolog
NEIL	nei endonuclease VIII-like 1
NER	Nucleotide Excision Repair
NF-YA	Nuclear factor –Y α
NHS	N-Hydroxysuccinimidyl
NLS	Nuclear localisation signal
O	Oxygen
OGG1	8-oxyguanine DNA glycosylase
PAGE	Polyacrylamide gel electrophoresis
PBS	Phosphate buffered saline
PCNA	Proliferating Cell Nuclear Antigen
Phe	Phenylalanine

PKC	Protein kinase C
Pro	Proline
R	Arginine
ROS	Reactive Oxygen Species
rS3	Ribosomal small protein 3
SDS	Sodium dodecyl sulphate
Ser	Serine
SNP	Single nucleotide polymorphism
T	Thymine
TCR	Transcription Coupled Repair
TFA	Trifluoroacetic acid
TFIIH	Transcription factor II H
Tris	tris(hydroxymethyl)aminomethane
Try	Tyrosine
TSC2	Tuberin sclerosis protein 2
Val	Valine
XPC	xeroderma pigmentosum complementation group C
XPG	xeroderma pigmentosum complementation group G
XRCC1	X-ray cross complementing protein 1

Chapter 1. Introduction

Reactive species (ROS) have a dichotomic role in living species; involved in both physiological and pathophysiological processes. ROS are responsible for the administration of oxidative burst in phagocytes, modulation of vascular tone and cellular signalling regulation of several kinases and transcriptions (Dröge 2002). Conversely they are responsible for cellular damage, mutagenesis and aging (Dröge 2002). Reactive species are oxygen-containing or nitrogen-containing molecules rendered highly reactive due to the presence of an unpaired electron or an open shell configuration. The cataclysmic effect this single subatomic imbalance has in orchestrating cellular level damage underpins the intricacy and complexity of cellular chemical reactions. The destructive effect of reactive oxygen species has been more widely examined since the establishment that ROS plays a role in the aetiologies of a number of chronic diseases such as cancer, CVD, atherosclerosis and diabetes (Dröge 2002; Simone *et al*. 2008). ROS can be either endogenous from mitochondrial respiration, cytochromes, and macrophage and neutrophil defences, or from exogenous sources such as UV light, environmental pollutants, drugs and alternatively from pathological processes such as inflammation (Dröge 2002).

Excessive reactive oxygen species induces oxidative stress wherein the steady state production and removal of ROS is imbalanced in the favour of ROS accumulation (Klaunig *et al.* 2011). As a result of oxidative stress there is an increased manifestation of lipid peroxidation, DNA oxidation and protein oxidation (Dröge 2002). Particular attention is given to oxidative damaged DNA as DNA is the blueprint on which survival is underpinned. As well as direct modification of nucleotides, ROS accumulation can lead to deoxyribose modifications, single strand and double strand breaks, and DNA crosslinks resulting in genomic instability (Klaunig *et al.* 2011). Consequently carcinogenesis, cell

death or cellular cytotoxicity are induced (Simonelli *et al*. 2011). Several repair mechanisms have been evolved to maintain DNA fidelity and overcome potentially lethal adducts. Choice of repair pathway is lesion-specific; however there is some overlap in the mechanisms. As most common form of oxidative DNA damage is single base adducts; base excision repair (BER) is the prime repair mechanism. BER repairs single nucleotide damage such as thymine glycols and uracil lesions (Barnes & Lindahl 2004). Base excision repair involves the specific excision of the damaged base, leaving an abasic site which is then filled by a DNA Polymerase and ligated to the phosphodiester backbone. Several evolutionarily conserved proteins have been assigned to this process, emphasizing the dependence on BER is correcting DNA damage (Grollman & Moriya 1993).

Owing to its low redox potential, guanine is most vulnerable to oxidative damage, resulting in the formation of 7,8-dihydro-8-oxoGuanine lesions (8-oxoG) (Radak & Boldogh 2010). 8-oxoG is a highly mutagenic lesion formed from the addition of an oxo group to C8 and a hydrogen to the nitrogen group at C7 (figure1.1)(David et al. 2007). The earliest evidence of 8-oxoG formation *in vitro* and *in vivo* was presented by Kasai and Nishimura who quantified the increase in 8-oxoG formation upon ionizing radiation, thus providing a link between oxygen radicals and 8-oxoG (Kasai *et al.* 1986; Kasai & Nishimura 1984). The mutagenic potential of 8-oxoG arises from its ability to mimic thymine residues. Upon generation 8-oxoG in its 6,8-diketo form and is paired with cytosine in the *anti* conformation by Watson-Crick pairing. The thermodynamic and structural preference of 8-oxoG to adopt the *syn* conformation results in the incorporation of adenine opposite 8-oxoG (David *et al*. 2007). The Hoogsteen base pairing of 8-oxoG:A is stabilised by 2 hydrogen bonds (figure1.2). (Klungland & Bjelland 2007, Wang *et al*. 1998). Further propagation of the DNA strands would result in the pairing of thymine opposite adenine, thus left unrepaired 8-oxoG can result in GC:TA transversions. The

functional consequence of 8-oxoG was identified by transfecting the c-HA-ras gene containing an 8-oxoG moiety into NIH3T3, which upon sequence analysis revealed the 8-oxoG had almost exclusively mutated to a thymine (Kamiya *et al.* 1992).

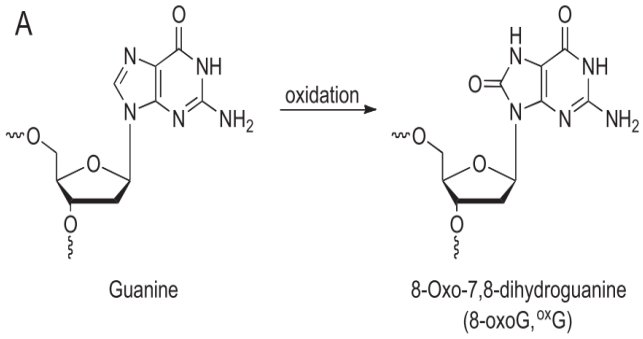

Figure 1.1 Guanine Oxidation (Jarem *et al*. 2011)

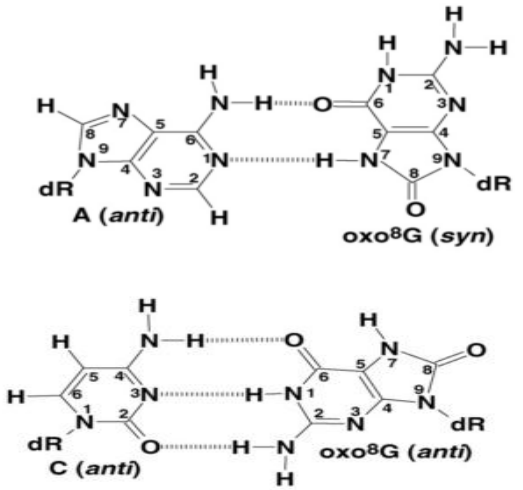

Figure.1.2 Base Pairs of 8-oxoG. In the *syn* conformation 8-oxoG base pairs with adenine and guanine. Its predominate keto form base pairs with cytosine. (Klungland & Bjelland 2007)

A 3-fold difference in the *in vivo* levels of 8-oxoG compared to *in vitro* suggested the presence of a repair mechanism(Kasai *et al.* 1986). The mutagenic potential of 8-oxoG is subdued by a complex defence system. Studies in model genetic organisms have identified repair enzymes which excise 8-oxoG; inactivation of these genes increased the accumulation of GC:TA transversions (Arai *et al.* 2006; Larsen *et al.* 2006). Similar repair proteins have been discovered in drosophila and mouse models (Dherin *et al*. 2000). The *E.coli* repair system has been fully characterised as an elaborate three-tiered system composed of the 8-oxoG-specific enzymes MutM, MutY and MutT collectively known as the GO system (Michaels & Miller 1992). Devoting three mechanisms to the correction of 8-oxoG emphasizes the significant avoidance in 8-oxoG accumulation, and the threat of 8-oxoG to genetic fidelity. Functional homologs of each GO system enzyme have been discovered in human cells (Bessho *et al.* 1993). MutM catalyses the excision of 8-oxoG opposite cytosine, the human functional homolog of MutM is OGG1 (Russo *et al.* 2007).

MutY, homolog of human NEH1, excises 8-oxoG opposite a misincorporated adenine (Hazra *et al.* 2002; Morland *et al.* 2002). Whilst these two enzymes act on DNA, MutT (mammalian MTH1 homolog) sanitises the nucleotide pool of free 8-oxoG bases (Colussi *et al.* 2002).

The critical activity of *E.coli* MutM in error avoidance propelled the search for its homolog in other species. The OGG1 protein was first identified in *S.cerivisiae* possessing the same function as MutM but structurally unrelated. Determination of the structure of yeast OGG1 lead to the identification of human and mouse homologs of OGG1 through sequences database search (Aburatani *et al.* 1997). OGG1 was identified as the major repair enzyme of 8-oxoG, demonstrated by a 7-fold increase in 8-oxoG levels in homozygous OGG1 knockout mice and a 200-fold increase when the knockout mice were subjected to the oxidising agent potassium bromate (Nishimura 2003). It is reported that upto 80% of 8-oxoG repair is performed by OGG1. OGG1 also excises FapyG lesions (David *et al.* 2007). Although functionally identical, MutM facilitated the discovery of OGG1 which has distinctly different structures and reaction mechanisms (Rosenquist *et al.* 1997). While MutM belongs to the Helix-two turn-Helix superfamily, OGG1 belongs to the Endonuclease III superfamily possessing the canonical Helix-Hairpin-Helix motif and the conserved Gly/Pro-rich-Asp residues (Hazra et al. 2002). The OGG1 gene was mapped on to 3p25 by FISH analysis and consisted of 8 exons, the gene site is associated with inhibition of lung cancer (Lu et al. 1997). The upstream region possesses a typical house-keeping gene sequence suggesting OGG1 is constitutively expressed, although at varying expression levels in different tissues (Boiteux & Radicella 2000).

Further investigation of OGG1 gene identified several alternatively spliced variants of which 2 cDNA sequences were dominantly expressed. The most prevalent, OGG1α consists of the first 7 exons whereas OGG1β consists of the first 6 exons and exon 8. Thus

both proteins share the first 316 amino acids, but differ at the c-terminus. OGG1α is a 36kDa nuclear protein whereas OGG1β is 40kDa and is translocated to the mitochondria (Boiteux & Radicella 2000). The localisation sequences were allocated to exon 1 for mitochondrial localisation and the exon 8 for nuclear localisation. The nuclear localisation signal consisted of the consensus signal KRKK-(X3-5)-K-XX-E also found in yeast OGG1 (Boiteux & Radicella 2000). The intracellular localisation was further verified by indirect immunofluorescence microscopy and counter-staining of mitochondria and nucleus; as expected the exogenously expressed OGG1 proteins colocalised to their respective compartments critically dependant on intact localisation signal (Nishioka *et al.* 1999). Nishioka *et al.* further pinpointed OGG1β to the inner mitochondrial membrane using electron microscopy (Nishioka *et al.* 1999). Relative mRNA levels were quantified in the kidney, thymus, testis, ovary, lungs and brain. Depletion of OGG1β did not affect the level of DNA glycosylase activity (Hashiguchi *et al.* 2004). *In vitro* excision assays established the lack of DNA glycosylase activity of OGG1β (Hashiguchi *et al.* 2004). The inactivity of OGG1β was ascribed to the C-terminal domain at which the gene sequences for OGG1α and OGG1β diverge (Hashiguchi *et al.* 2004). This surprising result leads to the speculation that other DNA glycosylases repair oxidative DNA damage in the mitochondria. The lack of activity of OGG1β is compensated for by OGG1α distributed within the nuclear and mitochondrial compartments at a calculated ratio of 4.2:1 (Hashiguchi *et al.* 2004). Exclusive targeting to mitochondria has further elucidated the role of wild-type OGG1 in maintaining mtDNA integrity while non-functional mutants reduced cell viability (Rachek *et al.* 2002; Chatterjee *et al.* 2006). Consistent with previous studies, OGG1 knockout models results in 20-fold increase in 8-oxoG lesions in mtDNA, emphasizing both the higher exposure to oxidative damage compared to nuclear DNA and importance of OGG1 repair (Souza-pinto et *al*. 2001; Bohr *et al*. 2002).

OGG1 is a bifunctional protein in the BER pathway of 8-oxoG elimination; it initiates the excision of the lesion via glycosylase activity and subsequently cleaves the strand at the site of nucleotide excision via AP lyase activity (David *et al.* 2007). The strand break is then restored to normality by the concerted action of a complex of proteins. The composition of the complex reflects the choice between short-patch pathway and long-patch pathway which diverge upon OGG1-catalysed cleavage of the N-glycosidic bond. The short-patch pathway requires DNA polymerase β, APE1, DNA ligase III and XRCC1 (van Loon *et al*. 2010). Using the activated lysine-249 residue, OGG1 introduces nucleophilic attack on the bond between the nucleotide and sugar-phosphate, resulting in β-elimination of the nucleotide and the formation of a covalent Schiff base intermediate between OGG1 and the deoxyribose at C1 position (Hill *et al.* 2001). Subsequent to nucleotide excision, a strand break at the apurinic (AP site) is catalysed by β-elimination via the APlyase activity of OGG1, forming a 3'-α,β-unsaturated aldehyde and a 5'phosphate (Hill *et al.* 2001). The intrinsic 3' phosphodiesterase activity of human AP endonucleases is required to remove the 3' terminus. Alternatively, APE1 can substitute for the AP lyase activity of hOGG1, by directly cleaving the generated AP site (Hirano 2008). The AP site is filled by DNA polymerase β and ligated into the DNA backbone by DNA ligase III. Whereas short-patch pathway replaces a single nucleotide, the long-patch pathway involves the ligation of 2-5 nucleotides. The abasic site is elongated 3' by several nucleotides catalysed by DNA polymerase δ/ε. Due the inability of these polymerases to process 5'rd-pase (sugar phosphate), Flap endonuclease FEN1 is required to process this single stranded flap structure containing a 5'-dRp group which is then a substrate for polymerisation and ligation (Sokhansanj *et al.* 2002). PCNA and protein A assist the long-patch pathway, whereas these auxiliary proteins are readily bypassed by DNA polymerase-β (Maga *et al.* 2008; Maga *et al.* 2007). Dianov *et al.* quantified the relative proportion of

8-oxoG BER pathways, with short-patch BER accounting for 72% of repair events. Long-patch BER only repairs 28% of 8-oxoG adducts (Dianov *et al*. 1998), however this proportion is increased to 50% in the experimental absence of polymerase β, leading to the speculation of another polymerase-β independent repair pathway. Additional to the two types of BER, 8-oxoG can be repaired by other mechanisms independent of OGG1. This reflects the presentation on the lesion on DNA depending on whether it is in the transcribed or nontranscribed strands, in dividing cells or quiescent cells, and if on proliferating cells whether it is in the parent strand. The Nucleotide excision repair (NER) system is considered as a backup system, using RAD14, and appears to recognize a helix distortion rather than specific lesions and can remove a variety of structurally unrelated base modifications (Mikkelsen *et al.* 2009). Mismatch repair (MMR) uses MSH2/MSK6 to repair 8-oxoG lesions on the transcribed strand (Russo et al. 2007). Further defence is provided by Transciption coupled repair (TCR) which is able to repair 8-oxoG relatively efficiently if the lesion is in the transcribed sequence, independent of OGG1 (Le Page *et al.* 2000). TCR contributes to the defences requiring several NER proteins such as XPG, TFIIH and CSB; these are able to repair 8-oxoG efficiently in the transcribed sequence independent of OGG1 but requires OGG1 for repair of 8-oxoG in the nontranscribed sequence (Le Page *et al.* 2000).

The base flipping mechanism is common to several BER repair proteins (Hollis *et al.* 2000; Faucher *et al*. 2009). Detection of the lesion is the first step and involves the repair protein recognising the local conformational change in the DNA backbone and the more widespread bending of the helix (Miller *et al*. 2003; Barone 2003). Positive recognition of the lesion initiates the superposition of glycosylase amino acid into the DNA helix adjacent to the site of lesion (Kuznetsov *et al*. 2005). The nucleotide is rotated out of DNA and the vacant site is occupied by an amino acid stabilising the DNA duplex (David *et al.*

2007). The enzyme-reaction mechanism is then activated upon entry of the nucleotide into a cavity within the repair protein (Bruner *et al.* 2000). The kinetics of OGG1 activity have been defined into 5 reaction steps (Kuznetsov *et al.* 2005). The first 3 are fast consecutive equilibrium steps involving lesion recognition, base extrusion, and enzyme reconfiguration (Kuznetsov *et al.* 2007). The final 2 steps are irreversible rate-limiting steps in which the N-glycosidic bond is cleaved and the 3'phosphate is eliminated (Kuznetsov *et al.* 2005). OGG1 scours the length of the DNA sampling millions of base pair per second in search of a 8-oxoG among every million guanines (Chen *et al*. 2002). Considerable optimisation of the DNA-protein interface is required to facilitate fast enzyme sliding (Blainey *et al*. 2006). 8-oxoG creates a local kink in the DNA and curvature to the strand. Atomic force microscopy has been used to visualise OGG1 detection of damage (Chen *et al.* 2002). The repair process is initiated by OGG1 detection of 8-oxoG residues; it can discriminate between undamaged DNA and 8-oxoG by the greater curvature of the DNA at 8-oxoG sites upon OGG1-mediated bending of DNA at the minor groove (Hashiguchi *et al.* 2004). Considerable distortion is observed adjacent to 8-oxoG lesions. Interestingly it is not the mutagenic syn conformation of 8-oxoG that the OGG1 active site recognises but the *anti* conformation which is quite similar the normal duplex DNA (Bruner *et al.* 2000).

Structure-mediated catalysis is one of the methods by which OGG1 exerts substrate specificity and ensures precision repair. Comparison of the active OGG1α and OGG1β not only elucidated potential causes for the inactivity of OGG1β but also identified catalysis-critical amino acids. Following this, site-directed mutagenesis of potentially critical amino acids confirmed their function and significance (Radom *et al.* 2007). The phenylalanine residue at 319 is known to be critical for 8-oxoG recognition (Bruner *et al*. 2000), as it interacts with the opposite π-faces of 8-oxoG with cooperation from Cys-253. However OGG1β possess a leucine at this position which may justify the absence in α-helix

formation in the c-terminus (Faucher et al. 2010). When the Phe-319 residue was mutated to leucine in OGG1α, the mutant maintained partial activity in the leucine mutant. Although the activity of the leucine-mutant is reduced 2.1-fold relative to the wild-type OGG1α, it confirms the feasible activity of OGG1β which is identical to the leucine mutant of OGG1α. It was proposed the mutation at Phe-319 destabilizes the interaction with 8-oxoG without perturbing the glycosylase activity, however binding cannot be restored by substitution to Phe indicating that binding requires several amino acids. Site-directed mutagenesis of the 317-323 region of OGG1α highlighted the importance of Valine-317, critical for glycosylase activity. The centrally located residue is likely to provide geometric stabilisation, virtue of its hydrophobicity, in the interaction with 8-oxoG. Once 8-oxoG is sandwiched into the active site by interactions of Cys253 and Phe315 with the opposite π-faces of 8-oxoG, the hOGG1 contacts the DNA backbone via an almost charge-neutral channel with the exception of the basic His27 residue. Discrimination between 8-oxoG and guanine is based on the opposite orientations of local dipoles as OGG1 can only specifically interact with dipole orientation of 8-oxoG via the complementary dipoles on active site amino acids Lys249-NH_3^+ and Cys-253-S^- (Seeberg *et al*. 2002). Phosphates of 8-oxoG strand provide the main contact interface between the lesion and OGG1. Only the final helix of the helix-hairpin-helix (HhH) motif directly interacts with the DNA via Val250, Gln 249 and the highly conserved Gly245. The HhH contacts the 3' region of the lesion to stabilise the DNA for maximum access of the lesion into the active-site cavity. Hydrated ions of either Ca^{2+} or Mg^{2+} stabilized the kinked conformation via the hydrogen bonds formed between the H_2O ligands and the DNA. Stabilisation is improved by the hydrogen bonding of the central residue (Asn150) of the conserved NNN motif with a phosphate on the DNA backbone (Seeberg *et al.* 2002). The first residue (Asn149) of the NNN motif binds the exocyclic NH_2 of the complementary

cytosine via hydrogen bonds to its amide carbonyl side chain. Gly-42 on the β-sheet forms hydrogen bonds with the N7 atom of 8-oxoG (Seeberg *et al*. 2002). Furthermore Gln 315 hydrogen bonds with 8-oxoG at the O6, N1 and N2H positions. Only 4 residues interact with the base on the complementary strand; these are critical to ensure accurate opposite base substrate-specificity (Seeberg *et al.* 2002). Tyr203 is wedged between the cytosine and its 5' neighbour creating a DNA kink. Arg154 and Arg204 form strong hydrogen bonds with N3 and O2 atoms of 8-oxoG. Finally Asn149 interacts with the carbonyl group of cytosine, completing the hydrogen-bond pentad between OGG1 and 8-oxoG (Priestley *et al.* 2010). The catalytic reactions then begins with the nucleophilic attack on C-1' by the ε-NH_2 on the critical lysine 249 (Kemp *et al.* 2004). The approximation of the 8-oxoG and Lys249 on OGG1 provide the enthalpic and entropic force for the completion of the reaction (Norman *et al.* 2001).

The interactions of OGG1 with the cytosine on the complementary strand underlie the significance of opposite base substrate specificity. Bjoras *et al.* measured the excision activity of hOGG1 for oligonucleotides containing 8-oxoG paired with C,G, T and A (Bjorâs *et al.* 1997). As expected the most efficient excision occurred when 8-oxoG was opposite C, followed by T>G>A (Bjorâs *et al.* 1997). The diversity in cleavage substrates is unexpected as excision of 8-oxoG against C, T or A can result in fix mutations. However the least efficient excision of 8-oxoG occurred when it was paired with A, despite this being the most common pairing during replication, this limits the possibility of repair-error mutations. The opposite base substrate specificity of OGG1 can be considered as a form of temporal regulation of 8-oxoG repair. The base opposite 8-oxoG is altered several times inherent to the mutagenicity of OGG1. As aforementioned there is some redundancy in the enzyme involved in oxidative DNA damage repair. OGG1 is the first

point of repair as it excises 8-oxoG opposite cytosine, the native state of this lesion. Transcription leads to 8-oxoG paired with adenine at which point it is no longer substrate for OGG1. It is then repaired by the human MutY homolog, NEH1which has broader substrate specificity (Hazra *et al*. 2002). Zharkov *et al.* have further characterised the substrate specificity according to the two activities of OGG1; glycosidic bond incision and strand cleavage (Sidorenko *et al.* 2009). Strand cleavage assays were conducted to investigate the AP endonuclease activity of OGG1. It was found that strand cleavage only occurs when 8-oxoG is paired with C. The inability of hOGG1 to cleave the strand at an AP site opposite the bases G, T and A is evidence that the activities occur independently and are regulated independently. This provides a secondary level of discrimination which prevents the continuation of excision and subsequent strand cleavage of mispaired 8-oxoG lesions which would otherwise result in fix mutations. Therefore strand continuity is preserved for mismatch removal which will allow error-free post-replication repair by strand exchanges until the AP-site is processed. Coupling of glycosylase and AP lyase activities is often observed with bifunctional DNA glycosylases demonstrated by comparable catalytic rates; however this is not the case with OGG1 (Norman *et al.* 2001). Base excision occurred at a 2-fold higher rate than DNA strand cleavage.The delay between base excision and β-elimination has been observed by sodium borohydryde trapping of OGG1 activity against 8-oxoG:C leading to the proposition of a two step reaction mechanism (Zharkov *et al*. 2000).

It is known that OGG1 is expressed constitutively and is not transcriptionally regulated by cell-cycle progression (Dhénaut *et al.* 2000). It is more likely its activity is modulated at the protein level, via direct interactions by protein partners or by changes in cellular environment. Both stimulation and inhibition of OGG1 activity have been reported on induction of oxidative stress (Pu *et al.* 2007; Bercht *et al*. 2007; Hodges *et al*. 2002). A

well established stimulator of OGG1 is APE1 (APEX1), increasing excision activity 5-fold in vitro (Hill *et al*. 2001). It is proposed that this coordination is to maintain APEX1 in close approximation to the OGG1-catalysed nucleotide gap (Sidorenko *et al.* 2007). P300 is a transcriptional coactivator implicated in the acetylation of Lys338/341, which stimulates OGG1 activity in cooperation with APE1 (Bhakat *et al*. 2006). XRCC1 also forms a complex with APE1, polymerase-β and DNA ligase during active BER, but its exact role is yet unknown (Boiteux & Radicella 2000). The human ribosomal protein rS3 interacts with OGG1 at high affinity, which if bound to OGG1 before OGG1-DNA interaction it can stimulate OGG1 activity 2-fold (Vijay *et al.* 2006). Conversely rS3 can bind 8-oxoG blocking OGG1 interaction and possibly induce apoptosis (Vijay *et al.* 2006). The multifunctional checkpoint complex Rad9-Rad1-Hus1 was shown to colocalise and interact with OGG1(Park *et al*. 2009). Though the complex is involved cell signalling, apoptosis and cycle arrest, it is likely to be acting in its DNA damage sensor and DNA repair capacity. Upon sensing DNA damage the Rad9-Rad1-Hus1 complex transmits further signals to downstream proteins involved in BER repair; it has previously shown to interact with APE, polymerase, FEN1, DNA Ligase 1, NEIL1 and the MutY homolog (Park *et al.* 2009). The increase in OGG1 activity was more pronounced when incubated with individual components of the complex, despite this the complex was able to stimulate OGG1 activity 4-fold (Park *et al. 2009).* The homologous-recombination protein RAD52 has been shown to confer resistance to oxidative stress by direct interaction with both OGG1 isoforms, suggesting interaction mediated by a common domain, increasing OGG1 incision activity 3-fold by increasing dissociation rate from Schiff-base intermediate (de Souza-Pinto *et al.* 2009). Reciprocally, OGG1 inhibits the activities of RAD52, thereby preventing RAD52-mediated single-strand annealing and DNA strand exchange (de Souza-Pinto *et al.* 2009), The RAD52 inhibition was inherent to OGG1 and not observed

in other DNA glycosylases, however RAD52 stimulation was observed in the induction of double strand DNA breaks (de Souza-Pinto *et al.* 2009). It is possible this mechanism ensure repair of 8-oxoG lesions prior to homologous recombination. Nuclear factor-YA (NF-YA) has a CCAAT box motif transcription factor that binds OGG1 promoter in a consensus sequence. The involvement of the Tuberin and NF-YA in OGG1 regulation has also been documented. Tuberin is a multifunctional protein encoded by the TSC2 gene, the deficiency of which has been associated with human malignancies. A marked decreased in OGG1 mRNA was observed in human renal epithelial cells when tuberin was down-regulated by siRNA interference (Habib *et al.* 2008). A similar pattern of decreased NF-YA expression was observed when tuberin was down-regulated in the tumour kidney tissue of Eker rats (Habib *et al.* 2003). NF-YA levels were measured in cytoplasmic and nuclear fractions of tuberin-deficient murine renal cells, the data suggested that tuberin-deficiency results in increased cytoplasmic localisation of NF-YA. The study has lead to the inference that tuberin is involved in the regulation of OGG1 via controlled expression and subcellular redistribution of NF-YA (Habib 2009). NEIL1 and NEIL2 are proteins structurally unrelated to OGG1 but have similar substrates particularly Fapy and 5-hydroxyuracil (David *et al.* 2007). They possess preferential activity on DNA bubble structures, as found during transcription and recombination, while OGG1 can only process 8-oxoG on duplex DNA (Dou *et al*. 2003). Therefore these proteins are involved in Transcription-coupled repair (TCR). Another protein involved in TCR is Cockayne syndrome B (CSB) protein which reportedly associates with OGG1 to overcome the transcription blockage and gene inactivation caused by 8-oxoG (Khobta *et al*. 2009). Furthermore, CSB has an OGG1 independent role and can repair 60% of 8-oxoG lesions in the absence of OGG1 (Osterod *et al.* 2002). Xeroderma Pigmentosum complementation group C (XPC) also contributes to 8-oxoG repair by stimulated OGG1 activity,

presumably by increasing the rate of dissociation of OGG1 from the AP site (Shimizu *et al.* 2010). As the prime enzyme of Mismatch repair (MMR), MSH2 is also associated with OGG1 to coordinate the repair of 8oxoG. The substrate of MSH2 is 8oxoG paired with adenine, thus MSH2 also reduces the GC:TA transversions (Ni *et al.* 1999). There is considerable cross-talk between the different pathways of DNA repair, ensuring back-up defences should OGG1 bypass the 8-oxoG lesion. The network of OGG1 interacting proteins is illustrated below (figure 1.3).

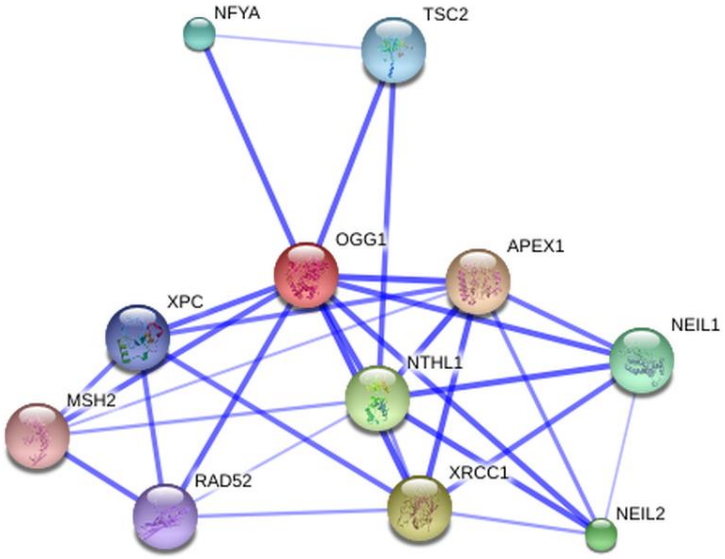

Figure 1.3 OGG1 Interactions Network from STRING 9.0
Evidence of interaction sourced from existing knowledge and experimental data.
The weight of the connecting line indicates strength of interaction. (STRING, 2012)

Alterations in individual amino acids have been shown to abolish catalytic activity and or recognition (van der Kemp *et al.* 2004; Radom *et al.* 2007). Several single-nucleotide polymorphisms have been identified in the population. The most common polymorphism in OGG1 is the Ser-326-Cys which is present at varying levels at different ethnicities. It is most frequent in Japanese populations present in 47.6% of the population (Daimon *et al.* 2009). The mutation is the result of a G:C transversion mutation at 1245 base pair on exon 7 (Li *et al.* 2008). Dherin *et al.* found the k_{cat}/K_m for the excision activity of Cys-OGG1 was $2.82x10^{-5}$ ($min^{-1}nM^{-1}$), which was 1.6-fold lower than the wildtype at $4.47x10^{-5}$ ($min^{-1}nM^{-1}$) (Dherin *et al.*1999). The significantly reduced repair activity was also observed *in vivo* in mononuclear blood cells of individuals of the Cys/Cys genotype (Jensen *et al.*

2012).This reduced repair activity has been associated with resistance to APE1 stimulation (Hill & Evans 2006). Several investigators have attempted to deduce the exact cause of reduced repair activity. Bravard et al. investigated the susceptibility of the variant to oxidative cellular environment (Bravard *et al.* 2009a). *In vitro* investigations using diamide-induced oxidation induced the reduced repair activity of the variant compared to the wild-type as observed *in vivo* (Bravard *et al.* 2009a). Enzymatic activity was restored by reducing agents, normalizing activity comparable to the wild-type. The regulatory effect of redox environment indicated the possible thiolation of OGG1. Crosslinking agents further confirmed the formation of the disulphide-bond, directly linking the redox sensitive cysteine to reduced activity (Bravard *et al. 2009a).* Hill and Evans expanded on the dimerisation theory suggesting that the disulphide bonds are formed between two OGG1 proteins resulting in homodimerisation in solution as confirmed by gel shift assays and size exclusion chromatography (Hill & Evans 2006). The allosteric effect and altered interface of the dimerisation is implicated in reduced repair ability (Hill & Evans 2006). Paradoxically Cys-326 is possibly inactivated by the same physiological condition (oxidative stress) from which it protects DNA. Epidemiological studies have attempted to elucidate the functional consequences of this polymorphism; however no definitive conclusion has been agreed. Kohno *et al.* identified loss of heterozygosity at the hOGG1 locus in lung tumours; however levels of 8-oxoG in peripheral leukocytes and lung cancer cells were normal (Kohno *et al*. 1998). No significant difference was observed in the mutation suppressibility between the variant and wildtype (S.-R. Kim *et al.* 2004). A case-control study found a significant association of lung adenocarcinoma risk in individual homozygous for the Cys variant allele (Kohno *et al.* 2006). Conversely a large scale meta-analysis of 6375 cancer subjects found no association of lung cancer with the Cys/Cys genotype (Li *et al*. 2008). The neuropathological CAG repeat was expanded in the Cys

variant, linking the Cys phenotype to accelerated manifestation of Huntingdon's disease (Jarem *et al.* 2009; Jarem *et al*. 2011). Heterozygotes and homozygotes for the variant present accelerated development of Type 2 Diabetes due to decreased glucose tolerance (Daimon *et al.* 2009) and ROS-mediated β-cell dysfunction (Thameem *et al.* 2010). Diabetes aetiology has been attributed to the loss of protective effect of OGG1 against free fatty acid-induced apoptosis (Rachek *et al.* 2006) in addition to its regulation of inflammation in type 1 diabetes, allergens and LPS-induced shock (Mabley *et al.* 2004). Lack of conformity between the biochemical properties of the Cys-326 variant and carcinogenesis may be due to a number of factors such as inter-individual variability(Lee *et al.* 2005; Collins *et al.* 2001), age-related oxidative-stress susceptibility (Mikkelsen *et al.* 2009; Radak & Boldogh 2010) and exposure to environmental factors (Aka *et al*. 2004; Wrońska-Nofer *et al*. 2012). Furthermore the redundancy of the oxidative DNA repair means that reduced activity of OGG1 may be nullified by other repair proteins.

Several studies have suggested post-transcriptional modification of OGG1, such as phosphorylation by Cdk4 (Hu *et al.* 2005), PKC (Dantzer *et al.* 2002), and acetylation by P300 (Bhakat *et al.* 2006). OGG1 interacts with many protein partners, many of which regulate activity. OGG1 exerts discrimination at an intermolecular level dictated by the amino acid sequence, and though these have an additive effect on recognition, a single amino acid change can disrupt the recognition properties of the protein. Thus it is theorised that altered sequence can directly affect the complement of protein partners. This study investigates the identity of protein partners of the variant compared to the wild-type in an attempt to examine whether altered interaction properties are responsible for the reduced repair activity of the Cys-326 variant. The delayed response of the Cys-326 OGG1 has recently been documented as well as decreased nuclear retention (Kershaw 2011).

Previous inconsistencies in the localisation of the variant have been documented, suggesting that while the wild-type consistently relocates to the nucleoli during S-phase the variant is excluded from this compartment (Luna *et al.* 2005). This study compares the localisation of the variant and the wild-type under normal and oxidative stress conditions.

Chapter 2 Materials and Methods

2.1 Chemicals

Materials were of the highest quality and from Sigma-Aldrich unless otherwise stated.

Abbreviations

DMEM Dulbecco's Modified Eagle's Medium (D6429, Sigma-Aldrich) with 4500 mg/L glucose, L-glutamine and sodium pyruvate, with pyridoxine (substitutes pyridoxine HCl for pyridoxal HCl), endotoxin tested, sterile filtered. Supplementated with foetal bovine serum (10% v/v) (FBS), L-glutamine (2 mM), penicillin (100 U/ml) and streptomycin (100 µg/ml).

PBS Phosphate Buffered Saline (Dulbecco A) (Oxoid, Basingstoke). Typical Formula:

Sodium Chloride 8.0, Potassium chloride 0.2, Di-sodium hydrogen phosphate 1.15, potassium dihydrogen phosphate 0.2.

2.2 Cell Culture

Cell culture was conducted in sterile conditions in a Bio Air Aura B4 Class II hood, which was spray cleaned with 70% ethanol before and after use. All instruments were sprayed with 70% ethanol before entering the hood.

2.2.1 Thawing Cells

A549 cells were removed from liquid nitrogen. The cryovial (1ml) (Naglene) containing the frozen cells were retrieved from liquid nitrogen storage and immediately placed in a 37ºC water bath. The cryovial was then transferred to the hood where the contents of the vial were transferred to a 15ml Falcon tube (BD Falcon™). Pre-warmed DMEM (9ml) was added to the 15ml Falcon tube. The tube was centrifuged for at 1000 x g for 5 minutes (MSE Falcon 6/300, Sanyo, Japan). The supernatant was aspirated and the pellet was

resuspended in 1ml fresh DMEM. The suspension was then split into 75cm^2 cell culture flasks (BD Falcon™) and fresh pre-warmed DMEM (15ml) was added to each flask.

2.2.2 Cell Maintenance

Cells were maintained in 75cm^2 cell culture flasks (BD Falcon™) containing Dulbecco's modified Eagle's medium (DMEM) supplemented with foetal bovine serum (10% v/v) (FBS), L-glutamine (2 mM), penicillin (100 U/ml) and streptomycin (100 µg/ml). Cells were incubated at 37°C in a humidified chamber (5% CO2, 95% air; MCO-15AC, Sanyo, Japan).

2.2.3 Cell Passage

Cells were reseeded upon reaching 70-80% confluency. DMEM media was removed from T75cm^2 flasks and the cells were washed with sterile PBS. As standard, cells were detached using trypsin-EDTA, incubated at 37ºC in a humidified chamber (5% CO2, 95% air; MCO-15AC, Sanyo, Japan) for approximately 3 minutes, transferred to 15ml Falcon tube with fresh media and centrifuged at 1500 x g for 5 minutes (MSE Falcon 6/300, Sanyo, Japan). The supernatant was then aspirated and the pellet was resuspended in 1ml fresh media. The resuspended media was split to achieve 50-60% confluency per T75cm^2 flask. Cells were maintained in 15ml of DMEM.

2.2.4 Cryopreservation

Cells were washed in sterile PBS and trypsinised as above. Following centrifugation at 1500 x g for 5 minutes, the supernatant was aspirated and cells were resuspended in 1ml of Freezing media. Freezing media consists of 1:9 mixture of sterile DMSO (10% v/v) and Feotal Bovine Serum (Sigma-Aldrich). The resuspended cells were then transferred to a cryopreservation vial (Naglene) and kept in a -80C freezer overnight before transfer to liquid nitrogen.

2.3 Oxidation Treatment

2.3.1 BSO Oxidation

Buthionine sulfoximine was used as the oxidative reagent of choice attributed to its rapid potent inhibition of GCL resulting in the depletion of cellular GSH. Depletion of cytoplasmic GSH by BSO has been documented to significantly increase ROS formation. A stock solution of 10mM of BSO was prepared by mixing 22.23mg DL-buthionine-sulfoximine (Sigma-Aldrich) in complete DMEM medium (10ml). Serial dilutions were conducted to prepare 1mM, 0.5mM, 0.25mM, 0.125mM and 0.0625mM concentrations of BSO which were stored in the freezer till use.

2.3.2 Cell Viability Assay

MTT (Thiazolyl Blue Tetazolium Bromide) (Sigma-Aldrich) was prepared in complete medium to a 0.5mg/ml solution and filter sterilised. Cells were seeded into 96 -Well plates (Corning) and incubated overnight in at 37ºC, 5% CO2, 95% air (MCO-15AC, Sanyo, Japan) to reach confluency. The growth media was removed and varying concentrations of BSO-containing media was added to cells which were then incubated for 24 hours at 37ºC. The oxidation treatment media was decanted from the 96-well plates and replaced with MTT-supplemented media. Cells were incubated for 2 hours at 37ºC in a humidified chamber (5% CO2, 95% air; MCO-15AC, Sanyo, Japan). Again the medium was removed and 100% DMSO was added to each well. The well plates were then either read immediately or stored at 4ºC till ready to read. The absorbance was read at 540nm using Bio-Tek FL600 microplate reader (Bio-Tek Instruments Inc. USA) against a DMSO blank.

2.4. EGFP-OGG1 Vectors

2.4.1 Vector Propagation

GFP-Ser326-hOGG1 and GFP-Cys326-hOGG1 cDNA plasmids (pcDNA3©) were propagated by transformation into E.*coli* and selection using Kanamycin antibiotic (30ug/ml). As a positive-control of transfection, a plasmid containing GFP was also selectively grown. Using a 200µl pipette tip a small aliquot of frozen glycerol stock *E.coli* cells transformed with the OGG1-GFP or GFP expression vector was scraped from the eppendorf and added to a 50ml Falcon tube (BD Falcon™). Then 30ml of Luria-Bertani Broth (MELFORD) was added to the falcon tube, followed by kanamycin (15µl). The *E.coli* culture was grown at 37ºC in a rotator (Aerotron INFORS AG) (225rpm) overnight.

2.4.2 Plasmid DNA Isolation

Plasmid extraction was conducted using the Bioline ISOLATE Plasmid Mini kit as per manufacturer's instructions (BIOLINE). Cultures were centrifuged at 6000 x g for 10 minutes (Mistral 2000, Meadowrose Scientific LTD) to pellet the bacterial cells. The remaining supernatant was removed and the cells were resuspended in 500µl in Resuspension buffer. Next, 500µl of Lysis Buffer P was added and the suspension was mixed by inverting 4-5 times. The mixture was transferred to a 1.5ml microcentrifuge tube to which 600µl of Neutralisation buffer is added. The contents are mixed by inverting 4-5 times to achieve a homogenous suspension. The suspension was centrifuged at maximum speed (16500 x g using Eppendorf Centrifuge 5415D) for 10 minutes. The supernatant was transferred to the spin column (BIOLINE) which was placed in a collection column and centrifuged for 1 minute at 10000 x g. The column was washed with 500µl of Wash Buffer AP and centrifuged for 1 minute at 10000 x g. The filtrate was discarded It was then washed with 700µl Wash Buffer BP and centrifuged for 1 minute at 10000 x g. The filtrate was discarded. The spin column was centrifuged at maximum speed (16500 x g using

Eppendorf Centrifuge 5415D) for 2 minutes. The spin column was then placed into a 1.5ml Elution tube. The plasmid DNA was eluted by the addition of 100µl of Elution buffer to the spin column and incubation at room temperature for 5 minutes followed by centrifugation at 10000 x g for 1 minute.

2.4.3 DNA Quantification

The concentration of the eluted DNA was measured by conducting a 1:20 dilution with ultrapure water into 100µl spectrophotometer curvette. The absorbance at 260nm determined using UVIKON spectrophotometer is an estimation of the DNA concentration expressed in µg/µl. Absorbance was also measured at 280nm to facilitate DNA purity calculation.

2.5 Transfection

2.5.1 Transfection of EGFP-OGG1

The ratios of the transfection reagent, DNA and media volume were adjusted according to the tissue culture vessal as suggested by manufacturer's instructions. Cells were cultured in 12-well plates/ 6-wells plates/ T25 flasks at 50-60% confluency and incubated (37ºC, 5% CO2, 95% air) overnight to grow to approximately 70-80% confluency. The quantity of DNA required per vector for each well/flask was calculated and then multiplied by the number of replicates for each vector type. The recommended amount of serum-free DMEM was added to the vector DNA in a 15ml Falcon tube or 1.5ml eppendorf. The recommended amount of TurboFect™ Transfection reagent (Fermentas, UK) was added according to vessel size and number of replicates. The mixture was briefly vortexed followed by incubation for 15-20 minutes at room temperature. The DNA:DMEM: Turbofect mixture was then added dropwise to each well and the cells were returned to the humidified chamber (37ºC, 5% CO2, 95% air) for 24-48 hours for vector expression.

2.5.2 Flow Cytometry

Quantitative transfection efficiency was determined by flow cytometry analysis. Cells were grown in 12-Well plates (Corning) and transfected (2µg DNA: 200µl serum-free DMEM: 4µl TurboFect™) according to the protocol above. Samples were prepared for flow cytometry following the 24-48 hour incubation period required to achieve vector expression. The DMEM was removed and cells were washed with PBS. Cells were detached by the addition of Trypsin:EDTA and incubation at 37ºC for 5 minutes. The detached cells suspension was transferred to a 1.5ml eppendorf and spun for 5 minutes at 8000 x g at room temperature using a benchtop centrifuge (Eppendorf Centrifuge 5145D). The supernatant was then aspirated and the cells were resuspended in 1ml non-sterile PBS. The suspension was transferred to a 5ml polystyrene round bottom flow cytometry tube (Becton Dickinson). Samples (10 000 live cells) were gently vortexed prior to analysis using a BD FACScalibur™ flow cytometer (Becton Dickinson). CellQuestPro™ software and Weasel software (Walter and Eliza hall institute of medical research, Australia) were used to process and analyse the data.

2.6 Immunoprecipitation of OGG1

2.6.1 Epifluorescence Microscopy

Having optimised transfection and quantitatively recorded efficiency levels, Epifluorescence microscopy was utilised to ensure adequate transfection of cells in T25 flasks prior to immunoprecipitation. Axiovert 10 (Zeiss) microscope was used to view GFP fluorescence under blue laser light.

2.6.2. Nuclear Protein Extraction

Nuclear protein was isolated from cultured to reduce sample complexity and enrich concentration of GFP-OGG1 protein. Growth medium was decanted from the culture flask

and cells were washed with cold sterile PBS. Ice cold Pierce IP Lysis buffer (25mM Tris-HCl pH 7.4, 150mM NaCl, 1mM EDTA, 1% NP-40 and 5% glycerol), supplemented with protease inhibitor cocktail (Sigma Aldrich), was added to the cells at the recommended volume per culture vessel. Cell detachment was further stimulated by vigorous scraping. The detached cell suspension was transferred to a 1.5ml eppendorf* and incubated at 4ºC for 20 minutes. Following this, cells were centrifuged at 3000 x g for 5 minutes at 4ºC using a benchtop centrifuge (Hawk 15/05 Refrigerated, Sanyo, Japan). The supernatant was aspirated and the nuclear pellet resuspended in Pierce IP Lysis buffer. Cells were further incubated at 4ºC for 30 minutes, with gentle vortexing every 10 minutes. The resuspension was subjected to centrifugation at 18 000 x g for 20 minutes at 4ºC, and the supernatant was collected in a sterile 1.5 ml eppendorf. *T25 flasks of cells transfected in duplicate were combined at this stage to increase the overall yield of nuclear protein.

2.6.4 Immunoprecipitation

Protein purification was conducted using Pierce ® Crosslink Immunoprecipitation Kit (ThermoScientific) according to manufacturer's instructions (Appendix 1). The protocol was optimised to troubleshoot a number of problems; the numbered points below correspond to the stage that was modified in the original protocol. The protocol was repeated several types with different variables altered each time, therefore to simplify the interpretation of results the attempts are annotated with the experiment number.

A. Binding Antibody to Protein A/G Plus Agarose

A.5. The initial antibody dilution used 10µl Rabbit Anti-GFP antibody (Ab290, Abcam) diluted into 400µl 1x Coupling Buffer and added (100µl) to each column. (Experiment 1)

A.5. The antibody dilution was reduced to 4µl Rabbit Anti-GFP antibody (Ab290, Abcam) diluted into 400µl 1x Coupling Buffer. Then 100µl of the solution was added directly to the resin in the column. (Experiment 2 and onwards).

B. Crosslinking the Bound Antibody

B.1. A single tube of DSS was dissolved in DMSO to prepare 10x DSS. (Experiment 1) The 10x DSS was stored in a foil pouch and used in subsequent experiments. (Experiment 1-5).

B.1. Inefficient crosslinking suggested degradation of 10xDSS. To address this possibility fresh 10x DSS was prepared per experiment. (Experiment 6-7).

B.5. The crosslinking reaction was incubated for 90 minutes which is longer than the recommended maximum time of 60 minutes. (Experiment 6-7).

C. Mammalian Cell Lysis

C.3. Supplement the IP Lysis buffer with protease inhibitor (1:10 dilution). For lysis of 12-well plate 250µl of IP lysis buffer was added to each well. (Experiment 1).

C.3. Due to high background to signal ratio, lysis of cells transfected with EGFP-Cys OGG1, EGFP-Ser OGG1 and non-transfected cells was proceeded by nuclear protein extraction as described above. (Experiment 2). Lysis of the positive-control GFP-transfected cells was conducted using the original cell lysis protocol; GFP localizes in the cytoplasm so nuclear protein extraction would be counterproductive. (Experiment 1 and onwards).

C.3. Due to insufficient protein yields, the cell culture and transfection was scaled up to T25 flasks (25cm^2). Therefore the cell lysis was also scaled up; 750 µl of IP Lysis buffer was used to lyse cells in T25s as described above. (Experiment 3 and onwards).

D. Pre-clearing lysate using Control Agarose Beads.

D.1. To respond to the low protein yields (~0.5mg), only 40µl of the Control Agarose Resin was added to each spin column. (Experiment 1 - 3).

D.1. At high protein yields the recommended amount (80µl) of Control Agarose Resin was added to each spin column. (Experiment 4 and onwards).

D.4. The volume of lysate added to the column varied with every immunoprecipitation attempt. The recommended amount of total protein per IP reaction is 500-1000µg. The amount of total protein per sample was determined using the Bradford Assay, then the maximum amount that could be consistently taken from each sample was calculated. This lysate volume was diluted with ice-cold IP Lysis buffer to achieve the general recommended sample volume (300-600µl) of 500µl.

E. Antigen Immunoprecipitation

E.1. This step was omitted as the antibody-crosslinked columns were freshly prepared on the day of immunoprecipitation. (Experiment 1 and onwards)

E.3. This step was omitted as the cell extract was diluted in IP Lysis buffer prior to pre-clearing. Subsequent to the pre-clearing (D.5), all of the flow-through collected per sample was applied to antibody-crosslinked columns.

F. Antibody Elution

F1. The spin column was placed into a new collection tube and 10µl of Elution buffer was added and the columns were centrifuged as suggested in the original protocol. Additionally the low pH of the Elution buffer was neutralised by adding 3µl of 1M Tris, pH 8.8, directly to the collection tube. (Experiment 1-6).

F3. Two additional elutions were conducted by repeating steps F1-F3. The elute was collected into 1.5 eppendorf and stored at -80 till further analysis by SDS-PAGE.

F1-3. To facilitate the downstream mass spectrometry of the purified protein, the Pierce Elution buffer was exchanged for an elution buffer of known composition and compatibility to mass spectrometry. The elution buffer was prepared of

TFA:H_2O:Acetonitrile at 1:20:20 ratio. Then 40µl of elution buffer was added to each column. The columns were rotated end-to-end gently for 10 minutes at room temperature, followed by centrifugation at 1000 x g for 1 minute at 4°C (Hawk 15/50 Sanyo, Japan). The supernatant was collected, and elution buffer was evaporated at 60°C using Eppendorf Vacufuge to achieve a dry pellet. The samples were then stored at -80 till downstream processing by mass spectrometry.

2.6.5 Bradford Assay

Protein concentration was determined colorimetrically using the Bradford assay (Bradford M.M 1976). Bio-Rad reagent was made to a 1/5 dilution with dH20 and syringe filtered. Bio-Rad reagent (1ml) was added to each curette with varying amounts (0-10 µl) of the BSA standard. Arbitrarily chosen amounts of samples were added to a cuvette containing Bio-Rad reagent and the absorbance was read at 595nm.

2.7 Protein Analysis

2.7.1 SDS-PAGE

Buffers

10% Resolving gel: Polyacrylamide 30% solution (10%), Tris-HCl pH 8.8 (1.5M), SDS (10% w/v), UHQ H_20 (11.9ml). Immediately prior to casting N,N,N,N-tetramethylethylenediamine (TEMED) (4 µl per 10ml) and 10% w/v ammonium persulphate (APS) (100 µl per 10 ml) were added.

4% Stacking gel: Polyacrylamide 30% solution (5%), Tris-HCl pH 6.8 (1M), SDS (10% w/v), UHQ H_2O (20.4ml). Immediately prior to casting N,N,N,N-tetramethylethylenediamine (TEMED) (10 µl per 10 ml) and 10% w/v ammonium persulphate (APS) (100 µl per 10 ml) were added.

1X TBS: Tris base (0.1 M) and NaCl (0.15 M), adjusted to pH 8.0.

1X TBS-0.05% Tween: 10x TBS, UHQ H_2O and Tween 20 (0.05%).

SDS-PAGE running buffer: Tris base (25 mM), glycine (192 mM), and SDS (0.1% w/v).

Transfer buffer: Tris base (20 mM), glycine (150 mM) and methanol (20% v/v).

Blocking buffer: Low-fat powdered milk (Marvel, U.K.) (5%) in 1X TBS-0.05% Tween

Following elution of the desired protein, 20µl was aliquoted into a 100µl microcentrifuge tube in preparation of SDS-PAGE. The eluted proteins were mixed with 20µl of 2x Laemmli loading buffer and centrifuged briefly. The sample was denatured by heating at 95ºC for 5 minutes. Sequentially the resolving gel and stacking gel were cast using the Mini-PROTEAN Tetra Electrophoresis System (Bio-Rad™). Ladder (Prestained Protein Marker, Broad Range, BioLabs) (10µl) was loaded followed by the samples; these were resolved in running buffer at 100V for approximately 90 minutes.

2.7.2 Western Blot and ECL Immunodetection

The SDS-polyacrylamide gel was washed with running buffer and the stacking gel was removed, prior to placing the gel into the transfer kit. The PVDF membrane (Millipore Immobilon) was primed to transfer by equilibration in 100% methanol and transfer buffer. The transfer unit was assembled in the following order: cathode cassette plate, fiber pad, filter paper, polyacrylamide gel, PVDF membrane, filter paper, fiber pad and anode cassette plate. The proteins were transferred using the Bio-Rad electrophoretic transfer system at 80V for 90 minutes. Following transfer the membrane was blocked, using Blocking buffer, overnight at 4C on a rocking platform. The membrane was washed with 1xTBS- 0.05% Tween before incubation with primary antibody, Rabbit Anti-GFP antibody (Abcam:ab290) (1:2500 dilution) for either 1 hour at room temperature or overnight at 4C on a rocking platform. Membranes were washed with 1x TBS-0.05% Tween solution (3 x 15 minutes) before incubation with secondary antibody, Goat Anti-

Rabbit HRP antibody (DAKO) (1/1000 dilution). Once again the membranes were washed with 1x TBS-0.05% Tween solution (3x15minutes) and then washed with 1x TBS for 15 minutes. The membrane was incubated with SuperSignal West Pico chemiluminescent detection reagent (Thermo Fisher Scientific, U.K.) for 5 minutes, prepared as per manufacturer's instructions. The membranes were exposed to ECL Hyperfilm (Amersham) in the dark and the film was developed using X-O-graph machine.

2.8 Mass Spectrometry

Samples underwent zip-tip desalting and trypsin digestion (Functional genomics and proteomics facility, University of Birmingham, UK). The peptide fragments were pipetted into 96-well and processed by LTQ Orbitrap Velos Mass spectrometer **(ThermoScientific)** (Functional genomics and proteomics facility, University of Birmingham, UK)

2.9 Confocal microscopy

Coverslips were washed in 70% ethanol and PBS before being placed into 6-well plates (Corning). Cells were seeded into 6-well plates at 40-50% confluency and incubated overnight. Wells were transfected (4µg DNA: 400µl serum-free DMEM: 6µl Turbofect™) in duplicate in to separate well plates. After 24 hours of transfection incubation, a 6-well plate was treated with BSO (10mM); the DMEM was removed and equal volume of fresh BSO- media (10mM) was added. Following 48 hour incubation since transfection, cells were counterstained with 1000x dilution of DAPI for 30 minutes at 37°C. DMEM media was aspirated and coverslips were washed twice with PBS and fixed using 2% paraformaldehyde, pH 7.4, for 15 minutes at room temp. Coverslips were washed twice with PBS before transfer to a microscope slide with an aqueous mountant (DAKO). Image acquisition was performed with a Leica TCS SP2 confocal microscope using a 63x oil immersion objective NA 1.32. Fluorochromes were excited using an argon laser at 488 nm for EGFP and 405 nm for DAPI. Images were processed using ImageJ (MacBiophotonics).

Chapter 3 Results

Various concentration of the oxidising agent BSO were tested to determine a suitable concentration without disruption of cell viability. The cells were transfected with GFP-OGG1 and then treated with the oxidising agent. These cells were then viewed under a confocal microscope and compared to non-treated cells. A second set of cells were transfected, and OGG1 with its protein partners was co-purified and the identities were confirmed by mass spectrometry.

3.1 Cell Viability Assay

Cell viability of the cells was measured to ensure that BSO did not have an adverse affect on the survival of the cells. Different concentrations of BSO were tested to determine a concentration effect on cell viability. Cell viability was determined using the MTT assay in which a yellow tetrazole dye is reduced to an insoluble purple formazan crystal, which is solubilised on addition of DMSO. The absorbance [540nm] is measured against a DMSO blank. No statistical difference was observed between any of BSO concentrations tested.

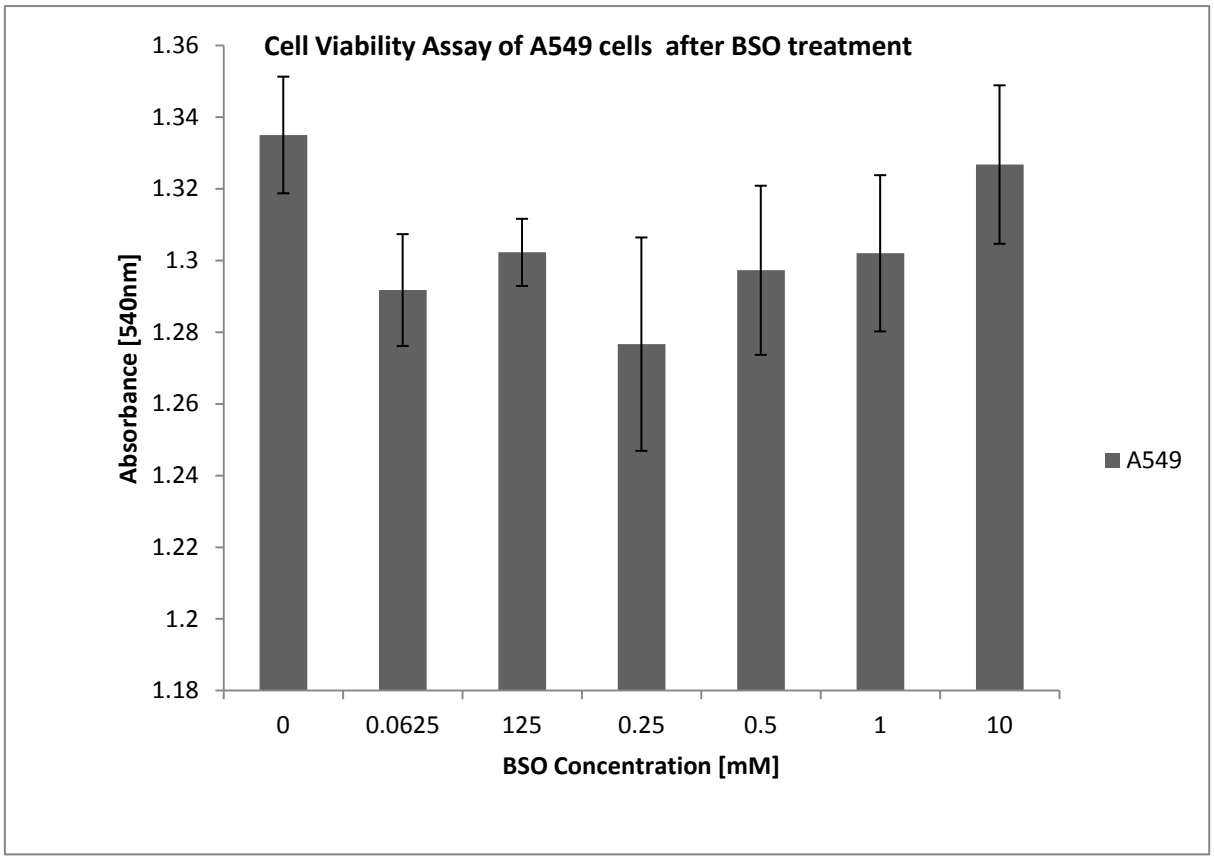

Figure 3.1 Cell Viability of A549s assessed after BSO treatment for 24 hours. Cell viability determined by MTT assay, measuring the absorbance of MTT reduction against a DMSO blank. No concentration dependant decrease is observed in A549 cells. One-way ANOVA analysis further confirmed that there was no statistical change ($P<0.05$) in the absorbance (540nm) at varying BSO concentrations in A549s ($P=0.647$ SD±0.058).

3.2 Flow Cytometry Analysis of Transfection Efficiency

The fluorescence emitted by GFP was measured to determine the transfection efficiency.

The measurement of GFP fluorescence was plotted against the forward scatter. A quadrant is chosen ($x=0, y=10^1$) to exclude background fluorescence and represent a threshold between transfection-dependant fluorescence and background fluorescence inherent to cells. The region below this quadrant represents non-transfection dependent inherent fluorescence. The fluorescence measured above the threshold is due to transfection and the percentage of cells above the threshold fluorescence is the transfection efficiency.

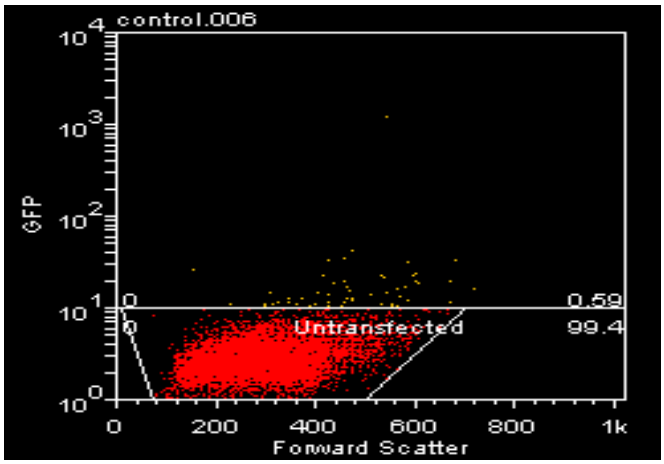

Figure 3.2.1 Graphical presentation of GFP fluorescence in negative control untransfected cells. Over 99% of the cells in the non-transfected negative control are below this threshold.

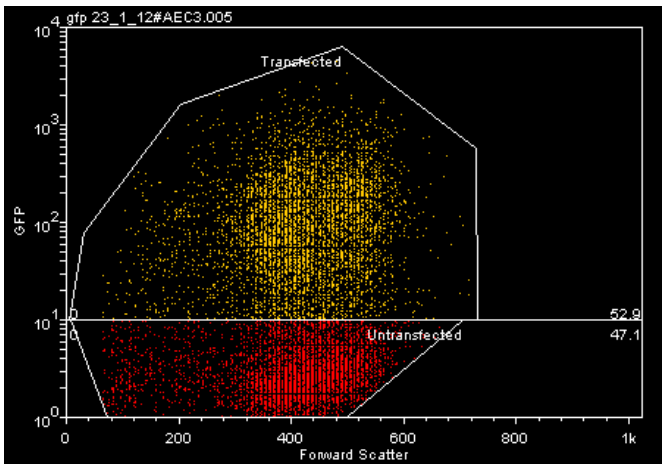

Figure 3.2.2 Graphical presentation of GFP fluorescence in positive control GFP-transfected cells. The standard threshold as determined by the negative-control is applied. The region above the threshold (yellow) represents GFP expression in transfected cells indicating a 52% transfection efficiency.

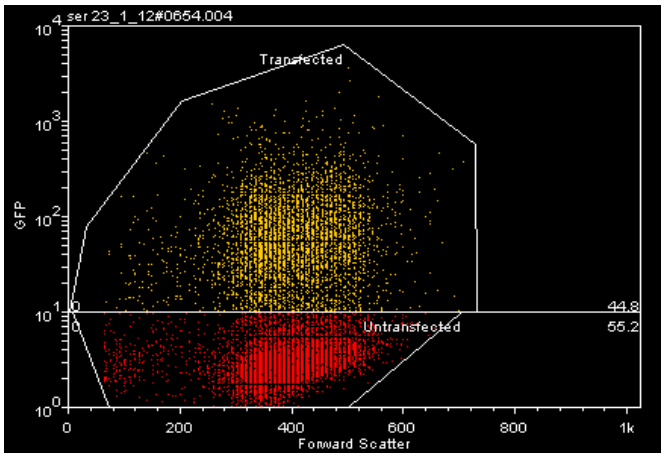

Figure 3.2.3 Graphical presentation of GFP fluorescence in GFP-Ser-OGG1 transfected cells. The region (yellow) above represents cells transfected with GFP-Ser-OGG1 vector (44.8% transfection efficiency).

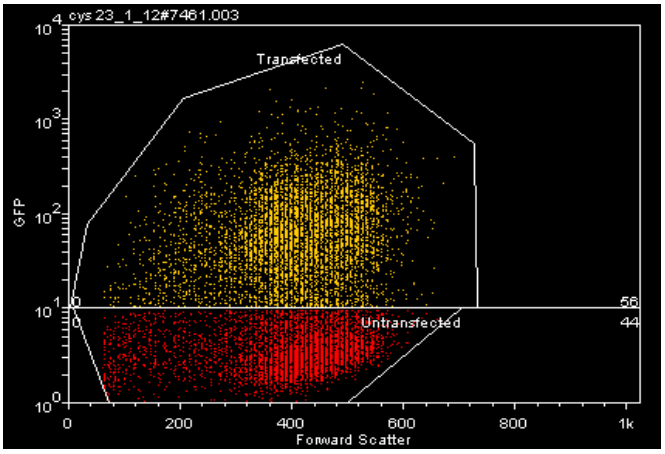

Figure 3.2.4 Graphical presentation of GFP fluorescence in GFP-Cys-OGG1 transfected cells. Expression of Cys-OGG1 is measured by GFP fluorescence above the threshold, the figure above shows 56% transfection efficiency.

3.3 Optimisation of Immunoprecipitation protocol

This study provides recommendations on the optimisation of the Pierce Crosslink Immunoprecipitation kit for the purification of GFP-OGG1, based on the experience of the author. The optimisation of immunoprecipitation is a common challenge encountered by investigators as protocols need to be modified to suit the type of protein, source of protein and the amount required. Optimisation of immunoprecipitation is further complicated by numerous factors which significantly influence the success of the experiment. Isolating the causal factor of a poor result is a scientific challenge that is dependent on the interpretation of the results. The usual strategy that is taken during method development is to alter one variable at a time which is often easy to implement and readily observed in the results. However, the trial and error method in which adjustments are made is time consuming and laborious. The starting point of any optimisation procedure is to perform the protocol without any deviations; the outcome of this pilot run would dictate the troubleshooting actions. Various immunoprecipitation methodologies are illustrated below (Figure.3.3.1), in general an antibody showing high specificity for the low-abundance target is coupled to a solid-phase matrix (protein A/G sepharose beads); this then binds proteins of interest and adsorbs the protein complex from the cell lysate (ThermoScientific 2010). Proteins that are not bound to the antibody-Protein A/G bead support are washed away and the proteins of interest are eluted from the antibody coupled beads. This is often followed by Western blot analysis to determine the identity of proteins that are associated with the protein of interest. This study utilised the Crosslink IP method whereby the antibody is covalently bound to the beaded support via a crosslinking reagent.

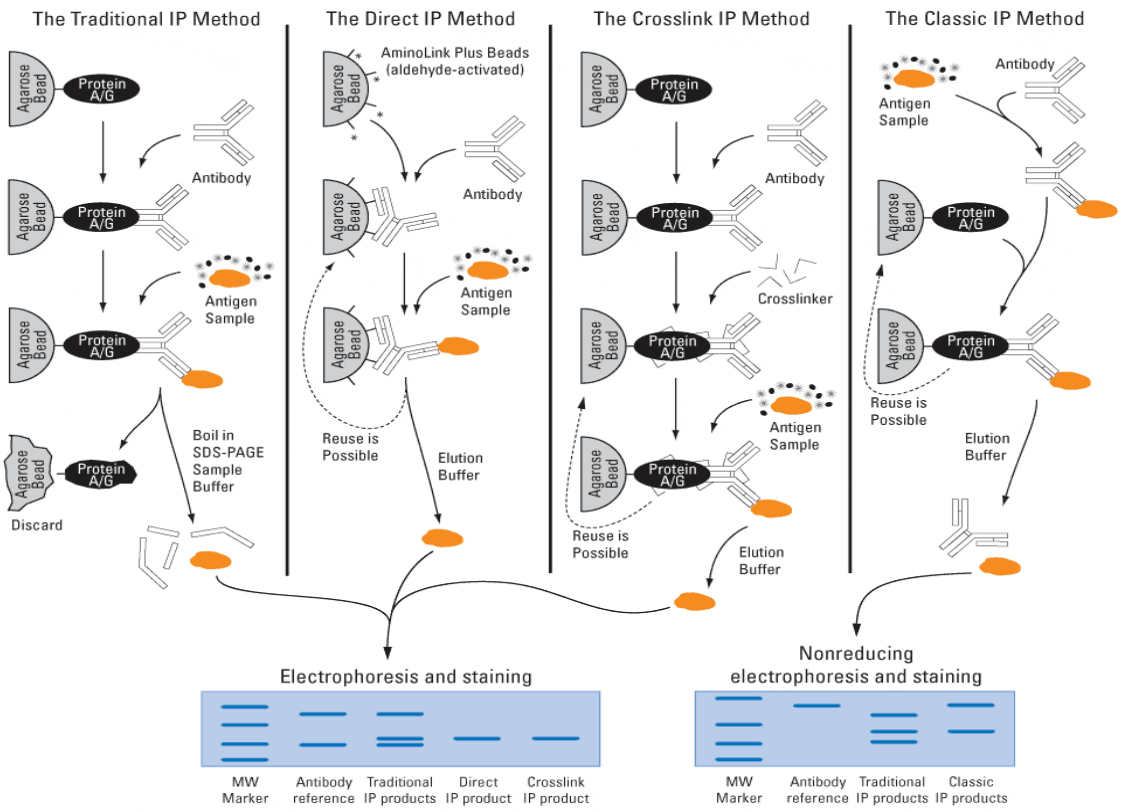

Figure 3.3.1 Immunoprecipitation Methodology. The various methodologies of immunporecipiation are summarised. The crosslink IP method is most relevant to this study (ThermoScientific 2010).

Several efforts were made to optimise the cross-link immunoprecipitation. The outcome of each immunoprecipitation was analysed by western blot. The results are analysed in the context of identifying the potential problem and the suitable troubleshooting reaction. The figure below (figure 3.3.2) summarises the immunoprecipitation protocol with the optimisation steps conducted, demonstrating that different variables were altered with each experiment of the immunoprecipitation protocol.

Optimisation of Sample Preparation

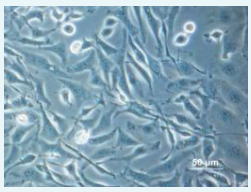

1. The initial run of the immunoprecipitation experiment indicated a high noise ratio and background. To minimise this, the sample preparation protocol was modified to include nuclear extraction.

Sample Preparation

3. Insufficient yields of initial protein sample was considered as a possible drawback. To address this, the cell culture vessal was up-scaled from 12-well plates to T_{25} flasks.

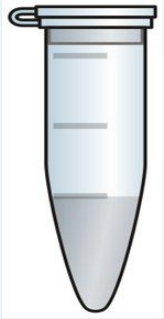

Antibody-Column Preparation

2. The excessive elution of the antibody indicated that the concentration of antibody was too high, resulting in elution of uncrosslinked antibody. To counteract this, the antibody concentration was lowered.

4. The presence of an antibody band in the control extract suggested inadequate crosslinking of antibody to the A/G Proteins. Fresh DSS crosslinker was utilised to increase efficiency of crosslinking reaction.

Elution

5. The elution buffer provided in the immunoprecipitation kit was incompatible with mass spectrometry, thus the elution buffer was changed to one with known composition suitable for mass spectrometry.

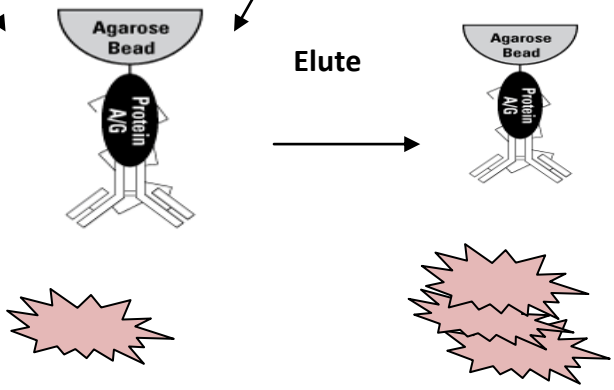

Figure 3.3.2 Schematic illustration of the cross-link immunoprecipitation. The stages that were altered to optimise the immunoprecipitation protocol are numbered in the order they were implemented.

Results of Experiment 1.

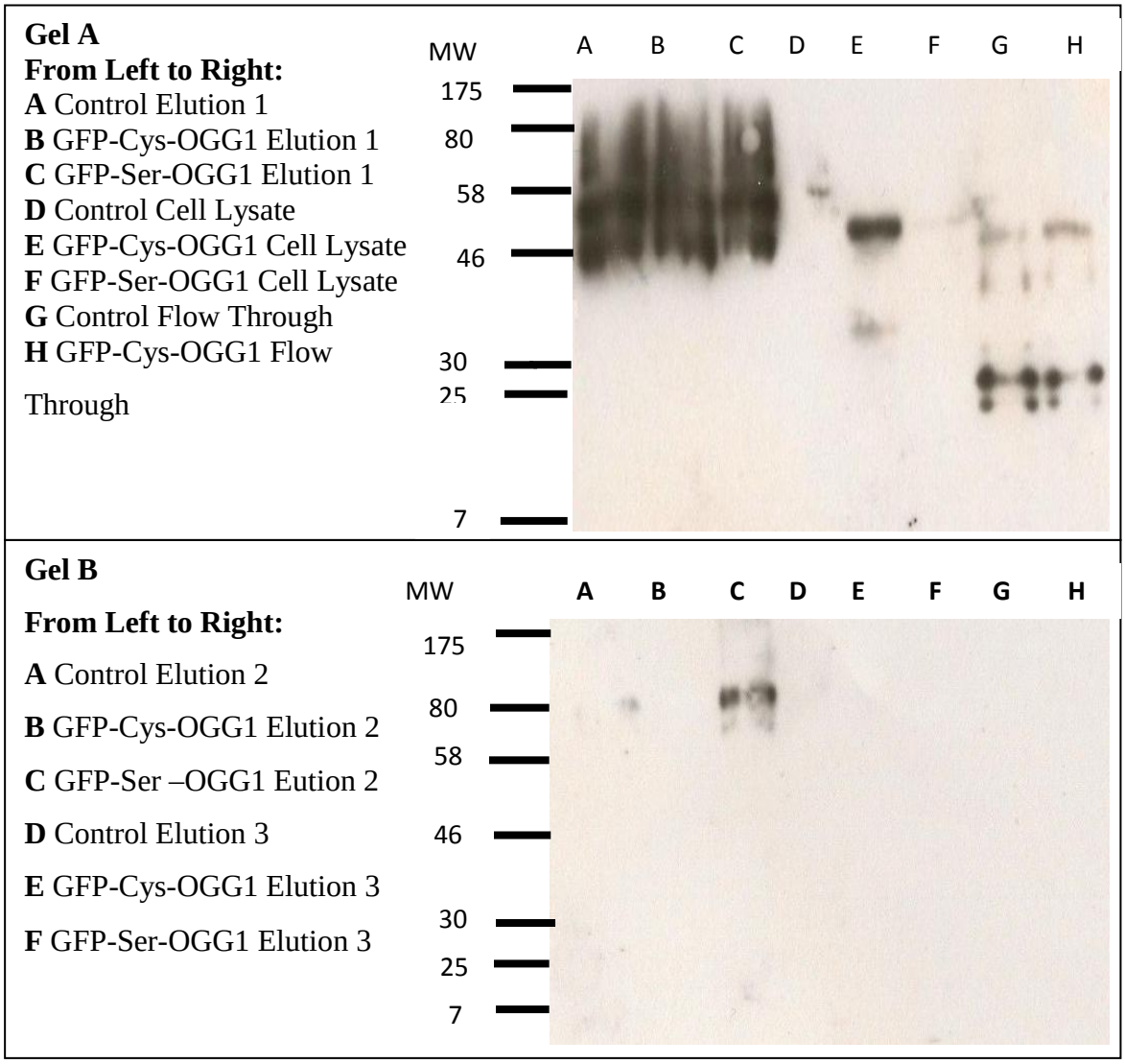

Figure 3.3.3 Western blots of Experiment 1. Gel A analysed the primary eluate, the starting material and the flow through allowing the comparison of protein bands at each stage of immunoprecipitation. Gel B analysed the secondary and tertiary elutions to evaluate the efficiency of the elution buffer is washing off GFP-OGG1.

The outcome of the immunoprecipitation was analysed by conducting a western blot of the eluates (Figure 3.3.3). Gross vertical streaking was observed in all the eluate samples. The control samples lack GFP so the presence of bands in the control column is likely due to contamination of the samples. GFP-Cys-OGG1 and GFP-Ser-OGG1 presented a similar

band pattern to the control, suggesting inherent processing problems. It is likely that the proteins have been degraded resulting in a number of polypeptides that have different molecular weights that can be detected by GFP antibody.

The starting cellular material was also analysed to confirm the presence of OGG1 in the cell sample. As expected no GFP was present in the cell lysate of the control. The cell lysate of GFP-Cys-OGG1 displayed a discrete band representing OGG1 protein with an approximate molecular weight of 60kDa which correlates to estimated combined molecular weights of GFP and OGG1. The lack of a band for GFP-Ser-OGG1 represents insufficient GFP-OGG1 present in the cell sample which would likely be a result of low transfection efficiency.

The flow-through was collected after overnight incubation of the cell lysate with the antibody-crosslinked resin (Step E.5, Immunoprecipitation Protocol, Appendix 1). The flow-through was analysed to determine the efficiency of the immunoprecipitation; the presence of discrete bands would indicate the proteins are not sufficiently bound to the resin and can be washed off the resin without elution buffer.

The additional elutions were also analysed, as presented on Gel B (figure 3.3.3). The band present in the GFP-Ser-OGG1 column is likely to represent GFP-OGG1. This indicates the primary elution is not sufficient to elute all of the protein. It also suggests that the GFP-antibody cross-linked resin was able to specifically detect and bind to GFP-OGG1. The absence of any bands in the remaining column indicates any bound GFP-OGG1 has been eluted completely from the resin.

Optimisation Step 1

The initial problem encountered was the high level of background noise relative to the signal of interest. From the SDS-PAGE analysis it is evident that the expected signal of

interest is masked in the background signal. High background is the result of non-specific binding of the cell lysate components to the antibody immobilised resin. As no resin is completely inert, non-specific interactions between cellular components and the Protein A/G resin are likely. Pre-clearing of starting material eliminates nonspecific high affinity proteins bound to the protein A/G resin, these proteins are omitted from the actual immunoprecipitation process. High background signal was repeatedly detected throughout the experiments despite the pre-clearing stage, suggesting either short-comings of the pre-clearing stage or other causes of non-specific signals. Several routes can be undertaken to reduce the background signal; in this investigation the first attempt was to reduce sample complexity by conducting nuclear extraction of the samples. Only the nuclear fraction was immunoprecipitated, therefore minimising the amount of non-specific proteins in the cell lysate sample. Reducing the presence of nonspecific proteins enriches the protein of interest in the lysis buffer

Results of Experiment 2.

Gel A
From Left to Right:
AControl Elution 1
B GFP-Cys-OGG1 Elution 1
C GFP-Ser-OGG1 Elution 1
D GFP Elution 1
E GFP-Cys-OGG1 Elution 2
F GFP-Ser-OGG1 Elution 2
G GFP Elution 2
H Control Elution 2

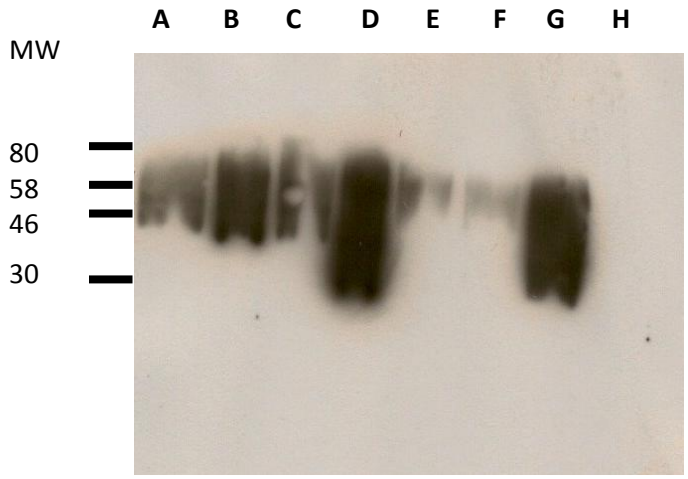

Gel B
From Left to Right:
A Control Flow Through
B GFP-Cys-OGG1 Flow Through
C GFP-Ser-OGG1 Flow Through
D GFP Flow Through
E Control Nuclear Extract
F GFP-Cys-OGG1 Nuclear Extract
G GFP-Ser-OGG1 Nuclear Extract
H GFP Cell Lysate

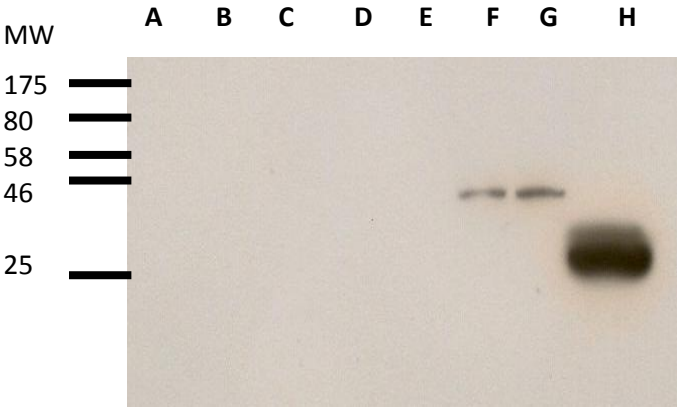

Figure 3.3.4 Western Blots of Experiment 2. Gel A compares the efficiency of the primary and secondary elution. Large amount of non-specific interactions are observed in all columns except Control Elution 2. Gel B doesn't present any bands in any flow through samples indicating that all antigen has been washed off. The nuclear extract samples indicate the presence of the protein of interest in each analyte.

The primary and secondary eluates were examined by western blot. As previously observed in Experiment 1, (Gel A - figure 3.3.3), vertical streaking in all of the columns was evident. It was established that these were likely the result of non-specific binding, which was minimised in the secondary elution. The large vertical bands presented in the GFP elution represent the relative affinity of GFP antibody to GFP compared to that of GFP-OGG1.

The flow through of the immunopreciptation (Gel B) did not produce any bands indicating that the GFP-antibody is interacting strongly with the components of the lysate. The analysis of the nuclear extracts confirms the absence of GFP-OGG1 in the control. The bands in the GFP-Cys-OGG1 and GFP-Ser-OGG1 columns represent GFP-OGG1 as these are of equal molecular weight. The band in the GFP nuclear extract is further down representing the smaller molecular weight GFP protein. The intensity of this band indicates large number of GFP transfected cells and also excessive GFP antibody concentrations.

Optimisation Step 2

The antibody dilution must be balanced to achieve adequate protein yield whilst reducing background reactions. The antibody concentrations are empirically determined using the manufactures' recommendations as a preliminary guideline. The initial dilution used was 1/1000 but as a result of strong antibody signal this concentration was reduced to 1/2500. This study utilised polyclonal antibodies which is a possible source of background reactions due to its ability to recognise various epitopes of the GFP proteins. An obvious solution to this would be the use of monoclonal antibodies, however due to the limited resources this was not feasible in this study.

Results of Experiment 3

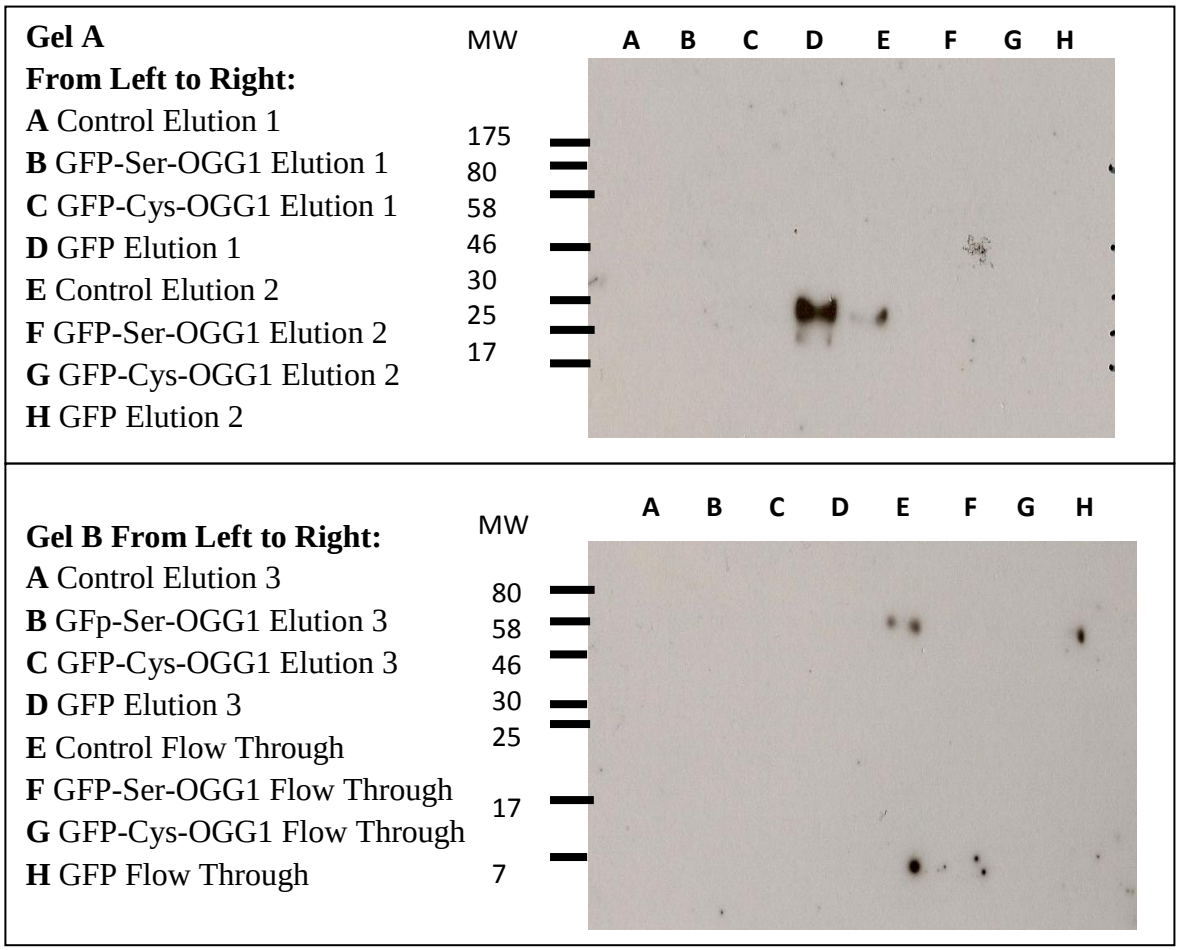

Figure 3.3.5 Western Blot of Experiment 3. Gel A only produced a single discrete band for GFP elution 1. Gel B generated no bands for elution 3 and produced speckled bands for flow through.

The western blots of experiment 3 were uncharacteristic of what had previously been observed with these samples. Various causes could be attributed to this, including preparation error. No bands were observed in elution 1 with the exception of a band for GFP elution 1. No bands were observed in elution 2 (Gel A) or elution 3 (Gel B). Analysis of the flow through resulted in speckled bands of various molecular weights, likely a result of non-specific proteins being detected. The lack of GFP-OGG1 bands in the flow through eliminate the possibility that the GFP-OGG1 was being washed off resulting in the absence of bands of elution samples. An analysis of the cell lysate was required to determine

whether the absence of GFP-OGG1 bands were a result of poor transfection efficiency. It is possible that the low amount of GFP-OGG1 proteins were insufficient enough to be detected.

Optimisation Stage 3

The lack of antigen signal prompted investigation into the possible causes; it was determined that the low initial OGG1 concentration prevented detection. Although the transfection was confirmed by epifluorescence microscopy, a quantitative measure of transfection efficiency was not determined. Possible resolutions for low antigen abundance include increasing cell lysate concentration, increasing antibody concentration and metabolically labelling cellular proteins. It was observed that the yield of nuclear extract protein was below the recommended sample volume. To ensure that the initial protein concentration corresponded to the recommended amount, the cell lysate yield was increased by up-scaling the cell culture vessel. Initially cells were cultured in 12-well plates, then 6-well plates and finally in T25 flasks. Furthermore cells were transfected in duplicate, thus the yield for each sample was doubled.

Results of Experiment 4

The western blots, (figure 3.3.6), of the eluates on Gel A show that the GFP-antibody is being eluted. Most of the antibodies are eluted in the primary elution with only faint bands present in the secondary elution. This suggests very weak or absent crosslinking of the GFP antibody to the Protein A/G resin. The GFP-OGG1 bands are not observed for the GFP-OGG1 transfected samples; however it is undetermined whether the immunoprecipitation purified these proteins as the signal is potentially concealed by the antibody bands which are of similar molecular weight to GFP-OGG1. The nuclear extract samples show the expected absence of a signal in the control, the presence of GFP-OGG1

bands in the transfected samples and the characteristically more mobile GFP band in the GFP nuclear extract. The absence of any bands in the flow through suggests that the antibodies are only removed from the resin on addition of elution buffer. Neither GFP-OGG1 nor GFP were observed in the flow through, suggesting that these are adequately bound to the GFP-antibody resin.

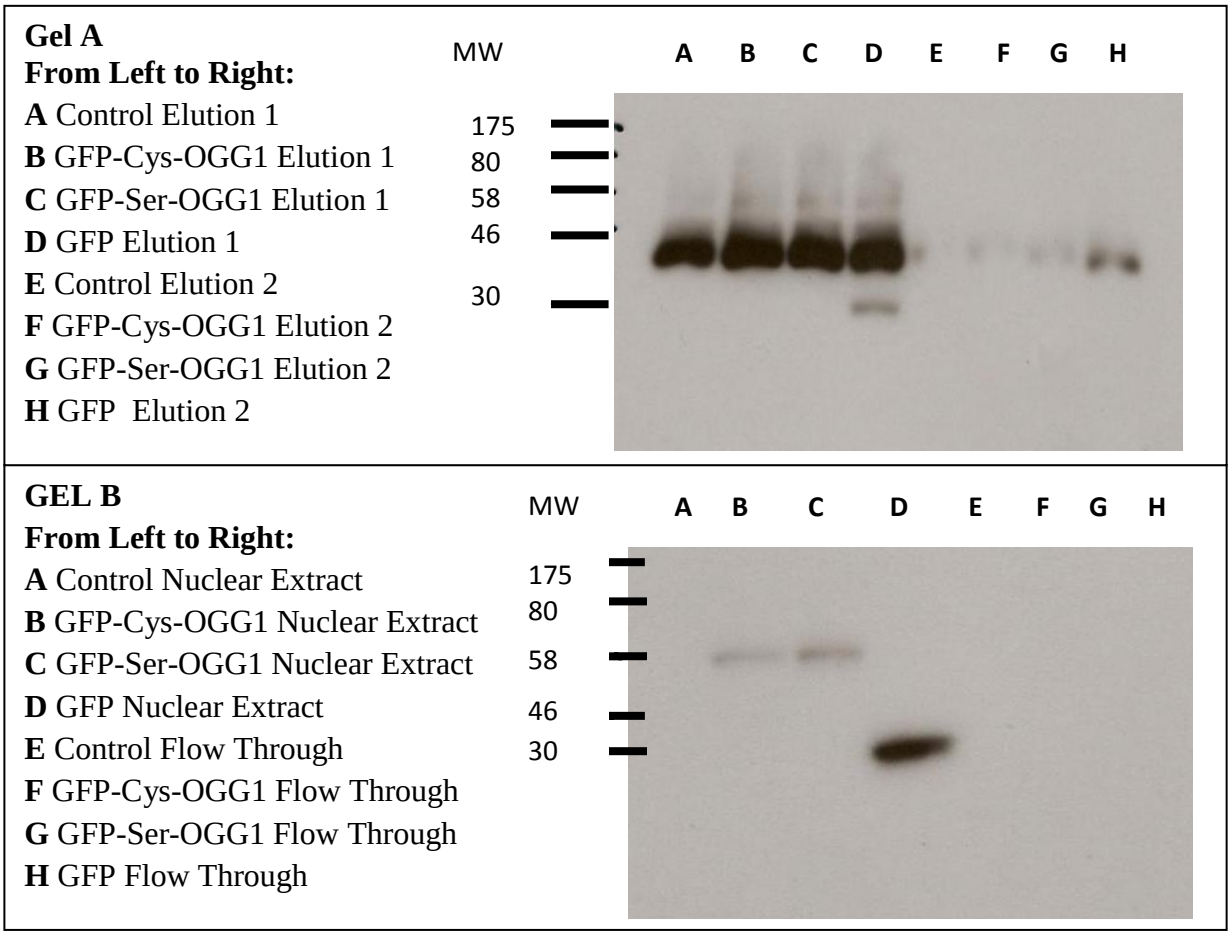

Figure 3.3.6 Western Blots of Experiment 4. Gel A shows equal molecular weight bands in all the samples, although these bands become fainter in Elution 2. This indicates the elution of the GFP antibody as it is present in all samples and of the corresponding molecular weight. A small band is seen in the GFP Elution 1 column which represents GFP. Gel B shows the presence of GFP-OGG1 and GFP in the nuclear extract of the corresponding transfected samples. No bands are observed in the Flow Through columns.

Optimisation Step 4

A common occurrence in immunopreciptation is elution of the antibody. Specific background refers to the co-elution of the antibody which masks the band of the protein of interest. Specific background is attributed to the antibody interactions with the immobilized resin. Crosslink immunoprecipitation kits allow the antibody to be crosslinked to the solid-phase bead matrix to prevent co-elution, which would otherwise interfere with antigen detection. The efficiency of the crosslinking reaction has been documented as incomplete, despite improving the overall quality of the immunoprecipitation. The crosslinking reaction between antibodies and Proteins A/G is attributed to the multiple primary amine groups of amino acids on both of the antibody and protein resins, resulting in the formation covalent amide bonds (ThermoScientific 2010). Common crosslinkers exploit this interaction by promoting the production reaction of N-Hydroxysuccinimidyl (NHS) esters. This study used a DSS crosslinker which contains reactive (NHS) esters on the ends of short carbon chains (ThermoScientific 2010). It is critical to optimise the dosage of DSS crosslinker to sufficiently link the antibody to Protein A/G without overwhelmingly crosslink Fc regions, modifying the binding site and preventing antigen recognition. It was determined that the DSS crosslinker had not been adequately preserved. Therefore a fresh batch of DSS crosslinker was prepared for the proceeding experiments.

Results of Experiment 5

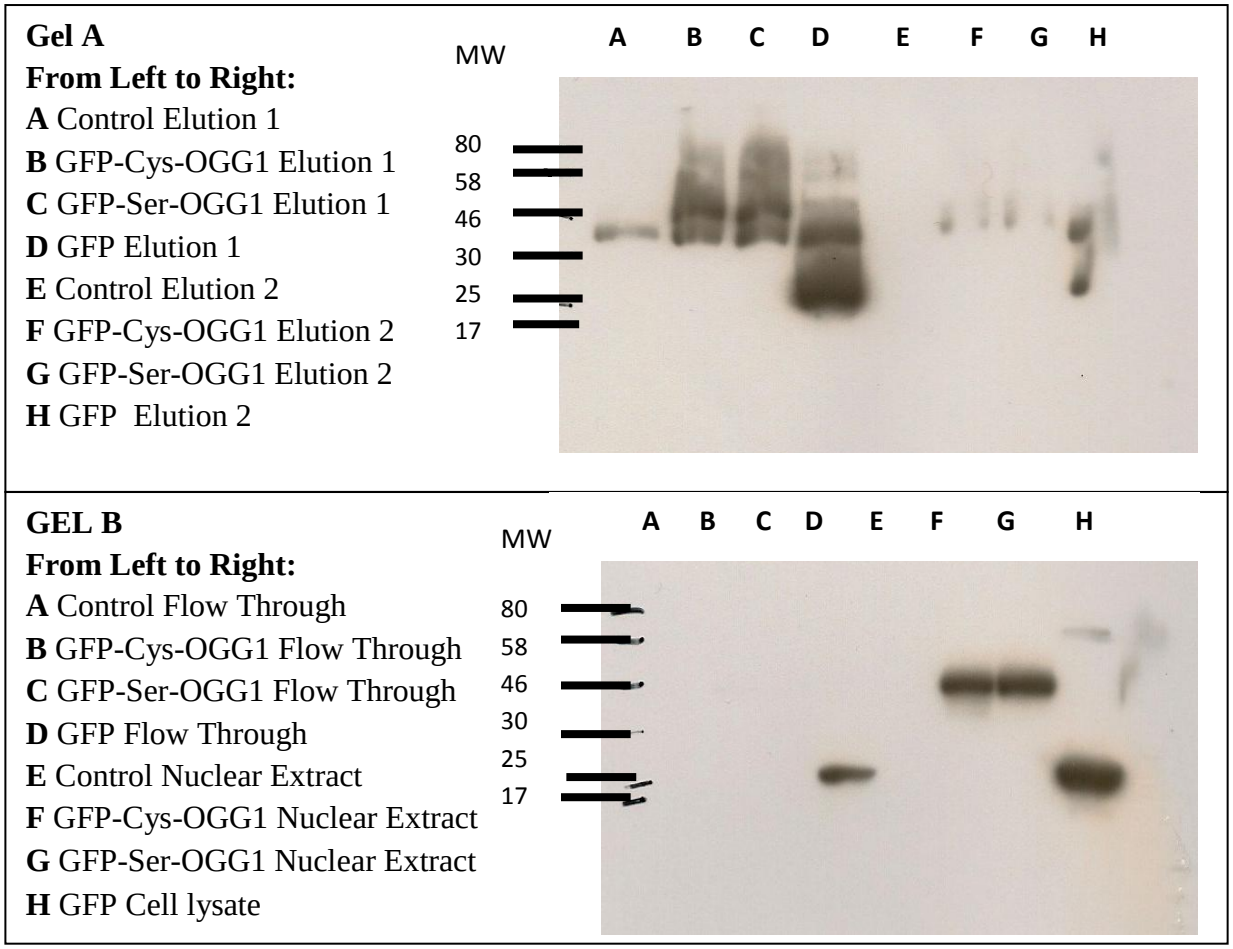

Figure 3.3.7 Western Blots of Experiment 5. Gel A shows the immunoprecipitation of OGG1 in the GFP-Cys-OGG1 and GFP-Ser-OGG1 column; the OGG1 band is less mobile than the antibody band. Gel B shows GFP-OGG1 and GFP is present in the same prior to immunoprecipitation.

Successful immunoprecipitation was observed in the western blot images of experiment 5. The control elution 1 shows a single band representing the GFP-antibody. The identity of the GFP-antibody was confirmed by the presence of an equal molecular weight band in all the samples of elution 1. Two bands were observed in GFP-Cys-OGG1 and GFP-Ser-OGG1 columns. The lower mobility band refers to the GFP-OGG1 protein. The bands of elution 2 show a similar pattern to elution 1. As expected no GFP signal is detected in the nuclear extract or flow through of the control. No bands were observed in the flow through

of the GFP-Cys-OGG1 and GFP-Ser-OGG1 suggesting adequate binding of OGG1 proteins to the GFP-antibody resin. A discrete band of GFP was observed in the flow through of GFP sample, this is likely due to high concentrations of GFP cell lysate resulting in unbound GFP. The characteristic bands of GFP-Cys-OGG1, GFP-Ser-OGG1, and GFP cell extracts were observed.

Optimisation Step 5

There are considerable restrictions on the solutions utilised to prepare samples for mass spectrometry, such as the absence of detergent and salts. The elution buffer provided with the immunoprecicipitation kit was unsuitable for mass spectrometry so the immunoprecipitation was repeated using an elution buffer with known compatibility to mass spectrometry. This elution buffer, however, was not compatible for SDS-PAGE analysis of the purity of the sample.

3.4 Mass Spectrometry Results

Cells transfected with GFP-Ser-OGG1 and GFP-Cys-OGG1 were lysed and the OGG1 proteins with associated partners were co-purified. The eluate was collected following immunoprecipitation and was analysed by mass spectrometry. The LQT Orbitrap Velos Mass Spectrometer requires trypsin digestion of the samples before high energy collisions with neutral gas atoms resulting in fragmentation of peptides. The fragmented ions of the peptides sequence are used to obtain a protein identify using the MASCOT database. A substantial proportion of the proteins identified in the samples were contaminating keratin and albumin proteins; these were excluded from the lists. Several variant forms of each protein were detected in the samples; here the precursor protein of the variants is presented (figure 3.3.8). The complete lists for each sample are available in Appendix 2. A selection of proteins was common to both samples. The proteins exclusive to the Cys-OGG1 sample were thioredoxin and lysozyme, both of which have known antioxidant properties.

Table 3.4.1 GFP-Ser-OGG1 Mass Spectrometry Results. The identities of several proteins from the Ser-OGG1 sample are presented below. The coverage refers to the amount of peptide sequence from which the protein identity was found.

Description	Coverage	# Proteins	# AAs	MW [kDa]
prolactin-inducible protein precursor [Homo sapiens]	10.17	1	118	13.514
glial fibrillary acidic protein [Homo sapiens]	16.67	1	66	7.5761
NCK-associated protein 1, isoform CRA_a [Homo sapiens]	7.09	1	141	16.3652
NCK-associated protein 1, isoform CRA_f [Homo sapiens]	5.24	1	401	43.6169
pHL E1F1 [Homo sapiens]	10.45	1	134	15.0876
prolactin-induced protein [Homo sapiens]	15.19	1	79	9.0777
prolactin-induced protein [Homo sapiens]	15.19	1	79	9.0596
prolactin-inducible protein precursor [Homo sapiens]	8.22	1	146	16.5618
sarcolectin [Homo sapiens]	3.84	1	469	51.3823

Table 3.4.2 GFP-Cys-OGG1 Mass Spectrometry Results. The identities of several proteins from the Cys-OGG1 sample are presented below.

Description	Coverage	# Proteins	# AAs	MW [kDa]
glial fibrillary acidic protein [Homo sapiens]	16.67	1	66	7.5761
prolactin-induced protein [Homo sapiens]	15.19	1	79	9.0596
thioredoxin [Homo sapiens]	15.29	1	85	9.4457
thioredoxin [Homo sapiens]	12.38	1	105	11.7297
Chain A, Buried Polar Mutant Human Lysozyme	9.23	1	130	14.6931
lysozyme {beta-sheet domain} [human, Peptide Mutagenesis, 130 aa]	9.23	1	130	14.6491
Chain A, Mutant Human Lysozyme With Foreign N-Terminal Residues	9.16	1	131	14.7482
prolactin-inducible protein precursor [Homo sapiens]	8.22	1	146	16.5618
lysozyme precursor [Homo sapiens]	8.11	1	148	16.4292
NCK-associated protein 1, isoform CRA_f [Homo sapiens]	2.74	1	401	43.6169
sarcolectin [Homo sapiens]	2.35	1	469	51.3823

3.5 Confocal Microscopy Results

Fig.3.5.1 Confocal images of untreated cells. Images show nuclear localisation of GFP-Ser- and GFP-Cys-OGG1 of untreated cells. Cells were counterstained with DAPI. The merge images show OGG1 is localised in the nucleus. Images of the positive control, GFP, demonstrates cytoplasmic localisation.

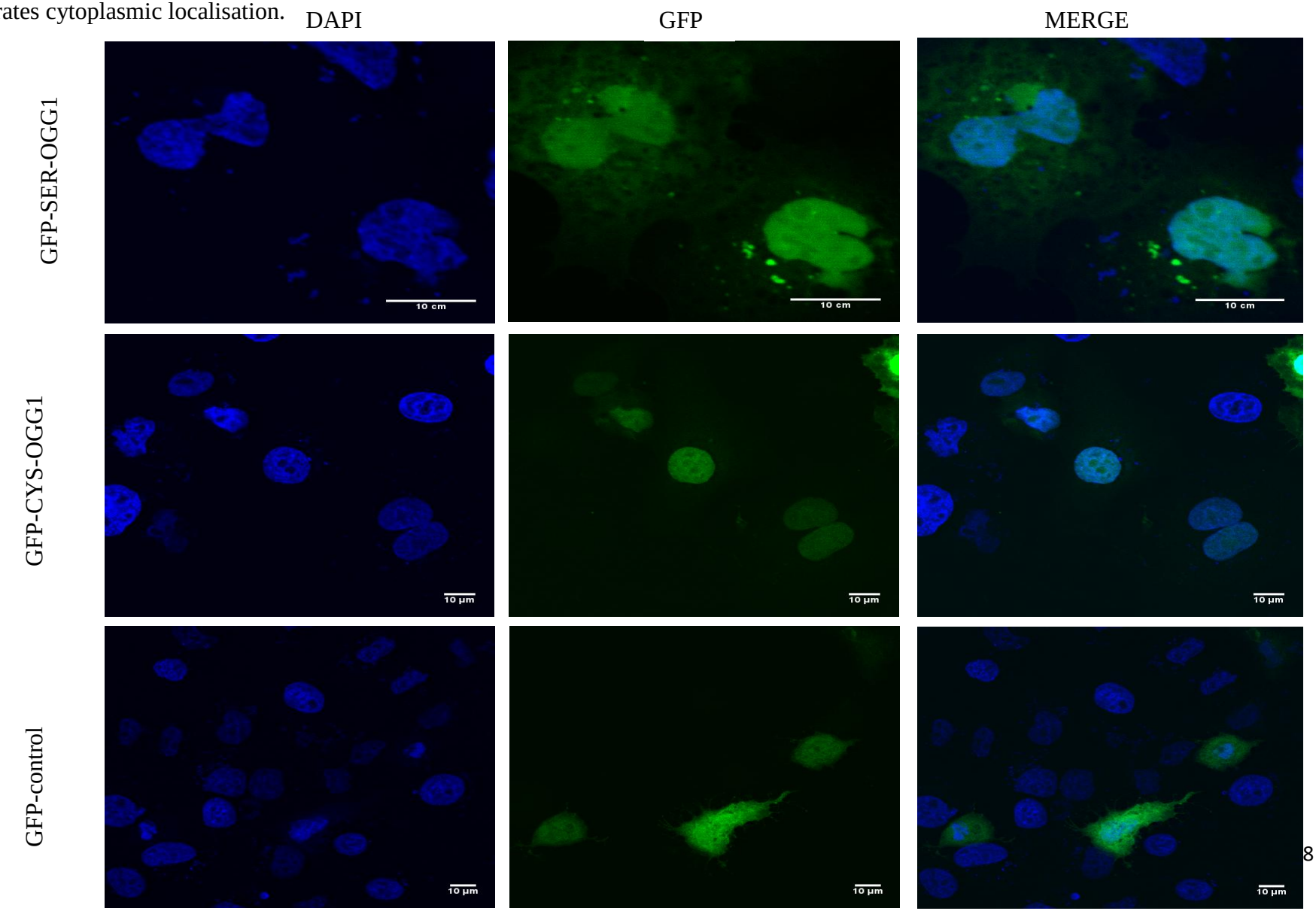

Figure 3.5.2. Confocal images of cells treated with 10mM BSO for 24 hours. Cells were counterstained with the nuclear stain DAPI. The GFP signal of the Ser-OGG1 and Cys-OGG1was localised in the nucleic material. The merge shows GFP-OGG1 in the nucleus. There was no change in localisation upon BSO treatment.

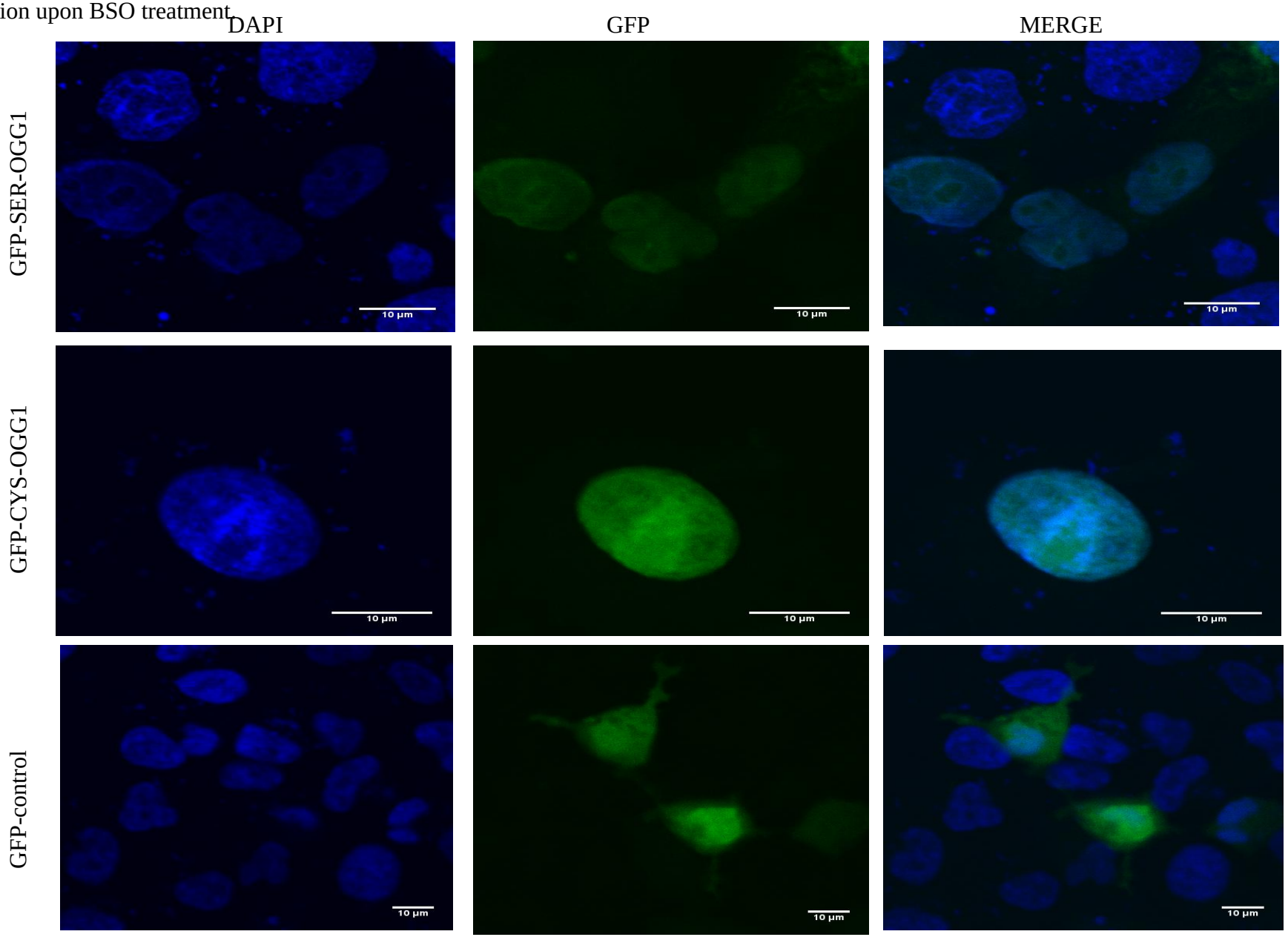

Figure 3.5.3. Confocal images showing localisation of GFP-OGG1 in apoptotic cells. Cells express exogenous GFP-OGG1. The DAPI panels show that the nucleic material has condensed into micronuclei apoptotic bodies. The merge shows GFP-OGG1 are discretely excluded from the apoptotic bodies.

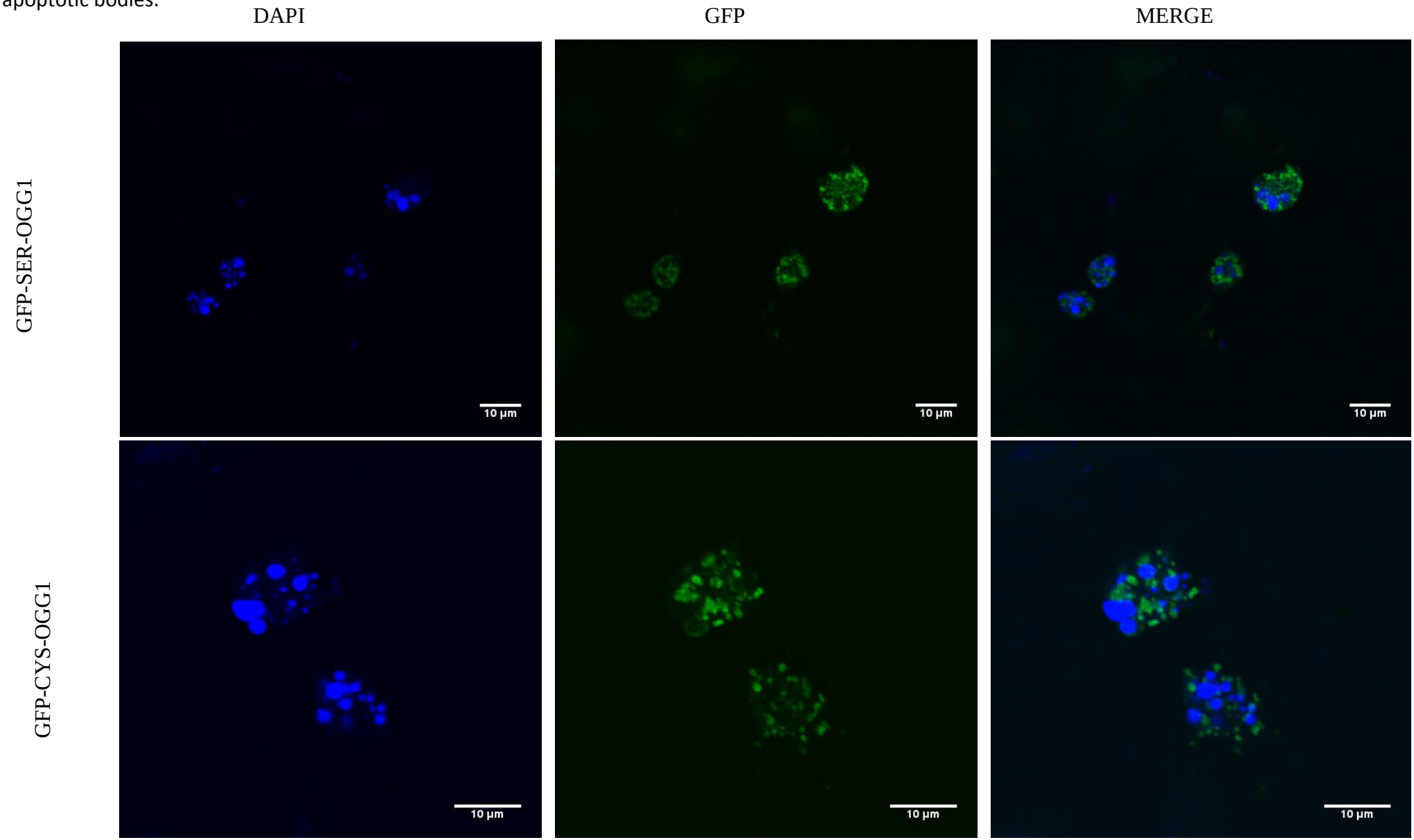

Figure 3.5.4. Merged Z-scan of an untreated Ser-OGG1 apoptotic cell. OGG1 is excluded from the apoptotic body at all cross sections of the nucleus.

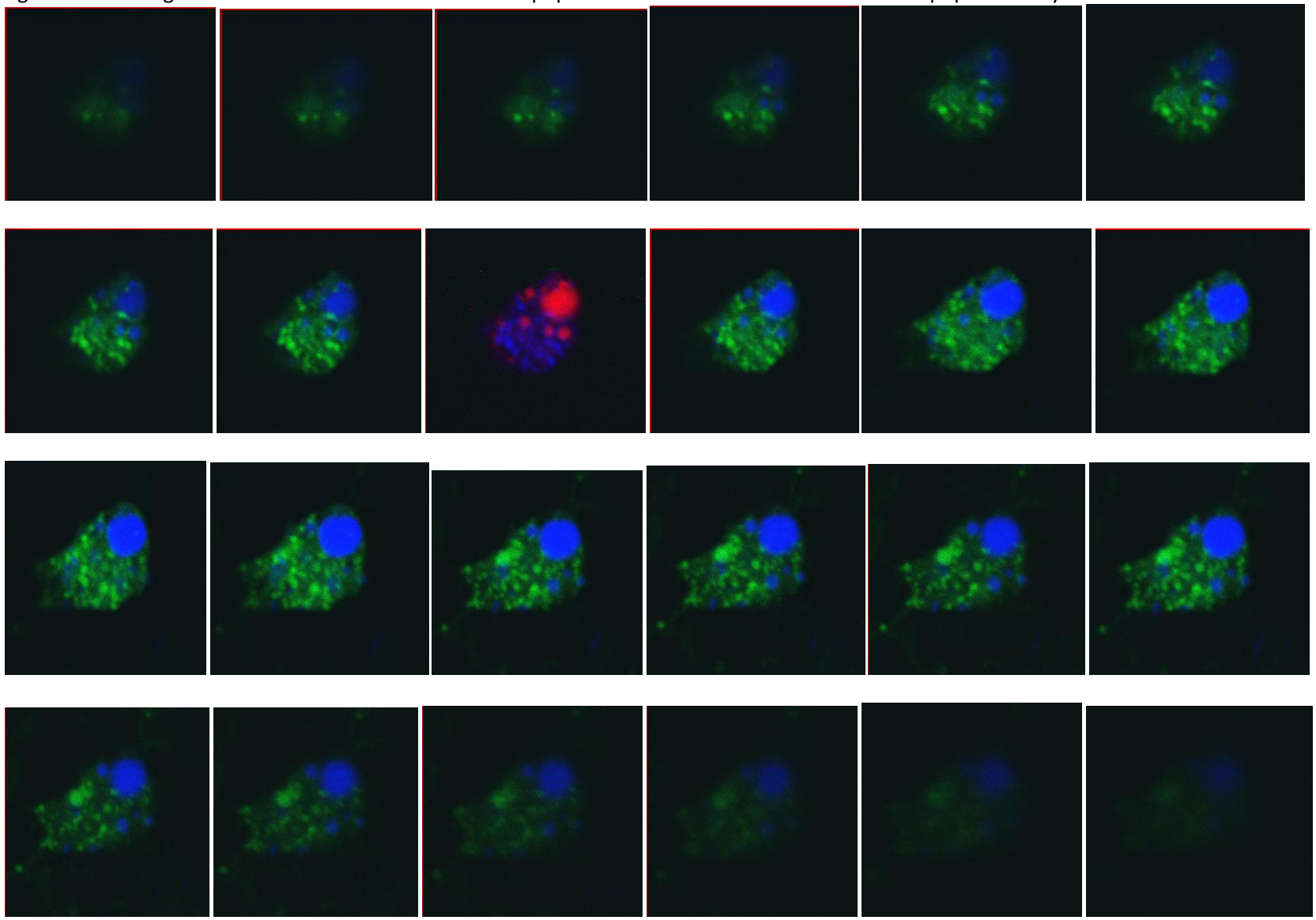

Figure 3.5.5. Confocal image of an untreated GFP-Ser-OGG1 apoptotic cell. The nuclear material, stained with DAPI, shows the condensation of nuclear material into apoptotic bodies. The GFP-OGG1 has a punctate pattern throughout the cell but as the merge demonstrates it is excluded from the apoptotic bodies.

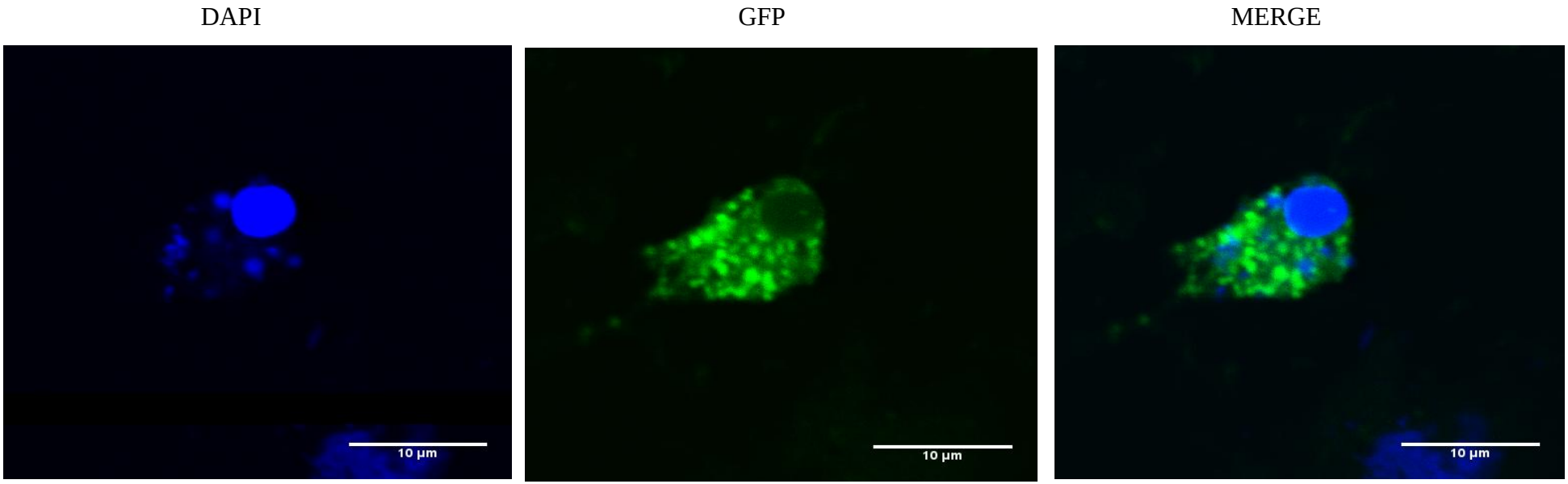

Figure 3.5.6. Orthogonal cross-section of an untreated GFP-Ser-OGG1 apoptotic cell. The GFP-OGG1 is excluded from the apoptotic body through the cell.

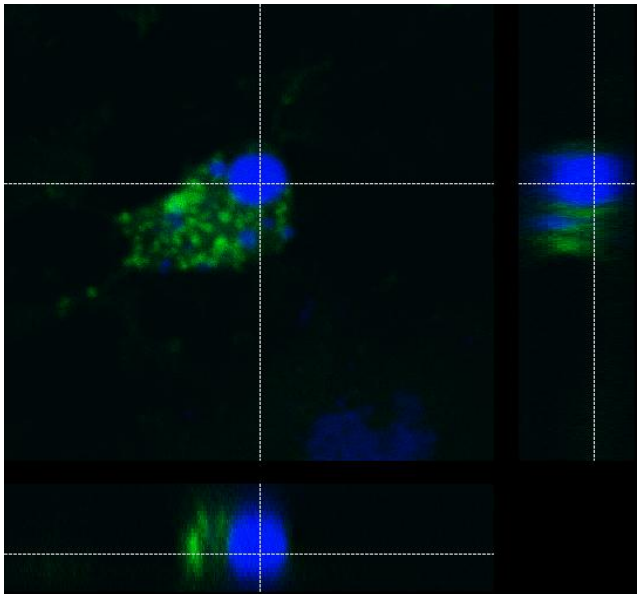

Figure 3.5.7. Confocal images of untreated GFP-Ser-OGG1 mitotic cells. The DAPI stain shows that the nuclear material is in the process of division. The GFP-OGG1 is diffusely distributed though out the cell. The merge shows the GFP-OGG1 is in both the nuclear and cytoplasmic compartment.

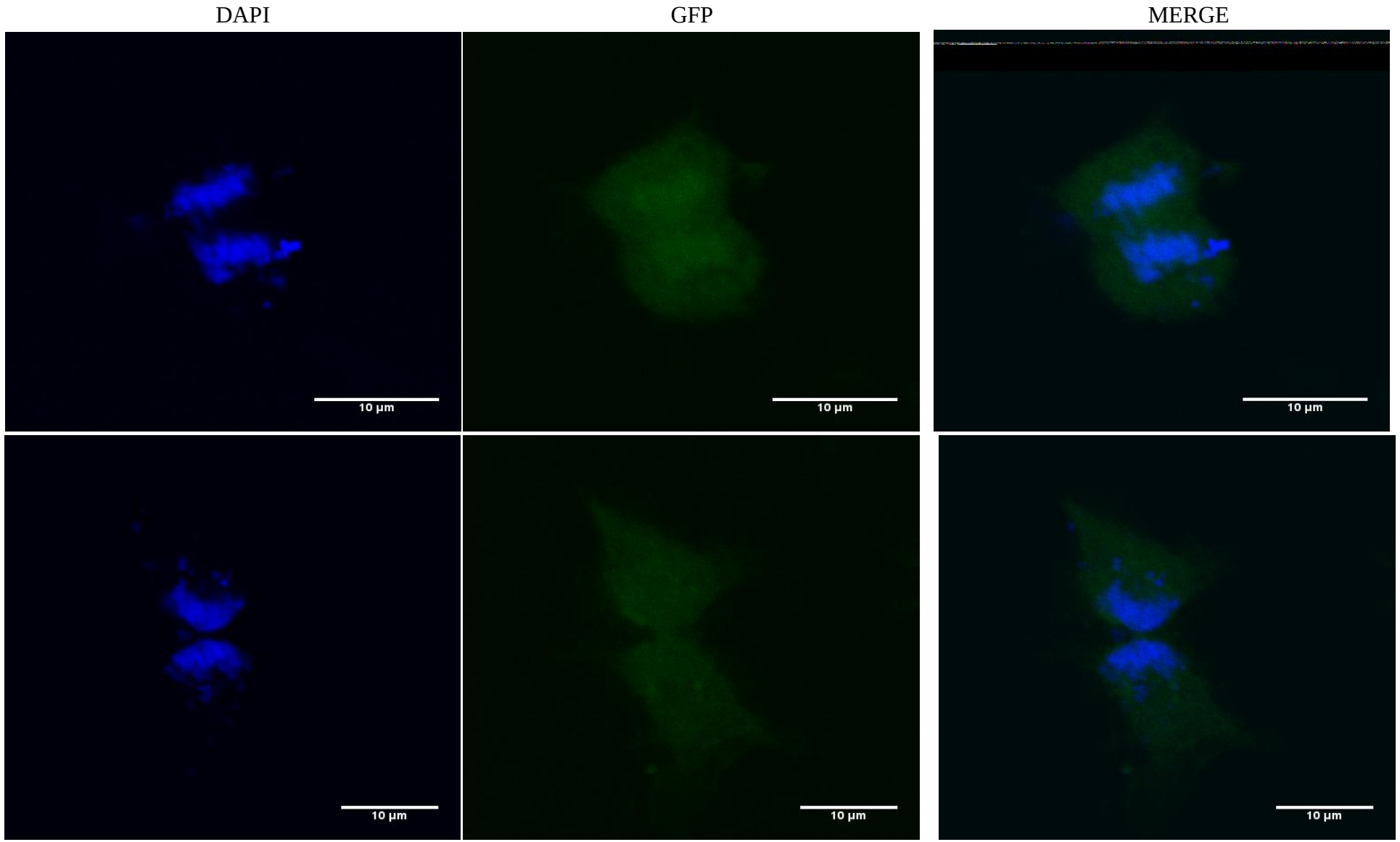

Chapter 4. Discussion

4.1 Cell Viability on BSO treatment

As a DNA repair protein for oxidised lesions it is critical to investigate OGG1 activity, localisation and regulation under its expected operating conditions of oxidative stress. Several studies have studied OGG1 upon inducement of oxidative stress by various means (Arai *et al.* 2006; Bercht *et al.* 2007; Dahle *et al*. 2008; Smart *et al*. 2006; Priestley *et al.* 2010; Green *et al*. 2006). This study used buthionine-sulphoximine to induce oxidative stress by reducing levels of reduced glutathione. Glutathione is a proven antioxidant in the cytoplasm, nucleus and mitochondria (Green *et al.* 2006), which reacts indirectly with various ROS or directly as a cofactor of glutathione peroxidase and dehydroascorbate dehydrogenase (Will *et al*. 1999). BSO depletes reduced glutathione by inhibition of the glutamate-cysteine ligase, the first enzyme in the biosynthesis of glutathione (Green *et al.* 2006). A BSO concentration dependant increase in glutathione was observed which correlates to the concentration dependant increase in reactive oxygen species; cells treated with 10mM BSO previously shown to increase ROS levels 4-fold compared to basal levels (Green *et al.* 2006). The levels of total cellular glutathione is inversely proportional to the levels of oxidative DNA damage i.e. 8-oxoG (Will *et al.* 1999; Lenton 1999; Martínez-Alfaro *et al.* 2006). The BSO concentrations used in this study produced no significant change in cell viability. Cell viability was determined by performing the MTT assay consisting of a yellow dye which is reduced to insoluble purple formazan crystals by the activity of mitochondrial succinate dehydrogenase. The highest concentration of BSO which did not change cell viability was 10mM BSO; this concentration was then used to treat cells prepared for confocal microscopy in order to achieve maximum change of cellular ROS levels without disrupting cell viability.

4.2 Transfection Efficiency

The bifunctionality of GFP as an affinity tag and fluorescent label is one of the reasons why it is the fusion-tag of choice, particularly in OGG1 research it has been used in both immunoprecipitation and fluorescence microscopy (Dantzer *et al.* 2002; Zielinska *et al.* 2011; Bravard *et al.* 2010). Cell samples were transfected with either Ser-OGG1-GFP, Cys-OGG1-GFP or GFP. Transfection efficiency was confirmed adequate to ensure sufficient expression of GFP-OGG1 prior to downstream experiments. Transient transfection in A549 cells overexpresses the OGG1 protein as A459s inherently possess low level endogenous OGG1 protein. As expected, overexpression of OGG1 enhances the activities of OGG1. When transfected into mammalian cells, the total OGG1 enzyme activity is increased 10-fold and the repair of 8-oxoG, as determined by the alkaline elution technique, is 3-fold higher than vector-only transfected cells (Hollenbach *et al.* 1999). Although the extent of difference in repair kinetics caused by overexpression varies depending on the source of oxidative stress (Dahle *et al.* 2008), the overall enhancement in repair efficiency is observed. Thus correlating exogenous OGG1 activity profile to endogenous OGG1 must take into consideration the overexpression of the OGG1 protein.

4.3 Immunoprecipitation

Many functions within the cell are the result of synergy between many protein interacting partners and/or multiprotein complexes. Studies have proposed the OGG1 contribution to a multiprotein complex, based on experiments demonstrating consistent colocalisation of DNA repair proteins and several cellular components displaying a regulatory effect on OGG1 possibly via direct interaction (Hu *et al.* 2005; Bhakat *et al.* 2006). This study aimed to compare the profile of protein-interactions between the wild-type Ser-326 OGG1 to the Cys-326 variant, as well as identifying any novel interactions. The first step was to purify OGG1 with all possible protein partners en masse. The co-purification of protein

partners is a compromise between removal all non-specific bound proteins (contaminants) using high stringency techniques, and preservation of specific interacting protein partners using low stringency techniques. In general, it is attempted to maintain all interaction events. For this reason low stringency techniques are utilised such as the pull-down assay which co-elute the proteins within a single experiment. To investigate further the proteins that directly interact with OGG1, a pull-down immunoprecipitation was performed. The 'bait' protein was recombinant GFP-OGG1 chimera synthesized in cells and allowed to interact with endogenous proteins and form stable complexes. These multiprotein complexes were harvested, purified, and then analysed by gel electrophoresis and mass spectrometry.

Untested immunoprecipitation techniques require considerable optimisation to adequately purify GFP-OGG1. A recurring issue was non-specific background; to resolve this antibody concentration was decreased to reduce the high-affinity low-specificity binding of contaminants to the antibody. Sample complexity was reduced by nuclear extraction, however this decreased the initial substrate for immunoprecipitation, therefore the cell culture was scaled up to increase the quantity of nuclear enriched OGG1. Consistent elution of the GFP antibody lead to the speculation that the DSS crosslinker was no longer active, therefore fresh crosslinker was utilised. Incompatibility of the ThermoScientific elution buffer to mass spectrometry analysis required substitution of the immunoprecipitation elution buffer to one of confirmed compatibility to mass spectrometry. The western blots of each experiment were sequentially analysed; the conclusion was that under these conditions immunoprecipitation is not suitable for mass spectrometry analysis. The incompatibility of the mass-spectrometry elution buffer to

SDS-PAGE prevented analysis of sample prior to mass spectrometry. This restriction means the purity of the sample cannot be verified before mass spectrometry.

4.4 Mass Spectrometry

The final immunoprecipitation was performed without SDS-PAGE analysis, instead the eluate was analysed by LQT Orbitrap Velos mass spectrometry to identify the peptide sequences of the co-eluted proteins. A substantial amount of the proteins identified were of the keratin family and albumin family which are common contaminants of mass spectrometry (Keller *et al.* 2008; Alphalyse Inc 2009). The presence of contaminants may reflect the stringency of the purification technique. The contaminating proteins that co-elute are due to nonspecific binding to the affinity matrix, antibody and/or fusion tag (Trinkle-Mulcahy *et al.* 2008). The challenge is then to distinguish the specific protein interacting partners from the abundant contaminants. The lists of proteins identified by mass spectrometry were filtered through a list of known non-specific binders of the agarose bead and the GFP tag (Global Proteomics Machine 2011). It was established that the accuracy in determining protein partners requires efficient depletion of the target protein, which can be stringently achieved using GFP binder (Trinkle-Mulcahy *et al.* 2008). A GFP binder is more efficient at specifically extracting GFP from a highly complex sample than anti-GFP antibody or endogenous antibody (Trinkle-Mulcahy *et al.* 2008). High depletion efficiency increases the signal of the target protein thus improving the signal to noise ratio (Trinkle-Mulcahy *et al.* 2008). Potential GFP-interacting proteins have been listed as cytokeratins 8 and 18, variants of heat-shock 70kDa protein, and ubiquitin (Trinkle-Mulcahy *et al*. 2008). Exclusion of such proteins from the mass spectrometry list reduces the list to possible protein partners which are then corroborated with previous publications.

Ser-OGG1-GFP Mass Spectrometry

The analysis of the Ser-OGG1 sample produced a large number of non-nuclear proteins. The most prevalent was Glial fibrillary acidic protein (GFAP). GFAP is a component of the intermediate filament family that provide structural support to cell (U.S National Library of Medicine 2008). Upon cellular trauma, astroglial cells produce GFAP to limit further structural and functional damage (U.S National Library of Medicine 2008). There is no previous evidence of the interaction between this protein and OGG1 so it is likely the presence of this protein in the sample is a result of contamination. Another possible contaminant is the Prolactin-induced protein (PIP), named as such due to its upregulation by prolactin (Kitano *et al.* 2006). It is secreted into the fluids of several glands, particularly the apocrine gland where it regulates water transport (Kitano *et al.* 2006). It was detected several times in the sample despite no previous indication of its interaction with OGG1. The NCK-associated protein 1 is preferentially expressed in the brain, heart and skeletal muscles. It is known to interact with RAC1, involved in cell growth, reorganisation of the cytokeleton and kinase activation (Kitamura *et al.* 1997). Its presence in the sample is unexpected as it has not previously been linked to OGG1. A proline-rich protein (pHL E1F1) was also detected twice in the sample, this protein is produced abundantly in the human lacrimal gland where it likely mediates a protective function (Dickinson & Thiesse 1995). This protein has not been cited in any study to associate with OGG1 so the function of this protein in relation to OGG1 is elusive. Sarcolectin is a tissue growth factor, was also detected in the sample. Its role is related to inhibition of interferon to reduce an antiviral state (Ibelguafts 2011). The proteins detected in the Ser-OGG1 sample were non-specific to OGG1 or were the result of contamination, thus it is not possible to relate these proteins to OGG1 function.

Cys-OGG1-GFP Mass Spectrometry

Several proteins were common to both the Ser-OGG1 and Cys-OGG1 sample; these included GFAP, PIP, NCK-associated protein and sarcolectin. The most abundant protein in the Cys-OGG1 sample is lysozyme. Various mutants and structures of lysozymes were detected. Lysozymes are ubiquitous enzymes in human secretions, such as tears, mucus, milk and saliva (Invitria 2010). Though Hen Egg Lysozyme C and human Lysozyme C have been implicated in contaminating mass spectrometry samples (Global Proteomics Machine 2011), such an unexpected abundance in lyzosymes in unexpected. The lack of detection of lysozymes in the Ser-OGG1 sample further obscures the cause of the lysozyme presence, as possible sources such as reagents can be excluded. However, considering the exogenous secretion of lysozyme it is likely a contaminant as a result of direct human contact with the sample. Lysozymes posses antimicrobial properties based on the ability to lyse bacterial cell walls (Hung *et al.* 2007). Lysozymes also help reduce oxidative stress by scavenging free radicals and hydroxyl molecules (Invitria 2010). Lysozymes detoxify advanced glycation end products (AGE) which produce ROS (Liu *et al*. 2006). Lysozymes also inhibit cell apoptosis and suppress the expression of AGE-induced p66 and c-Jun which are involved in stress response (Liu *et al.* 2006). As lysozymes are proven to reduce oxidative stress there is a possibility the abundant expression of lysozyme in the sample is due to enhanced oxidative stress.

Thioredoxin was also considerably prevalent in the mass spectrometry results. As with lysozymes, several mutant forms were detected. Thioredoxin has a significant role in oxidative stress and redox signalling. The prime role of thioredoxin is as a disulphide reductase which prevents the formation of disulphide bonds between free sulphydryl groups of proteins in oxidizing conditions (Arnér & Holmgren 2000). The proteins are then maintained in their reduced state via the synergy of thioredoxin, NADPH and

thioredoxin reductase. The disulphide within the active site of oxidized thioredoxin is reduced to dithiol by a reaction catalysed by thioredoxin reductase and NADPH (Arnér & Holmgren 2000). The reduced thioredoxin then reduces protein disulphides. Additionally thioredoxin also possesses several organism specific functions but it is its role in apoptosis in response to oxidative stress that is particularly relevant to this study. The apoptosis signalling kinase 1(ASK1) and reduced thioredoxin form a complex which associates with DNA polymerase (Arnér & Holmgren 2000). This inhibitory complex is able to regulate apoptosis according to redox states within the cell. Increasing oxidative stress would decrease the levels of reduced thioredoxin, preventing the formation of the inhibitory complex, allowing activation of apoptosis. Both oxidised and reduced forms of thioredoxin were present in our mass spectrometry analysis this it is not feasible to deduce the relative prevalence of each in the cell. Furthermore thioredoxin is involved in redox modulation of several transcription factors such as NF-kB and AP-1 involved in inflammation and apoptosis, respectively (Arnér & Holmgren 2000). Thus thioredoxin can modulate the cellular response to oxidative stress in contribution to its intrinsic antioxidant activity. Thioredoxin is upregulated in response to oxidative stress thus it is likely that the enhanced oxidative stress due impaired activity of Cys-OGG1 increased thioredoxin expression. However no previous study has linked thioredoxin to OGG1 directly. The redox regulation imposed by thioredoxin is reminiscent to the regulation proposed for OGG1. Bravard *et al.*, demonstrated the effect of altering the cellular redox on OGG1 activity (Bravard, *et al.* 2009a). Cadmium induced an redox environment which lead to the reduction of OGG1 (Bravard, *et al.* 2009a). The glycosylase activity was then measured at different doses to show a cadmium-specific inhibition of OGG1. It is not the general oxidative conditions which impair glycosylase activity, nor does cadmium directly interact with OGG1 but oxidative modifications of either possible 8 cysteine residues on OGG1(Bravard, *et al.*

2009a). Using cysteine-modifying reagents these redox-sensitive residues on OGG1 were verified as critical for glycosylase activity. After 60 minutes the glycosylase activity was restored indicating normalisation of the oxidation conditions, further reconfirmed when cadmium was sequestered by a metal chelator (Bravard, *et al* 2009a). Thus the redox-induced inhibition was reversible leading to the speculated involvement of thioredoxin which reverses protein thiolation. Yeast strain defective of thioredoxin are considerably vulnerable to the effect of cadmium, further highlighting a possible link between OGG1 and thioredoxin. The impaired activity of Cys326-OGG1 was then justified in terms of extra cysteine and its sensitivity to oxidation. Upon addition of reducing agents, which prevent oxidation of cysteine residues, the DNA glycosylase activity was rescued and comparable to the wildtype (Bravard, *et al.* 2009b). Using thiol-specific crosslinkers they were able to identify a disulphide bond exclusively present in Cys-OGG1 (Bravard, *et al.* 2009b). It is speculated that the additional cysteine increases the susceptibility to oxidation, forms a disulphide bond and therefore increases the sensitivity of OGG1 to inactivation by oxidative stress (Bravard, *et al.* 2009b). Thus the exclusive presence of thioredoxin in the Cys-OGG1 sample may reflect the requirement of thioredoxin to inhibition formation of disulphide bonds on Cys-OGG1 to maintain intact DNA glycosylase activity.

Conclusion

Overall the mass spectrometry did not yield any expected partners of OGG1 or even OGG1 itself. This suggests problems during the processing stages which has lead to the accumulation of large amount of human skin contaminants and non-specific proteins. However this was only a pilot study to determine the efficiency of the immunoprecipitation: mass spectrometry workflow in studying OGG1 and its interacting proteins. Thus the results here cannot be accepted conclusively as further repeats would be

required in addition to downstream validation techniques to verify the *bona fide* interaction of the partners. Several flaws in methodology have been identified such as lack of compatibility in the reagents of the two processes and the laborious optimisation of immunoprecipitation. Mass spectrometry does, however, provide an en mass identification of proteins from a complex sample in a single experiment. This reflects the high sensitivity and resolution of current mass spectrometry technology. Despite this, mass spectrometry is still prone to experimental errors and system errors which can lead to inaccurate identification of a peptide (Trinkle-Mulcahy *et al.* 2008). The inability to discriminate between native proteins, non-specific proteins and contaminants is a considerable problem when attempting to identify novel associations. Cell lysis inevitably mixes the pool of proteins which would otherwise be separated in organelle compartments. The subsequent protein interactions would not reflect the putative interactions in the cell, leading to inaccurate conclusions on protein-partners. Researchers have begun to challenge this drawback by the development of techniques which can distinguish between specific and non-specific interactions (Trinkle-Mulcahy *et al.* 2008; Tackett *et al*. 2005).

4.5 Confocal Microscopy

Comparison of BSO-treated cells to non-treated cells

Several investigations into the localisation of OGG1 have been conducted by means of conjugated photosensitive and fluorescent dyes in order to track the distribution and dynamic relocalisation in response to different physiological conditions and cell-cycle stages. Some studies have also attempted to compare the localisation of the wild-type OGG1 to mutant variants to elucidate whether aberrant spatial modulation is responsible for reduced repair activity. This study found no difference in the localisation of exogenous hOGG1 of either the wild-type or Cys-326 variant under oxidative stress induced by BSO (figure 3.5.1 and figure 3.5.2)

The confocal images generated in this study presented heterogenous localisation pattern of GFP-OGG1 in cells with no BSO-dependant difference (figure 3.5.2). At the organelle level the GFP-OGG1 was consistently localised in the nucleus and occasionally in the cytoplasm, but no GFP foci were observed in the mitochondria. Contrarily a molecular beacon tracked the dynamic activity of mOGG1 to dominate in the mitochondria in KO-MEFs (Mirbahai *et al.* 2010). The fluorescence denoting OGG1 excision activity increased in a concentration dependant manner of potassium bromate-induced oxidative stress. The possibility that this increase in mitochondrial mOGG1 was due to mRNA stabilisation or transcriptional activation was eliminated by RT-PCR (Mirbahai *et al.* 2010). The authors suggest the presence of mOGG1 activity in mitochondria may reflect the relative burden of the particular oxidising agent on mitochondrial DNA (Mirbahai *et al*. 2010). However without the use of 8-oxoG antibodies, the mitochondrial translocation cannot be directly correlated to increasing DNA damage. The surprising absence of nuclear mOGG1 activity observed in the study by Mirbahai *et al.*, may also be due to lack of authentic mOGG1 in knockout cells, maintaining normal levels of OGG1 and thus exclusively measuring the activity of ectopically expressed mOGG1. When the same authors transfected the mOGG1-beacon into wild-type MEFs a similar pattern of strong nuclear expression was observed, corresponding to overexpression of OGG1, as observed in this study.

Differential localisation of the Cys-OGG1 variant compared to wild-type was not observed in this study in either treated cells or non-treated cells. However Zielinski *et al.*, utilised quantitative live cell imaging to demonstrate that the repair kinetics of Cys-OGG1 is 3.4-4-fold slower than wild-type (Zielinska *et al.* 2011). Measuring colocalisation of GFP-OGG1 to acute foci of DNA damage, Cys-OGG1 was shown to be slower as it only repaired 20% of damage in 15 minutes compared to the 50% of damage repaired by the wild-type in 10 minutes.

Apoptotic Cells

Confocal images of apoptotic cells displayed differential GFP expression in the nuclear substructure (3.5.3). We observed that GFP-OGG1 was acutely excluded from the condensed Dapi-stained nuclear material in a non-treated GFP-Ser-OGG1. This distinctly differs from the diffuse GFP-OGG1 expression observed throughout the nucleus of non-apoptotic cells. The hallmark nuclear morphology of apoptosis is the presence of apoptotic bodies (also known as micronuclei) (Martelli *et al.* 2001), which characterise the confocal images from this study. The apoptotic pathway is intertwined with many components involved in oxidative stress, notably OGG1 protects against apoptosis activation as demonstrated in knockout models (Oka *et al.* 2008). For example, the earliest substrates of caspase-3 are poly(ADP-ribose) polymerase (PARP) and DNA-PK which are both involved in DNA repair (Robertson *et al.* 2000). Furthermore OGG1 binding to PARP during oxidative stress enhances its poly(ADP-ribosyl)ation activity, the absence of OGG1 results in total decrease in PARP and the PARP-mediated translocation of apoptosis-inducing factor (Hooten *et al.* 2011; Oka *et al*. 2008). DNA-PK mediates the DNA fragmentation by phosphorylation of histone H2AX (Mukherjee *et al.* 2006). To counteract this OGG1 inhibits activation of DNA-PK which would otherwise lead to the oxidative stress-induced apoptosis by phosphorylation of p53 (Youn *et al.* 2007). Caspase-6 then cleaves the nuclear proteins Lamin and NuMA which results in DNA fragmentation and chromatin condensation (Robertson *et al*. 2000). The protease cathepsin B diffuses into the nucleus where it degrades the transcription factor SP1 (Robertson *et al.* 2000). Suppression of SP1 has previously been shown to reduce OGG1 activity in response to the oxidative metal cadmium (Youn *et al.* 2005). Thus the consequence of cathepsin B-degradation of SP1 would be reduced OGG1. Moreover cathepsin B initiates chromatin detachment from nuclear matrix and endonuclease activation resulting in DNA fragmentation.

To our knowledge, this is the first study which visualizes OGG1 localisation in apoptotic cells. The nucleic material is condensed into a ball which is typical apoptotic morphology. OGG1 is discretely excluded from the nucleic material. Possible justifications for this distinctive morphology is to sequester DNA repair proteins from damaged DNA to which they have a high affinity. Gerner *et al.*, provided evidence of considerable exchange in the protein composition of the chromatin and nuclear matrix during apoptosis (Gerner *et al.* 2002). Apoptotic chromatin condensation resulted in the degradation of several proteins and the translocation of others to the nuclear matrix (Gerner *et al.* 2002). DNA repair proteins in particular become accumulated in the nuclear matrix (Gerner *et al.* 2002). It is likely that the inactivation of several DNA repair proteins is to prevent any counterproductive repair events when the cell is committed to death.

Mitotic cells

OGG1 expression was then observed in mitotic cells (figure3.5.7). The characteristic division of nucleic material was prevalent. The OGG1 was diffusely distributed throughout the cell. Surprising the characteristic localisation to the nuclear compartment was not observed in mitotic cells. Several studies have previously investigated the expression and localisation of OGG1 during cell cycle progression. Cell-cycle dependent expression is characteristic of a number DNA repair proteins, such as RAD52, APE and hMYH which are known associates of OGG1 (Luna *et al*. 2005; Fung *et al*. 2001; Kim 2001). The mRNA expression of hOGG1 increased with increased transcription in a cell-cycle dependant manner. The hOGG1 promoter contains two consensus transcription factor binding sites for NF-Y and E2F, which regulate the expression of several genes in a cell-cycle dependant manner (Luna *et al*. 2005). However other studies have presented evidence suggesting constitutive expression of OGG1, as a housekeeping protein (Youn *et al.* 2005). Reporter gene technology has been used to examine the transcription-level

regulation of hOGG1; the fusion of luciferase gene to the OGG1 promoter in HeLa cells did not suggest cell-cycle dependant increase in transcription (Dhénaut *et al.* 2000).

The localisation of GFP-OGG1 was tracked through cell cycle progression. During interphase OGG1 was localised in the nuclear matrix, a protein-RNA rich network, and chromatin (Dantzer *et al.* 2002). The OGG1 translocates dynamically to the condensed chromatin on the onset of mitosis (Dantzer *et al.* 2002). This translocation was further characterised in context of chromatin; oxidative stress induced the relocalisation of OGG1 from euchromatin to heterochromatin (Amouroux *et al.* 2010). The euchromatin is easily accessible and is the preferred site of OGG1-mediated BER (Amouroux *et al.* 2010). Heterochromatin, like mitotic condensed chromatin, is a barrier to OGG1-mediated BER (Amouroux *et al*. 2010). OGG1 also been suggested to associate with the spindle assembly during mitosis but translocates to the centriole and cytoskeleton during interphase (Conlon *et al.* 2004). Microtubule-associated shuttling has been suggested as the mode of translocation (Conlon *et al.* 2004).

The localisation of the wild-type and variant mutants in HaCat cells was studied in detail in context of cell-cycle dependant changes. Characteristically WT-OGG1 is located in the soluble chromatin and nuclear matrix during interphase. It is homogenously present in the nucleus during G1 and G2. However during S-phase, OGG1 is dynamically translocated to the nucleoli, discerned by counter-staining for nucleoli specific proteins, nucleolin and fibrallin. During S-phase the nucleoli is the site of high speed low fidelity of DNA synthesis which inherently requires DNA repair. Live time-lapse imaging confirmed the active localisation of OGG1 in the nucleoli during S-phase when counter-stained with PCNA, indicating active DNA replication. A similar pattern of localisation was observed with the repair deficient Cys-326 variant and the phosphomimetic variant Glu-326. During

mitosis, OGG1 is detected in the condensed chromatin; the site of DNA division. This is expected as many other DNA repair proteins become concentrated on chromatin during division of the nucleic material. The inhibition of DNA-dependant transcription saw the relocalisation of hOGG1 to condensed regions in the segregated nucleoli. Dantzer et al., observed hOGG1-GFP in nuclear speckles but attributed the displacement of hOGG1 from the soluble chromatin and nuclear matrix to condensed chromatin due to progression of cells from interphase to mitosis (Dantzer *et al.* 2002). They suggested relocalisation mechanism involved phosphorylation by PKC, as the wild-type distribution pattern was not observed with the Cys-326 variant but with the phosphomimetic Glu-326 variant (Dantzer *et al.* 2002). PKC is under redox regulation (Korichneva 2005), as is OGG1(Bravard et al. 2006), thus the activation of PKC during oxidative stress would enhance the response and localisation of OGG1.

Other investigators have attempted to study the distribution of OGG1 within the nuclear sub-architecture. Campalans *et al.,* demonstrated the dynamic localisation OGG1-GFP upon UVA radiation from soluble nucleoplasm to nuclear speckles where it is strongly associated with interchromatin and excluded from heterochromatin and nucleoli (Campalans *et al.* 2007). Distinct foci of OGG1-GFP colocalised with nuclear speckles independent of 8-oxoG interaction but possibly dye oxidative burst (Campalans et al. 2007). The colocalisation of GFP-OGG1 to nuclear speckles cannot be verified in the present study without counterstaining for SC35. Blocking transcription resulted in chromatin condensation and subsequent OGG1 translocation from nuclear speckles to heterochromatin (Campalans *et al.* 2007).

The exclusion of OGG1 from condensed chromatin/nucleoli was observed in a study by Conlon *et al.,* wherein nutrient starvation was used to established oxidative stress in cells. Under normal conditions the mOGG1, as detected by anti-mOGG1 antibodies was

observed diffusely distributed throughout the cell (Conlon *et al.* 2003). These initial cytoplasmic pools redistribute to the nucleus in response to 2 hours of nutrient deprivation. A punctuate pattern of condensed structures of mOGG1 is then visible in the nucleus. The investigators did not counterstain for nucleic structures to reduce possible bleedthrough of multiple fluorescent signals. This lack of nuclear staining makes it difficult to discern the pattern of OGG1 distribution with respect to nuclear material, although the authors suggested the lack of OGG1 in the nucleoli as discerned by phase-contrast microscropy. Detection using 8-oxoG antibodies showed a similar localisation pattern within the nuclear interior but excluded from nucleoli. The increased prevalence of OGG1 in the nucleus was attributed to the increased translation of stockpiled mRNA, although possible explanations such as increased nuclear import, protein stability and increased accessibility to antibodies have not been ruled out. The time frame eliminated the possibility of *de novo* synthesis of mRNA as the mRNA levels were not altered within the first hours of oxidative stress.

The mitotic cells examined in this study did not directly corroborate with existing evidence. Whilst nucleic staining indicates mitotic division, the OGG1 is diffusely distributed throughout the nucleus. Without further characterisation of the cell cycle stage it is not feasible to delineate the expected localisation of OGG1.

4.6 Conclusion

The investigation into OGG1 protein partners by immunoprecipitation and mass spectrometry workflow proved problematic for a number of reasons. Further optimisation and repetition of the experiment would be required to study OGG1 partners. This study found the critical parameters in OGG1 coimmunopurification to be antibody concentration, sample volume and crosslinker activity. The presence of the antioxidants thioredoxin and lysozyme reflect the oxidative stress environment in the Cys-OGG1 sample. The high resolution found many contaminants, indicating further optimisation of workflow to enrich

amount of purified OGG1.The investigation into the localisation of wild-type OGG1 in comparison to the Cys-326 variant suggested no difference under normal conditions or oxidative conditions. Thus the impaired repair activity of Cys-326 is not due to aberrant spatial modulation. Observation of the localisation of OGG1 in apoptotic cells was novel; further research is required to understand the dynamics of the separate compartments in the apoptotic nucleus. Examination of synchronous mitotic cells would be required to draw conclusions on OGG1 localisation. Overall no localisation difference between the wild-type and variant was observed.

Appendix

Appendix I

INSTRUCTIONS

Pierce® Crosslink Immunoprecipitation Kit

26147 2134.7

Number 26147

Description

Pierce Crosslink Immunoprecipitation Kit, contains sufficient reagents to perform 50 reactions using 10µL of immobilized antibody support

Kit Contents:

Pierce Protein A/G Plus Agarose, 0.55mL of settled resin supplied as a 50% slurry (e.g., 100µL of 50% slurry is equivalent to 50µL of settled resin)

20X Coupling Buffer, 25mL, when diluted results in 0.01M sodium phosphate, 0.15M NaCl; pH 7.2

DSS (disuccinimidyl suberate), **No-Weigh™ Format**, 8 · 2mg microtubes

IP Lysis/Wash Buffer, 2 · 50mL, 0.025M Tris, 0.15M NaCl, 0.001M EDTA, 1% NP-40, 5% glycerol; pH 7.4

100X Conditioning Buffer, 5mL, neutral pH buffer

20X Tris-Buffered Saline, 25mL, when diluted results in 0.025M Tris, 0.15M NaCl; pH 7.2

Elution Buffer, 50mL, pH 2.8, contains primary amine

Lane Marker Sample Buffer, Non-reducing, (5X), 5mL, 0.3M Tris•HCl, 5% SDS, 50% glycerol, lane marker tracking dye; pH 6.8

Pierce Spin Columns – Screw Cap, 50 columns, includes accessories

Microcentrifuge Collection Tubes, 2mL, 100 tubes

Microcentrifuge Sample Tubes, 1.5mL, 50 tubes

Pierce Control Agarose Resin (crosslinked 4% beaded agarose), 2mL of settled resin supplied as a 50% slurry (e.g., 100µL of 50% slurry is equivalent to 50µL of settled resin)

Storage: Upon receipt store at 4°C. Store DSS desiccated at 4ºC. Kit is shipped at ambient temperature.

Introduction

The Thermo Scientific Pierce Crosslink Immunoprecipitation (IP) Kit enables highly effective and efficient antigen immunoprecipitations by covalently crosslinking antibodies onto Protein A/G resin. This kit combines the reliable crosslinking chemistry of DSS and the versatile high-binding capacity of Pierce Protein A/G Plus Agarose to produce an
excellent method for performing IPs. The kit includes optimized buffers for high antigen yield using less than 10 ∝g of antibody and efficient spin columns and collection tubes for minimizing handling and mixing. The included 5X sample buffer is ideal for preparing samples for SDS-PAGE without significant dilution. This complete kit enables researchers to perform easy high-yield IPs that are free from antibody contamination.

Important Product Information

- Perform all steps at 4°C unless otherwise indicated.
- Perform all resin centrifugation steps for 30-60 seconds at low speed (i.e., 1000-3000 · *g*). Centrifuging at speeds greater than 5000 · *g* may cause the resin to clump and make resuspension difficult.
- When centrifuging spin columns, the flow-through volume should not exceed 600µL when using a 2mL collection tube and 300µL when using a 1.5mL collection tube. Exceeding these volumes may result in back pressure in the column and incomplete washing or elution.
- Before performing the immunoprecipitation, pre-clear lysates using the Control Agarose Resin to reduce nonspecific protein binding.
- When using serum, the antibody specific for the antigen of interest may comprise only 1-2% of the total IgG in the serum. If recovery of high amounts of antigen is desired, use an affinity-purified antibody for optimal results.
- IP Lysis/Wash Buffer has been tested on representative cell types including but not limited to the following cell lines: HeLa, Jurkat, A431, A549, MOPC, NIH 3T3 and U2OS. Typically, 10^6 HeLa cells yields ~10mg of cell pellet and ~3∝g/∝L (or 300∝g) when lysed with 100µL of IP Lysis/Wash Buffer.
- For best results, add Thermo Scientific Halt Protease (Product No. 78430) and Phosphatase (Product No. 78428) Inhibitor Cocktails to minimize degradation and dephosphorylation of cell lysate proteins. These inhibitors are also available as a combined cocktail (Product No. 78440). See the Related Thermo Scientific Products Section for more information.
- The IP Lysis/Wash buffer is compatible with the Thermo Scientific Pierce BCA Protein Assay (Product No. 23225).
- Proper controls are vital for identifying relevant interactions. The supplied Pierce Control Agarose Resin is composed of a similar support material used for Pierce Protein A/G Agarose Resin and can be used as a negative control.
- The Pierce Spin Columns package includes columns, screw caps, plugs, Luer-Lok™ Adapter Caps, large frits and a large frit tool. The large frit is not needed for the standard IP protocol. When scaling-up (i.e., > 200µL of resin), the large frit can be inserted into the column to facilitate washing. The Luer-Lok Caps have a flip top that may be used during wash steps. Use the screw caps for sealing the spin columns during storage. (See the Additional Information Section.)

Procedure for the Pierce Crosslink IP Kit

A. Binding of Antibody to Protein A/G Plus Agarose

Note: The following protocol is optimized for coupling 10∝g of antibody but can be used for 2-50∝g. For antibody amounts > 50∝g, proportionally scale the resin, crosslinker and buffer volumes.

1. Prepare 2mL of 1X Coupling Buffer for each IP reaction by diluting the 20X Coupling Buffer with ultrapure water.
2. Gently swirl the bottle of Pierce Protein A/G Plus Agarose to obtain an even suspension. Using a wide-bore or cut pipette tip, add 20µL of the resin slurry into a Pierce Spin Column. Place column into a microcentrifuge tube and centrifuge at 1000 · *g* for 1 minute. Discard the flow-through.
3. Wash the resin with 200µL of 1X Coupling Buffer, centrifuge and discard the flow-through. Repeat this wash once.
4. Gently tap the bottom of the column on a paper towel to remove any excess liquid. Insert the bottom plug.
5. Prepare 10 ∝g of antibody for coupling. Adjust the volume to 100µL with sufficient ultrapure water and 20X Coupling Buffer to produce 1X Coupling Buffer. For example, for a 1∝g/∝L of antibody solution, add 5µL of 20X Coupling Buffer and 85µL of water and 10µL of antibody. Add the ultrapure water, 20X Coupling Buffer and affinity-purified antibody directly to the resin in the column.
6. Attach the screw cap to the column and incubate on a rotator or mixer at room temperature for 30-60 minutes, ensuring that the slurry remains suspended during incubation.
7. Remove and retain the bottom plug and remove the cap. Place the column into a collection tube and centrifuge. Save the flow-through to verify antibody coupling.
8. Wash the resin with 100µL of 1X Coupling Buffer, centrifuge and discard the flow-through.
9. Wash the resin with 300µL of 1X Coupling Buffer, centrifuge and discard the flow-through. Repeat this wash once.

B. Crosslinking the Bound Antibody

Note: Conventional IP can be performed by omitting crosslinking; however, if crosslinking is omitted, the antibody will co-elute with the antigen during the elution steps.

Note: The DSS crosslinker is moisture-sensitive. Keep DSS in foil pouch after use. Dissolve DSS in DMSO or DMF immediately before use. DSS is not compatible with amine-containing buffers (e.g., Tris, glycine).

1. Puncture the foil covering of a single tube of DSS with a pipette tip and add 217µL of DMSO or DMF to prepare a 10X solution (25mM). Use the pipette to thoroughly mix the solution (i.e., draw up and expel the solution) until the DSS is dissolved.
2. Dilute the DSS solution 1:10 in DMSO or DMF (100µL of 10X DSS with 900µL solvent) to make 2.5mM DSS.
3. Tap the bottom of the column on a paper towel to remove excess liquid and insert the bottom plug.
4. Add 2.5µL of 20X Coupling Buffer, 9µL of 2.5mM DSS and 38.5µL of ultrapure water to the column. The total solution volume will be 50µL. The DSS is added at 10X molar excess to Protein A/G on the resin with a working concentration of 450∝M.
5. Incubate the crosslinking reaction for 30-60 minutes at room temperature on a rotator or mixer.
6. Remove and retain the bottom plug and open the cap. Place the column into a collection tube and centrifuge.
7. Add 50µL of Elution Buffer to the column and centrifuge. Save the flow-through to verify antibody crosslinking.
8. Wash twice with 100µL of Elution Buffer to remove non-crosslinked antibody and quench the crosslinking reaction.
9. Wash twice with 200µL of cold IP Lysis/Wash Buffer and centrifuge after each wash.
10. Proceed to immunoprecipitation protocol. If desired, the antibody-crosslinked resin can be stored for up to 5 days in IP Lysis/Wash Buffer. For longer storage, store resin in 1X Coupling Buffer (PBS). When storing the resin, place plug in bottom of spin column, add 200µL of storage buffer, attach the screw cap and store at 4°C

C. Mammalian Cell Lysis

Protocol I: Lysis of Cell Monolayer (Adherent) Cultures

1. Carefully remove culture medium from cells.
2. Wash the cells once with 1X Coupling Buffer.
3. Add ice cold IP Lysis/Wash Buffer (Table 1) to the cells and incubate on ice for 5 minutes with periodic mixing.

Table 1. Suggested volume of IP Lysis/Wash Buffer to use for different standard culture plates.

Plate Size/Surface Area	Volume of IP Lysis/Wash Buffer
100 · 100mm	500-1000µL
100 · 60mm	250-500µL
6-well plate	200-400µL per well
24-well plate	100-200µL per well

4. Transfer the lysate to a microcentrifuge tube and centrifuge at ~13,000 · *g* for 10 minutes to pellet the cell debris.
5. Transfer supernatant to a new tube for protein concentration determination and further analysis.

Protocol II: Lysis of Cell Suspension Cultures

1. Centrifuge the cell suspension at 1000 · *g* for 5 minutes to pellet the cells. Discard the supernatant.
2. Wash cells once by suspending the cell pellet in PBS. Centrifuge at 1000 · *g* for 5 minutes to pellet cells.
3. Add 500µL of ice cold IP Lysis/Wash Buffer per 50mg of wet cell pellet (i.e., 10:1 v/w). If using a large amount of cells, first add 10% of the final volume of IP Lysis/Wash Buffer to the cell pellet and pipette the mixture up and down to mix. Add the remaining volume of IP Lysis/Wash Buffer to the cell suspension.
4. Incubate lysate on ice for 5 minutes with periodic mixing. Remove cell debris by centrifugation at ~13,000 · *g* for 10 minutes. Transfer supernatant to a new tube for protein concentration determination and further analysis.

D. Pre-clear lysate using the Control Agarose Resin

1. For 1mg of lysate, add 80µL of the Control Agarose Resin slurry (40µL of settled resin) into a spin column.
2. Centrifuge column to remove storage buffer.
3. Add 100µL of 1X Coupling Buffer to the column, centrifuge and discard the flow-through.
4. Add 1mg of lysate to the column containing the resin and incubate at 4ºC for 30 minutes to 1 hour with gentle end-over-end mixing.
5. Centrifuge column at 1000 × *g* for 1 minute. Discard the column containing the resin and save the flow-through, which will be added to the immobilized antibody.

E. Antigen Immunoprecipitation General Protocol

Note: The amount of sample needed and the incubation time are dependent upon each specific antibody-antigen system and may require optimization for maximum yield.

1. If the antibody-crosslinked resin was stored in PBS, wash twice with IP Lysis/Wash Buffer. Discard the flow-through after each wash.
2. Tap bottom of the column on a paper towel to remove excess liquid. Replace bottom plug.
3. Dilute the cell extract in IP Lysis/Wash Buffer. The recommended sample volume in the spin column is 300-600µL. The suggested amount of total protein per IP reaction is 500-1000 ∝g as determined by the Pierce BCA Protein Assay.
4. Add the pre-cleared lysate to the antibody-crosslinked resin in the column. Attach the screw cap and incubate column with gentle end-over-end mixing or shaking for 1-2 hours or overnight at 4°C.
5. Remove bottom plug, loosen the screw cap and place the column in a collection tube. Centrifuge column and save the flow-through. Do not discard flow-through until confirming that the IP was successful.
6. Remove the screw cap, place the column into a new tube, add 200µL of IP Lysis/Wash Buffer and centrifuge.

   Note: An alternative wash buffer (20X TBS) is supplied if a detergent-free wash is required. Dilute TBS to 1X before use.
7. Wash sample twice with 200µL IP Lysis/Wash Buffer and centrifuge after each wash.
8. Wash sample once with 100µL of 1X Conditioning Buffer.

F. Antigen Elution

Note: To neutralize the low pH of the Elution Buffer (e.g., for downstream enzymatic or functional assays), add 5µL of 1M Tris, pH 9.5 to the collection tube, which will neutralize the pH upon centrifugation (Step F3). Alternatively, use a neutral pH elution buffer (i.e., Thermo Scientific Gentle Elution Buffer, Product No. 21027).

1. Place the spin column into a new collection tube, add 10µL of Elution Buffer and centrifuge.
2. Keep the column in the tube and add 50µL of Elution Buffer. Incubate for 5 minutes at room temperature. The column does not need to be closed or mixed.

   Note: For a more concentrated eluate, less Elution Buffer may be used; however, overall yield might be reduced.
3. Centrifuge the tube and collect the flow-through. Analyze the eluate for presence of antigen. Perform additional elutions (i.e., Steps F1-F3) as needed. Analyze each eluate separately to ensure that the antigen has completely eluted.
4. To preserve activity of the antibody-coupled resin, immediately proceed to Section G, Resin Regeneration and Storage.

G. Resin Regeneration and Storage

1. Add 100µL of 1X Coupling Buffer to the column, centrifuge and discard the flow-through. Repeat this step once.
2. Replace the bottom plug on the column. Add 200µL of 1X Coupling Buffer to column. Replace screw cap. Wrap the bottom of the tube with laboratory film to prevent resin from drying. For long-term storage (i.e., > 2 weeks) add sodium azide at a final concentration of 0.02%.

Appendix II

Mass Spectrometry Results of GFP-Ser-OGG1

Accession	Description	Score	Coverage	# Proteins	# Unique Peptides	# Peptides	# PSMs	# AAs	MW [kDa]	calc. pI
145579641	prolactin-inducible protein precursor [Homo sapiens] (Chain B, Crystal Structure Of The Complex Formed Between Mhc-Like Zinc Alpha2-Glycoprotein And Prolactin Inducible Protein At 3 A Resolution	73.34	10.17	1	0	1	1	118	13.514	5.55
38566198	GFAP protein [Homo sapiens]	68.06	2.55	1	0	1	1	431	49.7186	5.52
226236	glial fibrillary acidic protein	68.06	11.7	1	0	1	1	94	10.9288	5.29
553302	glial fibrillary acidic protein [Homo sapiens]	68.06	16.67	1	0	1	1	66	7.5761	7.25
16265836	glial fibrillary acidic protein [Homo sapiens]	68.06	2.55	1	0	1	1	432	49.7776	5.59
4503979	glial fibrillary acidic protein isoform 1 [Homo sapiens]	68.06	2.55	1	0	1	1	432	49.8496	5.52
196115290	glial fibrillary acidic protein isoform 2 [Homo sapiens]	68.06	2.55	1	0	1	1	431	49.4776	6.13
334688844	glial fibrillary acidic protein isoform 3 [Homo sapiens]	68.06	2.51	1	0	1	1	438	50.2578	5.67
62896925	glial fibrillary acidic protein variant [Homo sapiens]	68.06	2.55	1	0	1	1	432	49.8197	5.59
119571952	glial fibrillary acidic protein, isoform CRA_a [Homo sapiens]	68.06	3.47	1	0	1	1	317	36.2764	5.74
119571954	glial fibrillary acidic protein, isoform CRA_c [Homo sapiens]	68.06	2.67	1	0	1	1	412	47.6105	5.5
57997051	hypothetical protein [Homo sapiens] GFAP	68.06	2.51	1	0	1	1	438	50.2137	5.57
119631357	NCK-associated protein 1, isoform CRA_a [Homo sapiens]	38.3	7.09	1	0	1	1	141	16.3652	5.26

119631362	NCK-associated protein 1, isoform CRA_f [Homo sapiens]	77.36	5.24	1	0	2	2	401	43.6169	5.03
1050983	pHL E1F1 [Homo sapiens]	82.43	10.45	1	0	1	1	134	15.0876	7.06
332838574	PREDICTED: proline-rich protein 4 isoform 2 precursor pHL E1F1	82.43	10.45	1	0	1	1	134	15.1156	7.66
169168829	PREDICTED: similar to hCG1643231 [Homo sapiens]	68.06	3.51	1	0	1	1	313	35.2769	8.15
116642261	prolactin-induced protein [Homo sapiens]	73.34	15.19	1	0	1	1	79	9.0777	5.31
116642259	prolactin-induced protein [Homo sapiens]	73.34	15.19	1	0	1	1	79	9.0596	5.31
4505821	prolactin-inducible protein precursor [Homo sapiens]	73.34	8.22	1	0	1	1	146	16.5618	8.05
4688900	sarcolectin [Homo sapiens]	80.46	3.84	1	0	2	2	469	51.3823	5.69
121934234	Unknown (protein for IMAGE:40134129) [Homo sapiens] (glial fibrillary acidic protein isoform 1)	68.06	8.8	1	0	1	1	125	14.5404	4.89
34536332	unnamed protein product [Homo sapiens] glial fibrillary acidic protein isoform 2	68.06	2.55	1	0	1	1	431	49.4756	6.13
194382434	unnamed protein product [Homo sapiens] glial fibrillary acidic protein isoform 1	68.06	2.65	1	0	1	1	415	48.1709	5.52
194383466	unnamed protein product [Homo sapiens] glial fibrillary acidic protein isoform 2	68.06	2.7	1	0	1	1	407	47.3073	5.33

Mass Spectrometry Results of GFP-Cys-OGG1

Accession	Description	Score	Coverage	# Proteins	# Unique Peptides	# Peptides	# PSMs	# AAs	MW [kDa]	calc. pI
914044	surface-associated sulphydryl protein, SASP=thioredoxin homolog [human, THP-1 monocytes, Peptide Partial, 21 aa, segment 1 of 2]	34.74	61.9	1	0	1	1	21	2.2791	4.91
553302	glial fibrillary acidic protein [Homo sapiens]	71.47	16.67	1	0	1	1	66	7.5761	7.25
116642261	prolactin-induced protein [Homo sapiens]	76.04	15.19	1	0	1	1	79	9.0777	5.31
116642259	prolactin-induced protein [Homo sapiens]	76.04	15.19	1	0	1	1	79	9.0596	5.31
3153859	thioredoxin delta 3 [Homo sapiens]	34.74	15.48	1	0	1	1	84	9.3146	6.04
55957946	thioredoxin [Homo sapiens]	34.74	15.29	1	0	1	1	85	9.4457	6.04
226236	glial fibrillary acidic protein	71.47	11.7	1	0	1	1	94	10.9288	5.29
119389938	Chain A, Crystal Structure Of C73s Mutant Of Human Thioredoxin-1 Oxidized With H2o2	34.74	12.38	1	0	1	1	105	11.7138	4.92
302566158	Chain A, Crystal Structure Of Human Thioredoxin C6973S DOUBLE MUTANT, REDUCED Form	34.74	12.38	1	0	1	1	105	11.6978	4.92
119390130	Chain A, Crystal Structure Of S-Nitroso Thioredoxin	34.74	12.38	1	0	1	1	105	11.7367	4.92
119389988	Chain A, Crystal Structure Of S-Nitroso Thioredoxin	34.74	12.38	1	0	1	1	105	11.7437	4.92
1065111	Chain A, High Resolution Solution Nmr Structure Of Mixed Disulfide Intermediate Between Mutant Human Thioredoxin And A 13 Residue Peptide Comprising Its Target Site In Human Nfkb	34.74	12.38	1	0	1	1	105	11.5719	4.92
157836899	Chain A, High-Resolution Three-Dimensional Structure Of Reduced Recombinant Human Thioredoxin In Solution	34.74	12.38	1	0	1	1	105	11.6997	4.92

157829897	Chain A, Human Thioredoxin (D60n Mutant, Reduced Form)	34.74	12.38	1	0	1	1	105	11.7288	5.03
313103750	Chain A, Human Thioredoxin C35s,C62s,C69s,C73s Mutant Showing Cadmium Chloride Bound To The Active Site	34.74	12.38	1	0	1	1	105	11.6658	4.92
290560081	Chain A, Human Thioredoxin Double Mutant C35s,C73r	34.74	12.38	1	0	1	1	105	11.7669	5.07
157831000	Chain A, Human Thioredoxin Double Mutant With Cys 32 Replaced By Ser And Cys 35 Replaced By Ser	34.74	12.38	1	0	1	1	105	11.6978	4.92
157834011	Chain A, The High-Resolution Three-Dimensional Solution Structures Of The Oxidized And Reduced States Of Human Thioredoxin	34.74	12.38	1	0	1	1	105	11.6038	4.92
50592994	thioredoxin [Homo sapiens]	34.74	12.38	1	0	1	1	105	11.7297	4.92
9280551	thioredoxin 1 [Homo sapiens]	34.74	12.38	1	0	1	1	105	11.6857	4.78
345100812	Chain C, Crystal Structure Of The Human Thioredoxin Reductase-Thioredoxin Complex	34.74	11.21	1	0	1	1	116	12.9643	6.4
145579641	Chain B, Crystal Structure Of The Complex Formed Between Mhc-Like Zinc Alpha2-Glycoprotein And Prolactin Inducible Protein At 3 A Resolution	76.04	10.17	1	0	1	1	118	13.514	5.55
6730357	Chain A, Role Of Amino Acid Residues At Turns In The Conformational Stability And Folding Of Human Lysozyme	64.78	9.38	1	0	1	1	128	14.5631	9
6730358	Chain A, Role Of Amino Acid Residues At Turns In The Conformational Stability And Folding Of Human Lysozyme	64.78	9.3	1	0	1	1	129	14.5351	8.82
157831908	Chain A, Amyloidogenic Variant (Asp67his) Of Human Lysozyme	64.78	9.23	1	0	1	1	130	14.7132	9.17
14278473	Chain A, Buried Polar Mutant Human Lysozyme	64.78	9.23	1	0	1	1	130	14.6931	9
14278474	Chain A, Buried Polar Mutant Human Lysozyme	64.78	9.23	1	0	1	1	130	14.7071	9
14278472	Chain A, Buried Polar Mutant Human Lysozyme	64.78	9.23	1	0	1	1	130	14.7071	9
14278467	Chain A, Buried Polar Mutant Human Lysozyme	64.78	9.23	1	0	1	1	130	14.6791	9

14278476	Chain A, Buried Polar Mutant Human Lysozyme	64.78	9.23	1	0	1	1	130	14.6931	9
14278470	Chain A, Buried Polar Mutant Human Lysozyme	64.78	9.23	1	0	1	1	130	14.7071	9
14278471	Chain A, Buried Polar Mutant Human Lysozyme	64.78	9.23	1	0	1	1	130	14.7071	9
14278475	Chain A, Buried Polar Mutant Human Lysozyme	64.78	9.23	1	0	1	1	130	14.6931	9
157835338	Chain A, Changes In Conformational Stability Of A Series Of Mutant Human Lysozymes At Constant Positions	64.78	9.23	1	0	1	1	130	14.6912	9
157834217	Chain A, Contribution Of Hydrogen Bonds To The Conformational Stability Of Human Lysozyme	64.78	9.23	1	0	1	1	130	14.6752	9.01
157834215	Chain A, Contribution Of Hydrogen Bonds To The Conformational Stability Of Human Lysozyme	64.78	9.23	1	0	1	1	130	14.6752	9.01
157834218	Chain A, Contribution Of Hydrogen Bonds To The Conformational Stability Of Human Lysozyme	64.78	9.23	1	0	1	1	130	14.6752	9.01
157834216	Chain A, Contribution Of Hydrogen Bonds To The Conformational Stability Of Human Lysozyme	64.78	9.23	1	0	1	1	130	14.6752	9.01
6729876	Chain A, Contribution Of Hydrogen Bonds To The Conformational Stability Of Human Lysozyme: Calorimetry And X-Ray Analysis Of Six Ser->ala Mutant	64.78	9.23	1	0	1	1	130	14.6752	9
6729705	Chain A, Contribution Of Hydrogen Bonds To The Conformational Stability Of Human Lysozyme: Calorimetry And X-Ray Analysis Of Six Ser->ala Mutants	64.78	9.23	1	0	1	1	130	14.6752	9
4388847	Chain A, Contribution Of Hydrogen Bonds To The Conformational Stability Of Human Lysozyme: Calorimetry And X-Ray Analysis Of Six Ser->ala Mutants	64.78	9.23	1	0	1	1	130	14.6752	9
6729879	Chain A, Contribution Of Hydrogen Bonds To The Conformational Stability Of Human Lysozyme: Calorimetry And X-Ray Analysis Of Six Ser->ala Mutants	64.78	9.23	1	0	1	1	130	14.6752	9
157834711	Chain A, Contribution Of Hydrophobic Effect To The Conformational Stability Of Human Lysozyme	64.78	9.23	1	0	1	1	130	14.5992	9.31
157834708	Chain A, Contribution Of Hydrophobic Effect To The Conformational Stability Of Human Lysozyme	64.78	9.23	1	0	1	1	130	14.5992	9.31
157834707	Chain A, Contribution Of Hydrophobic Effect To The Conformational Stability Of Human Lysozyme	64.78	9.23	1	0	1	1	130	14.6132	9.31

157835340	Chain A, Contribution Of Hydrophobic Effect To The Conformational Stability Of Human Lysozyme	64.78	9.23	1	0	1	1	130	14.6912	9
157834704	Chain A, Contribution Of Hydrophobic Effect To The Conformational Stability Of Human Lysozyme	64.78	9.23	1	0	1	1	130	14.6132	9.31
157834716	Chain A, Contribution Of Hydrophobic Effect To The Conformational Stability Of Human Lysozyme	64.78	9.23	1	0	1	1	130	14.5992	9.31
157834709	Chain A, Contribution Of Hydrophobic Effect To The Conformational Stability Of Human Lysozyme	64.78	9.23	1	0	1	1	130	14.5992	9.31
157834710	Chain A, Contribution Of Hydrophobic Effect To The Conformational Stability Of Human Lysozyme	64.78	9.23	1	0	1	1	130	14.5992	9.31
157834703	Chain A, Contribution Of Hydrophobic Effect To The Conformational Stability Of Human Lysozyme	64.78	9.23	1	0	1	1	130	14.6132	9.31
157834712	Chain A, Contribution Of Hydrophobic Effect To The Conformational Stability Of Human Lysozyme	64.78	9.23	1	0	1	1	130	14.5992	9.31
157834714	Chain A, Contribution Of Hydrophobic Effect To The Conformational Stability Of Human Lysozyme	64.78	9.23	1	0	1	1	130	14.5992	9.31
157834715	Chain A, Contribution Of Hydrophobic Effect To The Conformational Stability Of Human Lysozyme	64.78	9.23	1	0	1	1	130	14.5992	9.31
157834713	Chain A, Contribution Of Hydrophobic Effect To The Conformational Stability Of Human Lysozyme	64.78	9.23	1	0	1	1	130	14.5992	9.31
157834292	Chain A, Contribution Of Hydrophobic Residues To The Stability Of Human Lysozyme: Calorimetric Studies And X-Ray Structural Analysis Of The Five Isoleucine To Valine Mutants	64.78	9.23	1	0	1	1	130	14.6771	9
157834289	Chain A, Contribution Of Hydrophobic Residues To The Stability Of Human Lysozyme: Calorimetric Studies And X-Ray Structural Analysis Of The Five Isoleucine To Valine Mutants	64.78	9.23	1	0	1	1	130	14.6771	9
157834288	Chain A, Contribution Of Hydrophobic Residues To The Stability Of Human Lysozyme: Calorimetric Studies And X-Ray Structural Analysis Of The Five Isoleucine To Valine Mutants	64.78	9.23	1	0	1	1	130	14.6771	9
157832579	Chain A, Contribution Of Hydrophobic Residues To The Stability Of Human Lysozyme: X-Ray Structure Of The V100a Mutant	64.78	9.23	1	0	1	1	130	14.6631	9
157832580	Chain A, Contribution Of Hydrophobic Residues To The Stability Of Human Lysozyme: X-Ray Structure Of The V110a Mutant	64.78	9.23	1	0	1	1	130	14.6631	9

157832581	Chain A, Contribution Of Hydrophobic Residues To The Stability Of Human Lysozyme: X-Ray Structure Of The V121a Mutant	64.78	9.23	1	0	1	1	130	14.6631	9
157832582	Chain A, Contribution Of Hydrophobic Residues To The Stability Of Human Lysozyme: X-Ray Structure Of The V125a Mutant	64.78	9.23	1	0	1	1	130	14.6631	9
157832583	Chain A, Contribution Of Hydrophobic Residues To The Stability Of Human Lysozyme: X-Ray Structure Of The V130a Mutant	64.78	9.23	1	0	1	1	130	14.6631	9
157832584	Chain A, Contribution Of Hydrophobic Residues To The Stability Of Human Lysozyme: X-Ray Structure Of The V2a Mutant	64.78	9.23	1	0	1	1	130	14.6631	9
157832585	Chain A, Contribution Of Hydrophobic Residues To The Stability Of Human Lysozyme: X-Ray Structure Of The V74a Mutant	64.78	9.23	1	0	1	1	130	14.6631	9
157832586	Chain A, Contribution Of Hydrophobic Residues To The Stability Of Human Lysozyme: X-Ray Structure Of The V93a Mutant	64.78	9.23	1	0	1	1	130	14.6631	9
157832587	Chain A, Contribution Of Hydrophobic Residues To The Stability Of Human Lysozyme: X-Ray Structure Of The V99a Mutant	64.78	9.23	1	0	1	1	130	14.6631	9
157835052	Chain A, Contribution Of Water Molecules In The Interior Of A Protein To The Conformational Stability	64.78	9.23	1	0	1	1	130	14.6491	9
157835057	Chain A, Contribution Of Water Molecules In The Interior Of A Protein To The Conformational Stability	64.78	9.23	1	0	1	1	130	14.6491	9
157835053	Chain A, Contribution Of Water Molecules In The Interior Of A Protein To The Conformational Stability	64.78	9.23	1	0	1	1	130	14.6491	9
15825835	Chain A, Crystal Structure Analysis Of A Human Lysozyme Mutant W64c C65a	64.78	9.23	1	0	1	1	130	14.5761	9
323462871	Chain A, Crystal Structure Of A Charge Engineered Human Lysozyme Variant	64.78	9.23	1	0	1	1	130	14.631	8.48
11514208	Chain A, Crystal Structure Of Mutant Human Lysozyme Substituted At Left-Handed Helical Positions	64.78	9.23	1	0	1	1	130	14.5921	8.82
11513937	Chain A, Crystal Structure Of Mutant Human Lysozyme Substituted At Left-Handed Helical Positions	64.78	9.23	1	0	1	1	130	14.6481	9
11513927	Chain A, Crystal Structure Of Mutant Human Lysozyme Substituted At Left-Handed Helical Positions	64.78	9.23	1	0	1	1	130	14.6061	8.82
11513929	Chain A, Crystal Structure Of Mutant Human Lysozyme Substituted At Left-Handed Helical Positions	64.78	9.23	1	0	1	1	130	14.5851	9.01

11513933	Chain A, Crystal Structure Of Mutant Human Lysozyme Substituted At Left-Handed Helical Positions	64.78	9.23	1	0	1	1	130	14.6251	9
11513935	Chain A, Crystal Structure Of Mutant Human Lysozyme Substituted At Left-Handed Helical Positions	64.78	9.23	1	0	1	1	130	14.6341	9
12084399	Chain A, Crystal Structure Of Mutant Human Lysozyme Substituted At The Surface Positions	64.78	9.23	1	0	1	1	130	14.7061	9
9955035	Chain A, Crystal Structure Of Mutant Human Lysozyme Substituted At The Surface Positions	64.78	9.23	1	0	1	1	130	14.6491	9
12084398	Chain A, Crystal Structure Of Mutant Human Lysozyme Substituted At The Surface Positions	64.78	9.23	1	0	1	1	130	14.7071	8.82
9955038	Chain A, Crystal Structure Of Mutant Human Lysozyme Substituted At The Surface Positions	64.78	9.23	1	0	1	1	130	14.7231	9
12084274	Chain A, Crystal Structure Of Mutant Human Lysozyme Substituted At The Surface Positions	64.78	9.23	1	0	1	1	130	14.7071	8.82
9955030	Chain A, Crystal Structure Of Mutant Human Lysozyme Substituted At The Surface Positions	64.78	9.23	1	0	1	1	130	14.6491	9
12084400	Chain A, Crystal Structure Of Mutant Human Lysozyme Substituted At The Surface Positions	64.78	9.23	1	0	1	1	130	14.7482	9.17
9955033	Chain A, Crystal Structure Of Mutant Human Lysozyme Substituted At The Surface Positions	64.78	9.23	1	0	1	1	130	14.7231	9
9955036	Chain A, Crystal Structure Of Mutant Human Lysozyme Substituted At The Surface Positions	64.78	9.23	1	0	1	1	130	14.7052	9
12084396	Chain A, Crystal Structure Of Mutant Human Lysozyme Substituted At The Surface Positions	64.78	9.23	1	0	1	1	130	14.6791	9
12084401	Chain A, Crystal Structure Of Mutant Human Lysozyme Substituted At The Surface Positions	64.78	9.23	1	0	1	1	130	14.7551	8.98
9955029	Chain A, Crystal Structure Of Mutant Human Lysozyme Substituted At The Surface Positions	64.78	9.23	1	0	1	1	130	14.7392	9
12084273	Chain A, Crystal Structure Of Mutant Human Lysozyme Substituted At The Surface Positions	64.78	9.23	1	0	1	1	130	14.7551	8.98
12084402	Chain A, Crystal Structure Of Mutant Human Lysozyme Substituted At The Surface Positions	64.78	9.23	1	0	1	1	130	14.7071	8.82

9256911	Chain A, Crystal Structure Of Mutant Human Lysozyme Substituted At The Surface Positions	64.78	9.23	1	0	1	1	130	14.6491	9
9955031	Chain A, Crystal Structure Of Mutant Human Lysozyme Substituted At The Surface Positions	64.78	9.23	1	0	1	1	130	14.7052	9
9955039	Chain A, Crystal Structure Of Mutant Human Lysozyme Substituted At The Surface Positions	64.78	9.23	1	0	1	1	130	14.7392	9
9955037	Chain A, Crystal Structure Of Mutant Human Lysozyme Substituted At The Surface Positions	64.78	9.23	1	0	1	1	130	14.7052	9
9955027	Chain A, Crystal Structure Of Mutant Human Lysozyme Substituted At The Surface Positions	64.78	9.23	1	0	1	1	130	14.7052	9
9955034	Chain A, Crystal Structure Of Mutant Human Lysozyme Substituted At The Surface Positions	64.78	9.23	1	0	1	1	130	14.7392	9
12084409	Chain A, Crystal Structure Of Mutant Human Lysozyme Substituted At The Surface Positions	64.78	9.23	1	0	1	1	130	14.7482	9.17
9955032	Chain A, Crystal Structure Of Mutant Human Lysozyme Substituted At The Surface Positions	64.78	9.23	1	0	1	1	130	14.7052	9
12084272	Chain A, Crystal Structure Of Mutant Human Lysozyme Substituted At The Surface Positions	64.78	9.23	1	0	1	1	130	14.7482	9.17
12084397	Chain A, Crystal Structure Of Mutant Human Lysozyme Substituted At The Surface Positions	64.78	9.23	1	0	1	1	130	14.7551	8.98
12084275	Chain A, Crystal Structure Of Mutant Human Lysozyme Substituted At The Surface Positions	64.78	9.23	1	0	1	1	130	14.7061	9
9955028	Chain A, Crystal Structure Of Mutant Human Lysozyme Substituted At The Surface Positions	64.78	9.23	1	0	1	1	130	14.7052	9
12084403	Chain A, Crystal Structure Of Mutant Human Lysozyme Substituted At The Surface Positions	64.78	9.23	1	0	1	1	130	14.7061	9
9955327	Chain A, Crystal Structure Of Mutant Human Lysozyme Substituted At The Surface Positions	64.78	9.23	1	0	1	1	130	14.7231	9
7767021	Chain A, Crystal Structures Of Salt Bridge Mutants Of Human Lysozyme	64.78	9.23	1	0	1	1	130	14.6902	9.17
7767016	Chain A, Crystal Structures Of Salt Bridge Mutants Of Human Lysozyme	64.78	9.23	1	0	1	1	130	14.6902	9.17

7767015	Chain A, Crystal Structures Of Salt Bridge Mutants Of Human Lysozyme	64.78	9.23	1	0	1	1	130	14.6902	9.17
157835322	Chain A, Crystal Structures Of The Apo-And Holomutant Human Lysozymes With An Introduced Ca2+ Binding Site	64.78	9.23	1	0	1	1	130	14.7221	8.66
157833900	Chain A, Dissection Of The Functional Role Of Structural Elements Of Tyrosine-63 In The Catalytic Action Of Human Lysozyme	64.78	9.23	1	0	1	1	130	14.5991	9.01
157833914	Chain A, Dissection Of The Functional Role Of Structural Elements Of Tyrosine-63 In The Catalytic Action Of Human Lysozyme	64.78	9.23	1	0	1	1	130	14.6752	9.01
157833921	Chain A, Dissection Of The Functional Role Of Structural Elements Of Tyrosine-63 In The Catalytic Action Of Human Lysozyme	64.78	9.23	1	0	1	1	130	14.7142	9.01
17942569	Chain A, G105a Human Lysozyme	64.78	9.23	1	0	1	1	130	14.7052	9
17942568	Chain A, G127a Human Lysozyme	64.78	9.23	1	0	1	1	130	14.7052	9
17942566	Chain A, G129a Human Lysozyme	64.78	9.23	1	0	1	1	130	14.7052	9
17942574	Chain A, G37a Human Lysozyme	64.78	9.23	1	0	1	1	130	14.7052	9
17942573	Chain A, G48a Human Lysozyme	64.78	9.23	1	0	1	1	130	14.7052	9
17942571	Chain A, G68a Human Lysozyme	64.78	9.23	1	0	1	1	130	14.7052	9
17942570	Chain A, G72a Human Lysozyme	64.78	9.23	1	0	1	1	130	14.7052	9
3659960	Chain A, Human Lysozyme Double Mutant A96l, W109h	64.78	9.23	1	0	1	1	130	14.6842	9
6980459	Chain A, Human Lysozyme E102 Mutant Labelled With 2',3'-Epoxypropyl Glycoside Of N-Acetyllactosamine	64.78	9.23	1	0	1	1	130	14.7052	9
6980458	Chain A, Human Lysozyme L63 Mutant Labelled With 2',3'-Epoxypropyl N, N'-Diacetylchitobiose	64.78	9.23	1	0	1	1	130	14.6412	9.01
3659958	Chain A, Human Lysozyme Mutant A96l	64.78	9.23	1	0	1	1	130	14.7332	9

157831552	Chain A, Human Lysozyme Mutant With Glu 35 Replaced By Ala	64.78	9.23	1	0	1	1	130	14.6331	9.17
157831551	Chain A, Human Lysozyme Mutant With Glu 35 Replaced By Asp	64.78	9.23	1	0	1	1	130	14.6771	9
157831554	Chain A, Human Lysozyme Mutant With Trp 109 Replaced By Ala	64.78	9.23	1	0	1	1	130	14.5761	9
157831553	Chain A, Human Lysozyme Mutant With Trp 109 Replaced By Phe	64.78	9.23	1	0	1	1	130	14.6521	9
13399627	Chain A, Mutant Human Lysozyme (A83kQ86DA92D)	64.78	9.23	1	0	1	1	130	14.7792	8.82
13399626	Chain A, Mutant Human Lysozyme (A92d)	64.78	9.23	1	0	1	1	130	14.7351	8.82
13399625	Chain A, Mutant Human Lysozyme (Q86d)	64.78	9.23	1	0	1	1	130	14.6781	8.82
1827553	Chain A, Mutant Human Lysozyme C77a	64.78	9.23	1	0	1	1	130	14.6592	9.14
5821956	Chain A, Mutant Human Lysozyme With Foreign N-Terminal Residues	64.78	9.23	1	0	1	1	130	14.6341	8.84
5821955	Chain A, Mutant Human Lysozyme With Foreign N-Terminal Residues	64.78	9.23	1	0	1	1	130	14.6941	8.84
157829561	Chain A, Role Of Arg 115 In The Catalytic Action Of Human Lysozyme. X-Ray Structure Of His 115 And Glu 115 Mutants	64.78	9.23	1	0	1	1	130	14.6721	8.82
157829563	Chain A, Role Of Arg 115 In The Catalytic Action Of Human Lysozyme. X-Ray Structure Of His 115 And Glu 115 Mutants	64.78	9.23	1	0	1	1	130	14.6641	8.66
157831824	Chain A, Role Of Proline Residues In Human Lysozyme Stability: A Scanning Calorimetric Study Combined With X-Ray Structure Analysis Of Proline Mutants	64.78	9.23	1	0	1	1	130	14.7172	9
157831820	Chain A, Role Of Proline Residues In Human Lysozyme Stability: A Scanning Calorimetric Study Combined With X-Ray Structure Analysis Of Proline Mutants	64.78	9.23	1	0	1	1	130	14.6891	9
50514025	Chain A, Structure Of T70n Human Lysozyme	64.78	9.23	1	0	1	1	130	14.7041	9

4930014	Chain A, T11a Mutant Human Lysozyme	64.78	9.23	1	0	1	1	130	14.6611	9
4930015	Chain A, T11v Mutant Human Lysozyme	64.78	9.23	1	0	1	1	130	14.6892	9
4930016	Chain A, T40a Mutant Human Lysozyme	64.78	9.23	1	0	1	1	130	14.6611	9
4930017	Chain A, T40v Mutant Human Lysozyme	64.78	9.23	1	0	1	1	130	14.6892	9
4930020	Chain A, T43a Mutant Human Lysozyme	64.78	9.23	1	0	1	1	130	14.6611	9
4930021	Chain A, T43v Mutant Human Lysozyme	64.78	9.23	1	0	1	1	130	14.6892	9
4930023	Chain A, T70v Mutant Human Lysozyme	64.78	9.23	1	0	1	1	130	14.6892	9
157831825	Chain A, The Crystal Structure Of A Mutant Lysozyme C77(Slash)95a With Increased Secretion Efficiency In Yeast	64.78	9.23	1	0	1	1	130	14.6272	9.31
6729883	Chain A, Verification Of Spmp Using Mutant Human Lysozymes	64.78	9.23	1	0	1	1	130	14.7622	9
6729882	Chain A, Verification Of Spmp Using Mutant Human Lysozymes	64.78	9.23	1	0	1	1	130	14.6752	9.17
157830185	Chain A, Verification Of Spmp Using Mutant Human Lysozymes	64.78	9.23	1	0	1	1	130	14.6791	9
6729885	Chain A, Verification Of Spmp Using Mutant Human Lysozymes	64.78	9.23	1	0	1	1	130	14.6902	9
385536	lysozyme {beta-sheet domain} [human, Peptide Mutagenesis, 130 aa]	64.78	9.23	1	0	1	1	130	14.6491	9
5821957	Chain A, Mutant Human Lysozyme With Foreign N-Terminal Residues	64.78	9.16	1	0	1	1	131	14.7482	9
7546189	Chain A, Crystal Structure Of Mutant Human Lysozyme With Four Extra Residues (Eaea) At The N-Terminal	64.78	8.96	1	0	1	1	134	15.0913	8.66
157831913	Chain A, Structural And Functional Analyses Of The Arg-Gly-Asp Sequence Introduced Into Human Lysozyme	64.78	8.96	1	0	1	1	134	15.1063	9

157831853	Chain A, Structure Of A Conformationally Constrained Arg-Gly-Asp Sequence Inserted Into Human Lysozyme	64.78	8.82	1	0	1	1	136	15.3124	8.78
157831914	Chain A, Structural And Functional Analyses Of The Arg-Gly-Asp Sequence Introduced Into Human Lysozyme	64.78	8.7	1	0	1	1	138	15.4325	9
4505821	prolactin-inducible protein precursor [Homo sapiens]	76.04	8.22	1	0	1	1	146	16.5618	8.05
307141	lysozyme precursor (EC 3.2.1.17) [Homo sapiens]	64.78	8.11	1	0	1	1	148	16.5442	9.16
847820	lysozyme precursor [Homo sapiens]	64.78	8.11	1	0	1	1	148	16.4292	8.98
119571952	glial fibrillary acidic protein, isoform CRA_a [Homo sapiens]	71.47	3.47	1	0	1	1	317	36.2764	5.74
119631362	NCK-associated protein 1, isoform CRA_f [Homo sapiens]	71.47	2.74	1	0	1	1	401	43.6169	5.03
119571954	glial fibrillary acidic protein, isoform CRA_c [Homo sapiens]	71.47	2.67	1	0	1	1	412	47.6105	5.5
38566198	GFAP protein [Homo sapiens]	71.47	2.55	1	0	1	1	431	49.7186	5.52
196115290	glial fibrillary acidic protein isoform 2 [Homo sapiens]	71.47	2.55	1	0	1	1	431	49.4776	6.13
16265836	glial fibrillary acidic protein [Homo sapiens]	71.47	2.55	1	0	1	1	432	49.7776	5.59
4503979	glial fibrillary acidic protein isoform 1 [Homo sapiens]	71.47	2.55	1	0	1	1	432	49.8496	5.52
62896925	glial fibrillary acidic protein variant [Homo sapiens]	71.47	2.55	1	0	1	1	432	49.8197	5.59
334688844	glial fibrillary acidic protein isoform 3 [Homo sapiens]	71.47	2.51	1	0	1	1	438	50.2578	5.67
4688900	sarcolectin [Homo sapiens]	71.47	2.35	1	0	1	1	469	51.3823	5.69

References

Aburatani, H. et al., 1997. Cloning and characterization of mammalian 8-hydroxyguanine-specific DNA glycosylase/apurinic, apyrimidinic lyase, a functional mutM homologue. *Cancer research*, 57(11), pp.2151-6. Available at: http://www.ncbi.nlm.nih.gov/pubmed/9187114.

Aka, P. et al., 2004. Are genetic polymorphisms in OGG1, XRCC1 and XRCC3 genes predictive for the DNA strand break repair phenotype and genotoxicity in workers exposed to low dose ionising radiations? *Mutation research*, 556(1-2), pp.169-81.

Alphalyse Inc, 2009. Common protein contaminants observed in mass spectrometric protein identification « Alphalyse Protein Analysis Blog. Available at: http://proteinanalysis.wordpress.com/2009/11/03/common-protein-contaminants-observed-in-mass-spectrometric-protein-identification/ [Accessed March 20, 2012].

Amouroux, R. et al., 2010. Oxidative stress triggers the preferential assembly of base excision repair complexes on open chromatin regions. *Nucleic acids research*, 38(9), pp.2878-90.

Arai, T. et al., 2006. The study using wild-type and Ogg1 knockout mice exposed to potassium bromate shows no tumor induction despite an extensive accumulation of 8-hydroxyguanine in kidney DNA. *Toxicology*, 221(2-3), pp.179-86.

Arnér, E.S. & Holmgren, a, 2000. Physiological functions of thioredoxin and thioredoxin reductase. *European journal of biochemistry / FEBS*, 267(20), pp.6102-9. Available at: http://www.ncbi.nlm.nih.gov/pubmed/11012661.

Barnes, D.E. & Lindahl, T., 2004. Repair and genetic consequences of endogenous DNA base damage in mammalian cells. *Annual review of genetics*, 38, pp.445-76. Available at: http://www.ncbi.nlm.nih.gov/pubmed/15568983 [Accessed June 20, 2011].

Barone, F., 2003. Influence of DNA torsional rigidity on excision of 7,8-dihydro-8-oxo-2'-deoxyguanosine in the presence of opposing abasic sites by human OGG1 protein. *Nucleic Acids Research*, 31(7), pp.1897-1903.

Bercht, M. et al., 2007. Is the repair of oxidative DNA base modifications inducible by a preceding DNA damage induction? *DNA repair*, 6(3), pp.367-73. Available at: http://www.ncbi.nlm.nih.gov/pubmed/17197252 [Accessed February 26, 2012].

Bessho, T. et al., 1993. Evidence for two DNA repair enzymes for 8-hydroxyguanine (7,8-dihydro-8-oxoguanine) in human cells. *The Journal of biological chemistry*, 268(26), pp.19416-21. Available at: http://www.ncbi.nlm.nih.gov/pubmed/8366089.

Bhakat, K.K. et al., 2006. Acetylation of Human 8-Oxoguanine-DNA Glycosylase by p300 and Its Role in 8-Oxoguanine Repair In Vivo Acetylation of Human 8-Oxoguanine-DNA Glycosylase by p300 and Its Role in 8-Oxoguanine Repair In Vivo. *Society*, 26(5), pp.1654-1665.

Bjorâs, M. et al., 1997. Opposite base-dependent reactions of a human base excision repair enzyme on DNA containing 7,8-dihydro-8-oxoguanine and abasic sites. *The EMBO journal*, 16(20), pp.6314-22.

Blainey, P.C. et al., 2006. A base-excision DNA-repair protein finds intrahelical lesion bases by fast sliding in contact with DNA. *Proceedings of the National Academy of Sciences of the United States of America*, 103(15), pp.5752-7.

Bohr, V. a, Stevnsner, T. & de Souza-Pinto, N.C., 2002. Mitochondrial DNA repair of oxidative damage in mammalian cells. *Gene*, 286(1), pp.127-34. Available at: http://www.ncbi.nlm.nih.gov/pubmed/11978482.

Boiteux, S. & Radicella, J P, 2000. The human OGG1 gene: structure, functions, and its implication in the process of carcinogenesis. *Archives of biochemistry and biophysics*, 377(1), pp.1-8. Available at: http://www.ncbi.nlm.nih.gov/pubmed/10775435 [Accessed July 26, 2011].

Bravard, A. et al., 2010. Inactivation by oxidation and recruitment into stress granules of hOGG1 but not APE1 in human cells exposed to sub-lethal concentrations of cadmium. *Mutation research*, 685(1-2), pp.61-9. Available at: http://www.ncbi.nlm.nih.gov/pubmed/19800894 [Accessed February 26, 2012].

Bravard, A., Vacher, M., Moritz, E., Vaslin, L., Hall, J., Epe, B. & Radicella, J Pablo, 2009a. Oxidation status of human OGG1-S326C polymorphic variant determines cellular DNA repair capacity. *Cancer research*, 69(8), pp.4-8.

Bravard, A., Vacher, M., Moritz, E., Vaslin, L., Hall, J., Epe, B. & Radicella, J Pablo, 2009b. Oxidation status of human OGG1-S326C polymorphic variant determines cellular DNA repair capacity. *Cancer research*, 69(8), pp.3642-9. Available at: http://www.ncbi.nlm.nih.gov/pubmed/19351836 [Accessed January 13, 2012].

Bravard, A. et al., 2006. Redox regulation of human OGG1 activity in response to cellular oxidative stress. *Molecular and cellular biology*, 26(20), pp.7430-6. Available at: http://www.pubmedcentral.nih.gov/articlerender.fcgi?artid=1636869&tool=pmcentrez&rendertype=abstract [Accessed July 24, 2011].

Bruner, S D, Norman, D.P. & Verdine, G L, 2000. Structural basis for recognition and repair of the endogenous mutagen 8-oxoguanine in DNA. *Nature*, 403(6772), pp.859-66. Available at: http://www.ncbi.nlm.nih.gov/pubmed/10706276.

Campalans, A. et al., 2007. UVA irradiation induces relocalisation of the DNA repair protein hOGG1 to nuclear speckles. *Journal of cell science*, 120(Pt 1), pp.23-32. Available at: http://www.ncbi.nlm.nih.gov/pubmed/17148573 [Accessed July 26, 2011].

Chatterjee, A. et al., 2006. Targeting of mutant hogg1 in mammalian mitochondria and nucleus: effect on cellular survival upon oxidative stress. *BMC cancer*, 6, p.235. Available at: http://www.pubmedcentral.nih.gov/articlerender.fcgi?artid=1633743&tool=pmcentrez&rendertype=abstract [Accessed February 16, 2012].

Chen, L. et al., 2002. Direct Visualization of a DNA Glycosylase Searching for Damage. *Science*, 9(02), pp.345-350.

Collins, a R. et al., 2001. Inter-individual differences in repair of DNA base oxidation, measured in vitro with the comet assay. *Mutagenesis*, 16(4), pp.297-301. Available at: http://www.ncbi.nlm.nih.gov/pubmed/11420396.

Colussi, C. et al., 2002. Removes DNA 8-oxodGMP Incorporated from the Oxidized dNTP Pool. *Current*, 12(02), pp.912-918.

Conlon, K., Zharkov, Dmitry O & Berrios, M., 2004. Cell cycle regulation of the murine 8-oxoguanine DNA glycosylase (mOGG1): mOGG1 associates with microtubules during interphase and mitosis. *DNA repair*, 3(12), pp.1601-15. Available at: http://www.ncbi.nlm.nih.gov/pubmed/15474421 [Accessed February 26, 2012].

Conlon, K. a., Zharkov, Dmitry O. & Berrios, M., 2003. Immunofluorescent localization of the murine 8-oxoguanine DNA glycosylase (mOGG1) in cells growing under normal and nutrient deprivation conditions. *DNA Repair*, 2(12), pp.1337-1352. Available at: http://linkinghub.elsevier.com/retrieve/pii/S1568786403001617 [Accessed February 26, 2012].

Dahle, J. et al., 2008. Overexpression of human OGG1 in mammalian cells decreases ultraviolet A induced mutagenesis. *Cancer letters*, 267(1), pp.18-25. Available at: http://www.ncbi.nlm.nih.gov/pubmed/18406515 [Accessed February 26, 2012].

Daimon, M. et al., 2009. Association of the Ser326Cys polymorphism in the OGG1 gene with type 2 DM. *Biochemical and biophysical research communications*, 386(1), pp.26-9. Available at: http://www.ncbi.nlm.nih.gov/pubmed/19486888 [Accessed February 26, 2012].

Dantzer, F. et al., 2002. Human OGG1 undergoes serine phosphorylation and associates with the nuclear matrix and mitotic chromatin in vivo. *Nucleic acids research*, 30(11), pp.2349-57. Available at: http://www.pubmedcentral.nih.gov/articlerender.fcgi?artid=117190&tool=pmcentrez&rendertype=abstract.

David, S.S., O'Shea, V.L. & Kundu, S., 2007. Base-excision repair of oxidative DNA damage. *Nature*, 447(7147), pp.941-50. Available at: http://www.pubmedcentral.nih.gov/articlerender.fcgi?artid=2896554&tool=pmcentrez&rendertype=abstract [Accessed June 13, 2011].

Dherin, C. et al., 1999. Excision of oxidatively damaged DNA bases by the human alpha-hOgg1 protein and the polymorphic alpha-hOgg1(Ser326Cys) protein which is frequently found in human populations. *Nucleic acids research*, 27(20), pp.4001-7. Available at: http://www.pubmedcentral.nih.gov/articlerender.fcgi?artid=148667&tool=pmcentrez&rendertype=abstract.

Dherin, C. et al., 2000. Repair of oxidative DNA damage in Drosophila melanogaster: identification and characterization of dOgg1, a second DNA glycosylase activity for 8-hydroxyguanine and formamidopyrimidines. *Nucleic acids research*, 28(23), pp.4583-92. Available at: http://www.pubmedcentral.nih.gov/articlerender.fcgi?artid=115177&tool=pmcentrez&rendertype=abstract.

Dhénaut, a, Boiteux, S. & Radicella, J P, 2000. Characterization of the hOGG1 promoter and its expression during the cell cycle. *Mutation research*, 461(2), pp.109-18. Available at: http://www.ncbi.nlm.nih.gov/pubmed/11765003.

Dianov, G. et al., 1998. Repair pathways for processing of 8-oxoguanine in DNA by mammalian cell extracts. *The Journal of biological chemistry*, 273(50), pp.33811-6. Available at: http://www.ncbi.nlm.nih.gov/pubmed/9837971.

Dickinson, D.P. & Thiesse, M., 1995. A major human lacrimal gland mRNA encodes a new proline-rich protein family member. *Investigative ophthalmology & visual science*, 36(10), pp.2020-31. Available at: http://www.ncbi.nlm.nih.gov/pubmed/7544782.

Dou, H., Mitra, S. & Hazra, T.K., 2003. Repair of oxidized bases in DNA bubble structures by human DNA glycosylases NEIL1 and NEIL2. *The Journal of biological chemistry*, 278(50), pp.49679-84. Available at: http://www.ncbi.nlm.nih.gov/pubmed/14522990 [Accessed October 10, 2011].

Dröge, W., 2002. Free radicals in the physiological control of cell function. *Physiological reviews*, 82(1), pp.47-95. Available at: http://www.ncbi.nlm.nih.gov/pubmed/11773609.

Faucher, F. et al., 2009. Crystal structures of two archaeal 8-oxoguanine DNA glycosylases provide structural insight into guanine/8-oxoguanine distinction. *Structure (London, England : 1993)*, 17(5), pp.703-12. Available at: http://www.pubmedcentral.nih.gov/articlerender.fcgi?artid=2758660&tool=pmcentrez&rendertype=abstract [Accessed February 3, 2012].

Faucher, F., Wallace, S.S. & Doublié, S., 2010. The C-terminal lysine of Ogg2 DNA glycosylases is a major molecular determinant for guanine/8-oxoguanine distinction. *Journal of molecular biology*, 397(1), pp.46-56. Available at: http://www.pubmedcentral.nih.gov/articlerender.fcgi?artid=3085930&tool=pmcentrez&rendertype=abstract [Accessed February 26, 2012].

Fung, H., Bennet, R.A.O. & Demple, B., 2001. Key Role of a Downstream Specificity Protein 1 Site in Cell Cycle regulated Transcription of the AP Endonuclease Gene APE1/APEX in NIH3T3 Cells. *Journal of Biological Chemistry*, 276(45), pp.42011-42017. Available at: http://www.jbc.org/content/276/45/42011.full.pdf [Accessed March 23, 2012].

Gerner, C. et al., 2002. Proteome analysis of nuclear matrix proteins during apoptotic chromatin condensation. *Cell death and differentiation*, 9(6), pp.671-81. Available at: http://www.ncbi.nlm.nih.gov/pubmed/12032676 [Accessed March 23, 2012].

Global Proteomics Machine, 2011. common Repository of Adventitious Proteins (cRAP). Available at: http://www.thegpm.org/crap/index.html [Accessed March 20, 2012].

Green, R.M. et al., 2006. Subcellular compartmentalization of glutathione: correlations with parameters of oxidative stress related to genotoxicity. *Mutagenesis*, 21(6), pp.383-90. Available at: http://www.ncbi.nlm.nih.gov/pubmed/17012304 [Accessed November 8, 2011].

Grollman, A.P. & Moriya, M., 1993. Mutagenesis by 8-oxoguanine: an enemy within. *Plasmid*, 9(7), pp.7-10.

Habib, S.L., 2009. Molecular mechanism of regulation of OGG1: tuberin deficiency results in cytoplasmic redistribution of transcriptional factor NF-YA. *Journal of molecular signaling*, 4, p.8. Available at: http://www.pubmedcentral.nih.gov/articlerender.fcgi?artid=2807420&tool=pmcentrez&rendertype=abstract [Accessed February 26, 2012].

Habib, S.L. et al., 2003. Reduced constitutive 8-oxoguanine-DNA glycosylase expression and impaired induction following oxidative DNA damage in the tuberin deficient Eker rat. *Carcinogenesis*, 24(3), pp.573-82. Available at: http://www.ncbi.nlm.nih.gov/pubmed/12663520.

Habib, S.L. et al., 2008. Tuberin regulates the DNA repair enzyme OGG1. *American journal of physiology. Renal physiology*, 294(1), pp.F281-90. Available at: http://www.ncbi.nlm.nih.gov/pubmed/17989114 [Accessed February 26, 2012].

Hashiguchi, K. et al., 2004. The C-terminal alphaO helix of human Ogg1 is essential for 8-oxoguanine DNA glycosylase activity: the mitochondrial beta-Ogg1 lacks this domain and does not have glycosylase activity. *Nucleic acids research*, 32(18), pp.5596-608. Available at: http://www.pubmedcentral.nih.gov/articlerender.fcgi?artid=524278&tool=pmcentrez&rendertype=abstract [Accessed January 25, 2012].

Hazra, T.K. et al., 2002. Identification and characterization of a human DNA glycosylase for repair of modified bases in oxidatively damaged DNA. *Proceedings of the National Academy of Sciences of the United States of America*, 99(6), pp.3523-8. Available at: http://www.pubmedcentral.nih.gov/articlerender.fcgi?artid=122556&tool=pmcentrez&rendertype=abstract [Accessed January 30, 2012].

Hill, J W et al., 2001. Stimulation of human 8-oxoguanine-DNA glycosylase by AP-endonuclease: potential coordination of the initial steps in base excision repair. *Nucleic acids research*, 29(2), pp.430-8. Available at: http://www.pubmedcentral.nih.gov/articlerender.fcgi?artid=29662&tool=pmcentrez&rendertype=abstract [Accessed December 19, 2011].

Hill, Jeff W & Evans, M.K., 2006. Dimerization and opposite base-dependent catalytic impairment of polymorphic S326C OGG1 glycosylase. *Nucleic acids research*, 34(5), pp.1620-32. Available at: http://www.pubmedcentral.nih.gov/articlerender.fcgi?artid=1405821&tool=pmcentrez&rendertype=abstract [Accessed January 30, 2012].

Hirano, T., 2008. Repair System of 7, 8-Dihydro-8-Oxoguanine as a Defense Line against Carcinogenesis. *Journal of Radiation Research*, 49(4), pp.329-340. Available at: http://joi.jlc.jst.go.jp/JST.JSTAGE/jrr/08049?from=CrossRef [Accessed February 11, 2012].

Hodges, N.J., 2002. Down-regulation of the DNA-repair endonuclease 8-oxo-guanine DNA glycosylase 1 (hOGG1) by sodium dichromate in cultured human A549 lung carcinoma cells. *Carcinogenesis*, 23(1), pp.55-60. Available at: http://carcin.oxfordjournals.org/cgi/content/abstract/23/1/55 [Accessed January 30, 2012].

Hollenbach, S. et al., 1999. Overexpression of Ogg1 in mammalian cells: effects on induced and spontaneous oxidative DNA damage and mutagenesis. *Carcinogenesis*, 20(9),

pp.1863-1868. Available at: http://carcin.oxfordjournals.org/cgi/content/abstract/20/9/1863 [Accessed January 30, 2012].

Hollis, T., Ichikawa, Y. & Ellenberger, T., 2000. DNA bending and a flip-out mechanism for base excision by the helix – hairpin – helix DNA glycosylase , Escherichia coli AlkA. , 19(4), pp.758-766.

Hooten, N.N. et al., 2011. Poly(ADP-ribose) Polymerase 1 (PARP-1) Binds to 8-Oxoguanine-DNA Glycosylase (OGG1). *The Journal of biological chemistry*, 286(52), pp.44679-90. Available at: http://www.jbc.org/cgi/content/abstract/286/52/44679 [Accessed January 23, 2012].

Hu, J. et al., 2005. Phosphorylation of human oxoguanine DNA glycosylase (alpha-OGG1) modulates its function. *Nucleic acids research*, 33(10), pp.3271-82. Available at: http://www.pubmedcentral.nih.gov/articlerender.fcgi?artid=1143695&tool=pmcentrez&rendertype=abstract [Accessed November 22, 2011].

Hung, C.-R., Chen, W.-H. & Wang, P.S., 2007. Protective effect of lysozyme chloride on gastric oxidative stress and hemorrhagic ulcers in severe atherosclerotic rats. *MedSciMonit*, 13(12), pp.271-280.

Ibelguafts, H., 2011. Sarcolectin (Cytokines & Cells Encyclopedia - COPE). *Cytokines & Cells Online Pathfinder Encyclopeadia*, p.Sarcolectin. Available at: http://www.copewithcytokines.de/cope.cgi?key=Sarcolectin [Accessed March 22, 2012].

Invitria, 2010. Lysozyme Is a Powerful Antimicrobial Commonly Used as a Preservative in Foods and Beverages And as a Microbial Cell Lysis Reagent. , p.Lysozyme. Available at: http://www.invitria.com/products-and-services/lysozyme.html [Accessed March 22, 2012].

Jarem, D. a et al., 2011. Incidence and persistence of 8-oxo-7,8-dihydroguanine within a hairpin intermediate exacerbates a toxic oxidation cycle associated with trinucleotide repeat expansion. *DNA repair*, 10(8), pp.887-96.

Jarem, D. a, Wilson, N.R. & Delaney, S., 2009. Structure-dependent DNA damage and repair in a trinucleotide repeat sequence. *Biochemistry*, 48(28), pp.6655-63. Available at: http://www.ncbi.nlm.nih.gov/pubmed/19527055 [Accessed November 17, 2011].

Jensen, A. et al., 2012. Influence of the OGG1 Ser326Cys polymorphism on oxidatively damaged DNA and repair activity. *Free radical biology & medicine*, 52(1), pp.118-25. Available at: http://www.ncbi.nlm.nih.gov/pubmed/22019439 [Accessed February 26, 2012].

Kamiya, H. et al., 1992. c-Ha-ras containing 8-hydroxyguanine at codon 12 induces point mutations at the modified and adjacent positions. *Cancer research*, 52(12), pp.3483-5. Available at: http://www.ncbi.nlm.nih.gov/pubmed/1596906.

Kasai, H. et al., 1986. Formation of 8-hydroxyguanine moiety in cellular DNA by agests producting oxygen radicals and evidence for its repair. *Carcinogenesis*, 7(11), pp.1849-1851.

Kasai, H. & Nishimura, S., 1984. Hydroxylation of deoxyguanosine at the C-8 position by ascorbic acid and other reducing agents. *Nucleic Acids Research*, 12(4), pp.2137-2145. Available at: http://nar.oxfordjournals.org/cgi/content/abstract/12/4/2137 [Accessed March 20, 2012].

Keller, B.O. et al., 2008. Interferences and contaminants encountered in modern mass spectrometry. *Analytica chimica acta*, 627(1), pp.71-81. Available at: http://www.ncbi.nlm.nih.gov/pubmed/18790129 [Accessed March 14, 2012].

van der Kemp, P.A. et al., 2004. Catalytic and DNA-binding properties of the human Ogg1 DNA N-glycosylase/AP lyase: biochemical exploration of H270, Q315 and F319, three amino acids of the 8-oxoguanine-binding pocket. *Nucleic acids research*, 32(2), pp.570-8. Available at: http://www.pubmedcentral.nih.gov/articlerender.fcgi?artid=373348&tool=pmcentrez&rendertype=abstract [Accessed February 11, 2012].

Kershaw, R.M., 2011. *Delayed response of the Cys326 variant of the DNA repair protein OGG1 to cellular oxidative stress By*. University of Birmingham.

Khobta, A. et al., 2009. 8-Oxoguanine DNA glycosylase (Ogg1) causes a transcriptional inactivation of damaged DNA in the absence of functional Cockayne syndrome B (Csb) protein. *DNA repair*, 8(3), pp.309-17. Available at: http://www.ncbi.nlm.nih.gov/pubmed/19061977 [Accessed February 26, 2012].

Kim, P.M., 2001. Overexpression of human RAD51 and RAD52 reduces double-strand break-induced homologous recombination in mammalian cells. *Nucleic Acids Research*, 29(21), pp.4352-4360. Available at: http://nar.oxfordjournals.org/cgi/content/abstract/29/21/4352 [Accessed March 23, 2012].

Kim, S.-R. et al., 2004. Suppression of chemically induced and spontaneously occurring oxidative mutagenesis by three alleles of human OGG1 gene encoding 8-hydroxyguanine DNA glycosylase. *Mutation research*, 554(1-2), pp.365-74. Available at: http://www.ncbi.nlm.nih.gov/pubmed/15450432 [Accessed February 26, 2012].

Kitamura, Y. et al., 1997. Interaction of Nck-associated protein 1 with activated GTP-binding protein Rac. *In Vitro*, 878, pp.873-878.

Kitano, T. et al., 2006. Origin and evolution of gene for prolactin-induced protein. *Gene*, 383, pp.64-70. Available at: http://www.ncbi.nlm.nih.gov/pubmed/16949771 [Accessed March 22, 2012].

Klaunig, J.E. et al., 2011. Oxidative stress and oxidative damage in chemical carcinogenesis. *Toxicology and applied pharmacology*, 254(2), pp.86-99. Available at: http://www.ncbi.nlm.nih.gov/pubmed/21296097 [Accessed July 26, 2011].

Klungland, A. & Bjelland, S., 2007. Oxidative damage to purines in DNA: role of mammalian Ogg1. *DNA repair*, 6(4), pp.481-8. Available at: http://www.ncbi.nlm.nih.gov/pubmed/17127104 [Accessed February 26, 2012].

Kohno, T. et al., 2006. Association of the OGG1-Ser326Cys polymorphism with lung adenocarcinoma risk. *Cancer science*, 97(8), pp.724-8. Available at: http://www.ncbi.nlm.nih.gov/pubmed/16800823 [Accessed March 27, 2012].

Korichneva, I., 2005. Redox regulation of cardiac protein kinase C. *Experimental and clinical cardiology*, 10(4), pp.256-61. Available at: /pmc/articles/PMC2716239/?report=abstract

Kuznetsov, N. a et al., 2007. Kinetic conformational analysis of human 8-oxoguanine-DNA glycosylase. *The Journal of biological chemistry*, 282(2), pp.1029-38. Available at: http://www.ncbi.nlm.nih.gov/pubmed/17090545 [Accessed December 7, 2011].

Kuznetsov, N. a et al., 2005. Kinetics of substrate recognition and cleavage by human 8-oxoguanine-DNA glycosylase. *Nucleic acids research*, 33(12), pp.3919-31. Available at: http://www.pubmedcentral.nih.gov/articlerender.fcgi?artid=1176011&tool=pmcentrez&rendertype=abstract [Accessed December 12, 2011].

Larsen, E. et al., 2006. Repair and mutagenesis at oxidized DNA lesions in the developing brain of wild-type and Ogg1-/- mice. *Oncogene*, 25(17), pp.2425-32. Available at: http://www.ncbi.nlm.nih.gov/pubmed/16369492 [Accessed December 14, 2011].

Lee, A.J., Hodges, Nikolas J & Chipman, James K, 2005. Interindividual variability in response to sodium dichromate-induced oxidative DNA damage: role of the Ser326Cys polymorphism in the DNA-repair protein of 8-oxo-7,8-dihydro-2'-deoxyguanosine DNA glycosylase 1. *Cancer epidemiology, biomarkers & prevention : a publication of the American Association for Cancer Research, cosponsored by the American Society of Preventive Oncology*, 14(2), pp.497-505.

Lenton, K.J., 1999. Glutathione and ascorbate are negatively correlated with oxidative DNA damage in human lymphocytes. *Carcinogenesis*, 20(4), pp.607-613. Available at: http://carcin.oxfordjournals.org/cgi/content/abstract/20/4/607 [Accessed March 19, 2012].

Li, H. et al., 2008. The hOGG1 Ser326Cys polymorphism and lung cancer risk: a meta-analysis. *Cancer epidemiology, biomarkers & prevention : a publication of the American Association for Cancer Research, cosponsored by the American Society of Preventive Oncology*, 17(7), pp.1739-45. Available at: http://www.ncbi.nlm.nih.gov/pubmed/18628426 [Accessed March 27, 2012].

Liu, H. et al., 2006. Amelioration of oxidant stress by the defensin lysozyme. *American journal of physiology. Endocrinology and metabolism*, 290(5), pp.E824-32. Available at: http://www.ncbi.nlm.nih.gov/pubmed/16317028 [Accessed March 22, 2012].

van Loon, B., Markkanen, E. & Hübscher, U., 2010. Oxygen as a friend and enemy: How to combat the mutational potential of 8-oxo-guanine. *DNA repair*, 9(6), pp.604-16. Available at: http://www.ncbi.nlm.nih.gov/pubmed/20399712 [Accessed June 20, 2011].

Lu, R., Nash, H.M. & Verdine, G L, 1997. A mammalian DNA repair enzyme that excises oxidatively damaged guanines maps to a locus frequently lost in lung cancer. *Current biology : CB*, 7(6), pp.397-407.

Luna, L. et al., 2005. Dynamic relocalization of hOGG1 during the cell cycle is disrupted in cells harbouring the hOGG1-Cys326 polymorphic variant. *Nucleic acids research*, 33(6), pp.1813-24.

Mabley, J.G. et al., 2004. Potential role for 8-oxoguanine DNA glycosylase in regulating inflammation. *The FASEB Journal*, 18, pp.1-18.

Maga, G. et al., 2007. 8-oxo-guanine bypass by human DNA polymerases in the presence of auxiliary proteins. *Nature*, 447(7144), pp.606-8.

Maga, G. et al., 2008. Replication protein A and proliferating cell nuclear antigen coordinate DNA polymerase selection in 8-oxo-guanine repair. *Proceedings of the National Academy of Sciences*, 105(52), pp.4-9.

Martelli, a M. et al., 2001. Nuclear apoptotic changes: an overview. *Journal of cellular biochemistry*, 82(4), pp.634-46. Available at: http://www.ncbi.nlm.nih.gov/pubmed/11500941.

Martínez-Alfaro, M. et al., 2006. Correlation between formamidopyrimidine DNA glycosylase (Fpg)-sensitive sites determined by a comet assay, increased MDA, and decreased glutathione during long exposure to thinner inhalation. *Toxicology letters*, 163(3), pp.198-205.

Michaels, M.L.E.O. & Miller, Jeffrey H, 1992. The GO System Protects Organisms from the Mutagenic Effect of the Spontaneous Lesion 10I0 I I. *Microbiology*, 174(20), pp.6321-6325.

Mikkelsen, L. et al., 2009. Aging and defense against generation of 8-oxo-7,8-dihydro-2'-deoxyguanosine in DNA. *Free radical biology & medicine*, 47(5), pp.608-15.

Miller, John H et al., 2003. 8-Oxoguanine Enhances Bending of DNA that Favors Binding to Glycosylases. *Journal of American Chemistry*, 125(5), pp.6331-6336.

Mirbahai, L. et al., 2010. Use of a molecular beacon to track the activity of base excision repair protein OGG1 in live cells. *DNA repair*, 9(2), pp.144-52. Available at: http://www.ncbi.nlm.nih.gov/pubmed/20042377 [Accessed January 27, 2012].

Morland, I. et al., 2002. Human DNA glycosylases of the bacterial Fpg / MutM superfamily : an alternative pathway for the repair of 8-oxoguanine and other oxidation products in DNA Ê s and Sequence analysis. *Analysis*, 30(22), pp.4926-4936.

Mukherjee, B. et al., 2006. DNA-PK phosphorylates histone H2AX during apoptotic DNA fragmentation in mammalian cells. *DNA repair*, 5(5), pp.575-90.

Ni, T.T., Marsischky, G.T. & Kolodner, R.D., 1999. MSH2 and MSH6 Are Required for Removal of Adenine Misincorporated Opposite 8-Oxo-Guanine in S. cerevisiae. *Molecular Cell*, 4(3), pp.439-444.

Nishimura, S., 2003. Serial Review : Oxidative DNA Damage and Repair 8-HYDROXYGUANINE RESIDUE IN DNA. *Free Radical Biology & Medicine*, 32(9), pp.813-821.

Nishioka, K. et al., 1999. Expression and differential intracellular localization of two major forms of human 8-oxoguanine DNA glycosylase encoded by alternatively spliced OGG1 mRNAs. *Molecular biology of the cell*, 10(5), pp.1637-52.

Norman, D.P.G., Bruner, Steven D & Verdine, Gregory L, 2001. Coupling of Substrate Recognition and Catalysis by a Human Base-Excision DNA Repair Protein. *Society*, (1), pp.359-360.

Oka, S. et al., 2008. Two distinct pathways of cell death triggered by oxidative damage to nuclear and mitochondrial DNAs. *The EMBO journal*, 27(2), pp.421-32. Available at: http://www.pubmedcentral.nih.gov/articlerender.fcgi?artid=2234344&tool=pmcentrez&rendertype=abstract [Accessed August 4, 2011].

Osterod, M. et al., 2002. A global DNA repair mechanism involving the Cockayne syndrome B (CSB) gene product can prevent the in vivo accumulation of endogenous oxidative DNA base damage. *Oncogene*, 21(54), pp.8232-9.

Le Page, F. et al., 2000. Transcription coupled repair of 8-oxoguanine in murine cells: the ogg1 protein is required for repair in nontranscribed sequences but not in transcribed sequences. *Proceedings of the National Academy of Sciences of the United States of America*, 97(15), pp.8397-402.

Park, M.J. et al., 2009. Repair activities of human 8-oxoguanine DNA glycosylase are stimulated by the interaction with human checkpoint sensor Rad9-Rad1-Hus1 complex. *DNA repair*, 8(10), pp.1190-200.

Priestley, C.C. et al., 2010. Anomalous genotoxic responses induced in mouse lymphoma L5178Y cells by potassium bromate. *Toxicology*, 267(1-3), pp.45-53.

Pu, Y.-S. et al., 2007. 8-Oxoguanine DNA glycosylase and MutY homolog are involved in the incision of arsenite-induced DNA adducts. *Toxicological sciences : an official journal of the Society of Toxicology*, 95(2), pp.376-82.

Rachek, L.I. et al., 2002. Conditional targeting of the DNA repair enzyme hOGG1 into mitochondria. *The Journal of biological chemistry*, 277(47), pp.44932-7.

Rachek, L.I. et al., 2006. Protection of INS-1 Cells From Free Fatty Acis-induced Apoptosis by targeting hOGG1 to Mitochondria. *Diabetes*, 55, pp.1022-1028.

Radak, Z. & Boldogh, I., 2010. 8-Oxo-7,8-dihydroguanine: links to gene expression, aging, and defense against oxidative stress. *Free radical biology & medicine*, 49(4), pp.587-96.

Radom, C.T., Banerjee, A. & Verdine, Gregory L, 2007. Structural characterization of human 8-oxoguanine DNA glycosylase variants bearing active site mutations. *The Journal of biological chemistry*, 282(12), pp.9182-94.

Robertson, J.D., Orrenius, S. & Zhivotovsky, B., 2000. Review: nuclear events in apoptosis. *Journal of structural biology*, 129(2-3), pp.346-58.

Rosenquist, T. a, Zharkov, D O & Grollman, a P., 1997. Cloning and characterization of a mammalian 8-oxoguanine DNA glycosylase. *Proceedings of the National Academy of Sciences of the United States of America*, 94(14), pp.7429-34.

Russo, M.T. et al., 2007. Different DNA repair strategies to combat the threat from 8-oxoguanine. *Mutation research*, 614(1-2), pp.69-76. Available at: http://www.ncbi.nlm.nih.gov/pubmed/16769088 [Accessed January 12, 2012].

STRING, STRING: functional protein association networks. , p.OGG1. Available at: http://string-

db.org/newstring_cgi/show_input_page.pl?UserId=W055Xo6tcADn&sessionId=_Pn3IXkHI_Ct [Accessed March 28, 2012].

ScienceDaily, 2010. Radical (chemistry). , p.Science Reference: Radical. Available at: http://www.sciencedaily.com/articles/r/radical_(chemistry).htm [Accessed March 27, 2012].

Seeberg, E. et al., 2002. Reciprocal Flipping'' Underlies Substrate Recognition and Catalytic Activation by the Human 8-Oxo-guanine DNA Glycosylase. *Journal of molecular biology*, 317, pp.171-177.

Shimizu, Y. et al., 2010. Stimulation of DNA Glycosylase Activities by XPC Protein Complex: Roles of Protein-Protein Interactions. *Journal of nucleic acids*, 2010. Available at: /pmc/articles/PMC2925305/?report=abstract [Accessed March 19, 2012].

Sidorenko, Viktoriya S et al., 2009. Substrate specificity and excision kinetics of natural polymorphic variants and phosphomimetic mutants of human 8-oxoguanine-DNA glycosylase. *The FEBS journal*, 276(18), pp.5149-62.

Sidorenko, Victoria S, Nevinsky, G. a & Zharkov, Dmitry O, 2007. Mechanism of interaction between human 8-oxoguanine-DNA glycosylase and AP endonuclease. *DNA repair*, 6(3), pp.317-28. Available at: http://www.ncbi.nlm.nih.gov/pubmed/17126083 [Accessed February 26, 2012].

Simone, S. et al., 2008. Mechanism of Oxidative DNA Damage in Diabetes. *Diabetes*, 57(October), p.2626.

Simonelli, V. et al., 2011. Gene susceptibility to oxidative damage: From single nucleotide polymorphisms to function. *Mutation research*, 731(1-2), pp.1-13. Available at: http://www.ncbi.nlm.nih.gov/pubmed/22155132 [Accessed January 13, 2012].

Smart, D.J., Chipman, J K & Hodges, N J, 2006. Activity of OGG1 variants in the repair of pro-oxidant-induced 8-oxo-2'-deoxyguanosine. *DNA repair*, 5(11), pp.1337-45. Available at: http://www.ncbi.nlm.nih.gov/pubmed/16861056 [Accessed February 26, 2012].

Sokhansanj, B. a et al., 2002. A quantitative model of human DNA base excision repair. I. Mechanistic insights. *Nucleic acids research*, 30(8), pp.1817-25. Available at: http://www.pubmedcentral.nih.gov/articlerender.fcgi?artid=113225&tool=pmcentrez&rendertype=abstract.

de Souza-Pinto, N.C. et al., 2009. The recombination protein RAD52 cooperates with the excision repair protein OGG1 for the repair of oxidative lesions in mammalian cells. *Molecular and cellular biology*, 29(16), pp.4441-54.

Souza-pinto, N.C.D. et al., 2001. Repair of 8-Oxodeoxyguanosine Lesions in Mitochondrial DNA Depends on the Oxoguanine DNA Glycosylase (OGG1) Gene and 8-Oxoguanine Accumulates in the Mitochondrial DNA of OGG1-defective Mice. *DNA Repair*, 61, pp.5378-5381.

Tackett, A.J. et al., 2005. I-DIRT , A General Method for Distinguishing between Specific and Nonspecific Protein Interactions research articles. *Journal of Proteome Research*, pp.1752-1756.

Thameem, F. et al., 2010. The Ser(326)Cys Polymorphism of 8-Oxoguanine Glycosylase 1 (OGG1) Is Associated with Type 2 Diabetes in Mexican Americans. *Human heredity*, 70(2), pp.97-101.

ThermoScientific, 2010. Selection Guide for Immunoprecipitation Kits. Available at: http://www.piercenet.com/browse.cfm?fldID=FE0FBC6F-61BB-41DF-AD2E-008247C95177 [Accessed March 28, 2012].

Trinkle-Mulcahy, L. et al., 2008. Identifying specific protein interaction partners using quantitative mass spectrometry and bead proteomes. *The Journal of cell biology*, 183(2), pp.223-39.

U.S National Library of Medicine, 2008. GFAP - glial fibrillary acidic protein. *Genetics Home Reference*, p.GFAP. Available at: http://ghr.nlm.nih.gov/gene/GFAP [Accessed March 22, 2012].

Vijay H, Wang Mu, Mian I. Saira, Spyres Lea, D.W.A., 2006. The high binding affinity of human ribosomal protein S3 to 7,8-dihydro-8-oxoguanine is abrogated by a single amino acid change 10.1016/j.dnarep.2006.04.001 : DNA Repair | ScienceDirect.com. *DNA repair*, pp.810-815.

Wang, D., Kreutzer, D.A. & Essigmann, J.M., 1998. Mutagenicity and repair of oxidative DNA damage: insights from studies using defined lesions. *Mutation Research/Fundamental and Molecular Mechanisms of Mutagenesis*, 400(1-2), pp.99-115.

Will, O. et al., 1999. Influence of glutathione levels and heat-shock on the steady-state levels of oxidative DNA base modifications in mammalian cells. *Carcinogenesis*, 20(2), pp.333-7. Available at: http://www.ncbi.nlm.nih.gov/pubmed/10069473.

Wrońska-Nofer, T. et al., 2012. Oxidative DNA damage and oxidative stress in subjects occupationally exposed to nitrous oxide (N(2)O). *Mutation research*, 731(1-2), pp.58-63. Available at: http://www.ncbi.nlm.nih.gov/pubmed/22085808 [Accessed February 26, 2012].

Youn, C.-K. et al., 2005. Cadmium down-regulates human OGG1 through suppression of Sp1 activity. *The Journal of biological chemistry*, 280(26), pp.25185-95. Available at: http://www.ncbi.nlm.nih.gov/pubmed/15760895 [Accessed January 13, 2012].

Youn, C.-K. et al., 2007. Human 8-oxoguanine DNA glycosylase suppresses the oxidative stress induced apoptosis through a p53-mediated signaling pathway in human fibroblasts. *Molecular cancer research : MCR*, 5(10), pp.1083-98.

Zharkov, D O et al., 2000. Substrate specificity and reaction mechanism of murine 8-oxoguanine-DNA glycosylase. *The Journal of biological chemistry*, 275(37), pp.28607-17. Available at: http://www.ncbi.nlm.nih.gov/pubmed/10884383 [Accessed February 13, 2012].

Zielinska, A. et al., 2011. Direct visualization of repair of oxidative damage by OGG1 in the nuclei of live cells. *Journal of biochemical and molecular toxicology*, 25(1), pp.1-7. Available at: http://www.ncbi.nlm.nih.gov/pubmed/21322094.

University of Birmingham

School of Biosciences

Project 2

THE ROLE OF SRC-LIKE ADAPTOR PROTEINS IN REGULATING GPVI SIGNALLING

A research project report submitted by

Sarah Akbar

as part of the requirement for the
degree of MRes in Molecular and Cellular Biology

This project was carried out at: The University of Birmingham

Under the supervision of: Dr M G Tomlinson Date:July 2012

Summary

GPVI is a glycoprotein platelet receptor integral to stable collagen binding at sites of vascular damage to activate haemostasis. GPVI is exclusively expressed on the platelet membrane dependent on its non-covalent association to ITAM-containing FcR-γ chains. As GPVI is a member of the immunoglobulin superfamily and shares considerable homology to ITAM-receptors, it was hypothesised that GPVI is regulated by Src-like adaptor proteins (SLAP) which are the key negative regulators of ITAM-containing receptors of B cells and T cells. The two homologs of SLAP proteins, SLAP1 and SLAP2, are expressed in platelets and consist of 4 homologous domains. The present study investigates the role of the SLAP proteins in GPVI signalling in DT40 cell line model using the robust NFAT/AP-1-luciferase assay. Furthermore the contribution of each SLAP2 domain to its inhibitory activity was investigated to elucidate a potential mechanism of SLAP2 mediated inhibition. The results show SLAP1 and SLAP2 significantly inhibit collagen-stimulated GPVI signalling. SLAP proteins did not alter GPVI expression levels indicating intrinsic inhibition of GPVI signalling. The c-terminal domain predominantly contributes to inhibitory activity followed by the SH2 domain, myristoylation sequence and the SH3 domain. Elucidation of GPVI regulation could have implications in the development of anti-thrombosis therapy.

Contents

List of Figures

Abbreviations

Ab	Antibody
ADP	Adenosine diphosphate
ADAM10	A disintegrin and metallopeptidase 10
ADAM17	A disintegrin and metallopeptidase 17
AP-1	Activator protein 1
BCR	B cell receptor
β-gal	B-galactosidase
BJAB	B-lymphoblastoid cell line
Btk	Bruton's tyrosine kinase
cAMP	Cyclic adenosine monophosphate
Cbl	Casitas B-lineage lymphoma
cDNA	Complementary deoxyribonucleic acid
CEACAM-1	Carcinoembyonic antigen-related cell adhesion molecule 1
CLEC-2	C-type lectin-like receptor 2
Cis	'on the same side' isomerism
CRP	Collagen related peptide
CVX	Convulxin
Cys	Cysteine (C)
DAG	Diacylglycerol
Eck	Epithelial cell receptor
ECL	Enhanced chemiluminescence
ECM	Extracellular matrix
EMMPRIN	Extracellular matrix metalloproteinase induces
Eph	Ephrin
Epo-R	Erythopoitein receptor
ER	Endoplasmic reticulum
Fab	Fragment antigen binding
Fc	Fragment crystallisable region
FcR	Fc receptor
FITC	Fluorescien isothiocyanate
FXa	Factor Xa
G	Glycine
Gads	Grb2 adaptor downstream of Shc
GDP	Guanosine diphosphate
GM-CSF	Granulocyte-macrophage colony-stimulated factor
GPVI	Glycoprotein VI
GST	Glutathione S-transferase
GTP	Guanosine-5'-triphosphate
HEK293	Human embryonic kidney cell line
HRP	Horseradish peroxidise
I_{CRAC}	Calcium-release-activated current
Ig	Immunoglobulin
IP_3	Inositol 1,4,5-trisphosphate
ITAM	Immunoreceptor tyrosine based activation motif
ITP	Idiopathic thrombocytopenic purpura
ITIM	Immunoreceptor tyrosine based inhibition motif
L	Leucine

LAIR	Leukocyte-associated Ig-like receptor
LAT	Linker for activation of T cells
Lck	Lymphocyte-specific protein tyrosine kinase
LRC	Leukocyte receptor cluster
K	Lysine
M	Methionine
M-CSF	Macrophage colony-stimulating factor
mAb	Monoclonal antibody
MAPK	Mitogen-activated protein kinase
MI	Myocardial infarction
Myc	c-myc derived protein tag sequence N-EQKLISEEDL-C
NFAT	Nuclear factor of activated T cells
P	Proline
PECAM-1	Platelet/endothelial cell adhesion molecule 1
PDGF	Platelet-derived growth factor
PH	Pleckstrin homology
PI3-kinase	Phosphatidyl inositol-3 kinase
PIP2	Phosphatidylinositol 4,5-bisphosphate
PIP3	Phosphatidylinositol 3,4,5-triphosphate
PKB	Protein kinase B
PKC	Protein kinase C
PLCγ2	Phospholipase C γ2
PMA	Phorbal 12-myristate 13-acetate
PRP	Platelet rich plasma
PVDF	Polyvinylidene fluorite
R	Arginine
Ras	Rat sarcoma GTPase family protein
RBL-2H3	Basophilic leukemia cells
RPMI	Roswell Park Memorial Institude medium
SDS-PAGE	Sodium dodecyl sulphate polyacrylamide gel electrophoresis
SH2	Src homology 2
SH3	Src homology 3
SHIP-1	SH2-containing polyinositol-5-phosphatase
SHP-1	SH2-containing tyrosine phosphatase 1
SHP-2	SH2-containing tyrosine phosphatase 2
SLAP	Src-like adaptor protein
SLP-76	SH2 containing leukocyte protein of 76kDa
SNP	Single nucleotide polymorphism
SOCE	Store-operated calcium entry
STIM1	Stromal-interacting molecule 1
Syk	Spleen tyrosine kinase
TBS	Tris buffered saline
TCR	T cell receptor
Trans	‘on the other side’ cis-trans isomerism
vWF	Von Willebrand factor
V	Valine
Vav	Guanine nucleotide-exchange factors of the Rho family
W	Tryptophan
WT	Wild type
ZAP-70	Zeta-chain associated protein kinase 70

Chapter 1. Introduction

1.1 Overview

Haemostasis has three fundamental tenets; (1) the formation of a haemostatic 'plug' to arrest bleeding into the vasculature, (2) sealing off localised tissue damage to prevent further damage at site, and (3) recruitment of reparative components to restore vascular integrity. Haemostasis exemplifies a feat of cellular signalling established on multi-component interconnections, bi-directional signal transduction and dynamic cellular changes such that a molecular-cellular process sufficiently responds to extensive vascular tissue damage. The importance of haemostasis is most emphasized by the bleeding disorders that manifest in its absence, such as thrombotic thrombocytopenia purpura, and von Willebrand disease (Coller 2011). Platelets survey the entirety of the vasculature, safeguard structural integrity in the event of damage and provide continuous support to repair of vessels (Ho-Tin-Noe et al. 2012). In recent years, however, the role of platelets has undergone a paradigm shift with their implication in pathologies such as MI, ischemic stroke, acute coronary syndrome, and atherosclerosis (Linden & Jackson 2010; Nieswandt *et al.* 2011; Bigalke *et al.* 2010; Huo & Ley 2004). The aetiologies of these disorders are associated with the formation of thrombotic lesions. Thrombotic lesions have the propensity to rupture and occlude blood vessals. Alternatively the thrombotic lesion uncontrollably extends resulting in intravascular intrusion and disruption of blood flow. Thrombosis is mechanistically identical to haemostasis, but due to deregulation of the haemostatic process clot formation is excessive either in magnitude or site. The dichotomic role of platelets in the maladaptive version of haemostasis, thrombosis, is investigated with the intention to produce anti-thrombotic agents. The most thrombotic ECM protein, collagen and its putative receptor is GPVI. The GPVI is associated with the ITAM-bearing FcR-γ chain and is critical to the early formation of stable contacts with the damaged vasculature. Here, the regulation of GPVI receptors via SLAP proteins, regulators of ITAM receptors, is investigated. Elucidation of GPVI regulation would contribute to our understanding of limiting thrombosis.

1.2 Platelet Physiology

Platelets are anuclear discoid cell fragments derived from megakaryocytes in the bone marrow (Ho-Tin-Noe *et al.* 2012). Platelets are the third major morphological component of the blood (Coller 2011). Highly adapted to their role, platelets display a number of receptors, produce secretory granules and undergo rapid cytoskeletal changes. Platelets traverse the length of the vasculature, and in resting conditions are maintained in a quiescent state by nitric oxide and prostacyclin released by the endothelium layer (Austin 2009). Discontinuity of the anti-thrombotic endothelium layer at the site of damage indicates a loss of vascular integrity. At the site of injury thrombin, shear stress, or various cytokines perturb antithrombotic activity of endothelial cells to inhibit the quiescent state of platelets and promote haemostasis (Austin 2009).

1.3 Haemostasis

Haemostasis is a complex dynamic process consisting of a seamless transition of 5 events (figure 1); a distinct ligand-receptor pairing characterises each stage of haemostasis resulting in increased stability of the haemostatic plug with each stage.

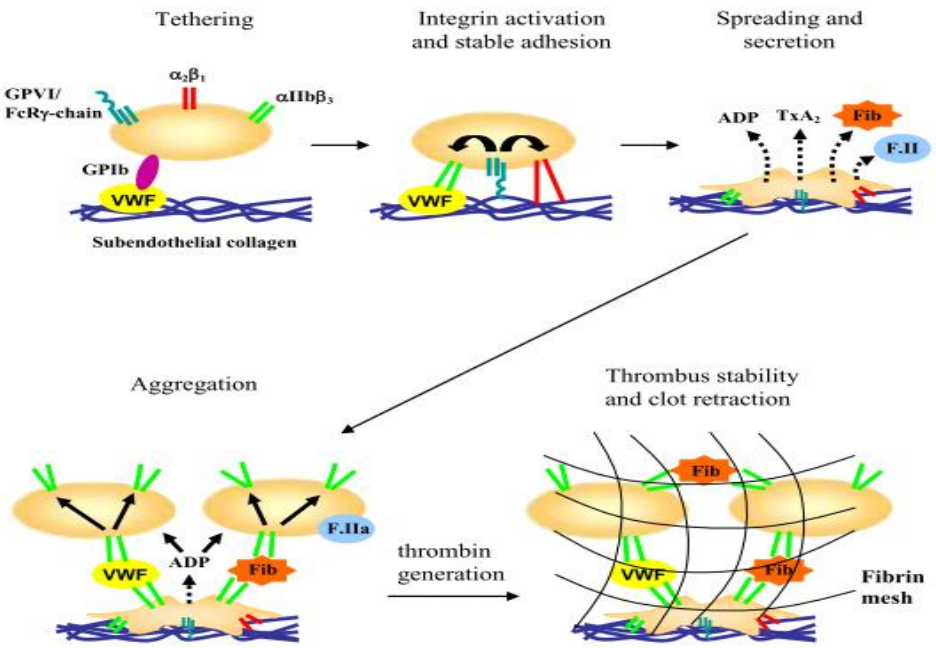

Figure 1.1 Haemostasis. An Illustrated representation of the major events in haemostasis plug formation (Ellison 2009).

1.***Rolling*** – The initiator of haemostasis is von Willibrand factor (vWF), a large highly abundant multimeric glycoprotein which is only platelet-reactive when attached to fibrillar collagen (Peyvandi, *et al* 2011). High shear conditions cause elongation of globular vWF to linear vWF, exposing the A1 domains of vWF to glycoprotein GPIbα (Savage, *et al* 1998). GPIbα is disulphide linked to GPIbβ and noncovalently associated to GP-IX and GP-V forming the glycoprotein receptor GPIb-V-IX (Broos, *et al* 2011). Under high velocity flow absolute immobilisation of platelets is not feasible; instead the shear forces incident on vWF-bound GPIbα elongates cytoskeletal-bound GPIbα into a tether (Ruggeri & Mendolicchio 2007). This tether impedes the flow of circulating platelets and gradually decelerates circulating platelets to facilitate other low binding-energy interactions. The transient interactions of vWF:GPIbα create a rolling effect along the vessal wall (Stegner & Nieswandt 2011).

2. ***Platelet Activation*** – At high shear stress direct collagen receptor binding is not possible due to the slow rate of interaction, however once platelets have been decelerated to site of damage, these interactions become feasible. Platelets have two receptors for collagen, GPVI and α2β1 (Clemetson, *et al* 1999). Platelet-exclusive GPVI activates tyrosine phosphorylation cascades, intracellular calcium flux, exteriorisation of phosphatidylserine on platelet membrane and release of soluble agonists (Clemetson 2012). Integrin receptor α2β1 undergoes 'inside-out activation'; ligand-induced transition from resting to high affinity state by extending extracellular domains upwards (Nuyttens, et al 2011). Integrin α2β1 synergises with GPVI to maximise the activation response of platelets. Exposure of negatively charged phosphatidylserine on the plasma membranes provides an interface for the catalytic generation of thrombin and coagulation cascade (Farndale 2006). The GPVI-dependent exocytosis of granules releases *secondary wave mediators*, ThromboxaneA_2 and ADP, which propagate autocrine platelet activation via binding to G-protein coupled receptors (Rivera, *et al* 2009).

3. Platelet-Platelet Adhesion **–** Activation via collagen receptors, extracellular matrix components and soluble agonists all converge to the activation of the integrin $\alpha_{IIb}\beta_3$ (Clemetson 2012). The receptor $\alpha_{IIb}\beta_3$ recognises the arginine-glycine-aspartic acid sequences in fibrinogen, fibrin, vWF, thrombospondin, fibronectin, and vitronectin (Varga-Szabo *et al.* 2008). The bivalent nature of fibrinogen allows the attachment of two integrins from separate platelets to a single fibrin molecule, thus bridging adjacent platelets. The fibrin mesh engulfs the microaggregate developing a stable platelet clot. Platelet-platelet adhesion occurs at less than 50nm of each other supported by indirect interactions of multivalent adhesive proteins and junctional proteins, and direct platelet-platelet interactions via surface Eph kinases which bind surface-bound ephrins (Brass *et al*. 2005). The receptor plays a central role in maintaining these interactions to prevent dissolution of the haemostatic plug (Langer & Gawaz 2008). The premature destabilisation of the growing clot may results in the detachment of fibrous clot which can occlude blood vessels. Site ruptures facilitate thrombus formation via the interaction of GPIb-V-IX and GPVI with the underlying fibrous tissue (Andrews & Berndt 2004).

4. Spreading – The adhesive contacts enforced by $\alpha_{IIb}\beta_3$ receptors result in the formation of a monolayer of platelets. Platelets undergo vast cellular conformation transforming from discoid cells to flattened cells with protuberant pseudopodia. Ligand-binding of α2β1 receptors critically contribute to the formation of filopodia and lamellaepodia. Increased intracellular calcium levels mediates phosphorylation of myosin-light chain of the cytoskeleton, facilitating dynamic cell changes and contractile motion of fibrin mesh (Allford & Machin 2004).

5. Aggregation – The haemostatic plug is stabilised by further deposition of platelets. However beyond the monolayer of platelets, circulating platelets do not have access to the attractive forces of the subendothelium. Therefore further recruitment and activation of platelets is dependent on secretion of soluble agonists in platelet granules (Clemetson 2012). vWF bridges interactions between deposited platelets and circulating platelets via the $\alpha_{IIb}\beta_3$ receptor (Clemetson 2012).

1.3 GPVI Identification

The first evidence of GPVI was indirectly acquired by the absence of collagen-induced platelet aggregation in patients harbouring antibodies to a 62-kDa membrane glycoprotein (Sugiyama *et al.* 1987). Sugiyama *et al.* investigated a patient presenting idiopathic thrombocytopenic purpura (ITP) finding normal platelet characteristics with the exception of collagen-responses. Purification of the $F(ab')_2$ fragments of this atypical antibody verified its specificity to GPVI as when mixed in normal platelet-rich plasma it caused collagen-dependent aggregation (Sugiyama *et al.* 1987). Sugiyama and colleagues deduced that the patient's IgG was directed to a membrane bound collagen receptor. Similar bleeding disorders alerted researchers to the absence of GPVI. One such patient exhibited inherited deficiency of GPVI (significantly reduced radioisotope incorporation into a 61kDa protein), reducing collagen- adhesion to 1.3%, significantly below the normal range 23-24% (Moroi, *et al* 1989). Having demonstrated α2β1-independent collagen-stimulated aggregation (Morton, *et al* 1995), the identity of the second collagen receptor was investigated. Several potential candidates were proposed however only GPVI fit the criterion of collagen-induced tyrosine phosphorylation of signalling proteins. The phosphorylation of Fc receptor γ-chain (FcR-γ), a prerequisite of collagen-induced aggregation, crosslinks GPVI (Poole *et al*. 1997). Increased collagen concentration corresponded to increased tyrosine phosphorylation of FcR-γ chain and increased co-precipitation with 60kDa membrane protein GPVI (Gibbins, *et al* 1997). The snake toxin, convulxin, and the synthetic collagen derivative, collagen-related peptide (CRP), induced platelet aggregation by mechanisms analogous to collagen, resulting in time-dependent tyrosine phosphorylation of FcR-γ and also co-immunoprecipitated with GPVI (Polanowska-Grabowska, *et al* 2003; Polgár *et al.*, 1997). Taken together, GPVI was identified as a platelet receptor directly binding the physiological ligand collagen. With this, a 'two-step, two-site' model of collagen-induced platelet activation was established as Santoro *et al* first proposed whereby binding of α2β1 is followed by GPVI activation (Santoro, *et al* 1991).

1.4 GPVI Genomic Structure

Isolation of GPVI facilitated early attempts to characterise GPVI and its gene (Tandon, *et al* 1989). The GPVI gene was mapped to chromosome 19q 13.4 consisting of 8 exons spanning 1017 base pairs encoding 339 amino acids (Clemetson et al. 1999; Ezumi *et al*. 2000). The mouse and human genes share 64% homology and the expression of GPVI is limited to the megakaryocytic lineage (Jandrot-Perrus *et al.* 2000). Common with other megakaryocytic genes, such as integrin α2, GPIX and GPV, the GPVI promoter has a consensus initiation sequence, which lacks TATA and CAAT boxes instead has multiple transcription start sites (Ezumi *et al.* 2000). Full-length cDNA cloning identified an N-terminal signal sequence followed by two IgG-like domains, a mucin-like serine/threonine-rich region, a transmembrane domain, and a unique c-terminus (Clemetson *et al.* 1999). The two IgG-like domains are disulphide linked and externalised on the plasma membrane. This hydrophobic extracellular portion is homologous to Type-1 transmembrane receptors (Clemetson *et al.* 1999; Jandrot-Perrus *et al*. 2000). Homology searching of this region identified GPVI as a member of the immunoglobulin super-family, closely related to FcR-α, mouse mast cell receptor and the natural killer receptor class (Clemetson *et al.* 1999). The 19 amino acid transmembrane domain contains a positively charged- arginine residue which forms an ionic bond with aspartic residue in the transmembrane portion of FcR-γ (Clemetson *et al.* 1999). The 51 amino acid cytoplasmic region is distinct from other family members, lacking a kinase consensus sequence or any phosphorylateable residue. Instead the cytoplasmic domain possesses a type-1 proline-rich sequence typical of SH3-binding sites (Miura, *et al* 2000). Genomic analysis found a discrepancy between the predicted molecular weight (38kDa) from the cDNA sequence and the ~60kDa molecular weight of purified GPVI. The incongruency was attributed to extensive glycosylation contributing an extra 20 kDa molecular weight to GPVI (Jandrot-Perrus *et al.* 2000). The cDNA sequence predicted one putative N-glycosylation site (Miura *et al.* 2000) confirmed by crystal analysis (Horii, *et al* 2006).

1.5 GPVI Structure

The general GPVI structure, as predicted by genomic analysis, consists of two Ig-like globular extracellular domains, a transmembrane domain and a long cytoplasmic tail. Though extensive regions of GPVI are reserved for ligand-recognition, ligand-binding is dominated by the two Ig-like domains (n-terminal D1 and D2) (Horii *et al*., 2006; Lecut *et al*., 2004). The D1 domain and to a lesser extent the D2 domain promote ligand binding and are critical for binding of collagen, CRP and convulxin (Dumont *et al*. 2006). Substitution of both domains abolished collagen binding, but restoring the D1 had a greater collagen-binding efficiency than D2 (Dumont *et al.* 2006). D1 domain is typical of an Ig fold, consisting of β-sheets (ABE and A`GFCC` strands) followed by a short 3_{10} helix and 2 polyproline type II helices. After the first β-strand of D1 a conserved *cis*-proline (P14) distorts the A'strand which then interacts with the G strand the final β-sheet of D1. Therefore to D1 domain is an I-type Ig fold. In contrasts the conserved proline (P100) at the end of the A strand of D2 results in *trans* conformation, and thus the D2 domain is a C2-type Ig fold. The D2 domain deviates from canonical C2-type Ig-fold, containing elongated C and C1 strands; these, like the AB loop, extend outwards and exhibit considerable flexibility. Atypical of the Leukocyte receptor cluster (LRC) family, GPVI has an 11-residue deletion intervening C'E loop resulting in a shallow hydrophobic groove in the D1 domain. The ligand binding residues were identified by generating monoclonal antibodies to selectively inhibit the binding of collagen, convulxin and collagen-related protein (CRP).

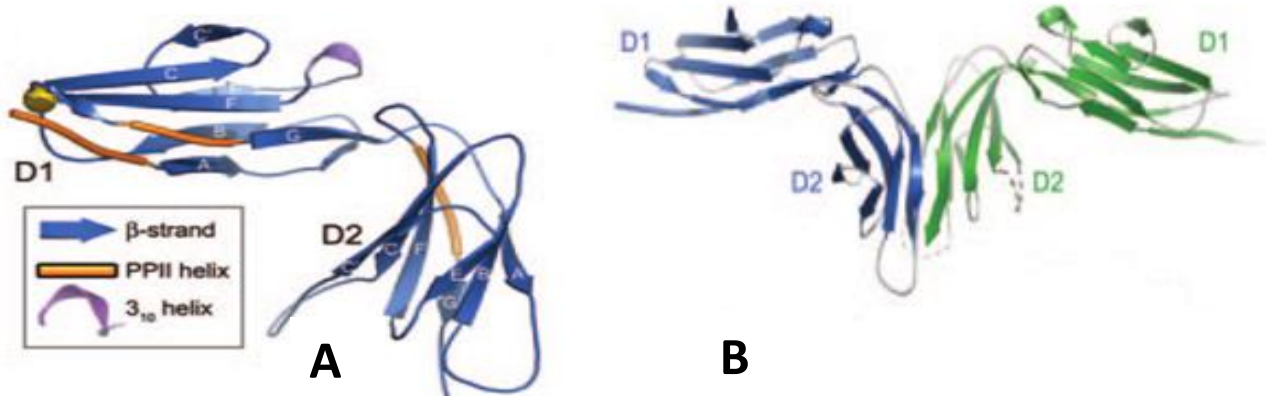

Figure 1.2. Structure of GPVI Ig-domains (Horii et al. 2006)**. A.** Ribbon diagram of GPVI representing the n-terminal D1 domain and the c-terminal D2 domain. The N-glycosylation site is indicated by a gold ball. **B.** Ribbon diagram of the dimeric structure of GPVI. The two D2 domains via hydrophobic interactions form a back to back dimer. The D1 domains are extended at 90˚ angles to form the ligand binding site.

Differential inhibition of collagen, CRP, and convulxin indicates GPVI possesses distinct binding sites for each ligand with some overlap of residues (Lecut *et al*. 2004). GPVI binding to convulxin involves charge residues on the D1 and the interdomain hinge, as mutation of both the linker region and D1 abolish convulxin binding (Dumont *et al.* 2006). Collagen binding residues are localised to a 30-35 residue loop bordering the hydrophobic groove on D1; these residues are charged polar residues such as K41, K59, and R60 (Horii *et al.* 2006). Residues K59, R60 and R166 on the apical surface of GPVI are critical for collagen binding (O'Connor *et al.* 2006; Smethurst *et al.* 2004). In a separate study the residues V34 and L36 were found critical for the binding of GPVI to collagen and CRP (Lecut *et al.* 2004). The homologous collagen-binding domains of both GPVI and LAIR presented 3 conserved residues R59, E61, and W109, which promote collagen binding (Brondijk *et al.* 2010). Crystal structure analysis found an N-glycosylated residue (N72) on an outward extending loop at the end of D1 (Horii *et al*. 2006). Glycosylation contributes to the maximal binding of GPVI agonists, as the oligosaccharides directly contact collagen, and preserve optimal orientation of the binding site (Kunicki, *et al* 2005). Disruption of the consensus N-glycosylation site Asn92-Gly-Ser94 decreased GPVI response to ligands (Kunicki *et al.* 2005). The transmembrane domain contains a positively charged arginine in position 3 which forms a salt-bridge with an aspartic acid of FcR-γ; the expression of GPVI is dependent on this constitutive cross linking (Nieswandt *et al*. 2000). The intracellular tail serves as an adaptor for downstream interactions via two autonomous domains; a highly basic region and a proline-rich region which mediate interaction with calmodulin and Src-family kinases, respectively (Locke *et al*. 2003). Loss of either domain significantly abrogates GPVI signalling, in the presence and absence of FcR-γ. The basic residues in 14 amino acids sequence between W292 and V306, presented on the interface of a helix, shares homology to classical calmodulin-binding motifs (Locke *et al.* 2003). Calmodulin binds GPVI in resting platelets but dissociates upon activation, and is therefore considered a regulator of GPVI (Bender *et al*. 2010).

1.6 GPVI Dimerisation

GPVI forms back-to-back dimers stabilised via the interaction between two hydrophobic D2 domains (Horii *et al.* 2006). The D2 domains orientate the D1 domains to favour ligand binding (Dumont *et al.* 2006). The binding affinity of monomeric GPVI was compared to recombinant dimeric GPVI; monomeric GPVI has no observable affinity for collagen (Miura *et al.* 2002). Conversely GPVI dimers enhance affinity for collagen, and reciprocally collagen-stimulation enhances GPVI dimerisation. Furthermore the dimer interface, consisting of 2 parallel grooves, displays surface complementarity and matches the dimensions of a collagen fiber (Horii *et al*. 2006). The penultimate residue Cys388 in the D2 domain is critical for the dimerisation of GPVI (Arthur *et al.* 2007). GPVI dimerisation is independent of FcR-γ phosphorylation, Src-kinases, Syk, PI-3Kinase and calmodulin (Arthur *et al*. 2007). Resting platelets present GPVI monomers until activated by soluble agonists, collagen-, vWF- or shear-induced platelet aggregation (Loyau *et al.* 2012). Monomers are maintained by high concentrations of intraplatelet cAMP, a general inhibitor of platelet activation (Dütting & Nieswandt, 2012). In contrast, Berlanga *et al.* demonstrated GPVI is dimerised in basal conditions and dimerisation is rapidly enhanced upon ligand binding (Berlanga *et al.* 2007). It is has been suggested GPVI operates via the multichain immune recognition receptor (MIRR) signalling model, whereby basal receptor dimers do not activate signalling until the disordered cytoplasmic domains of MIRR subunits homooligomerise (Sigalov 2007). The clustering of receptors is a requisite of collagen binding due to the multivalent and highly polymerised structure of collagen (Jarvis *et al*. 2008). Studies have demonstrated optimal binding to collagen is favoured dimerisation (Loyau *et al.* 2012; Jung *et al.* 2009; Miura *et al.* 2002). The clustering of GPVI was first indicated by the ability of bivalent F(ab')2 fragments of GPVI antibodies to induce platelet aggregation and activation (Sugiyama *et al*. 1987). In support of clustering- induced activation, Jung *et al*. demonstrated crosslinking of GPVI dimers by bivalent IgG or monovalent Fab induced platelet aggregation (Jung *et al.* 2009).

1.7 GPVI- ITAM signalling

GPVI signalling is underpinned on its interaction with the FcR-γ chain. GPVI lacks intrinsic enzymatic or kinase activity (Moroi & Jung 2004). Signal transduction is dependent on the constitutive association with the ITAM-bearing FcR-γ chain. GPVI is an ITAM-receptor, like BCR and TCRs, and signals through the ITAM motif of the FcR-γ. The ITAM motif consists of YXXL/IX_{6-8}YXXL/I sequence where X denotes any amino acid (Watson & Gibbins 1998). Phosphorylation of the tyrosine (Y) residues within the ITAM motif form SH2-domain docking sites. Recruitment of SH2-domain proteins initiates downstream signalling.

Ligand binding results in dimerisation of the GPVI receptor, and subsequently GPVI-associated Src-kinases phosphorylate the ITAM motif of the FcR-γ chain. Src-kinases Lyn and Fyn are constitutively associated with the proline rich regions of the GPVI cytoplasmic tail via their SH3 domains (Suzuki-Inoue *et al.* 2002). Despite the constitutive association of Lyn and Fyn to GPVI, no kinase activity is observed in the absence of ligand, these kinases are primed for activity, emphasising the requirement of GPVI clustering to bring Lyn and Fyn in proximity of FcR-γ (Schmaier *et al.* 2009). Phosphorylation of conserved tyrosines in the ITAM motif of FcR-γ creates docking sites for SH2-domain bearing proteins. Other downstream substrates of Lyn include the kinase C-δ and SHIP-1 (SH2-domian-containing inositol phosphatase-1) which upon GPVI-induced phosphorylation result in the secretion of dense granules (Chari *et al.* 2009).

The docking site created by the phosphorylated ITAM motif facilitates the binding of Syk (Suzuki-Inoue *et al.* 2004). Subsequent autophosphorylation of Syk activates kinase activity targeted at a number of substrates including LAT, SLP-76, Vav and PLCγ2 (Watson *et al.* 2005). Syk mediates the formation of a signalosome with LAT, SLP-76 and Gads which regulates phospholipase Cy2 (PLCγ2) activity (Watson *et al.* 2005). Activated LAT and SLP-76 associate with the GPVI cytoplasmic tail to orchestrate the phosphorylation of PLCγ2, PI3-kinase, and G-protein coupled receptors (Leo *et al*. 2002; Judd *et al.* 2002). SLP-76 is involved

in granule secretion to maximise collagen-stimulated aggregation (Leo *et al.* 2002).

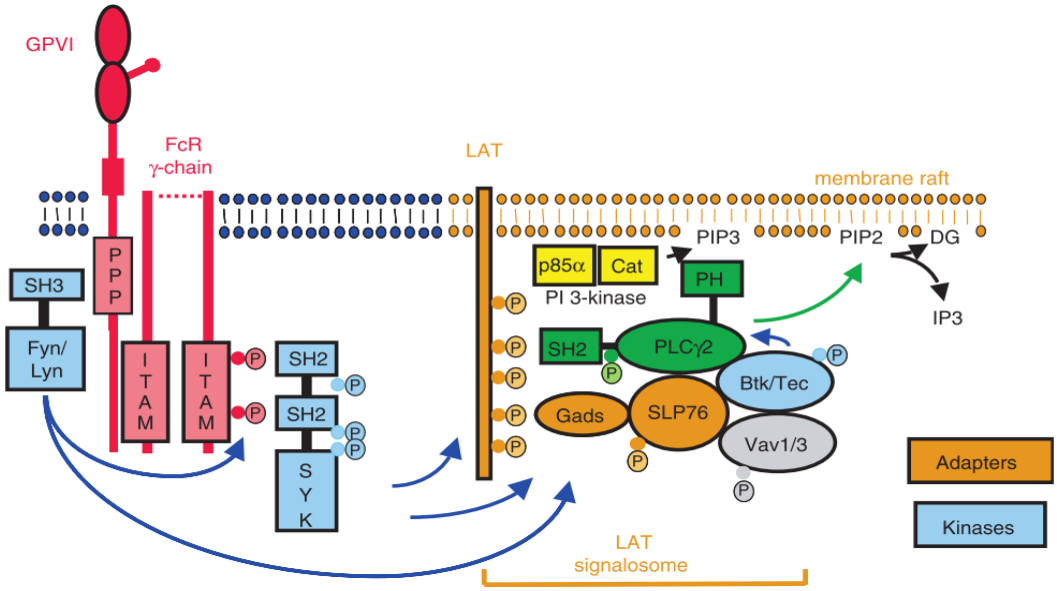

Figure 1.3. The GPVI signalling cascade (S P Watson et al. 2005)**.** GPVI ligand binding induces dimerisation of GPVI. Fyn and Lyn phosphorylate the ITAM motif of the FcR-γ chain. The recruitment of Syk to the results in the formation of a signalosome and PLCγ2 activation.

The phosphorylation of PLCγ2 is integral to the amplification of GPVI signalling. PLCγ2 translocates to the membrane where it cleaves phosphatidylinositol 4,5-bisphosphate (PIP2) into inositol 1,4,5-triphosphate (IP_3) and diacylglycerol (DAG) (Falet *et al.* 2000). The liberated IP_3 is a cytosol-soluble substrate of IP_3-receptors in the endoplasmic reticulum membrane. IP_3-mediated calcium channels are opened creating an influx of calcium. The cooperation of calcium and the membrane bound DAG activates PKC (Falet *et al.* 2000). Calcium mobilisation and PKC activation are major endpoints in GPVI signalling, resulting in the exocytosis of dense granules, integrin activation, platelet adhesion and platelet spreading by filopodia formation (Nieswandt & Watson 2003; Watson *et al.* 2005; Quinton 2002).

As the precursor to calcium influx and PKC activation, PLCγ2 is critical to haemostasis, such that no platelet aggregation is observed in PLCγ2-/- deficient mice (Nonne *et al.* 2005). Upon collagen-stimulation Syk, SLP-76, Lyn, LAT and FcR-γ interact with the c-terminal SH2 domain of PLCγ2 (Gross *et al.* 1999). The activation of PLCγ2 is also supported by PI3-kinase, Tec family and Vav proteins which are activated directly downstream of Syk (Watson *et al.* 2005). Vav proteins serve as critical adaptor proteins in PLCγ2 phosphorylation as deficiency

in certain members of the Vav family markedly reduces of PLCγ2 phosphorylation and GPVI signalling (Pearce *et al.* 2004).

Btk is a nonreceptor tyrosine kinase of the Tec family activated by Syk in response to GPVI and GPIb-Ix-V stimulation. Activated Syk recruits Btk which associates with PI3-kinase via its PH domain, and is simultaneously translocated to the plasma membrane (Dangelmaier *et al.* 2005). Btk phosphorylates PLCγ2 at Try753 and Tyr759 residues (Suzuki-Inoue *et al*. 2004). PI3-kinase is non-redundantly critical for GPVI-induced thrombus formation (Gilio *et al.* 2009). In addition to Btk translocation, PI3-kinase mediates the serine/threonine phosphorylation of protein kinase B (PKB) and translocates activated PKB to cell membranes where PKB modulates of dense granule secretion (Barry & Gibbins 2002). PKB regulates ADP secretion, enhances PLCγ2-mediated calcium flux, and induce exteriorisation of phosphatidylserine under flow conditions (Barry & Gibbins 2002).

The activities of several proteins converge to the activation of PLCγ2 which in turn activates several signalling pathways. The two products of PLCγ2 are exploited in the NFAT/AP-1 luciferase assay to measure the relative level of signalling. The IP_3 opens ER-calcium channels producing cytoplasmic calcium influx. Following depletion of IP_3-gated calcium stores, intraluminal calcium levels are replenished by opening of the membrane-bound I_{CRAC} channel composed of Orai1 oligomers and the calcium sensor STIM1(Gilio *et al.* 2010). Store-operated calcium entry (SOCE) produces sustained calcium influx activating several calcium sensitive proteins such as calcineurin. Calcineurin dephosphorylates NFAT exposing the nuclear translocation signal facilitating entry of NFAT into the nucleus. The second PLCγ2 product, DAG, activates the membrane-bound GTPase Ras. Ras undergoes conformation switch from inactive GDP-bound form to active GTP-bound state. Ras activates MAP3K which activates MAP2K. Successive activation of MAPK by MAP2K translocates MAPK to the nucleus where it promotes dimerisation of c-Fos and c-Jun forming the AP-1 transcription factor. NFAT and AP-1 promote transcription of luciferase reporter gene of the NFAT assay.

1.8 GPVI Membrane localisation

The clustering of GPVI receptors upon ligand-binding is promoted by the membrane localisation in lipid rafts which concentrate GPVI receptors (Quinter *et al*. 2007). Lipid rafts are heterogenous microdomains within the plasma membrane, highly enriched in glycoproteins such as glycosphingolipids, phospholipids and cholesterol (Lingwood & Simons 2010). Lipid rafts selectively sequester receptors in microenviroments where the selective composition of proteins is conducive to signal activation. Reported members of lipid rafts include acylated src-family kinases such as Lyn and Fyn, and palmitoylated transmembrane proteins such as LAT (Dorahy & Burns 1998; Horejsí et al. 1999; Zhang et al. 1998). Locke *et al*. reported the existence of convulxin-dependent presence GPVI in lipid rafts in platelets (Locke *et al*. 2002). The presence of GPVI in lipid rafts is comparable to the translocation of TCR, BCR and CLEC-2 (Kabouridis 2006; Gupta & DeFranco 2007; Pollitt et al. 2010). Uncoupling the GPVI:FcR-γ complex established FcR-γ association is required for GPVI presence in lipid rafts (Locke *et al.* 2002). Cvx-stimulation increased the prevalence of LAT and recruited SLP-76 and PLCγ2 to lipid rafts (Locke *et al*. 2002; Wonerow *et al.* 2002). The selective lipid raft disruption by methyl-β cyclodextrin reduces collagen-, CVX-, and CRP- induced aggregation (Ezumi *et al.* 2002; Quinter *et al*. 2007).The inhibition of GPVI induced aggregation, calcium mobilisation and dense-granule secretion upon methyl-β cyclodextrin treatment indicated lipid raft integrity is required for maximal GPVI activation (Wonerow *et al*. 2002). Ezumi *et al*. reported lipid raft disruption inhibited of phosphorylation of FcR-γ, Syk, PLC, LAT and SLP-76, whereas Quinter *et al*. found no affect on the phosphorylation of Syk, LAT and PLC in methyl-β cyclodextrin-treated cells in response to collagen and convulxin stimulation (Ezumi *et al.* 2002; Quinter *et al.* 2007). CRP stimulated responses were sensitive to lipid raft disruption, exhibiting reduced platelet aggregation, Syk phosphorylation and calcium mobilisation (Quinter *et al.* 2007). The resistance of collagen and convulxin to lipid raft disruption may indicate the ability of these agonists to induce clustering without lipid rafts.

1.9 GPVI Regulation

Several GPVI regulatory mechanisms have been proposed but it is likely the regulation of GPVI involves the synergy of several mechanisms providing tiered level of regulation whereby expression level is regulated by (i) ectodomain shedding or (ii) internalisation, or GPVI activation is attenuated by (iii) ITIM receptors or (iv) by direct inhibition of signalling proteins. GPVI undergoes ectodomain shedding whereby the extracellular portion is rapidly and irreversibly cleaved resulting in a soluble 55kDa sGPVI and the 10kDa membrane bound remnant (Gardiner *et al.* 2004). The soluble 55kDa sGPVI is observed in plasma upon incubation with GPVI agonists in a time-dependent manner (Gardiner *et al.* 2004). GPVI shedding is also induced by incubation of platelets with anti-GPVI antibody *in vitro* and *in vivo* (Stephens *et al*. 2005; Al-Tamimi *et al*. 2009; Boylan *et al.* 2006). Shedding was inhibited by inhibitors of GPVI signalling molecules Syk, PI-3kinase, and Src kinases indicating shedding is dependent on components downstream of GPVI-ligand activation (Wijeyewickrema *et al.* 2007).The mechanism of agonist-induced degradation involves the dissociation of the calmodulin bound to the cytoplasmic tail of GPVI (Gardiner *et al*. 2004). Loss of the protective calmodulin molecules makes GPVI susceptible to ectodomain shedding. Antibody-induced ectodomain shedding is also dependent on LAT and PLCγ2 (Rabie *et al.* 2007).Shedding is mediated by metalloproteinases, ADAM10 upon calmodulin inhibition and ADAM17 in cell cytotoxic conditions (Bender *et al*. 2010). Concomitant loss of GPVI shortly after ligand-binding attenuates the haemostatic response to external stimuli. Furthermore the resulting sGPVI inhibits platelet aggregation (Massberg *et al.* 2004). Metalloproteinases-dependent shedding is induced by the coagulation factor FXa in a time-dependent manner, controlling the procoagulant property of GPVI following coagulation (Al-Tamimi *et al.* 2011; Siljander *et al.* 2001). The metalloproteinase-dependent shedding is supported by EMMPRIN, an immunoglobulin receptor, which induces synthesis of matrix metalloproteinase and is capable of making semi-adhesive contacts with GPVI (Seizer *et al.* 2009).

GPVI internalisation was demonstrated by antibody-induced loss of GPVI expression and concomitant absence of cleaved GPVI ectodomain in the supernatant; this effect was exclusive to the hF1232 anti-GPVI antibody (Takayama *et al*. 2008). A fluorescent endocytic probe was tagged to the antibody and monitored GPVI internalisation upon introduction into monkeys. The fluorescence maximised within 1 hour, indicating high levels of GPVI endocytosis. *In vitro* studies confirmed the endocytosis fluorescence was specific to GPVI internalisation and was dependent on high levels of cAMP (Takayama *et al.* 2008). The JAQ1 anti-GPVI antibody was able to induce both endocytic-internalisation and the ectodomain shedding; the distinction between the two pathways was the differential requirement of LAT and PLC for ectodomain shedding (Rabie *et al.* 2007). JAQ1 mediated internalisation was dependent on the ITAM motif of FcR-γ as mutation of two conserved tyrosines (residues 65 and 76) inhibited internalisation (Rabie *et al*. 2007).

Analogous to BCR and TCR regulation, GPVI is susceptible immunoreceptor tyrosine-based inhibitory motif (ITIM) -receptor mediated regulation. ITIM receptors are diametric opposites of ITAM receptors, where the conserved ITIM motif is phosphorylated to create docking sites for SH2-domain phosphatases. Platelets express ITIM receptors PECAM-1, CEACAM-1, and G6b which have been shown to decrease platelet response to collagen (Patil *et al*. 2001; Wong *et al*. 2009; Mori *et al*. 2008). Phosphorylated ITIM motif recruits the phosphatases SHP-1, SHP-2, and SHIP1 which then inhibit PLCγ2 activation and dephosphorylate docking sites (Unkeless & Jin 1997).

Downregulation of individual signalling components is a regulatory mechanism observed in BCRs and TCRs (Rao *et al*. 2002; Lupher *et al.* 1999); the potential of this mechanism to regulated GPVI has been suggested due to the commonality of signalling components. Receptor stimulation recruits Cbl proteins to phosphorylated signalling components where Cbl catalyses the transfer of ubiquitin to lysine residues on the substrate protein resulting in ubiquitinylation and subsequent lysosomal or proteosomal degradation (Thien & Langdon

2005). The inhibitory capacity of the Cbl family in GPVI signalling has previously been established by the Cbl-b dependent inhibition of PLCγ2, Btk and GPVI induced aggregation (Daniel *et al*. 2010). c-Cbl is a ubiquitously expressed member of the Cbl family of E3 ligases composed of an N-terminal tyrosine-kinase binding domain, an ring finger domain and a c-terminal proline-rich SH3-recognition domain (Rao *et al.* 2002). c-Cbl complexes with phosphotyrosines of tyrosine kinases, such as Lyn, Fyn, Lck, ZAP70 and Syk, via the 4 helix bundle, calcium-binding EF domain and a SH2 domain of the tyrosine kinase binding domain (Rao *et al.* 2002; Thien & Langdon 2005). c-Cbl also interacts with non-tyrosine kinases, some of which are common to the GPVI signalling pathway such as PI 3-kinase, Vav and Grb2 (Rao *et al*. 2002). Analogous to the stimulation-dependent recruitment of c-Cbl in TCR and BCR complexes, GPVI stimulation results in phosphorylation/activation of c-Cbl (Polgár *et al.* 1997). Lck-dependent phosphorylation of c-Cbl in TCR parallels the Lyn- and Fyn- mediated phosphorylation of c-Cbl in GPVI signalling (Auger *et al.* 2003). c-Cbl then complexes with phosphorylated Syk which is rapidly ubiqinylated and degraded (Dangelmaier et al. 2005). Knockout analysis in platelets demonstrated the absence of c-Cbl coincided with the increase phosphorylation of FcR-γ, PLCγ2, and Syk (Auger *et al.* 2003). However an ubiquitinylation-inhibitor had no effect on the tyrosine phosphorylation of these proteins. Researchers have reported c-Cbl is phosphorylation-independently bound to Src-like Adaptor Proteins (SLAP) which are recruited to signalling complexes in receptor-stimulating conditions and supplement the activity of c-Cbl (Tang *et al.* 1999). SLAP proteins translocate c-Cbl to membranes upon receptor stimulation resulting in enhanced c-Cbl activity as c-Cbl is juxtaposed to substrates and SLAP further stabilises c-Cbl-to-protein interactions (Swaminathan *et al*. 2007).

1.10 SLAP Proteins

Src-like adaptor proteins (SLAP) are non-enzymatic adaptors which share considerable homology to the Src family of tyrosine kinase possessing homologous N-terminal regions, SH3 domains and SH2 domains but divergent c-terminus regions (Pandey *et al.* 1995). SLAP1 and

SLAP2 are homologous at n-terminal (21%), SH3 domain (36%) and SH2 domain (59% but have unique c-terminus. SLAP1 was identified via two independent yeast-hybrid screens for interacting molecules of tyrosine kinase Eck and c-Cbl (Pandey *et al.* 1995; Tang *et al*. 1999). SLAP2 was identified by bioinformatic searches informed by the genetic structure of SLAP1 (Holland *et al.* 2001). The SLAP1 gene was mapped to chromosome 8q22.3-qter in the 3' end of the thyroglobin gene (Angrist *et al.* 1995; Meijerink *et al.* 1998). The SLAP2 gene was localised to 20q11.23 (Loreto & McGlade 2003). Expression profiling found SLAPs predominantly present in cells of the lymphoid and myeloid lineage, with differential expression of SLAP1 and SLAP2 in spleen, lungs, and thymus (Dragone *et al*. 2009). The regulatory activity of SLAP was first recognised when SLAP1 overexpression inhibited DNA synthesis and cell growth (Roche *et al.* 1998). The co-immunoprecipitation of SLAP1 with the PDGF receptor indicated that the activity of SLAP1 was specific to receptors rather than a global inhibition of mitogenesis (Roche *et al*. 1998). Till date SLAP proteins have demonstrated negative regulation of PDGF receptor, BCR, TCR, GM-CSF, M-CSF, Epo-R, osteoclasts, fibroblasts and mast cells (Sirvent *et al.* 2008; Dragone *et al*. 2006; Myers *et al.* 2005; Liontos *et al.* 2011; Lebigot *et al.* 2003; Kim *et al.* 2010; Park & Beaven 2010; Swaminathan *et al.* 2007; Hiragun *et al.* 2006). Knockout studies have defined the *in vivo* role of SLAP proteins in lymphocytes. The $SLAP1^{-/-}$ deficiency results in a 3-5 fold increase in TCR expression on double-positive cells (DP) attributed to increased TCR recycling and decreased TCRζ degradation (Sosinowski et al. 2001). The $SLAP1^{-/-}$ phenotype of increased surface activation-markers, increased positive selection and rescue of $ZAP70^{-/-}$ induced inhibition of thymocyte development was no different from the $c\text{-}Cbl^{-/-}$ phenotype (Sosinowski et al. 2001). SLAP1 deficiency elevated BCR levels and generated hyporesponsive mature B-cells (Dragone et al. 2006). No phenotype in either B-cells or T-cells was observed in SLAP2 knockout studies (Dragone et al. 2009). In attempt to characterise the pathway of SLAP-induced regulation, interacting proteins have been coimmunoprecipitated under receptor

stimulating conditions. SLAP1 overexpression in T-cell line purified ZAP-70, Syk, Vav, SLP-76, c-Cbl, Lck, TCRζ and LAT (Tang *et al*. 1999; Loreto *et al.* 2002; Sosinowski *et al.* 2000). Interacting partners of SLAP2 in B-cells included c-Cbl and IgAα (Holland *et al.* 2001; Dragone *et al.* 2006). These interactions were dependent on the SH2 domain of SLAP proteins, with the exception of c-Cbl which associates with the c-terminal of SLAP proteins (Loreto *et al.* 2002; Sosinowski *et al*. 2000; Holland *et al.* 2001). The overexpression of SLAP proteins in T- and B-lymphocytes reduced NFAT transcription, calcium mobilisation, and reduced expression of CD69, a lymphocyte-specific marker of ligand-receptor activation (Holland *et al.* 2001). Overexpression of SLAP1 increased TCR degradation in a manner dependent on Lck-mediated phosphorylation of TCRζ followed by cooperative activities of c-Cbl and SLAP1 (Myers *et al.* 2005). Overexpressed SLAP1 decreased surface and total BCR levels by approximately 40-50% via c-Cbl-dependent alteration of BCR recycling and internalisation (Dragone *et al*. 2006). SLAP2 overexpression in T-cells decreased levels of ZAP-70 and CD3ε and in B-cells decreased Syk levels (Dragone *et al.* 2009). Sugihara *et al.* demonstrated the presence of SLAP proteins in platelets and implicated SLAP2 in the negative regulation of GPVI signalling, due to its stimulation-dependent displacement from the soluble cytoplasmic compartment to the insoluble cytoskeletal compartment accompanied with c-Cbl, LAT and Syk (Sugihara *et al.* 2010). The effect of SLAP proteins on GPVI signalling has not been characterised and is the subject of this study.

1.11 GPVI Levels and Polymorphisms

Population studies have reported tight regulation of GPVI levels among healthy population; the mean receptor density is 3730± 453 and the surface density ranges between 1.5-5% (Best *et al.* 2003; Furihata *et al.* 2001). GPVI is expressed in the early stages of megakaryocytic differentiation but is not functionally adherent to collagen till later differentiation stages (Lagrue-Lak-Hal *et al.* 2001). GPVI expression increases with megakaryocte differentiation (Berlanga *et al.* 2000). Platelets GPVI levels are maintained throughout lifetime and are not

affected by the protease-activated receptors or the Src-kinase inhibitor PP2 or prostacyclin (Best *et al.* 2003). Some variation of GPVI levels has been correlated to the presence of GPVI gene polymorphisms. Five of the 10 polymorphisms within the population are inherited as a haplotype with 5 single nucleotide polymorphisms (SNPs) within the mucin and cytoplasmic domains. Two common haplotypes of the GPVI gene, 'a' and 'b', are present in the population at frequencies of 0.85 and 0.13, respectively, and differ at residues Ser219Pro, Lys237Glu, Thr249Ala, Gln317Leu and His322Asn (Best *et al.* 2003; Arthur *et al.* 2007). The low frequency 'b' genes possess 3-fold reduced platelet aggregation, reduced tyrosine phosphorylation, platelet activation, reduced thrombin generation and reduced Syk phosphorylation (Joutsi-Korhonen *et al*. 2003; Trifiro *et al.* 2009). The most functionally relevant SNP is the Ser219Pro, a thymine to cytosine substitution at 13254 base, which modifies an O-glycosylation site (Arthur *et al.* 2007). This mutation has been associated with myocardial infarction and coronary thrombosis (Croft *et al.* 2001; Ollikainen *et al.* 2004). In a study of 102 healthy participants, one individual was homozygous for the Ser219Pro polymorphism, 77% were heterozygotes and 22% were Ser/Ser homozygotes; the GPVI expression levels were 2598 sites, 3437±353, and 3814±439 respectively (Best *et al.* 2003). The functional consequence of Ser219Pro is reduced collagen adhesion under high stress and reduced GPVI expression (Best *et al*. 2003). In contrast Trifiro *et al*. found that under static system there was no difference in the ligand binding capacities of the ectodomains of the two haplotypes, though the Gln317Leu and His322Asn of the 'b' haplotype increased binding to calmodulin and reduced binding to Lyn and Fyn, respectively (Trifiro *et al.* 2009). Though GPVI polymorphisms disrupt structure-function relationships and expression levels, the overall effect of gene polymorphisms on GPVI-mediated platelet responses is relatively subtle compared to the marked reduction in patients with anti-GPVI antibodies, congenital deficiency, immune disorders or defective GPVI signalling (Arthur *et al.* 2007). A review of GPVI deficiency reported a number of clinical defects that accompany the typical bleeding disorder

such as recurrent purpura, menorrhagia, post-surgery/trauma and postpartum bleeding, epistaxis, subcutaneous and gingival bleeding, and recurring bleeding episodes requiring multiple transfusions (Arthur *et al.* 2007). However there is inter-patient variability with some GPVI-deficient individuals exhibiting only mildly increased bleeding times (Moroi *et al.* 1989).

1.12 Therapeutic Potential of GPVI Regulation

The role of GPVI in coronary arterial thrombosis, atherosclerosis and acute coronary syndrome and its associated complications is well established (Nieswandt *et al*. 2011, Bigalke *et al*. 2011, Bigalke *et al.* 2010). GPVI deficiency exhibits anti-thrombotic properties as established by the abolition of thrombus formation in carotid artery injury model in GPVI null mice (Furie & Furie 2006). Researchers have observed the inhibition GPVI activity provides considerable protection from thrombosis. The established modes of GPVI inhibition involve anti-GPVI antibodies and soluble GPVI-Fc dimers which function via the same mechanism of competing with endogenous GPVI for collagen binding. Irreversible depletion of GPVI, via monoclonal antibody JAQ1, provided long-term protection from thrombosis with minimal effect on bleeding times (Nieswandt *et al.* 2001). Schulte *et al.* reported a two-phase anti-thrombotic effect of GPVI inhibition, first thrombin is partially and transiently inhibited followed by the prolonged unresponsiveness to collagen (Schulte *et al.* 2006). The anti-thrombotic capacity of anti-GPVI antibodies is due to the inhibition of several GPVI mediated events such as collagen-induced aggregation (Muzard *et al*. 2009), procoagulant activity of GPVI (Lecut *et al.* 2003), ATP release, thromboxane A2 formation, and platelet adhesion (Matsumoto *et al*. 2007) and shear-induced thrombosis (Walker *et al.* 2009). Soluble GPVI-Fc dimers also inhibit collagen-induced aggregation, though with less potency than anti-GPVI antibodies, and unlike anti-GPVI antibodies permit haemostasis in injured arterial walls (Grüner *et al.* 2005). Existing anti-platelet agents target fibrinogen, ADP, thromboxane increase the bleeding risks (Jackson

& Schoenwaelder 2003). The ability to protect against thrombosis without increased bleeding risk is exclusive to GPVI, and therefore GPVI an attractive target for anti-thrombotic therapy.

1.13 Objectives

The development of anti-GPVI agents promotes research into the mechanisms of GPVI regulation and inhibition. As GPVI is of the ITAM-family of receptors and shares considerable signalling homology with BCRs and TCRs it is proposed that GPVI is also regulated via similar mechanisms regulating BCRs and TCRs involving SLAP proteins. In this study the regulatory effect of SLAP proteins on GPVI signalling is investigated in a cell line model using the NFAT-luciferase assay. The DT40 B-cell line was selected as a representative of platelets; the limited endogenous expression signalling receptors on DT40s facilitates the investigation of isolated signalling pathways (Buerstedde 2002). The NFAT-luciferase assay exploits the ability of GPVI-induced calcium mobilisation and DAG synthesis to activate NFAT and MAPK, respectively, which then promote the transcription of the reporter gene, luciferase. The relative levels of luciferase are representative of GPVI-activation. Surface GPVI levels are also detected to identify any concomitant changes in GPVI levels. Furthermore SLAP2 mutants of each domain are also investigated with the NFAT-luciferase assay to determine the relative contributions of each domain to the inhibitory activity of SLAP2 proteins.

Chapter 2 Material and Methods

2.1 Materials

Materials were of the highest quality and obtained from Sigma-Aldrich unless otherwise stated. Cells, GPVI and SLAP1/SLAP2 constructs, agonists and antibodies were provided by Dr.M.Tomlinson. The C-terminal mutant, SH2 domain, and myristoylation SLAP2 mutants were provided by Dr. McGlade (University of Toronto); these contained function blocking mutations generated by PCR-based mutagenesis. The c-terminal mutant was truncated at 70 amino acids from the c-terminus. The SH2 domain was inactivated by mutation of arginine-120 to lysine. The myristoylation mutant was generated by substitution of glycine-2 to alanine. The SH3-mutant was generated by Jing (Tomlinson lab) by mutagenesis of the proline-recognition domain.

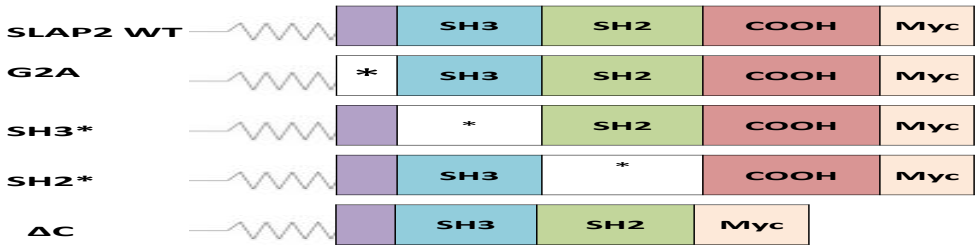

Figure 2.1 SLAP2 structure and domain mutants. A representation of the SLAP2 variants investigated in this study.

2.2.1 Cell Culture

DT40 B cells were provided by the laboratory. These were maintained in RPMI supplemented with foetal bovine serum (10% v/v), L-glutamine (2 mM), penicillin (100 U/ml) and streptomycin (100 µg/ml), β2-mercaptoethanol (50µM) and chicken serum (1% v/v). Cells were kept in 175cm^2 cell culture flasks (BD Falcon™) and incubated at 37°C in a humidified chamber (5% CO2, 95% air). Cells were maintained under 10^6cells/ml by subculturing every two days or in preparation for downstream experiments. Prior to cell passage, cell density was determined using trypan blue exclusion of cells loaded onto a haemocytometer and viewed under a microscope at low magnification. The cell count was calculated and used to inform the dilution required to obtain suitable seeding density.

2.3 DT40Transfection

2.3.1 Transfection

DT40 cells were counted by Trypan blue exclusion and reseeded to a density of $2x10^6$ cells/ml approximately 24 hours before transfection. On the day of the transfection, cells were counted by trypan blue exclusion and the volume required for $1.5x10^7$ cells/ml per transfection was transferred to 50ml falcon tubes (BD Falcon™) and centrifuged at 1200 x g for 5 minutes. The cell pellets were resuspended in serum-free RPMI and combined to a final volume of 50ml. The cells were centrifuged again at 1200 x g for 5 minutes and the supernatant was discarded. The pellet was then resuspended in serum-free RPMI (0.4ml per transfection) and 20µg NFAT reporter/ 2µg Lac-Z per transfection was added to the cells. The cell suspension was then aliquoted to electroporation cuvette in addition to combination of expression constructs for pEF6/pcDNA3, GPVI/FcR-γ, and either SLAP1, SLAP2 or SLAP2 mutants. After a 10minute room-temperature incubation, the cells are electroporated at 350V, 500µF using GenePulser II Electroporator (BioRad,Hercules,CA, USA). After a10 minute room-temperature incubation the transfected cells were transferred from the electroporation cuvette to a 6-well plate (BD Falcon™) containing 8ml serum-supplemented RPMI medium. The cells were incubated (37˚C, 5% $CO_{2)}$ for 16-20hours and harvested the next day.

2.3.2 Harvesting transfected cells

Following an overnight incubation, the transfected samples were transferred from 6-well plates to 15ml Falcon tubes. Two of these samples were used for trypan-blue cell counting. The samples were then centrifuged for 5 minutes at 1200 x g and the supernatant was discarded. Each pellet was resuspended in the appropriate volume of serum-supplemented medium required to adjust the cell concentration to 2 x 10^6 cells/ml. From this cell suspension aliquots were taken for NFAT-luciferase assay, β-galactosidase assay (250µl), flow cytometry (125µl), and western blot analysis (1000µl).

2.4 NFAT-Luciferase Assay

2.4.1 Agonist incubation

Immediately after harvesting transfected cells, aliquots were reseeded into a 96-well plate for NFAT-luciferase assay. Triplicates of transfected cells were individually stimulated with collagen (5µg/ml), RPMI media (negative control) and the positive control agonists PMA (phorbol myristate acetate) and ionomycin. First, aliqouts of transfected cells were transferred to separate troughs. Next, 50µl of transfected cells were pipetted into each well of a triplicate, for three triplicates for the three stimulation conditions. The negative control stimulated triplicates recieved 50µl of supplemented RPMI media. Soluble collagen (5µg/ml) was obtained by diluting Horm collagen with supplemented RPMI, briefly vortexed and then transferred 50µl to collagen-stimulated triplicates. The positive control stimulation was conducted by suspending together 50ng/ml PMA and 1µM ionomycin in supplemented RPMI and transferring 50µl to each well of a triplicate. The well-plate was then incubated at 37C for 6 hours, after which the plate was transferred to -80C or assayed immediately.

2.4.2 Luciferase Assay

The NFAT plate was read by first thawing cells at 37˚C for 15 minutes. Lysis buffer was prepared of 200 mM potassium phosphate buffer (pH7.8), 12.5% Triton X-100 and 1mM DTT. Lysis buffer (11µl) was multi-pipetted into each well, and cells were left to lyse at room temperature for 5 minutes. Assay buffer was prepared (200 mM phosphate buffer pH 7.8, 20 mM MgCl2 and 10 mM ATP) and 100µl was added to each well of a white, opaque 96-well luminometer plate. Upon completion of lysis, the 100µl cell lysate is transferred to assay-buffer containing wells of the luminometer plate. The luminescence produced upon injection of 50µl of 1mM luciferin over a 10 second period was measured using a Mithras LB 960 luminometer. Data were averaged, deducted from blank and normalised with β-galactosidase activity. Data was expressed a relative NFAT activation of the mean and standard error of the mean of three independent experiments.

2.5 β-galactosidase assay

The β-galactosidase assay was conducted using the Galacto-Light™ kit as per manufacturers` instructions. Briefly, cells were lysed with 80µl of provided lysis buffer, vortexed and lysed at room temperature for 5 minutes. Galacton™ was diluted (1:100) in Reaction buffer and aliquoted (70µl) in to wells of the luminometer plate. Lysed samples (20µl) were added to the Galacton-containing wells in triplicates and then incubated in the dark at room temperature for 30-minutes. β-galactosidase activity was measured using a luminometer after an injection of Light Emission Accelerator (100µl).This assay facilitates normalisation of the NFAT-Luciferase assay data for variation in transfection efficiencies of each sample.

2.6 Flow cytometry

Harvested cells were aliquoted into FACs tubes. Transfected cells were centrifuged at 1200 x g for 5minutes and the supernatant was aspirated. The cells were incubated in 50µl mouse anti-human GPVI mAb (HY101, 10µg/ml) for 30 minutes at 4C. Cells were washed in FACS buffer (PBS, 0.2% BSA, 0.02% sodium azide), centrifuged for 5 minutes and the supernatant was aspirated. The cells were then incubated in 50µl FITC-conjugated anti-mouse IgG for 30 minutes at 4°C. The cells were resuspended in 500µl FACs buffer containing the cell-viability dye propidium iodide. Cells were analysed using FACScalibur flow cytometer. Data was analysed using CellQuest™ software.

2.7 Western Blot

2.7.1 Buffers

1% Triton-X-100 lysis buffer: 1%(v/v) Triton X-100, 10mM Tris pH 7.5, 150mM NaCl, 1mM EDTA, 0.01% (w/v) sodium azide and Protease cocktail inhibitor.

12% Lower Gel: 30% Acrylamide (4ml), Lower gel buffer (2.5ml), distilled water (3.4ml), 10% w/v Ammonium persulphate (APS) (100µl) and Temed (N,N,N,N-tetramethylethylenediamine) (3.3µl). Lower gel buffer: 183g Trizma base (pH8.8) and 500ml water, store at 4°C.

Stacking Gel: 30% Acrylamide (0.43ml), Stacking gel buffer (0.83ml), distilled water (2.1ml), 10% w/v ammonium persulphate (APS) (17µl) and Temed (N,N,N,N-tetramethylethylenediamine) (3.3µl). **Stacking gel buffer:** 80g Trizma base (pH6.8) and 500ml water, store at 4°C.

1x TBS: Tris base (20mM), NaCl (137mM), adjusted to pH 7.6.

1xTBST: Tris base (20mM), NaCl (137mM), Tween 20 (0.1%) adjusted to pH 7.6.

TBST High Salt: 1xTBST and NaCl (5M).

SDS-PAGE running buffer: Tris base (25mM), glycine (192mM) and SDS (0.1%)

Transfer Buffer: Tris base (20mM), glycine (150mM) and methanol (20%v/v) stored at 4°C.

Blocking buffer: Low-fat powdered milk (Marvel, U.K.) (5%) in 1X TBS-0.05% Tween.

2.7.2 Cell Lysis

Samples were first placed on ice. Next 75µl of 1% Triton-100 lysis buffer was added and tubes were vortexed. Lysis was allowed to proceed for 30 minutes on ice, with vortexing every 10 minute intervals. Samples were centrifuged for 10minutes at 14000 x g. Cell lysates were transferred to fresh 1.5ml eppendorf tubes containing 16.25µl 5x Non-reducing Laemmli sample buffer. Following brief vortexing, samples were boiled at 100°C for 5 minutes.

2.7.3 Gel Electrophoresis

Sequentially 12% SDS-resolving gel and stacking gel were cast into a gel cassette (1.5mm). Broad range protein ladder (Prestained Protein Marker, Broad Range, BioLabs) was added followed by the samples (40µl). The gels were submerged in running buffer and resolved at 125V for approximately 90 minutes. Upon completion, gels were placed in transfer buffer for 30 mintues. The Immobilon/PVDF membrane was then equilibrated in 100% methanol for approximately two mintues and then placed in transfer buffer for approximately 30 minutes. The transfer unit was assembled and run at 30V for 90 minutes. After transfer the membranes were placed blotted in 5% Blocking buffer overnight at 4˚C on a rocking platform. Membranes were washed with 1xTBS- 0.05% Tween and then incubated in the primary antibody, Mouse

Anti-Myc antibody (1:1000 dilution), overnight at 4˚C on a rocking platform. Three 10 minute washes were conducted in High-salt TBST and the membranes were incubated in secondary antibody, Anti-Mouse 800-Odyssey antibody (1:1000) or Goat Anti-mouse HRP antibody (1:6000) overnight at 4˚C on a rocking platform. Following four 15 minute washes with High-salt TBST and final wash with TBS, the membranes were analysed either with the Odyssey system or ECL immunodetection.

2.7.4 Odyssey

Following the final TBS wash, the Immobilon membranes were dried with filter paper and scanned on the Odyssey system (Licor Biosciences). Immobilon membranes were maintained in the dark to prevent loss of signal.

2.7.5 ECL Immunodetection

SuperSignal West Pico chemiluminesce reagent (Thermo Fisher Scientific, U.K.) was preprased as per manufacturers` instructions and applied to the membrane for 1 minute. Membranes were exposed in the dark to ECL film and developed using an X-O-graph.

3.1.1 SLAP1 and SLAP2 inhibit GPVI/FcR-γ signalling in a cell line model

SLAP inhibition of GPVI/FcR-γ was investigated using the NFAT/AP-1 luciferase assay established in the DT40 chicken B cell line. NFAT/AP-1 activation is an assay for intercellular calcium mobilisation and MAPK activation, respectively, downstream of ITAM-containing receptors. DT40 cells were transfected with NFAT/AP-1 reporter and GPVI/FcR-γ in the presence or absence SLAP1 and SLAP2. Non-stimulated cells transfected with GPVI/FcR-γ induced a basal NFAT/AP-1 activation that was 6.9-fold higher than the control-transfected cells. Stimulation with the GPVI agonist collagen increased the NFAT/AP-1 activation 3-fold. DT40 cells were individually co-transfected with SLAP1 or SLAP2. SLAP1 and SLAP2 reduced GPVI/FcR-γ signalling by 4- and 9-fold, respectively in collagen-stimulated cells.

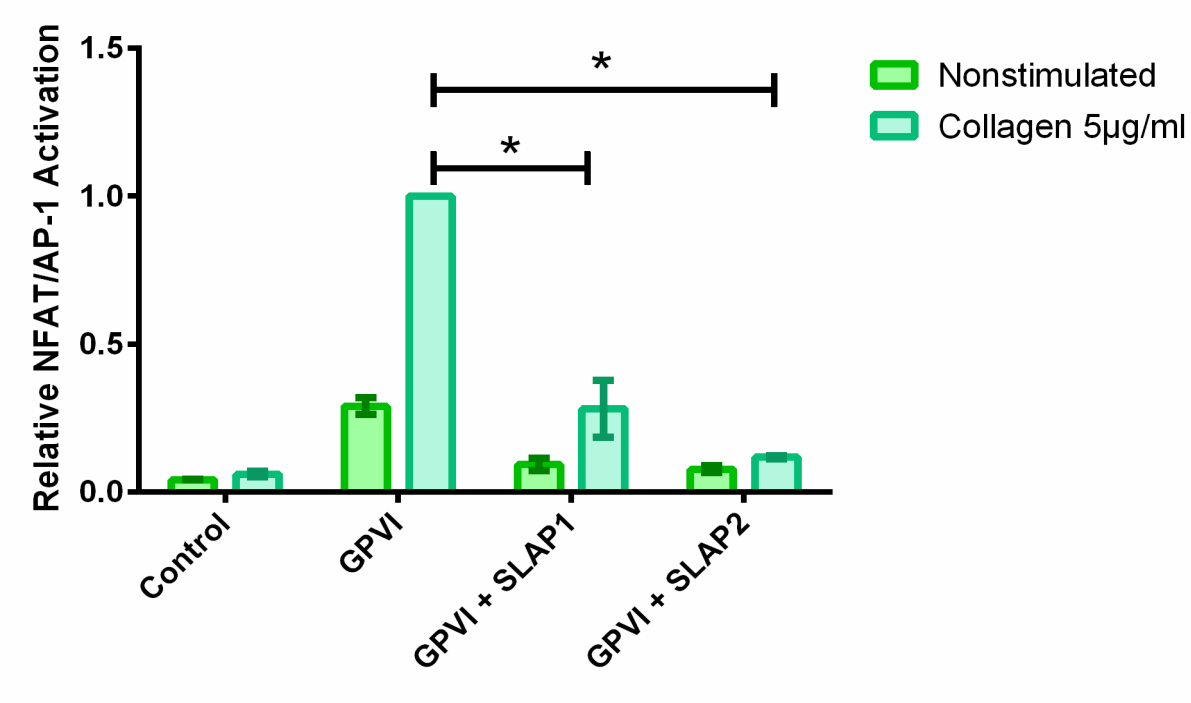

Figure 3.1.1 SLAP proteins inhibit basal and collagen-induced GPVI/FcR-γ signalling. Representative β-gal normalised arithmetic mean ±SEM of 3 data sets analysed with 1-tail, unpaired Student's t-test (P≤0.05). Data divided by collagen-stimulated GPVI value to obtain logarithmic data thus collagen-stimulated GPVI has no error bar. DT40 cells were transfected with 4µg GPVI/FcR-γ and 5µg SLAP1 or SLAP2. Collagen-stimulated GPVI induced substantial NFAT/AP-1 activation which was significantly reduced SLAP 1 (P=0.0431) and SLAP2 (P=0.0448). * ≤0.05

3.1.2 SLAP-mediated inhibition is specific to GPVI/FcR-γ signalling

Transfected cells were stimulated with positive control agonists, phorbol myristate acetate (PMA) and ionomycin, for calcium mobilisation and MAPK kinase activation independent of ITAM-receptor signalling. All samples stimulated with PMA and ionomycin responded robustly and to similar levels, indicating little variation in the calcium mobilisation and MAPK activation capacities of transfected cells. Furthermore it indicates the inhibitory effect of SLAP proteins was specific to GPVI and not due to a global inhibition of cell signalling (Figure 3.1.2).

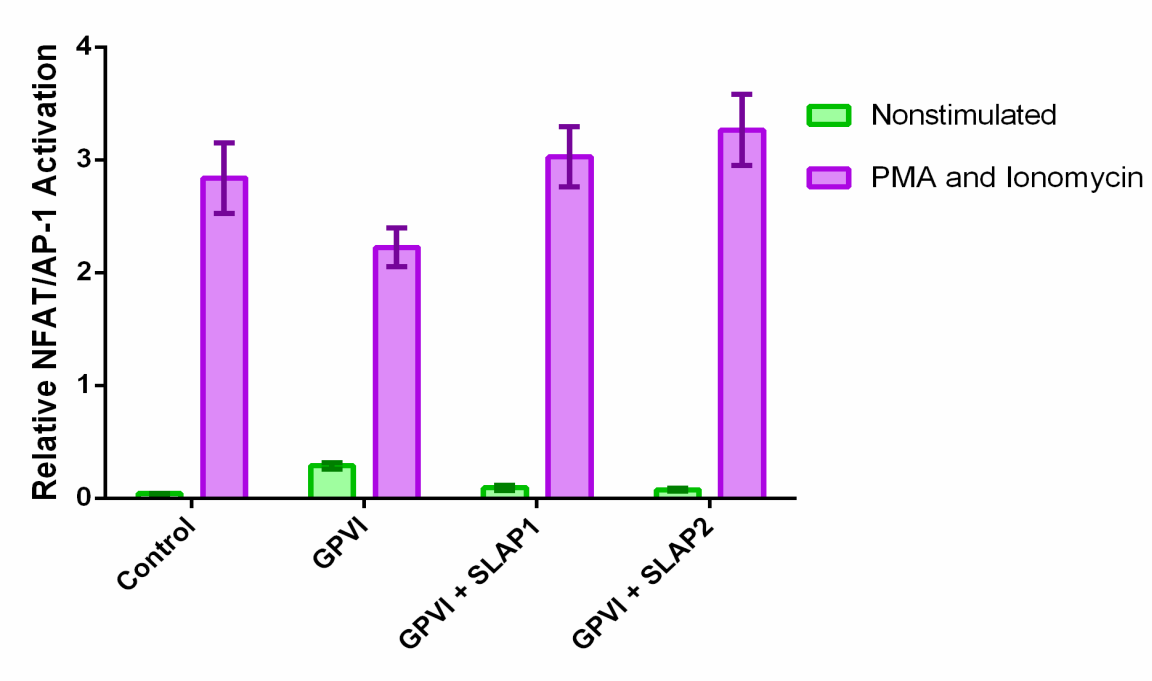

Figure 3.1.2 The PMA and ionomycin stimulation is not altered by SLAP proteins. Representative arithmetic mean ±SEM of 3 data sets normalised for β-gal. DT40 cells were transfected with NFAT/AP-1 reporter, β-galactosidase reporter and vector controls or 4µg GPVI/FcR-γ and 5µg SLAP1 or SLAP2, and stimulated with PMA and ionomycin. Relatively similar levels of NFAT/AP-1 activation observed upon PMA and ionomycin stimulation of DT40 cells. Co-transfection of SLAP proteins did not affect the PMA and ionomycin response.

3.1.3 Flow cytometry analysis of GPVI expression in SLAP-expressing DT40 cells

The GPVI expression levels were measured to determine whether the reduced GPVI/FcR-γ was due to decreased presentation of GPVI/FcR-γ on cell surface. Flow cytometry using FITC-conjugated anti-GPVI antibody was used to measure GPVI expression. The results show that

no GPVI is detected in control-transfected cells, whereas fluorescence is markedly increased in the GPVI/FcRγ transfected cells (Figure 3.1.3). The GPVI expression is not affected by co-transfection of SLAP proteins, indicating the decreased GPVI signalling is not due to decreased GPVI receptors.

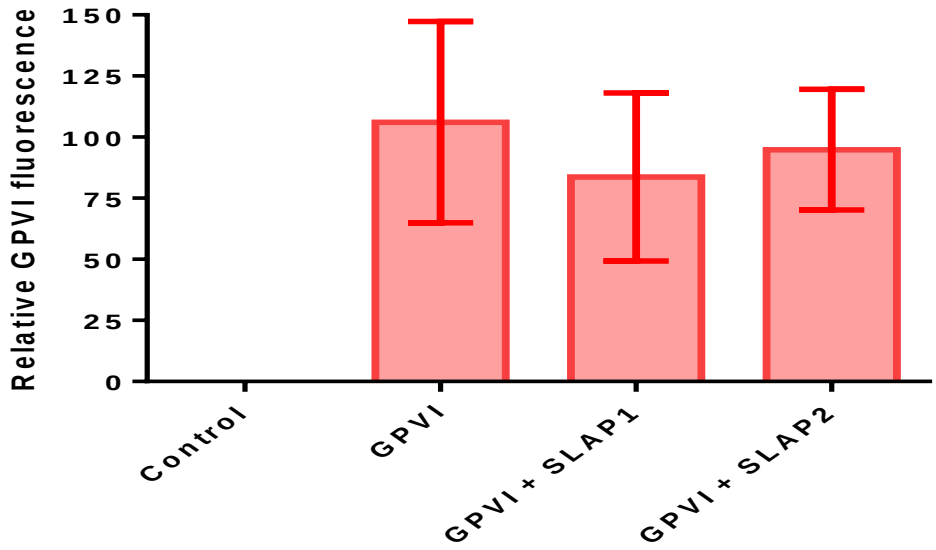

Figure 3.1.3 GPVI expression in not altered by co-expression of SLAP proteins. Representative arithmetic mean ±SEM of 3 data sets corrected for auto-fluorescence. DT40 cells were transfected with 4µg GPVI/FcR-γ and 5µg SLAP1 or SLAP2. Flow cytometric analysis of GPVI expression levels found similar GPVI expression levels in the absence or presence of SLAP proteins.

3.2.1 Optimisation of the NFAT/AP-1 Assay for analysis of GPVI/FcR-γ signalling

Comparing the data presented in Figure 3.1.1 to previous data, it was evident the basal GPVI/FcR-γ signalling response of non-stimulated cells was higher than previously observed in research establishing the DT40 cell line NFAT/AP-1 assay for GPVI signalling (Tomlinson *et al*. 2007). The high basal signal reduced the fold increase of GPVI signalling upon collagen stimulation. The high basal GPVI signalling and reduced collagen-stimulation distorts the relationship of collagen-induced signalling and misrepresents the magnitude of SLAP mediated inhibition. Therefore the assay was optimised to minimise the confounding basal GPVI signalling. To this end, the relationship between NFAT/AP-1 activation and the amount of

GPVI/FcR-γ construct was investigated to determine whether increased basal GPVI signal is due to increased GPVI receptors. DT40s were transfected with varying amounts of GPVI/ FcR-γ constructs (0, 0.25, 0.5, 1, 2µg) and the NFAT/AP-1 assay was conducted. The results demonstrate an inverse dose-dependent relationship where the NFAT/AP-1 activation is increased with decreasing quantities of GPVI/FcR-γ construct (Figure 3.2.1). Cells transfected with 2µg GPVI construct increased GPVI/FcR-γ signalling 8.8-fold upon collagen-stimulated whereas cells transfected with 0.25µg GPVI increased collagen-stimulated GPVI/FcR-γ signalling 33.8-fold over basal. The greater fold-increase in collagen stimulation increased the ratio of basal signal over collagen signal, therefore the basal signal was proportionally lesser with decreasing quantity of GPVI/FcR-γ construct. Higher proportion of collagen-stimulated signalling to basal signal was more comparable to previous NFAT/AP-1 assay data.

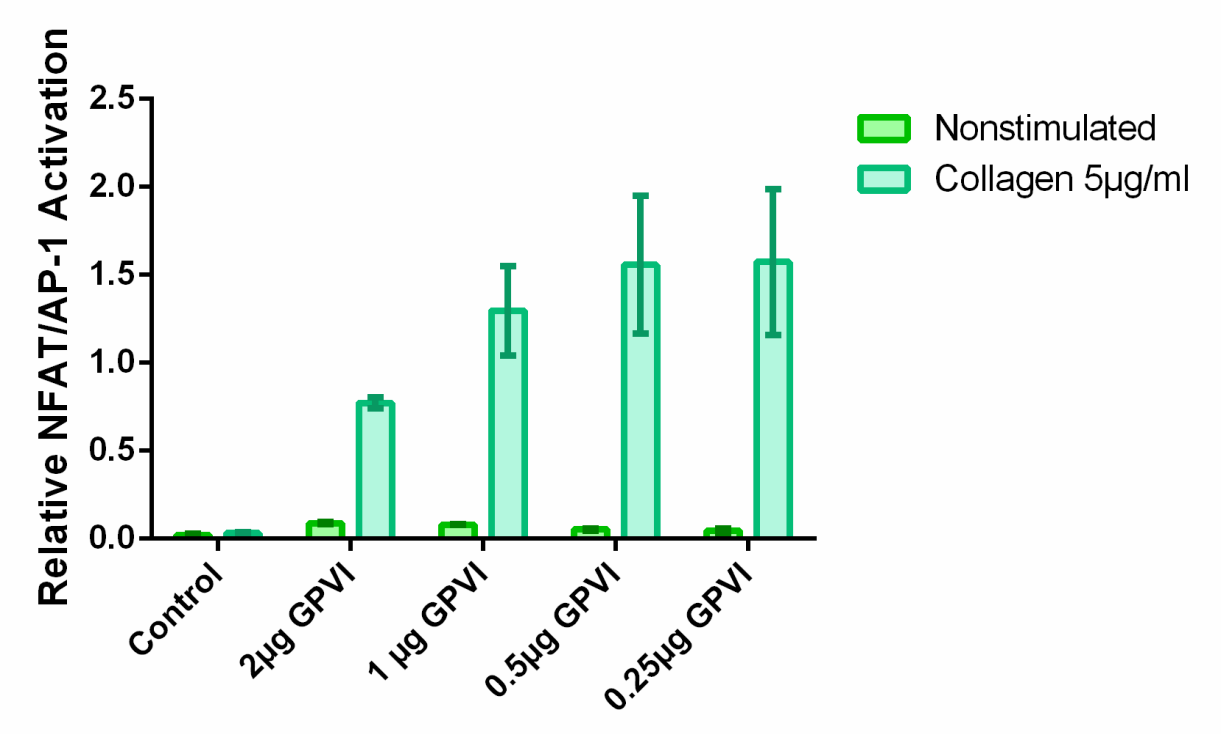

Figure 3.2.1 GPVI/FcR-γ induces collagen-stimulated NFAT/AP-1 activation in an inverse dose dependent manner. Representative β-gal normalised arithmetic mean ±SEM of 3 data sets. DT40 cells were transfected with 0,2,1,0.5 and 0.25µg of GPVI/FcR-γ construct. Nonstimulated cells displayed similar levels of basal signalling. The collagen-stimulated response increased with decreasing amounts of GPVI, increasing the proportion of collagen-response to basal signal.

3.2.2 Transfection with higher quantity of GPVI/FcR-γ construct does not alter calcium-mobilisation and MAPK activation capacities of DT40 cells

The NFAT/AP-1 assay was repeated with positive control agonists PMA and ionomyin (Figure 3.2.2). The response to PMA and ionomycin stimulation was not varied by the amount of GPVI DNA transfected into cells indicating all transfected samples were receptive to calcium mobilisation and MAPK activation to similar levels. Therefore the amount of GPVI/FcR-γ plasmid does not affect the global machinery involved in calcium mobilisation and MAPK activation. Thus the dose-dependent variation of collagen-stimulated NFAT/AP-1 activation is specific to increase in GPVI/FcR-γ signalling.

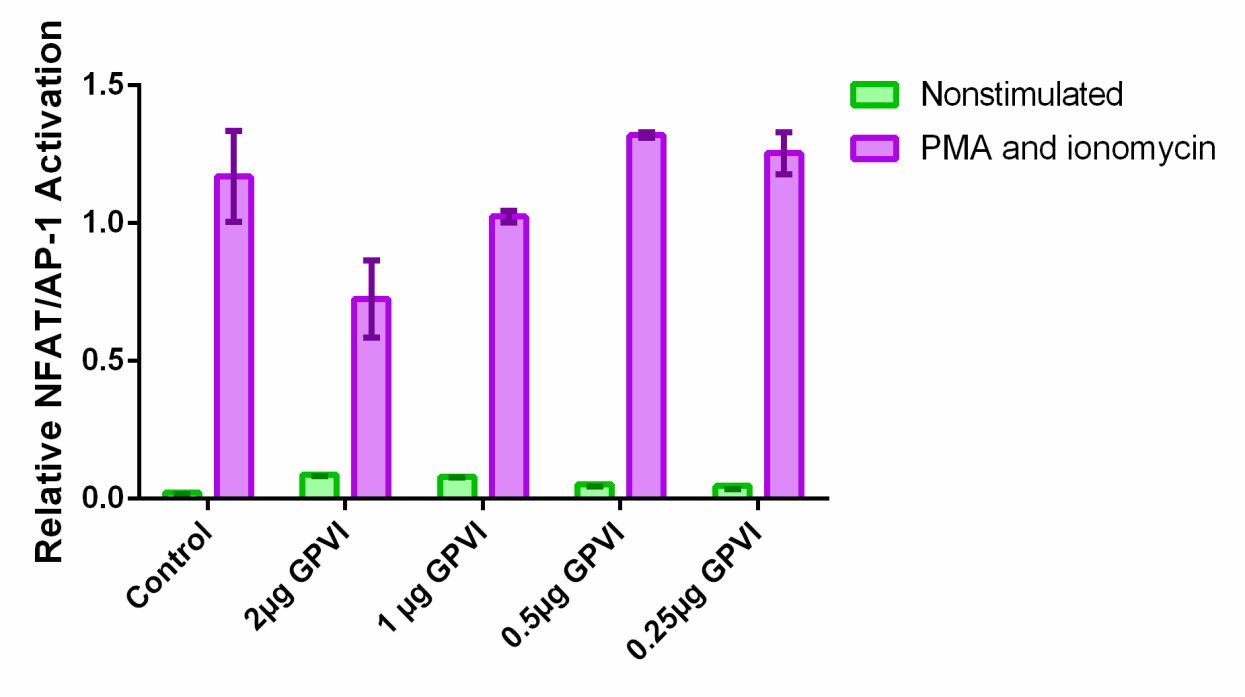

Figure 3.2.2 The PMA and ionomycin response is not affect by the quantity of GPVI/FcR-γ construct. Representative arithmetic mean ±SEM of 3 data sets normalised for β-gal values. DT40 cells transfected with varying quantities of GPVI/FcR-γ construct (0, 2, 1, 0.5, 0.25µg) were stimulated with PMA and ionomycin. All samples similarly responded robustly to PMA and ionomycin stimulation.

3.2.3 GPVI expression levels decrease in dose-dependent manner

To correlate the reduced NFAT/AP-1 activation to GPVI levels, the surface expression levels of GPVI were quantified by flow cytometry. As expected GPVI levels decreased with decreased construct transfection. This suggested the high levels of NFAT/AP-1 activation occurred at lower GPVI expression levels. Transfection with 2µg and 1µg of GPVI construct produced similar levels of GPVI expression, indicating a plateau of GPVI expression at 1µg GPVI construct. Therefore when cells were transfected with 2µg GPVI/FcR-γ construct, the excessive expression of GPVI is repressed by down-regulation of GPVI receptor. Measurement of GPVI expression levels precedes the 6-hour collagen-incubation of the NFAT/AP-1 assay, during this period cells transfected with higher quantities of GPVI/FcR-γ construct can substantially downregulate the GPVI receptor. As a result the NFAT/AP-1 activation at higher quantities of GPVI construct is lower than smaller quantities of GPVI construct.

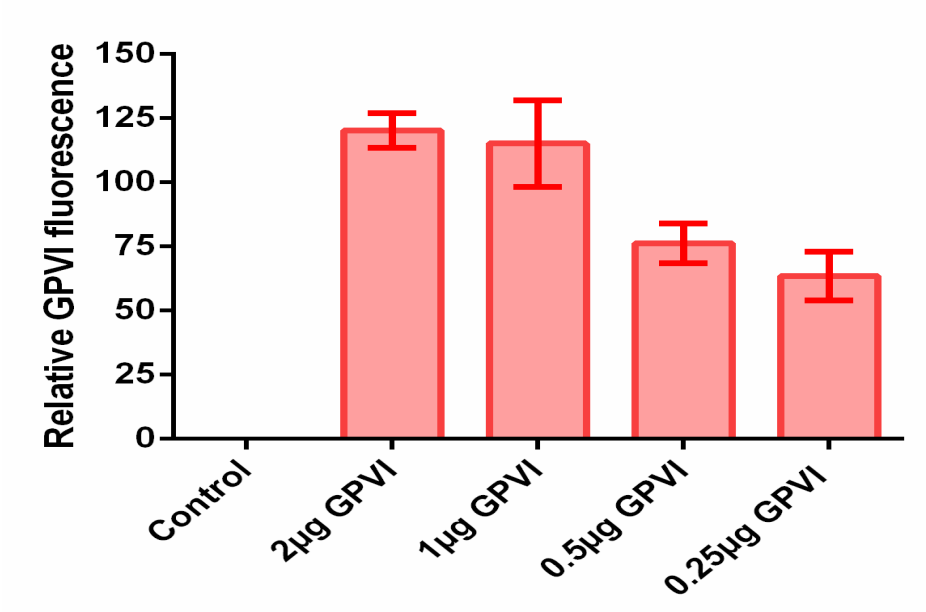

.

Figure 3.2.3 GPVI expression is reduced in decreasing quantities of GPVI/FcR-γ construct. Representative arithmetic mean ±SEM of 3 data sets corrected for auto-fluorescence. DT40 cells were transfected with varying quantities of the GPVI/FcR-γ construct. Analysis of GPVI expression levels demonstrated GPVI levels decreased with decreasing dose of GPVI/FcR-γ.

3.3.1 SLAP-mediated inhibition at optimised GPVI/FcR-γ concentration

The previous investigation demonstrated the collagen-stimulated NFAT/AP-1 activation was enhanced at lower concentrations of GPVI/FcR-γ. Transfections with lower amounts of GPVI increase GPVI/FcR-γ signalling by increasing the retainment of the receptor complex on the cell surface. High GPVI/FcR-γ concentrations and initial overexpression activate negative feedback pathways to downregulate the receptor. The greatest proportion of collagen-induced GPVI signalling was observed at 0.25µg of GPVI/FcR-γ construct. Therefore the NFAT/AP1 assay was repeated with optimised quantity (0.25µg) of GPVI construct. Implementation of the optimised concentration decreased basal signalling and diminished variation between the basal signals of samples. The collagen-induced GPVI signalling was 33-fold higher the basal (Figure 3.3.1). At optimised GPVI/FcR-γ concentrations, SLAP1 and SLAP2 significantly inhibited collagen-induced signalling by 22 and 12 fold, respectively, an improvement from our previous observation of 4 and 9 fold inhibition, respectively (Figure 3.1.1).

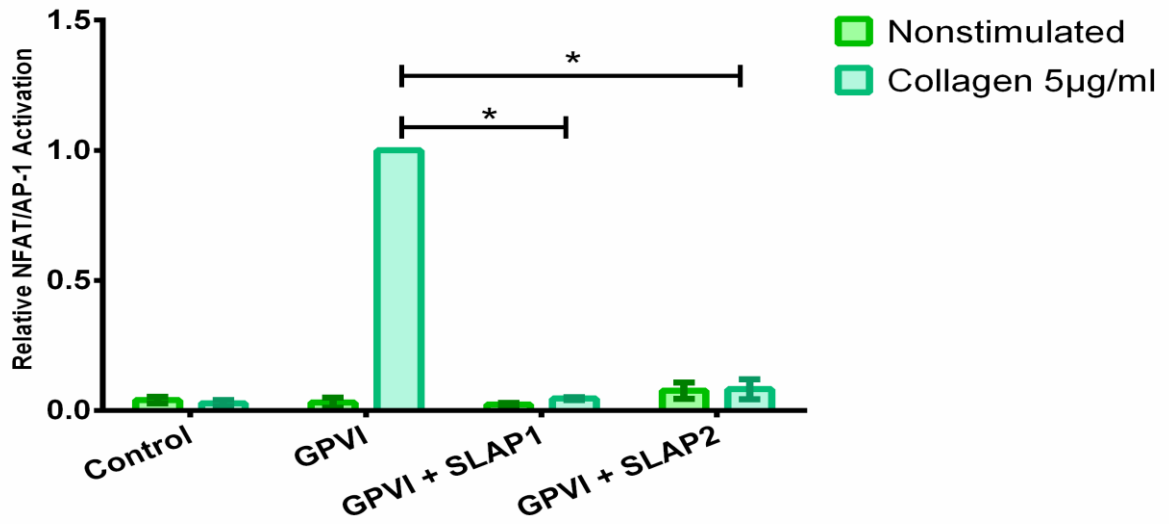

Figure 3.3.1 SLAP proteins inhibit GPVI signalling at optimised concentrations of GPVI/FcR-γ. Representative arithmetic mean±SEM of 3 data sets, normalised for β-gal, analysed with 1-tail, unpaired Student's t-test (P≤0.05). Data divided by collagen-stimulated DT40 cells were transfected with NFAT/AP-1reporter, β-galactosidase reporter and 0.25µg GPVI/FcR-γ and 5µg SLAP1 or SLAP2. Collagen-stimulated GPVI signalling was significantly reduced SLAP1 (P=0.0361) and SLAP2 (P=0.0389). * ≤0.05

3.3.2 SLAP proteins do not affect GPVI/FcR-γ signalling induced by positive control agonists PMA and ionomycin

DT40 cells transfected with optimised GPVI/FcR-γ concentrations were investigated for response to positive control agonists for calcium mobilisation and MAPK activation. The nonstimulated NFAT/AP-1 activation was substantially increased upon stimulation with PMA and ionomycin. Stimulation induced similar level of response in all transfected samples. These results restate those presented in Figure 3.1.1 except the variation between the nonstimulated and collagen-stimulated GPVI/FcR-γ signalling is distinctly increased attributed to optimisation of GPVI concentration. As aforementioned the co-expression of SLAP proteins in GPVI-transfected DT40s does not alter the calcium mobilisation and MAPK activation response to agonists. Therefore SLAP proteins inhibit receptor-proximal signalling. SLAP inhibition is specific to GPVI/FcR-γ and not due to cell-wide disruption of signalling.

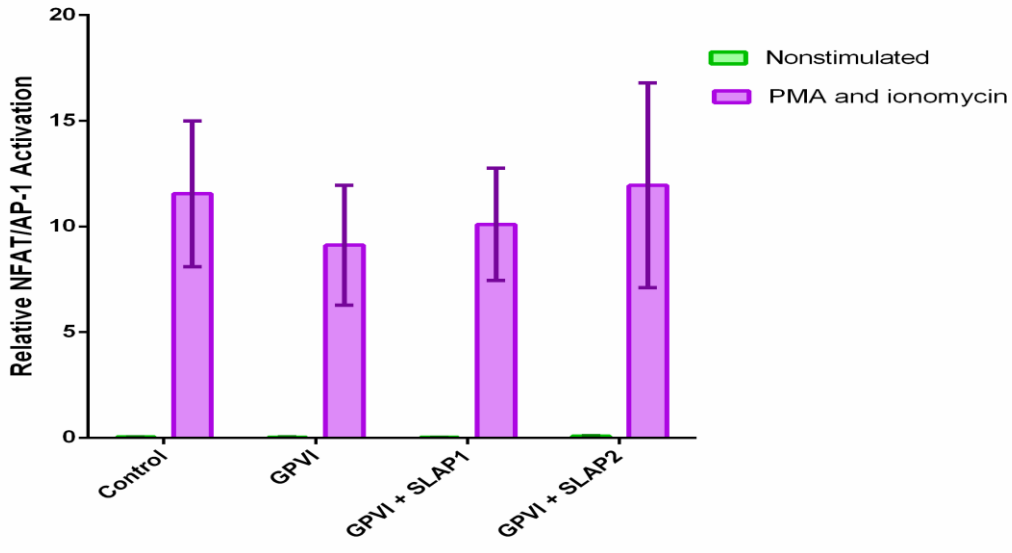

Figure 3.3.2 SLAP proteins do not affect PMA- and ionomycin-stimulated GPVI signalling. Representative arithmetic mean±SEM of 3 data sets normalised for β-gal values. DT40 cells transfected with NFAT/AP-1 reporter, β-galactosidase construct, and 0.25µg GPVI/FcR-γ and 5µg SLAP1 or SLAP2. Cells stimulated with PMA and ionomycin produced relatively similarly levels of NFAT/AP-1 activation. Co-transfection of SLAP proteins did not affect the PMA and ionomycin- stimulated GPVI signalling.

3.3.3 Investigation of GPVI expression levels in SLAP-transfected DT40 cells at optimised concentrations of GPVI/FcR-γ

The surface GPVI expression levels determined whether SLAP-mediated reduction of GPVI/FcR-γ signalling was due to reduced number of membrane GPVI/FcR-γ complexes. DT40s were transfected with the optimised concentration of GPVI/FcR-γ (0.25µg) to detect expression level variation at lower concentrations which would be overlooked at higher construct concentrations. The results (Figure 3.3.3) demonstrate non-significant variation of GPVI expressions levels in the presence of SLAP proteins. Unexpectedly GPVI expression levels were slightly increased in the presence of SLAP1 and SLAP2. These results eliminate the receptor degradation mechanism of SLAP-mediated inhibition and support the earlier finding (Figure 3.1.3) that SLAP-mediated inhibition is independent of GPVI expression levels.

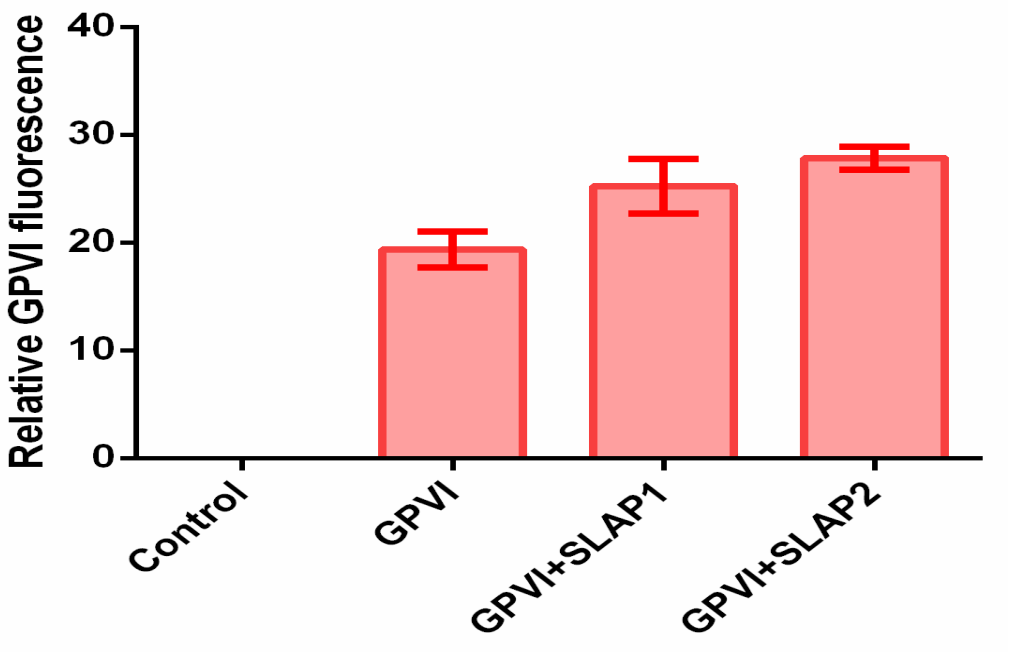

Figure 3.3.3 SLAP proteins do not alter GPVI expression levels. Representative arithmetic mean±SEM of 3 data sets corrected for auto-fluorescence. DT40s were transfected with 0.25µg GPVI/FcR-γ and 5µg SLAP1 or SLAP2. GPVI expression levels are relatively similar in the absence or presence of SLAP proteins.

3.4.1 SLAP2 mutants inhibit collagen-stimulated GPVI/FcR-γ signalling to varying degrees

Previous research has indicated the predominant presence of SLAP2 proteins in platelets (Sugihara, *et al* 2010). In order to further investigate the inhibitory activity of SLAP2 proteins, SLAP2 domain mutants were acquired and investigated using the NFAT/AP-1 assay. Each SLAP2 variant was mutated in one domain whilst the rest of the SLAP2 structure was intact. Function-blocking mutation of each domain investigated the contribution of the domain to SLAP2 inhibitory function and implied the potential mechanism of inhibition. DT40 cells were transfected with NFAT/AP-1 reporter and β-galactosidase construct, and then with either empty vector control, GPVI only, or GPVI and SLAP2 mutants. All transfected samples had similar levels of basal signalling. The GPVI signalling response was measured following 6-hour collagen stimulation. GPVI-transfected cells exhibited substantial increase in NFAT/AP-1 activation upon collagen stimulation. In contrast, empty-vector controls did not increase collagen-stimulated signalling. The SLAP2 wild-type demonstrated maximal inhibition (57-fold) of collagen-stimulated GPVI signalling whilst the SLAP2 mutants presented intermediate levels of inhibition. The inhibitory activity of the c-terminal truncated mutant, SLAP2 ΔC, was impaired most demonstrating 2-fold inhibition of collagen-stimulated GPVI signalling. Signal inhibition was reduced by mutation of the SH2 domain mutant, exhibiting 7-fold inhibition. Mutation of myristoylation domain (SLAP2 G2A) reduced inhibitory activity and only inhibited collagen-stimulation GPVI signalling 9-fold. Mutation of the SH3 domain did not vastly disrupt inhibitory activity as the 35-fold inhibition was comparable to the SLAP2 wild-type. Taken together, these results indicate a greater role of the c-terminal in the SLAP2-mediated GPVI inhibition followed by the SH2 domain, and the myristoylation sequence. The results indicate the SH3 domain has a minimal contribution to inhibition activity.

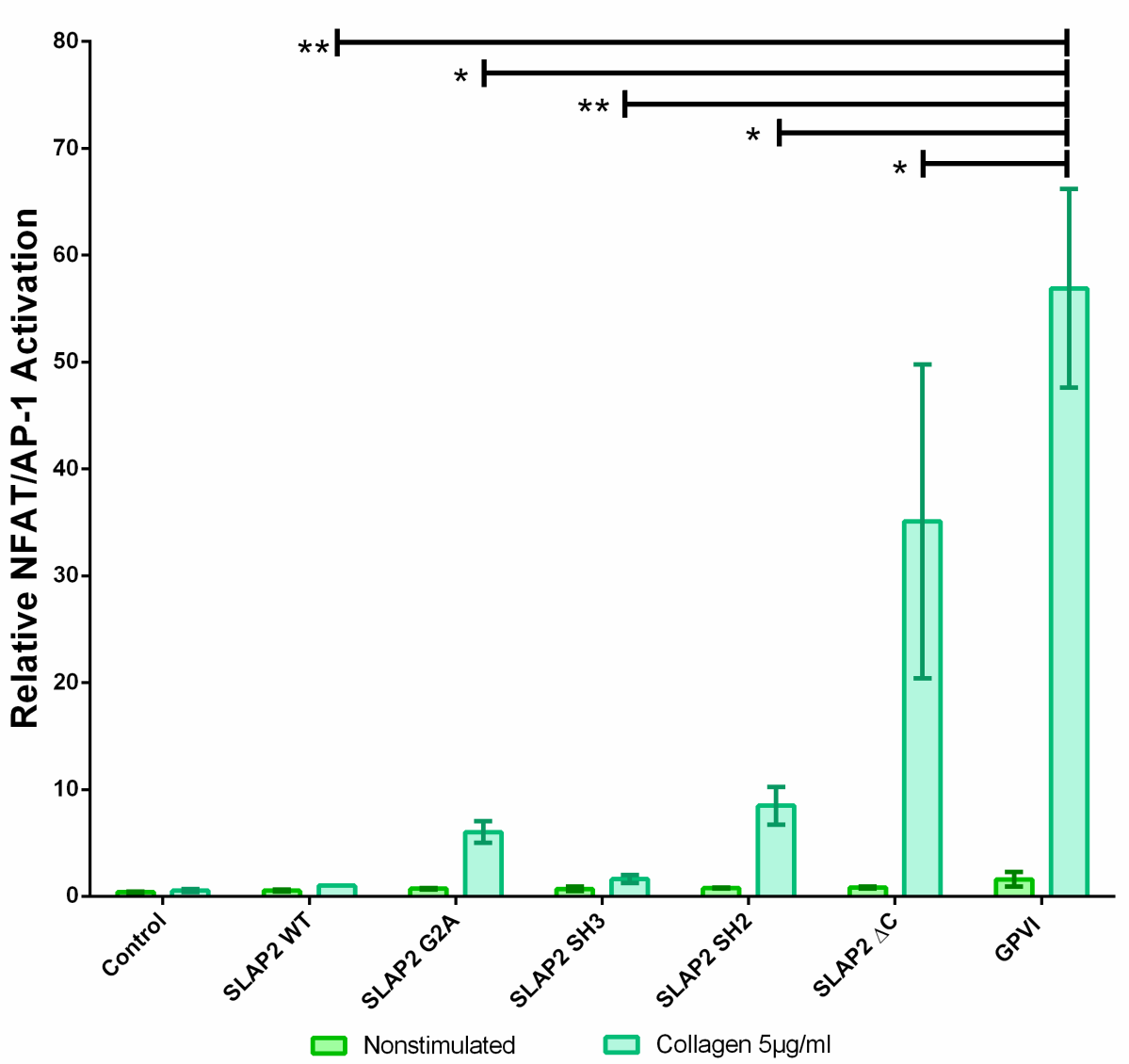

Figure 3.4.1 SLAP2 mutants inhibit collagen-induced GPVI/FcR-γ signalling to varying degrees. Representative β-gal normalised arithmetic mean ±SEM of 3 data sets analysed with 1-tail, unpaired Student's t-test ($P<0.05$). Data divided by collagen-stimulated SLAP WT value to obtain logarithmic data thus collagen-stimulated SLAP WT has no error bar. DT40 cells were transfected with NFAT/AP-1reporter, β-galactosidase reporter and 0.25µg GPVI/FcR-γ and 5µg SLAP2 variants. Collagen-stimulated GPVI/FcR-γ signalling was significantly inhibited by the SLAP2 WT ($P=0.0093$), SLAP2 G2A ($P=0.0112$), SLAP2 SH3 ($P=0.0094$), SLAP2 SH2 ($P=0.0123$) and SLAP ΔC ($P=0.0415$).

* ≤0.05

**≤0.01

3.4.2 SLAP2 mutants do not affect GPVI/FcR-γ signalling induced by positive control agonists PMA and ionomycin

GPVI/FcR-γ signalling was measured in response to positive control agonist for calcium mobilisation and MAPK activation. All transfected samples responded to stimulation with PMA and ionomycin. There was some non-significant variation between samples but on the whole the relative levels of NFAT/AP-1 activation were similar. These results indicated the co-expression of SLAP2 mutants did not disrupt cell-wide signalling responses. Instead the inhibitory activity of SLAP2 is specific to collagen-stimulated GPVI/FcR-γ signalling.

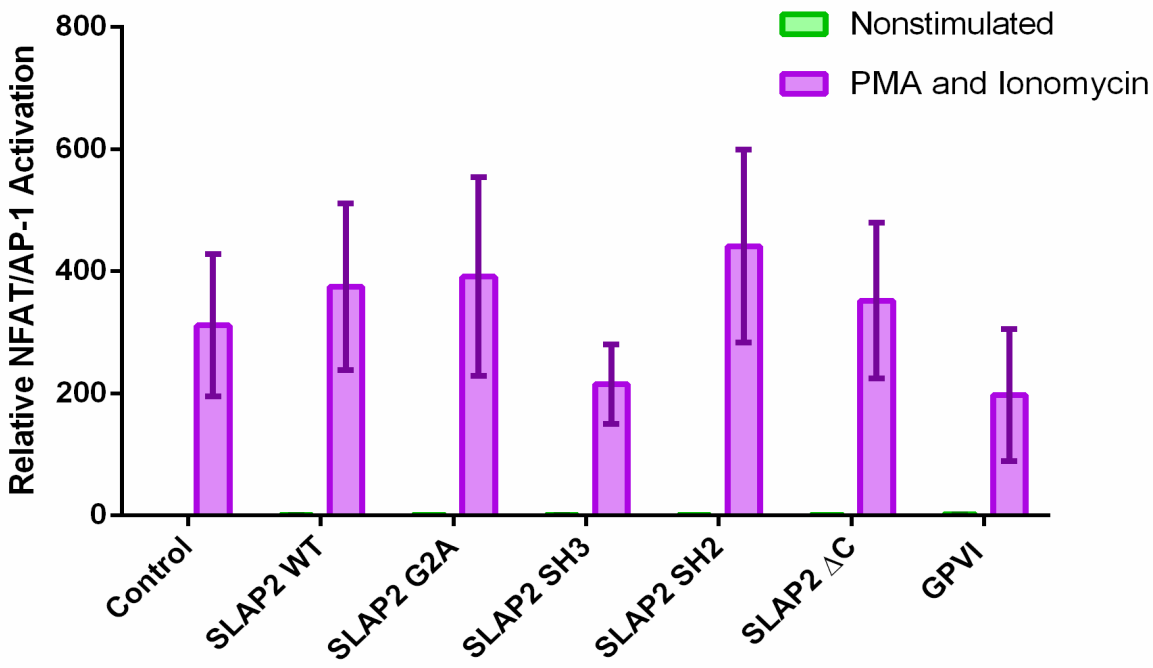

Figure 3.4.2 SLAP2 mutants do not affect PMA- and ionomycin-stimulated GPVI signalling. Representative arithmetic mean±SEM of 3 data sets normalised for β-gal values. DT40 cells were transfected with NFAT/AP-1 reporter, β-galactosidase construct, and vector control or 0.25µg GPVI/FcR-γ and 5µg SLAP2 mutants. The nonstimulated response was considerably small in comparison the PMA- and ionomycin- stimulated NFAT/AP-1 activation. PMA- and ionomycin-stimulation increased NFAT/AP-1 activation in all transfected samples.

3.4.3 Co-expression of SLAP2 mutants does not alter surface GPVI expression levels

The GPVI levels were quantified by flow cytometry to determine whether the inhibition of GPVI/FcR-γ was due to decreased receptor expression. The results demonstrated cells co-transfected with the SLAP2 mutants expressed GPVI to similar levels as cell transfected with GPVI only (Figure 3.4.3). The results indicate SLAP2 mutants inhibit GPVI signalling independent of GPVI expression levels.

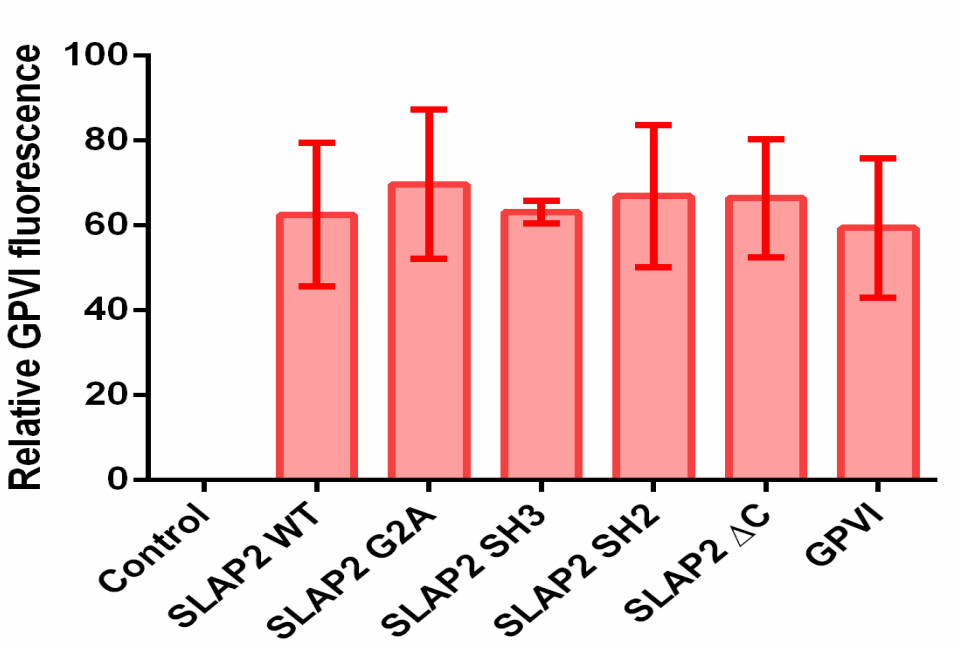

Figure 3.4.3 GPVI expression in not altered by co-expression of SLAP2 mutants. Representative arithmetic mean ±SEM of 3 data sets corrected for auto-fluorescence. DT40 cells were transfected with NFAT/AP-1 reporter, β-galactosidase construct, and vector control or 0.25µg GPVI/FcR-γ and 5µg SLAP2 mutants. Flow cytometric analysis of GPVI expression levels found GPVI expression levels were unaffected by the co-expression of SLAP2 mutants.

3.4.4 Western Blot analysis confirmed SLAP2 mutants are expressed to similar levels in transfected DT40 cells

Western blot of myc-tagged SLAP2 mutants confirmed the presence of SLAP proteins in transfected DT40s and demonstrated qualitatively similar levels of expression. Whole-cell lysate of transfect cells were analysed by SDS-PAGE blotted with anti-myc antibody and processed using the Odyssey system (Figure 3.4.4) The SLAP2 wild-type, SH2 domain mutant and the c-terminal mutant were expressed to similar levels. The myristoylation mutant SLAP2 G2A was expressed at slightly higher levels. Preliminary laboratory observations found the SLAP2 SH3 was not detected in western blots processed with the Odyssey system. In attempt to optimise detection of SLAP SH3 mutant, western blots were conducted with the more sensitive detection method of ECL immunoblotting (Figure 3.4.5). The SLAP2 wild-type, the SLAP2 G2A mutant and the SLAP2 SH3 mutant were detected. A faint band was detected for the SLAP2 ΔC mutant. The SLAP2 SH2 mutant was not detected possibly due to sample preparation error. There was some variation in the level of expression of SLAP2 mutants; however without quantitative analysis it cannot be determined whether the expression variation would have a significant effect on inhibition cannot be determined. Qualitative observations suggest the variation of expression is not sufficient to account for the pattern of inhibition observed with SLAP2 mutants.

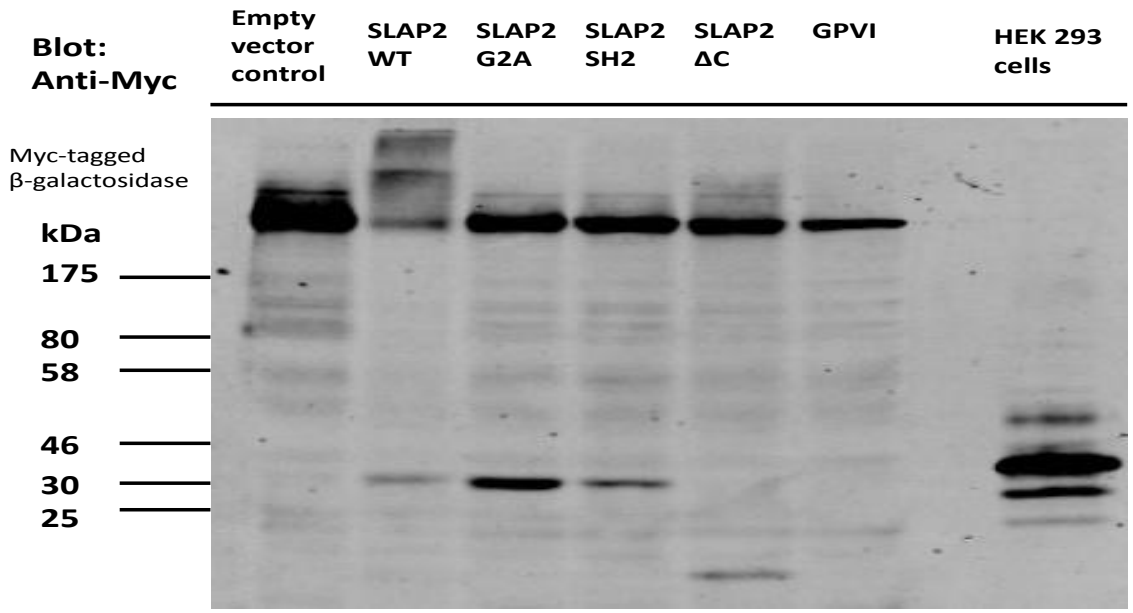

Figure 3.4.4 Anti-myc western blot of SLAP2 mutants detected using Odyssey system. Whole-cell lysates were blotted with anti-myc antibody to detect myc-tagged SLAP proteins. SLAP2-transfected HEK293 cells is a positive control. Tetrameric myc-tagged β-galactosidase (465kDa) was the loading control. SLAP2 WT and mutants were expressed to relatively similar levels.

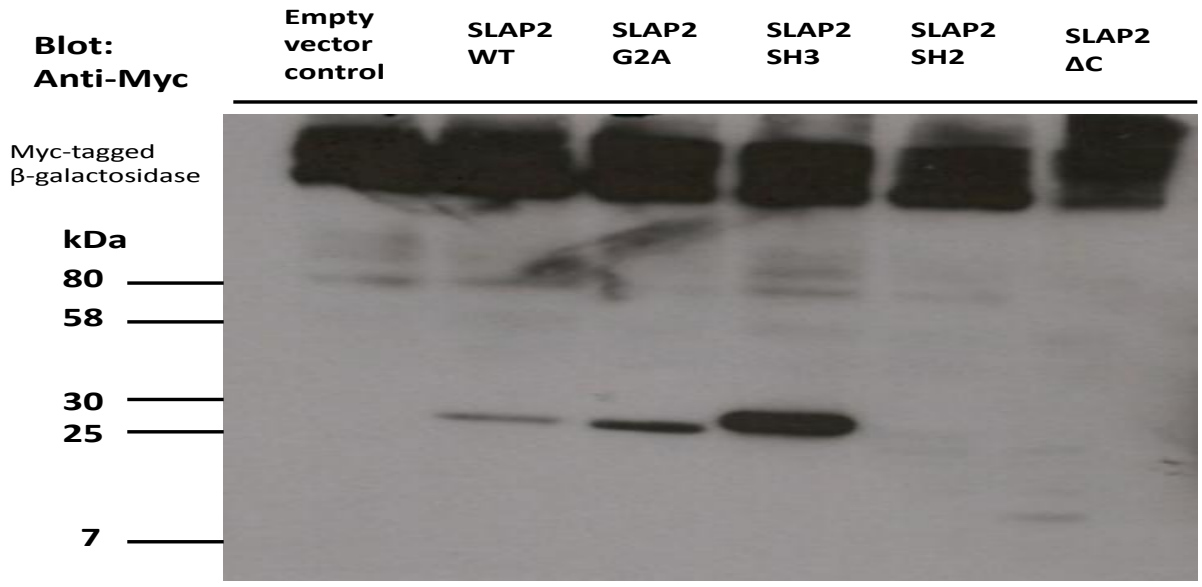

Figure 3.4.5 Anti-myc western blot of SLAP2 mutants detected by ECL. Whole-cell lysates were blotted with anti-myc antibody to detect myc-tagged SLAP proteins. Tetrameric myc-tagged β-galactosidase (465kDa) served as a loading control. The SLAP2 WT, G2A mutant and SH3-domain mutant were detected.

Chapter 4. Discussion

4.1 **SLAP1 and SLAP2 inhibit GPVI/FcR-γ signalling in a cell line model**

In this study the potential role of Src-Like Adaptor Proteins (SLAP) in regulating GPVI signalling was investigated in a cell line model using the NFAT-luciferase reporter assay. DT40 cells transfected with GPVI/FcR-y increased NFAT/AP-1 activation, which is a measure of GPVI-induced calcium mobilisation and MAPK activation. The GPVI signalling response was markedly increased by collagen-stimulation. The collagen-stimulated GPVI signalling was reduced in the presence of SLAP1 and SLAP2. The calcium mobilisation and MAPK activation capacities of cells were unaltered in the presence or absence of SLAP proteins, demonstrating the inhibition of NFAT/AP-1 activation was specific to GPVI receptor-proximal signalling, rather than a global inhibition of signalling. Furthermore GPVI expression levels were not affected by co-expression of SLAP proteins indicating that this reduction of signalling was not due to direct degradation of the receptor at the plasma membrane. Therefore a hypothesis is proposed where the inhibition of signalling involves disruption of the intrinsic signalling pathway.

Preliminary evidence of SLAP-mediated regulation of GPVI signalling was provided by the Nieswandt, Watson and Tomlinson groups [unpublished data]. Platelets of $SLAP1^{-/-}/SLAP2^{-/-}$ double knockout mice had significantly elevated levels of GPVI mRNA relative to control mice and GPVI stimulated-platelet aggregation was hyper-responsive in the absence of SLAP proteins (Appendix 1.A). To determine whether hyper-responsive GPVI signalling in $SLAP1^{-/-}SLAP2^{-/-}$ deficient mice was due to elevated GPVI expression levels, a GPVI gene was deleted in SLAP-double knockout mice to normalise GPVI expression levels. The signalling response of the $SLAP1^{-/-}/SLAP2^{-/-}/GPVI^{+/+}$ knockout mice was then compared to $SLAP1^{-/-}/SLAP2^{-/-}/GPVI^{+/-}$ mice. As expected, mice homozygous for GPVI had significantly elevated expression levels of GPVI and significantly increased signalling response compared to

control mice (Appendix 2.A). In GPVI heterozygous mice, despite the normalised GPVI expression levels, the signalling remained hyper-responsive relative to control mice (Appendix 2.B). These findings correlate with the data presented in this study demonstrating SLAP-mediated inhibition does not target GPVI expression levels; instead it is directed at the signalling pathway.

The inhibitory activity of SLAP proteins has been established for a number of receptors such as PDGF, BCRs, TCRs, GM-CSF and Epo-R (Manes *et al*. 2000; Dragone *et al.* 2006; Myers et al. 2005; Liontos *et al*. 2011; Lebigot *et al*. 2003). These reports suggest SLAP proteins mediate downregulation of receptor-specific activities. The *in vivo* expression of SLAP proteins in platelets indicates a regulatory role of SLAP proteins in receptor-specific events in platelets responses. Convulxin stimulation, a GPVI-specific agonist, increased the expression of SLAP2 and translocation to the plasma membrane in human platelets (Sugihara *et al.* 2010). The SLAP2 proteins co-immunoprecipitated with c-Cbl, Syk and LAT upon GPVI stimulation and were unaffected by inhibitors of *secondary wave mediators* and integrins (Sugihara *et al.* 2010). However the crude immunoblotting method of adding exogenous GST-SLAP2 to lysed platelets does not accurately reflect putative intracellular interactions and concentrates SLAP proteins above physiological range favouring interactions which would not occur at endogenous levels of SLAP2.Though Sugihara *et al.* demonstrated that SLAP2 is responsive to GPVI activation, the effect on signalling response could not be inferred, thus this study provides a valuable continuation of Sugihara *et al*. study where the signalling response is indirectly measured. Receptor activation is a requisite of SLAP activity and localisation; previous studies have demonstrated receptor stimulation activates Lck-mediated recruitment of SLAP to TCRζ chain (Myers *et al*. 2005), and induces SLAP colocalisation with the IgM chain of BCRs (Dragone *et al.* 2006). Accordingly, GPVI stimulation potentiates the inhibitory activity of SLAP proteins. Additionally SLAP proteins

reduced basal GPVI signalling in the absence of stimulation. It was suspected that this was due to a confounding error as the basal signal in GPVI-transfected cells was high than previous data collected with this assay (Tomlinson *et al*. 2007). Unaccounted NFAT/AP-1 activation in the absence of GPVI stimulation misrepresents the relationship between nonstimulated and stimulated GPVI signalling. For this reason the assay was optimised in attempt to minimise basal signalling.

4.2 Optimisation of the NFAT/AP-1 Assay for analysis of GPVI/FcR-γ signalling

The data presented in Figure 3.1.1 was not comparable to previously conducted NFAT-luciferase assays for GPVI signalling in DT40s (Tomlinson *et al.* 2007).The collagen-stimulation GPVI signalling (3.5-fold over basal) was grossly lower than previous data which reported a 700-fold increase upon collagen stimulation (Tomlinson *et al.* 2007). Also the basal signal was higher in GPVI-transfected cells compared to vector-transfected controls, whereas previously the nonstimulated signals in control and GPVI-transfected samples were approximately proportional. The high basal GPVI signal alters the ratio between non-stimulated and collagen-stimulated signalling and therefore misrepresents the capacity of collagen to induce GPVI signalling. Furthermore the extraneous basal GPVI signal misrepresents the relationship between GPVI and SLAP proteins in the nonstimulated samples, and diminishes the level of SLAP-mediated inhibition observed in collagen-stimulated samples. For this reason an objective in this study was to optimise the assay to reduce basal GPVI signalling and enhance collagen-stimulated signalling.

The basal GPVI/FcR-γ has been previously investigated by the uncoupling of the GPVI/FcR-γ complex into its constituent components and transfection into DT40s (Mori *et al*. 2008). GPVI was not expressed in the absence of FcR-γ. FcR-γ is expressed independent of GPVI and constitutively activates NFAT/AP-1 production. Furthermore, FcR-γ -induced

NFAT/AP-1 was increased upon collagen stimulation (Mori *et al.* 2008). Mori *et al*. observed a dose-dependent increase in collagen-stimulated NFAT/AP-1 activation upon increasing concentrations of the FcR-γ plasmid. Thus the high basal NFAT/AP-1 activation observed in this study corresponds to the relatively high quantity of the GPVI/FcR-γ construct. To address this, a series of transfections were conducted with decreasing quantities of the GPVI/FcR-γ construct (2, 1, 0.5 and 0.25µg). Subsequently the GPVI signalling was measured under nonstimulated and collagen-stimulated conditions by means of the NFAT-luciferase reporter assay (Section 3.2). All transfected samples exhibited reduced basal signalling due to the decreased FcR-γ plasmid concentration and consequently reduced FcR-γ-mediated NFAT/AP-1 activation. An inverse dose-dependent relationship of collagen-induced signalling was observed, such that increasing GPVI/FcR-γ concentration reduced the NFAT/AP-1 activation. The assay was repeated with positive control agonists for MAPK activation and calcium influx demonstrating that the quantity of GPVI/FcR-γ transfected into cells did not substantially affect the cellular receptiveness to calcium mobilisation and MAPK activation. GPVI expression levels were reduced corresponding to decreasing quantity of GPVI/FcR-γ construct. Taken together these results indicate that decreasing GPVI levels increases GPVI signalling upon collagen-stimulation. It is notable at higher concentrations of the GPVI/FcR-γ construct the ratio between the non-stimulated and stimulated response is reduced, indicating the responsiveness of these receptors to collagen stimulation is reduced.

The inverse relationship between quantity of GPVI construct and collagen-stimulated GPVI signalling can be explained in the context of adaptation. To limit the duration of signalling, receptors undergo adaptation, a process of ligand-induced internalisation or desensitisation (Shankaran *et al.* 2007). Adaptation facilitates temporal regulation of receptor sensitivity; in the presence of sustained stimuli cells enter a refractory state to prevent over-responding and continuously activating downstream process which could have detrimental effect on cells.

Collagen exerts a strong and prolonged signal in GPVI-transfected DT40s, inducing a 700-fold NFAT/AP-1 activation over basal signalling (Tomlinson *et al.* 2007). The strong sustained stimulation of collagen results in desensitisation of the GPVI receptor to limit further receptor activation. High concentrations of GPVI plasmid initially overexpress GPVI at the plasma membrane and activate negative feedback pathways to internalise or desensitise the receptor. This phenomenon is more prevalent at higher concentrations of GPVI plasmid as the initial high GPVI expression activates negative feedback and accelerates GPVI downregulation. At high GPVI concentrations the combination of collagen-induced desensitisation and GPVI-concentration dependent downregulation reduces the collagen-stimulated response. The lower concentrations of GPVI/FcR-γ plasmid exhibited lower levels of FcR-γ-mediated basal signalling. The absence of adaptation at low GPVI/FcR-γ concentrations enhances the collagen-stimulated response. The proportional ratio of basal signalling to collagen-stimulated signalling was increased. Therefore in effort to optimise this assay, the lowest concentration of GPVI/FcR-γ tested (0.25μg) was utilised in further experiments.

4.3 SLAP-mediated inhibition at optimised GPVI/FcR-γ concentration

The investigation into the inhibitory effect of SLAP1 and SLAP2 on GPVI signalling was repeated with optimised levels of GPVI/FcR-γ. The limited basal signalling and enhanced collagen-stimulated response more accurately represented the effect of collagen-stimulation on GPVI signalling and the magnitude of SLAP-mediated inhibition. At optimised GPVI concentrations the basal signalling was reduced and diminished variation of the basal signal among samples. The GPVI signalling increased following collagen stimulation. The presence of SLAP proteins decreased collagen-induced signalling with no effect on the basal GPVI signalling. The inhibitory activity of SLAP proteins was greater at optimised GPVI concentrations compared to previous concentrations of the GPVI construct. Stimulation with

positive control agonists, ionomycin and PMA, demonstrated no variation in global levels of calcium mobilisation and MAPK activation. Co-transfection of SLAP proteins did not affect GPVI expression levels. Consistent with earlier observations, SLAP family proteins inhibit GPVI signalling without altering GPVI surface expression levels. These results indicate SLAP-mediated inhibition is independent of GPVI-expression levels; instead inhibition is dependent on receptor stimulation and occurs at the signalling level.

Several studies have attempted to elucidate the mechanism of signalling inhibition by means of the NFAT-luciferase assay and *in vitro* binding studies. In one such study, levels of endogenous SLAP1 in a lymphoma cell line were determined, and this quantity was then transfected into Jurkat T-cells to demonstrate the sufficiency of physiological levels of SLAP1 to potently inhibit TCR signalling (Sosinowski *et al*. 2000). Exogenously expressed SLAP1 proteins inhibit TCR signalling, in a dose-dependent manner, operating on membrane-proximal signalling components (Sosinowski *et al*. 2000). A similar investigation of SLAP1 in B-lymphocyte cell line, BJAB, yielded analogous results to those found with the TCR in Jurkats; SLAP1 significantly reduced NFAT activation upon anti-IgM stimulation of the B-cell receptor (Holland *et al.* 2001). In both Jurkat T cells and BJAB B cells SLAP2 proteins, like SLAP1, inhibited NFAT induction in receptor stimulating conditions in a dose dependent manner (Holland *et al*. 2001). Furthermore SLAP2-mediated inhibition was overcome by the positive agonists for MAPK activation and calcium influx signifying the specificity of SLAP2 proteins to act on receptor-proximal components (Holland *et al.* 2001). Screening for CD69, an endogenous marker of early activation events in BCR and TCR signalling, both BJAB and Jurkat cells exhibited strong upregulation of CD69 upon stimulation of their representative lymphocyte receptors (Holland *et al*. 2001). Co-expression of either SLAP1 or SLAP2 inhibited CD69 induction and activation of anti-IgM stimulated BCRs and anti-CD3 stimulated TCRs (Holland *et al.* 2001).

The pattern of tyrosine phosphorylation is not affected by SLAP1 proteins, instead the downstream calcium mobilisation has been implicated as the mechanism of inhibition (Sosinowski *et al.* 2000). Fluorescent-based calcium indicator Indo-1 tracked the calcium level changes in stimulated Jurkat cells indicating an acute suppression of calcium mobilisation in SLAP1-expressing cells which is relieved upon addition of the calcium ionophore ionomycin (Sosinowski *et al.* 2000). Reversible suppression of calcium mobilisation was also observed in BJAB and Jurkat cells expressing SLAP2 following BCR and TCR stimulation, respectively (Holland *et al.* 2001).

In vivo models have correlated the inhibitory activity of SLAP proteins to the degradation of TCRs and BCRs at the plasma membrane (Myers *et al.* 2006; Dragone *et al.* 2006). In these cases the recruitment of the ubiquitin-ligase c-Cbl is the *modus operandi* of inhibition. SLAP-proteins constitutively associate with c-Cbl and are recruited to receptor-proximal components upon receptor stimulation (Dragone *et al.* 2009). In contrast the expression of GPVI receptors in not altered by the co-expression of SLAP proteins. The variation can be potentially attributed to the difference substrate specificity of c-Cbl. Targeting the CD3ε chain of TCRs and the IgM chain of BCRs, c-Cbl induces the degradation of these components (Myers *et al*. 2006; Dragone *et al.* 2006). Loss of these critical components accompanies downregulation of receptor complexes. As GPVI expression is not affected, it is likely c-Cbl does not target expression-critical components but rather SLAP and c-Cbl operate downstream of the receptor complex and instead interfere with the signalling pathway.

4.4 SLAP2 mutants inhibit collagen-stimulated GPVI/FcR-γ signalling to varying degrees

In attempt to further elucidate the mechanism of inhibitory activity, SLAP2 domain mutants were tested for their ability to reduce GPVI signalling. The mechanistic investigations

focused on SLAP2 due to proportionally greater expression of SLAP2 than SLAP1 in the platelets (Appendix 3). Also the role of SLAP1 has previously been studied in lymphocytes, by comparison much less is known of the role of SLAP2 though it has been linked to platelets (Dragone *et al.* 2009; Sugihara *et al.* 2010). Function-blocking mutations were generated in one domain per SLAP2 mutant and the inhibitory activities of these were evaluated using the NFAT-luciferase assay. Individual elimination of each domain of SLAP2 proteins inferred the relative importance of each domain to inhibitory activity. The inhibitory activities of all the mutants decreased compared to wildtype with the SH3 mutant possessing closest semblance to the wildtype followed by the myristoylation sequence, the SH2 domain and the c-terminal mutant. The c-terminal mutant was most affected by disruption at this site indicating its importance in SLAP2 inhibitory function. The expression of GPVI receptor was not altered by the co-expression of SLAP2 mutants. The relatively similar levels of SLAP2 mutants were determined by western blot to verify the pattern of inhibitory activity was not due to differences in expression levels.

Primarily these results indicate the capacity of SLAP2 proteins for intermediary levels of inhibition; disruption of a single domain did not abolish inhibitory activity inferring more than one domain contributes to inhibition. These findings are concurrent with similar studies of SLAP2 mutants in lymphocyte cell lines demonstrating mutations in each domain impair inhibitory activity to a varying degree. The relative levels of impairment reported in this study is SH3>G2A>SH2>ΔC, in descending order of inhibitory activity. These results differed from the pattern observed by Pandey *et al.* describing the SH2 domain as the most impaired followed by the G2A myristoylation mutant with the SH3 domain exhibiting inhibitory activity greater than the wild-type (Pandey *et al*. 2002). Loreto *et al*. described the c-terminal mutation is better tolerated than SH2-domain mutation, followed by the G2A myristoylation mutant which is least impaired in Jurkat T cells (Loreto *et al*. 2002). Holland

et al. demonstrated the c-terminal mutant and the G2A myristoylation mutant diminished SLAP2 activity in lymphocytes to an approximately equal degree and concomitantly increased CD69 induction (Holland *et al*. 2001).

The C-terminal region is critical for SLAP2 activity as compromise of its integrity vastly perturbs inhibitory ability. The results might reflect the greater proportional loss of protein mass of the c-terminal mutant relative to other SLAP2 mutants however the c-terminal region of SLAP1 and SLAP2 has been recognised as the site to which c-Cbl associates via its n-terminus region (Tang *et al*. 1999; Holland *et al.* 2001). Endogenously expressed SLAP2 constitutively associates with c-Cbl with enhanced interaction upon TCR activation (Loreto *et al*. 2002). Furthermore overexpression of both c-Cbl and SLAP2 enhances inhibition of NFAT activation in stimulated Jurkat cells (Loreto *et al.* 2002). An endogenously expressed SLAP-2 isoform, which lacks the c-terminal due to alternative splicing, is unable to associate with c-Cbl and does not inhibit TCR-induced NFAT activation (Loreto & McGlade 2003). SLAP1 was also observed to constitutively associate with c-Cbl in primary thymocytes and subsequently both are localised to endosomes (Myers *et al.* 2006; Sosinowski *et al.* 2000). In lymphocytes the inhibitory activity of SLAP proteins is attributed to their ability to associate with ubiquitin-ligase c-Cbl. c-Cbl has a dual role in receptor regulation in mediating ubiquitinylation-dependent degradation and endocytic-internalisation (Jacob *et al*. 2008). c-Cbl mediated ubiquitinylation of the Zap-70, Syk and CD3ε results in elimination of the TCR complex from the plasma membrane (Loreto *et al.* 2002; Myers *et al. 2*006). Likewise c-Cbl associates with proximal components of BCRs resulting in the downregulation of the receptor at the plasma membrane dependent on Src-family kinase activity (Dragone *et al.* 2006). This study rejects receptor-degradation mechanism of inhibition as GPVI expression was unaltered by the expression of SLAP proteins. However degradation of signalling proteins and subsequent elimination from signalling cascades is a potential mechanism of GPVI inhibition.

Cbl-dependent reduction of Fyn expression, transcription, substrate phosphorylation has been observed in T cells (Andoniou *et al.* 2000). Similar c-Cbl-mediated observations have been made for Lyn, Lck and Syk (Kaabeche *et al.* 2004; Rao, Miyake, *et al.* 2002; Katkere *et al.* 2012). It is notable that Syk co-eluted with SLAP2 and c-Cbl (Sugihara *et al.* 2010) and is ubiquitinylated upon GPVI stimulation (Dangelmaier *et al.* 2005).The non-redundant requirement of these signalling proteins in GPVI signalling indicates c-cbl mediated degradation of these signalling proteins would impose a feasible mechanism of GPVI inhibition. Upon GPVI stimulation, c-Cbl is tyrosine phosphorylated at the N-terminal (Polgár *et al.* 1997). Phosphorylation was dependent on Src-kinases and occurred downstream of Lyn and Fyn, these kinases contribute directly or indirectly (via FcR-γ phosphorylation) to the c-Cbl phosphorylation (Auger *et al.* 2003; Hunter *et al.* 1999). In the presence of mutated c-Cbl the phosphorylation of the FcR-γ, LAT, Syk and PLCγ2 is increased upon GPVI stimulation and c-Cbl mutant platelets aggregate in response to subthreshold concentrations of CRP (Auger *et al*. 2003). The delayed aggregation response indicated the enhanced aggregation magnitude was due to loss of feedback mechanism (Auger *et al.* 2003). Auger *et al*. provided strong evidence of the negative regulatory role of c-Cbl in GPVI signalling, however they found ubiquitin inhibitors had no effect on pattern of tyrosine phosphorylation (Auger *et al.* 2003). In conclusion, this study is consistent with previous SLAP studies supporting the involvement of c-Cbl constitutively complexed to c-terminus of SLAP proteins; however the precise role of c-Cbl remains to be elucidated as the GPVI expression data disputes the ubiquitinylation-degradation role of c-Cbl. Further investigation with c-Cbl-deficient DT40 cell line would indicate the role of c-Cbl in the SLAP-mediated regulation of GPVI.

Several researchers have identified the SH2 domain of SLAP proteins as the binding site for a number of signalling proteins. The conserved FXXR motif of the SH2 domain forms the

phosphotyrosine binding pocket which binds components of the TCR signalling complex such as TCRζ, Syk, ZAP-70, SLP-76, Vav and LAT (Tang *et al*. 1999; Myers *et al.* 2005; Sosinowski *et al*. 2000). SLAP2 also interacts with the proximal components of the BCR complex such as IgM via the SH2 domain (Dragone *et al.* 2006). These interactions are phosphorylation-dependent and diminished by mutation of the SH2 domain (Tang *et al*. 1999; Myers *et al.* 2005; Sosinowski *et al.* 2000). The inhibitory activity of SH2-domain SLAP1 is diminished and the downregulation of the CD3ε is reduced (Myers *et al.* 2006). Optimum inhibition is dependent on the SH2 domain of SLAP proteins binding GM-CSFRα (Liontos *et al.* 2011). The intact SH2 domain is also required for the characteristic cellular distribution and colocalisation with TCR and BCR complexes (Sosinowski *et al.* 2000; Dragone *et al.* 2006). Disruption of the SLAP2 SH2 domain diminishes binding of ZAP-70 and SLP-76 coincides with impaired ability to inhibit NFAT activation (Loreto *et al.* 2002). Likewise loss of ZAP-70 and CD3 interactions with overexpressed SLAP2 SH2 mutant correlated to decreased inhibition of NFAT induction (Pandey *et al.* 2002). Consistent with these studies, the mutation of the SH2 domain compromises the ability of SLAP2 to inhibit NFAT/AP-1 activation. Mutation of the SH2 domain impaired inhibitory function greater than mutation of the myristoylation sequence or SH3 domain, indicating the SH2 domain has a significant contribution to SLAP2-mediated inhibition but lesser than the c-terminus. In contrast, Pandey *et al.* reported the SH2 mutant exhibited lower inhibitory activity than the c-terminal mutant, indicating a greater role of SH2 domain in the inhibition of TCR activation (Pandey *et al.* 2002). The role of SH2 domain in the inhibition of the GPVI signalling is proposed to mediate the interaction of GPVI signalling components. Syk and LAT co-purify with SLAP2 in convulxin-stimulated platelets dependent of Src- and Syk-kinase activity (Sugihara *et al.* 2010). Therefore it is likely SLAP2 interacts with tyrosine-phosphorylated proteins via its SH2 domain and relays these proteins to the adjoined c-Cbl. A similar

scenario has been observed in the fibroblasts whereby SLAP1 recruits p85-PI3kinase via SH2 domain and connects p85-PI3kinase to c-Cbl to mediate c-Cbl-dependent cytoskeletal events (Swaminathan *et al.* 2007).

The reduced inhibitory activity of the myristoylation-mutant (G2A) can be explained in the context of the cellular localisation of SLAP proteins. Myristoylation domains facilitate interactions with plasma membranes attributed to the lipophilic myristoyl moiety (McIlhinney 1998). Previous research has suggested a role of the n-terminal myristoylation domain in facilitating the localisation of SLAP proteins to membranes. SLAP1 localises to the cytoplasm, plasma membrane and perinuclear regions (Manes *et al.* 2000), and both SLAP1 and SLAP2 have been localised to late endosomes (Sosinowski *et al.* 2000; Loreto *et al.* 2002). The presence of SLAP proteins in endosomes, typically involved in intracellular trafficking, is notable as previous evidence indicates the c-Cbl:SLAP complex mediates the endocytic internalisation of BCR (Dragone *et al.* 2006). The characteristic membrane distribution of wildtype SLAP proteins was abrogated when the second residue of the myristoylation sequence was mutated from glycine to alanine (G2A). The SLAP1 G2A mutant was strongly detected in the nucleus and diffusely present in the cytoplasm (Manes *et al.* 2000). Endogenously expressed SLAP2 variant, which lacks the myristoylation domain due to alternative translation initiation, is also mislocalised to the nucleus (Loreto & McGlade 2003). Differential localisation of the SLAP2 G2A myristoylation mutant was confirmed by detection of G2A mutants in the soluble cytosolic fraction, whereas the wildtype SLAP2 precipitated in the membrane pellet fraction (Holland *et al.* 2001; Loreto *et al.* 2002). The cytoplasmic retention of the SLAP2 G2A mutant coincided with reduced capacity to inhibit CD69 expression and NFAT activation (Holland *et al.* 2001; Loreto *et al.* 2002). Aberrant localisation is correlated to reduced SLAP2 activity indicating importance of myristoylation-mediated translocation. Accordingly the increased NFAT-activation of the G2A mutant

relative to the wild-type in this study indicates a potential role of the myristoylation domain in SLAP2-induced inhibition of GPVI signalling. Upon GPVI stimulation SLAP2 is transiently translocated from the cytosol to the membrane fraction (Sugihara *et al*. 2010). It is likely the myristoylation-targeting of SLAP proteins to membranous and vesicular structures transports SLAP and c-Cbl to the vicinity of GPVI signalling components. It has also been proposed the localisation of SLAP proteins is due to the synergy between the myristoylation site and the SH2 domain, as SH2 mutants have similarly disrupted cellular distribution (Sosinowski *et al.* 2000). Sosinowski *et al.* suggested the SH2-mediated binding to tyrosine phosphorylated proteins facilitates relocalisation to signalling complexes (Sosinowski *et al.* 2000). The loss of the myristoylation domain may be compensated by the SH2 domain; therefore the mutational-loss of myristoylation domain is better tolerated than disruption of the c-terminus or the SH2 domain.

The c-terminal region, the SH2 domain and myristoylation sequences have to some extent been assigned roles in SLAP-mediated inhibition. In contrast, the role of SH3 domain has remains elusive. This study found the mutation of the SH3 domain had little effect on inhibitory activity, such that the wild-type and SH3 mutant had closely equivalent levels of NFAT induction. Another research group also found the NFAT-activation was reduced by the co-expression of the SH3 mutant, to levels comparable to the wild-type SLAP2, on anti-CD3 stimulation of Jurkat T cells (Pandey *et al*. 2002). In contrast, the SLAP1-SH3 mutant was relatively impaired in its ability to inhibit TCR-induced NFAT activity (Sosinowski *et al.* 2000), highlighting potential differences in the mechanisms of SLAP1 and SLAP2. Thus the SH3 domain has a minor contribution to SLAP2-mediated inhibition but is likely to be more crucial to the activity of SLAP1. Characterisation of SH3 domain has defined it as ~60 residue region which recognises proline-rich binding motif (PxxP) on a diverse range of proteins facilitating adaptable and low specificity interactions (Mayer 2000). Initially it was

suspected that SH3 domain of SLAP2 competes with Fyn and Lyn for the cognate binding site on the tail-region of GPVI in order to inhibit GPVI signalling. To this end the NFAT-luciferase assay was repeated in an excess of Fyn to determine whether overexpression of Fyn can reverse the proposed competitive inhibition (Appendix 4). The results indicate the overexpression of Fyn did not rescue GPVI signalling in the presence of wild-type SLAP1 and SLAP2, contradicting the hypothesis of competitive inhibition. An alternative explanation of the SH3-mutant induced inhibition is based on the potential of the SH3 domain to interact with c-Cbl, via proline-rich sequences within c-Cbl (Sosinowski *et al.* 2000). It can be hypothesized that the interaction between c-Cbl and SH3 domains of SLAP proteins stabilises the c-Cbl:SLAP complex. However further research would be required to determine whether the SH3-mutant retains the ability to interact with c-Cbl. To conclude the findings of this project indicate the SH3 domain has a minimal undefined role in the inhibitory activity of SLAP2 proteins.

The present study investigated the effect of SLAP proteins on the signalling response of the platelet receptor GPVI in a cell-based model. The findings concur with previous evidence of SLAP-induced inhibition of lymphocyte receptors. However platelet research would be required to determine whether SLAP proteins are *bona fide* inhibitors of GPVI signalling. Mutational analysis was employed to elucidate the mechanism of SLAP2-mediated inhibition. To the best of our knowledge this the first study where the full complement of SLAP domain mutants have been investigated; on the whole the findings are in agreement with previous investigations of SLAP mutants. The SLAP2 mutants exhibited impaired inhibitory activity indicating all the domains contribute to inhibitory activity to varying degrees. The findings of this study can be integrated with previous research to infer a mechanistic version of SLAP-mediated inhibition. A model of SLAP inhibition of GPVI signalling is proposed (Figure 4.1). Following GPVI stimulation Src-kinase and Syk-kinase

phosphorylate of a number of components such as LAT and Syk. Subsequently SLAP proteins transiently translocate to the plasma membrane facilitated by the myristoylation sequence. At the membrane SLAP proteins are recruited to the phospho-tyrosines of signalling proteins. SLAP proteins bind signalling proteins via the SH2 domain. As a result the constitutively bound c-Cbl on the SLAP c-terminus is translocated to the membrane compartment and juxtaposed to phosphorylated signalling components. c-Cbl is also tyrosine phosphorylated in response to GPVI stimulation by activated Src-kinases. The role of the SH3 domain remains elusive; however, consistent with other studies the SH3 domain is not integral to inhibitory activity. SLAP proteins then enhance the activity of c-Cbl as adaptor proteins stabilising protein-protein interactions and concentrating c-Cbl substrates (Swaminathan *et al.* 2007). The role of c-Cbl has not been implicitly defined in the context of GPVI regulation; further research would be required to determine whether the SLAP and c-Cbl complex interferes with signalling or targets signalling components for degradation. Removal of receptor complexes is receptor-specific activity of c-Cbl as GPVI expression is not altered unlike BCRs and TCRs which are typically degraded in the presence of SLAP and c-Cbl. It is likely c-Cbl mediates ubiquitinylation of individual signalling components, as reported for Syk (Dangelmaier *et al.* 2005), and therefore attenuates GPVI signalling. In conclusion, SLAP proteins inhibit GPVI signalling and potentially regulate GPVI activation to control unwanted platelet activation and thrombosis.

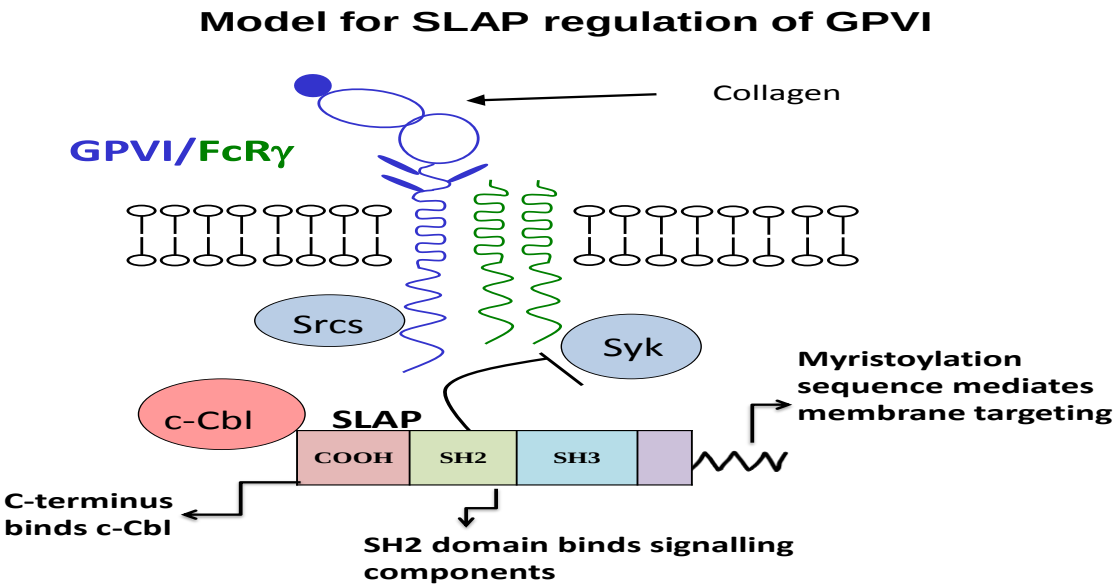

Figure 4.1 Model for SLAP2 regulation of GPVI. Each domain has a non-competitive and sequential role membrane localisation, protein-interaction and c-Cbl binding to mediate GPVI inhibition.

APPENDICES

Appendix 1.
Preliminary data provided by Bender, Cherpokova, and Nieswandt

A. SLAP1/SLAP2-deficient mice have elevated platelet GPVI levels. In the GPVI-dependent stroke model, SLAP1-/- SLAP2-/- mice have larger necrotic areas than wild-type mice (Markus Bender)

Protein	Control	*Slap/Slap2*$^{-/-}$	Significance
GPIb	335 ± 12	306 ± 25	n.s.
GPIX	536 ± 40	509 ± 37	n.s.
GPV	357 ± 19	344 ± 34	n.s.
CD9	1437 ± 60	1464 ± 101	n.s.
GPVI	57 ± 2	70 ± 3	***
CLEC-2	133 ± 7	146 ± 4	*
αIIbβ3	528 ± 41	599 ± 55	n.s.
α2	52 ± 2	53 ± 5	n.s.
β1	146 ± 7	154 ± 14	n.s.

* ≤0.05

**≤0.01

***≤0.001

Appendix 2
Prelinimary data provided by Nieswandt, Watson and Tomlinson Groups.

A. SLAP1/SLAP2 deficient platelets are hyper-response to subthreshold levels of GPVI agonists.

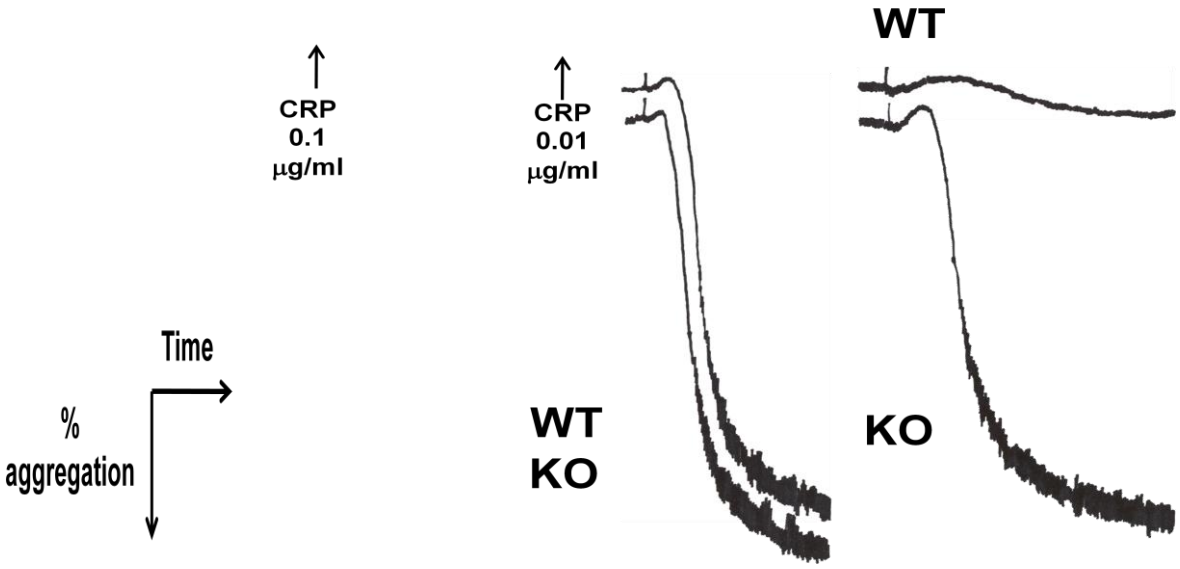

B. GPVI signalling is hyper-responsive despite normalisation of GPVI expression levels. The increased GPVI levels are not responsible for the enhanced signalling in the SLAP1/SLAP2 double knockouts.

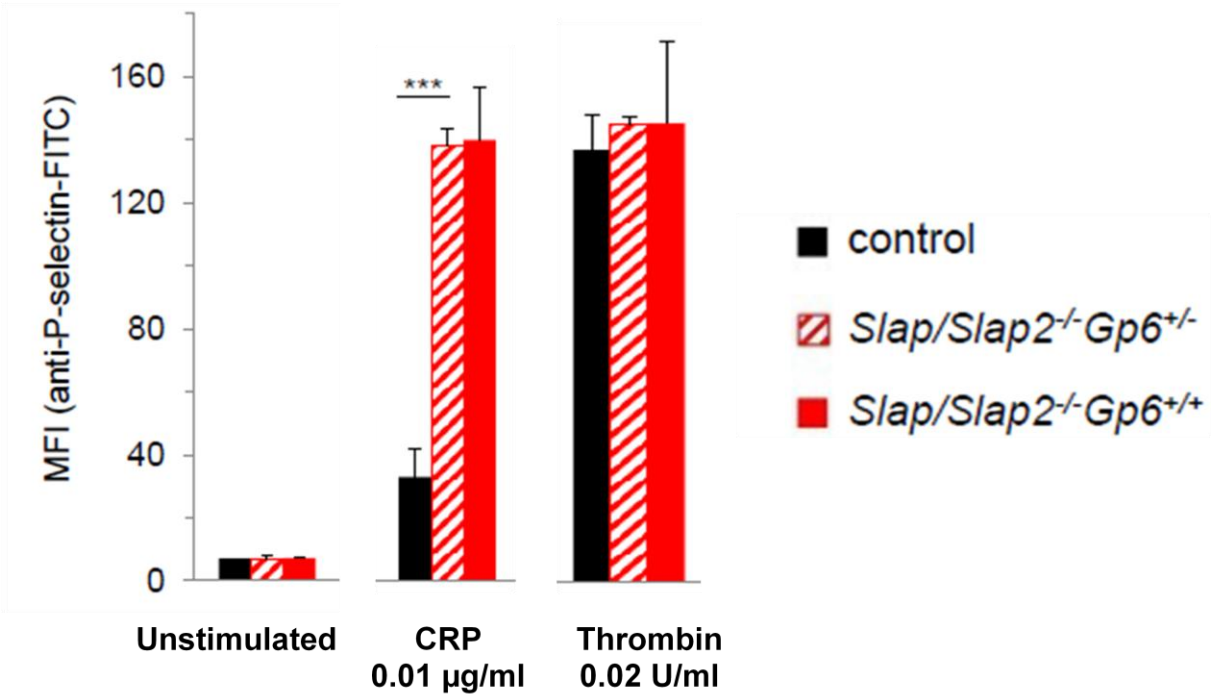

Appendix 3.

Mouse megakaryocytes and platelets express both SLAP1 and SLAP2 however the expression of SLAP2 is greater than that of SLAP1. Data provided by MG Tomlinson.

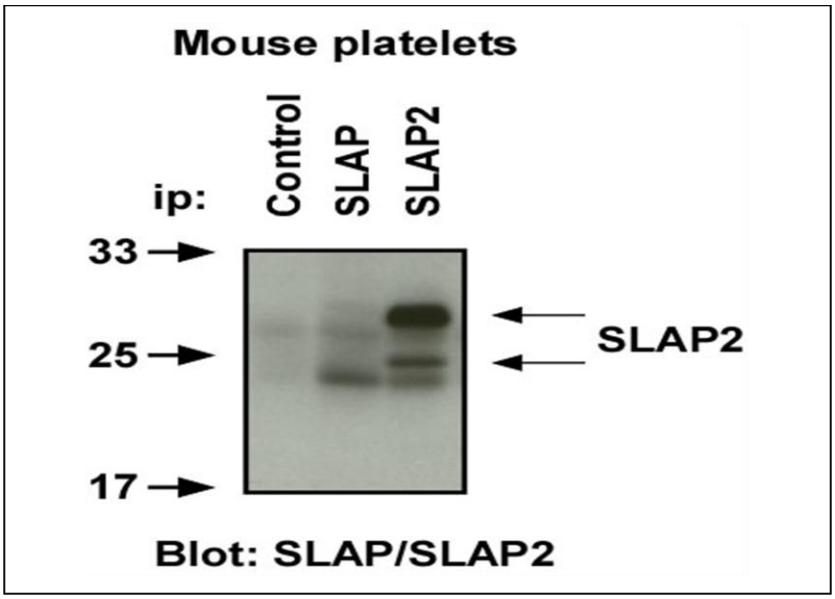

Appendix 4.

SLAP2-mediated inhibition of collagen-stimulated GPVI signalling is not affected by the overexpression of the Src-kinase Fyn.

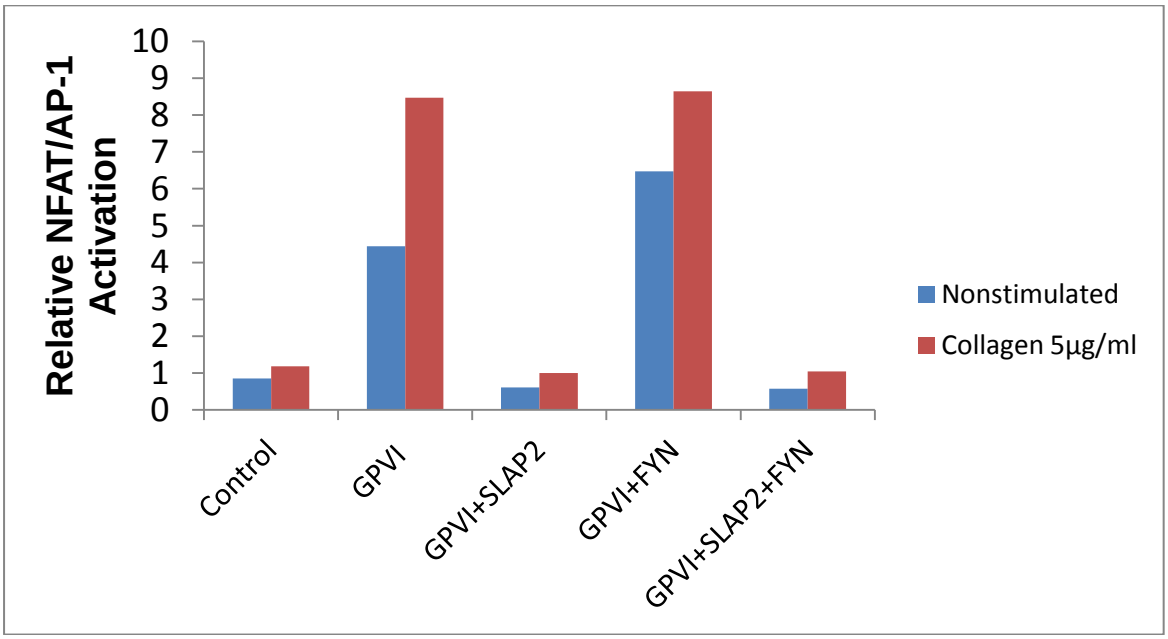

All transfected samples were responsive to positive agonists, PMA and ionomycin, indicating samples have similar levels of basal and stimulated calcium mobilisation and MAPK activation. SLAP2 inhibition does not affect the global response to calcium mobilisation and MAPK activation. The co-expression of Fyn has no effect on calcium mobilisation and MAPK activation.

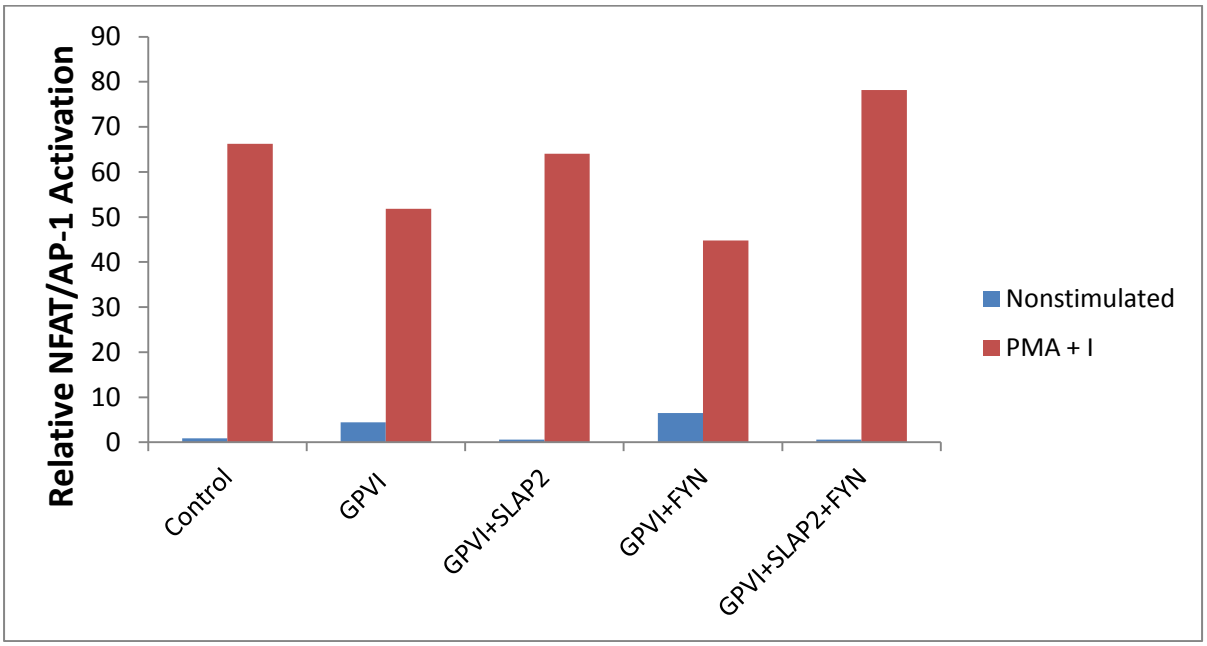

References

Al-Tamimi, M. et al., 2009. Anti-glycoprotein VI monoclonal antibodies directly aggregate platelets independently of FcgammaRIIa and induce GPVI ectodomain shedding. *Platelets*, 20(2), pp.75-82. Available at: http://www.ncbi.nlm.nih.gov/pubmed/19235048 [Accessed April 14, 2012].

Al-Tamimi, M. et al., 2011. Coagulation-induced shedding of platelet glycoprotein VI mediated by factor Xa. *Blood*, 117(14), pp.3912-20. Available at: http://www.ncbi.nlm.nih.gov/pubmed/21252089 [Accessed April 14, 2012].

Allford, S.L. & Machin, S., 2004. Haemostasis. *Medicine*, 32(5), pp.11-14. Available at: http://linkinghub.elsevier.com/retrieve/pii/S1357303906700056.

Andoniou, C.E. et al., 2000. The Cbl proto-oncogene product negatively regulates the Src-family tyrosine kinase Fyn by enhancing its degradation. *Molecular and cellular biology*, 20(3), pp.851-67. Available at: http://www.pubmedcentral.nih.gov/articlerender.fcgi?artid=85202&tool=pmcentrez&rendertype=abstract.

Andrews, Robert K & Berndt, M.C., 2004. Platelet physiology and thrombosis. *Thrombosis research*, 114(5-6), pp.447-53. Available at: http://www.ncbi.nlm.nih.gov/pubmed/15507277 [Accessed March 20, 2012].

Angrist, M. et al., 1995. Chromosomal localization of the mouse Src-like adapter protein (Slap) gene and its putative human homolog SLA. *Genomics*, 30(3), pp.623-5. Available at: http://dx.doi.org/10.1006/geno.1995.1289 [Accessed July 25, 2012].

Arthur, J., Dunkley, S. & Andrews, R K, 2007. Platelet glycoprotein VI-related clinical defects. *British journal of haematology*, 139(3), pp.363-72. Available at: http://www.ncbi.nlm.nih.gov/pubmed/17910626 [Accessed April 14, 2012].

Arthur, J.F., Shen, Y., et al., 2007. Ligand binding rapidly induces disulfide-dependent dimerization of glycoprotein VI on the platelet plasma membrane. *The Journal of biological chemistry*, 282(42), pp.30434-41. Available at: http://www.ncbi.nlm.nih.gov/pubmed/17690106 [Accessed April 14, 2012].

Auger, J.M. et al., 2003. c-Cbl negatively regulates platelet activation by glycoprotein VI. *Journal of Thrombosis and Haemostasis*, 1(May), pp.2419-2426.

Austin, S.K., 2009. Haemostasis. *Medicine*, 37(3), pp.133-136. Available at: http://linkinghub.elsevier.com/retrieve/pii/S1357303909000280 [Accessed July 2, 2012].

Barry, F. a & Gibbins, J.M., 2002. Protein kinase B is regulated in platelets by the collagen receptor glycoprotein VI. *The Journal of biological chemistry*, 277(15), pp.12874-8. Available at: http://www.ncbi.nlm.nih.gov/pubmed/11825911 [Accessed April 14, 2012].

Bender, Markus et al., 2010. Differentially regulated GPVI ectodomain shedding by multiple platelet-expressed proteinases. *Blood*, 116(17), pp.3347-55. Available at: http://bloodjournal.hematologylibrary.org/cgi/content/abstract/116/17/3347 [Accessed August 17, 2012].

Berlanga, O. et al., 2000. Expression of the collagen receptor glycoprotein VI during megakaryocyte differentiation. *Blood*, 96, pp.2740-2745.

Berlanga, O. et al., 2007. GPVI oligomerisation in cell lines and platelets. *Journal of Thrombosis and Haemostasis*, 5(5), pp.1026-1033.

Best, D. et al., 2003. GPVI levels in platelets : relationship to platelet function at high shear. *Hemostasis, Thrombosis and Vascular Biology*, 102(8), pp.2811-2818.

Bigalke, B. et al., 2010. Glycoprotein VI as a prognostic biomarker for cardiovascular death in patients with symptomatic coronary artery disease. *Clinical research in cardiology : official journal of the German Cardiac Society*, 99(4), pp.227-33. Available at: http://www.ncbi.nlm.nih.gov/pubmed/20049463 [Accessed April 16, 2012].

Bigalke, B. et al., 2011. Imaging of injured and atherosclerotic arteries in mice using fluorescence-labeled glycoprotein VI-Fc. *European journal of radiology*, 79(2), pp.e63-9. Available at: http://www.ncbi.nlm.nih.gov/pubmed/21497471 [Accessed April 14, 2012].

Boylan, B. et al., 2006. Activation-independent, antibody-mediated removal of GPVI from circulating human platelets: development of a novel NOD/SCID mouse model to evaluate the in vivo effectiveness of anti-human platelet agents. *Blood*, 108(3), pp.908-14. Available at: http://www.pubmedcentral.nih.gov/articlerender.fcgi?artid=1895852&tool=pmcentrez&rendertype=abstract [Accessed August 17, 2012].

Brass, L.F., Zhu, L. & Stalker, T.J., 2005. Review series Minding the gaps to promote thrombus growth and stability. *Journal of Clinical Investigation*, 115(12), pp.3385-3392.

Brondijk, T.H.C. et al., 2010. Crystal structure and collagen-binding site of immune inhibitory receptor LAIR-1: unexpected implications for collagen binding by platelet receptor GPVI. *Blood*, 115(7), pp.1364-73. Available at: http://www.ncbi.nlm.nih.gov/pubmed/20007810 [Accessed March 8, 2012].

Broos, K. et al., 2011. Platelets at work in primary hemostasis. *Blood reviews*, 25(4), pp.155-67. Available at: http://www.ncbi.nlm.nih.gov/pubmed/21496978 [Accessed April 1, 2012].

Buerstedde, J.-M., 2002. The DT40 web site: sampling and connecting the genes of a B cell line. *Nucleic Acids Research*, 30(1), pp.230-231. Available at: http://nar.oxfordjournals.org/cgi/content/abstract/30/1/230.

Chari, R. et al., 2009. Lyn, PKC-delta, SHIP-1 interactions regulate GPVI-mediated platelet-dense granule secretion. *Blood*, 114(14), pp.3056-63. Available at:

http://www.pubmedcentral.nih.gov/articlerender.fcgi?artid=2756209&tool=pmcentrez&rendertype=abstract [Accessed April 16, 2012].

Clemetson, J.M. et al., 1999. The platelet collagen receptor glycoprotein VI is a member of the immunoglobulin superfamily closely related to FcalphaR and the natural killer receptors. *The Journal of biological chemistry*, 274(41), pp.29019-24. Available at: http://www.ncbi.nlm.nih.gov/pubmed/10506151.

Clemetson, K.J., 2012. Platelets and primary haemostasis. *Thrombosis research*, 129(3), pp.220-4. Available at: http://www.ncbi.nlm.nih.gov/pubmed/22178577 [Accessed March 14, 2012].

Coller, B.S., 2011. Historical perspective and future directions in platelet research. *Journal of thrombosis and haemostasis : JTH*, 9 Suppl 1, pp.374-95. Available at: http://www.pubmedcentral.nih.gov/articlerender.fcgi?artid=3163479&tool=pmcentrez&rendertype=abstract [Accessed March 16, 2012].

Croft, S.A. et al., 2001. Novel Platelet Membrane Glycoprotein VI Dimorphism Is a Risk Factor for Myocardial Infarction. *Circulation*, 104(13), pp.1459-1463. Available at: http://circ.ahajournals.org/cgi/content/abstract/104/13/1459.

Dorahy, D. & Burns, G, 1998. Active Lyn protein tyrosine kinase is selectively enriched within membrane microdomains of resting platelets. Available at: http://www.biochemj.org/bj/333/0373/bj3330373.htm.

Dangelmaier, C. a et al., 2005. Rapid ubiquitination of Syk following GPVI activation in platelets. *Blood*, 105(10), pp.3918-24. Available at: http://www.pubmedcentral.nih.gov/articlerender.fcgi?artid=1895068&tool=pmcentrez&rendertype=abstract [Accessed April 16, 2012].

Daniel, J.L. et al., 2010. Cbl-b is a novel physiologic regulator of glycoprotein VI-dependent platelet activation. *The Journal of biological chemistry*, 285(23), pp.17282-91.

Dragone, L.L. et al., 2009. SLAP, a regulator of immunoreceptor ubiquitination, signaling, and trafficking. *Immunological reviews*, 232(1), pp.218-28. Available at: http://www.ncbi.nlm.nih.gov/pubmed/19909366.

Dragone, L.L. et al., 2006. Src-like adaptor protein (SLAP) regulates B cell receptor levels in a c-Cbl-dependent manner. *PNAS*, 103(48), pp.18202-18207.

Dumont, B. et al., 2006. Chimeric Fc receptors identify ligand binding regions in human glycoprotein VI. *Journal of molecular biology*, 361(5), pp.877-87. Available at: http://www.ncbi.nlm.nih.gov/pubmed/16876821 [Accessed April 16, 2012].

Dütting, S. & Nieswandt, Bernhard, 2012. Better safe than sorry: glycoprotein VI dimerization as a novel checkpoint and early biomarker of platelet activation. *Arteriosclerosis, thrombosis, and vascular biology*, 32(3), pp.552-3. Available at: http://www.ncbi.nlm.nih.gov/pubmed/22345591 [Accessed April 16, 2012].

Ellison, S.M., 2009. *CD148 : a positive regulator of GPVI and αIIbβ3 proximal signalling in platelets Centre for Cardiovascular Sciences*.

Ezumi, Y, Uchiyama, T. & Takayama, H, 2000. Molecular cloning, genomic structure, chromosomal localization, and alternative splice forms of the platelet collagen receptor glycoprotein VI. *Biochemical and biophysical research communications*, 277(1), pp.27-36. Available at: http://www.ncbi.nlm.nih.gov/pubmed/11027634 [Accessed April 16, 2012].

Ezumi, Yasuharu et al., 2002. Constitutive and functional association of the platelet collagen receptor glycoprotein VI − Fc receptor γ -chain complex with membrane rafts. *Blood*, 99(9), pp.3250-3255.

Falet, H. et al., 2000. Roles of SLP-76, phosphoinositide 3-kinase, and gelsolin in the platelet shape changes initiated by the collagen receptor GPVI/FcR gamma-chain complex. *Blood*, 96(12), pp.3786-92. Available at: http://www.ncbi.nlm.nih.gov/pubmed/11090061.

Farndale, R.W., 2006. Collagen-induced platelet activation. *Blood cells, molecules & diseases*, 36(2), pp.162-5. Available at: http://www.ncbi.nlm.nih.gov/pubmed/16464621 [Accessed July 3, 2012].

Furie, B.C. & Furie, B., 2006. Tissue factor pathway vs. collagen pathway for in vivo platelet activation. *Blood cells, molecules & diseases*, 36(2), pp.135-8. Available at: http://www.ncbi.nlm.nih.gov/pubmed/16513378 [Accessed April 16, 2012].

Furihata, K. et al., 2001. Variation in Human Platelet Glycoprotein VI Content Modulates Glycoprotein VI-Specific Prothrombinase Activity. *Arteriosclerosis, Thrombosis, and Vascular Biology*, 21(11), pp.1857-1863.

Gardiner, E.E. et al., 2004. Regulation of platelet membrane levels of glycoprotein VI by a platelet-derived metalloproteinase. *Blood*, 104, pp.3611-3617.

Gibbins, J.M. et al., 1997. Glycoprotein VI is the collagen receptor in platelets which underlies tyrosine phosphorylation of the Fc receptor γ-chain. *FEBS Letters*, 413(2), pp.255-259.

Gilio, K. et al., 2009. Non-redundant roles of phosphoinositide 3-kinase isoforms alpha and beta in glycoprotein VI-induced platelet signaling and thrombus formation. *The Journal of biological chemistry*, 284(49), pp.33750-62.

Gilio, K. et al., 2010. Roles of platelet STIM1 and Orai1 in glycoprotein VI- and thrombin-dependent procoagulant activity and thrombus formation. *The Journal of biological chemistry*, 285(31), pp.23629-38.

Gross, B.S., Melford, S.K. & Watson, S P, 1999. Evidence that phospholipase C-gamma2 interacts with SLP-76, Syk, Lyn, LAT and the Fc receptor gamma-chain after stimulation of the collagen receptor glycoprotein VI in human platelets. *European journal of biochemistry / FEBS*, 263(3), pp.612-23. Available at: http://www.ncbi.nlm.nih.gov/pubmed/10469124.

Grüner, S. et al., 2005. Relative antithrombotic effect of soluble GPVI dimer compared with anti-GPVI antibodies in mice. *Blood*, 105(4), pp.1492-9. Available at: http://www.ncbi.nlm.nih.gov/pubmed/15507524 [Accessed April 16, 2012].

Gupta, N. & DeFranco, A.L., 2007. Lipid rafts and B cell signaling. *Seminars in cell & developmental biology*, 18(5), pp.616-26.

Hiragun, T., Peng, Z. & Beaven, M. a, 2006. Cutting edge: dexamethasone negatively regulates Syk in mast cells by up-regulating SRC-like adaptor protein. *Journal of immunology (Baltimore, Md. : 1950)*, 177(4), pp.2047-50. Available at: http://www.ncbi.nlm.nih.gov/pubmed/16887961.

Ho-Tin-Noe, B., Demers, M. & Wagner, D.D., 2012. How platelets safeguard vascular integrity. *Journal of Thrombosis and Haemostasis*, 9(Suppl 1), pp.56-65.

Holland, S.J. et al., 2001. Functional cloning of Src-like adapter protein-2 (SLAP-2), a novel inhibitor of antigen receptor signaling. *The Journal of experimental medicine*, 194(9), pp.1263-76.

Horejsí, V. et al., 1999. GPI-microdomains: a role in signalling via immunoreceptors. *Immunology today*, 20(8), pp.356-61. Available at: http://www.ncbi.nlm.nih.gov/pubmed/10431155.

Horii, K., Kahn, M.L. & Herr, A.B., 2006. Structural basis for platelet collagen responses by the immune-type receptor glycoprotein VI. *Blood*, 108(3), pp.936-42. Available at: http://www.ncbi.nlm.nih.gov/pubmed/16861347 [Accessed March 8, 2012].

Hunter, S. et al., 1999. Fyn associates with Cbl and phosphorylates tyrosine 731 in Cbl, a binding site for phosphatidylinositol 3-kinase. *The Journal of biological chemistry*, 274(4), pp.2097-106.

Huo, Y. & Ley, K.F., 2004. Role of platelets in the development of atherosclerosis. *Trends in cardiovascular medicine*, 14(1), pp.18-22. Available at: http://www.ncbi.nlm.nih.gov/pubmed/18571912.

Jackson, S.P. & Schoenwaelder, S.M., 2003. Antiplatelet therapy: in search of the "magic bullet". *Nature reviews. Drug discovery*, 2(10), pp.775-89. Available at: http://www.ncbi.nlm.nih.gov/pubmed/14526381 [Accessed June 22, 2012].

Jacob, M. et al., 2008. Dual role of Cbl links critical events in BCR endocytosis. *International immunology*, 20(4), pp.485-97.

Jandrot-Perrus, M. et al., 2000. Cloning, characterization, and functional studies of human and mouse glycoprotein VI: a platelet-specific collagen receptor from the immunoglobulin superfamily. *Blood*, 96(5), pp.1798-807. Available at: http://www.ncbi.nlm.nih.gov/pubmed/10961879.

Jarvis, G.E. et al., 2008. Identification of a major GpVI-binding locus in human type III collagen. *Blood*, 111(10), pp.4986-96. Available at:

http://www.pubmedcentral.nih.gov/articlerender.fcgi?artid=2602586&tool=pmcentrez&rendertype=abstract [Accessed March 15, 2012].

Joutsi-Korhonen, L. et al., 2003. The low-frequency allele of the platelet collagen signaling receptor glycoprotein VI is associated with reduced functional responses and expression. *Blood*, 101(11), pp.4372-9.

Judd, B. a et al., 2002. Differential requirement for LAT and SLP-76 in GPVI versus T cell receptor signaling. *The Journal of experimental medicine*, 195(6), pp.705-17.

Jung, S.M., Tsuji, K. & Moroi, M., 2009. Glycoprotein (GP) VI dimer as a major collagen-binding site of native platelets : direct evidence obtained with dimeric GPVI- specific Fabs. *Journal of Thrombosis and Haemostasis*, 7(May), pp.1347-1355.

Kaabeche, K. et al., 2004. Cbl-mediated degradation of Lyn and Fyn induced by constitutive fibroblast growth factor receptor-2 activation supports osteoblast differentiation. *The Journal of biological chemistry*, 279(35), pp.36259-67. Available at: http://www.ncbi.nlm.nih.gov/pubmed/15190072.

Kabouridis, P.S., 2006. Lipid rafts in T cell receptor signalling . *Molecular membrane biology*, 23(1), pp.49-57.

Katkere, B., Rosa, S. & Drake, J.R., 2012. The Syk-binding ubiquitin ligase c-Cbl mediates signaling-dependent B cell receptor ubiquitination and B cell receptor-mediated antigen processing and presentation. *The Journal of biological chemistry*, 287(20), pp.16636-44.

Kim, H.-J. et al., 2010. Src-like adaptor protein regulates osteoclast generation and survival. *Journal of cellular biochemistry*, 110(1), pp.201-9. Available at: http://www.ncbi.nlm.nih.gov/pubmed/20225239 [Accessed July 21, 2012].

Kunicki, T.J. et al., 2005. The influence of N-linked glycosylation on the function of platelet glycoprotein VI. *Blood*, 106(8), pp.2744-9. Available at: http://www.pubmedcentral.nih.gov/articlerender.fcgi?artid=1895313&tool=pmcentrez&rendertype=abstract [Accessed April 16, 2012].

Lagrue-Lak-Hal, a H. et al., 2001. Expression and function of the collagen receptor GPVI during megakaryocyte maturation. *The Journal of biological chemistry*, 276(18), pp.15316-25. Available at: http://www.ncbi.nlm.nih.gov/pubmed/11278467 [Accessed April 16, 2012].

Langer, H.F. & Gawaz, M., 2008. Platelet-vessel wall interactions in atherosclerotic disease. *Thrombosis and haemostasis*, 99(3), pp.480-6. Available at: http://www.ncbi.nlm.nih.gov/pubmed/18327395 [Accessed March 27, 2012].

Lebigot, I. et al., 2003. Up-regulation of SLAP in FLI-1-transformed erythroblasts interferes with EpoR signaling. *Blood*, 102(13), pp.4555-62. Available at: http://www.ncbi.nlm.nih.gov/pubmed/12946994 [Accessed August 4, 2012].

Lecut, C et al., 2003. Human platelet glycoprotein VI function is antagonized by monoclonal antibody-derived Fab fragments. *Journal of Thrombosis and Haemostasis*, 1, pp.2653-2662.

Lecut, Christelle et al., 2004. Identification of residues within human glycoprotein VI involved in the binding to collagen: evidence for the existence of distinct binding sites. *The Journal of biological chemistry*, 279(50), pp.52293-9. Available at: http://www.ncbi.nlm.nih.gov/pubmed/15466473 [Accessed April 16, 2012].

Leo, L. et al., 2002. Role of the adapter protein SLP-76 in GPVI-dependent platelet procoagulant responses to collagen. *Blood*, 100(8), pp.2839-44. Available at: http://www.ncbi.nlm.nih.gov/pubmed/12351393 [Accessed April 16, 2012].

Linden, M.D. & Jackson, D.E., 2010. Platelets: pleiotropic roles in atherogenesis and atherothrombosis. *The international journal of biochemistry & cell biology*, 42(11), pp.1762-6. Available at: http://www.ncbi.nlm.nih.gov/pubmed/20673808 [Accessed June 26, 2012].

Lingwood, D. & Simons, K., 2010. Lipid rafts as a membrane-organizing principle. *Science (New York, N.Y.)*, 327(5961), pp.46-50. Available at: http://www.ncbi.nlm.nih.gov/pubmed/20044567 [Accessed July 13, 2012].

Liontos, L.M. et al., 2011. The Src-like adaptor protein regulates GM-CSFR signaling and monocytic dendritic cell maturation. *Journal of immunology*, 186(4), pp.1923-33. Available at: http://www.ncbi.nlm.nih.gov/pubmed/21220694 [Accessed July 21, 2012].

Locke, D. et al., 2003. Fc Rgamma -independent signaling by the platelet collagen receptor glycoprotein VI. *The Journal of biological chemistry*, 278(17), pp.15441-8. Available at: http://www.ncbi.nlm.nih.gov/pubmed/12594225 [Accessed April 16, 2012].

Locke, D. et al., 2002. Lipid rafts orchestrate signaling by the platelet receptor glycoprotein VI. *The Journal of biological chemistry*, 277(21), pp.18801-9. Available at: http://www.ncbi.nlm.nih.gov/pubmed/11844795 [Accessed April 16, 2012].

Loreto, M.P., Berry, D.M. & Mcglade, C.J., 2002. Functional Cooperation between c-Cbl and Src-Like Adaptor Protein 2 in the Negative Regulation of T-Cell Receptor Signaling. *Molecular and cellular biology*, 22(12), pp.4241-4255.

Loreto, M.P. & McGlade, C.J., 2003. Cloning and characterization of human Src-like adaptor protein 2 and a novel splice isoform, SLAP-2-v. *Oncogene*, 22(2), pp.266-73. Available at: http://www.ncbi.nlm.nih.gov/pubmed/12527895 [Accessed July 21, 2012].

Loyau, S. et al., 2012. Platelet Glycoprotein VI Dimerization, an Active Process Inducing Receptor Competence, Is an Indicator of Platelet Reactivity. *Arteriosclerosis, thrombosis, and vascular biology*, 32(3), pp.778-85. Available at: http://www.ncbi.nlm.nih.gov/pubmed/22155453 [Accessed March 14, 2012].

Lupher, M.L. et al., 1999. The Cbl protooncoprotein: a negative regulator of immune receptor signal transduction. *Immunology Today*, 20(8), pp.375-382.

Manes, G., Bello, P. & Roche, S., 2000. Slap negatively regulates Src mitogenic function but does not revert Src-induced cell morphology changes. *Molecular and cellular biology*, 20(10), pp.3396-406. Available at: http://www.pubmedcentral.nih.gov/articlerender.fcgi?artid=85632&tool=pmcentrez&rendertype=abstract.

Massberg, S. et al., 2004. Soluble glycoprotein VI dimer inhibits platelet adhesion and aggregation to the injured vessel wall in vivo. *FASEB journal : official publication of the Federation of American Societies for Experimental Biology*, 18(2), pp.397-9. Available at: http://www.ncbi.nlm.nih.gov/pubmed/14656994.

Matsumoto, Y. et al., 2007. Highly potent anti-human GPVI monoclonal antibodies derived from GPVI knockout mouse immunization. *Thrombosis research*, 119(3), pp.319-29. Available at: http://www.ncbi.nlm.nih.gov/pubmed/16566959 [Accessed April 16, 2012].

Mayer, B.J., 2000. SH3 domains : complexity in moderation. , 2.

McIlhinney, R.A., 1998. Membrane targeting via protein N-myristoylation. *Methods in molecular biology (Clifton, N.J.)*, 88, pp.211-25. Available at: http://www.springerlink.com/content/q472m23582l422l0/.

Meijerink, P.H. et al., 1998. The gene for the human Src-like adaptor protein (hSLAP) is located within the 64-kb intron of the thyroglobulin gene. *European journal of biochemistry / FEBS*, 254(2), pp.297-303. Available at: http://www.ncbi.nlm.nih.gov/pubmed/9660183.

Miura, Y. et al., 2002. Analysis of the interaction of platelet collagen receptor glycoprotein VI (GPVI) with collagen. A dimeric form of GPVI, but not the monomeric form, shows affinity to fibrous collagen. *The Journal of biological chemistry*, 277(48), pp.46197-204. Available at: http://www.ncbi.nlm.nih.gov/pubmed/12356768 [Accessed March 14, 2012].

Miura, Y. et al., 2000. Cloning and Expression of the Platelet-specific Collagen Receptor Glycoprotein VI. *Thrombosis research*, 98, pp.301-309.

Mori, J. et al., 2008. G6b-B inhibits constitutive and agonist-induced signaling by glycoprotein VI and CLEC-2. *The Journal of biological chemistry*, 283(51), pp.35419-27. Available at: http://www.pubmedcentral.nih.gov/articlerender.fcgi?artid=2602894&tool=pmcentrez&rendertype=abstract [Accessed April 16, 2012].

Moroi, M. et al., 1989. A Patient with Platelets Deficient in Glycoprotein VI That Lack Both Collagen-induced Aggregation and Adhesion. *Journal of Clinical Investigation*, 84(November), pp.1440-1445.

Moroi, M. & Jung, S.M., 2004. Platelet glycoprotein VI: its structure and function. *Thrombosis research*, 114(4), pp.221-33. Available at: http://www.ncbi.nlm.nih.gov/pubmed/15381385 [Accessed April 2, 2012].

Morton, L.F. et al., 1995. Integrin a2b1-independent activation of platelets by simple collagen-like peptides : collagen tertiary (triple-helical) and quaternary (polymeric) structures are sufficient alone for a2b1-independent platelet reactivity. *Journal of Biochemistry*, 344, pp.337-344.

Muzard, J. et al., 2009. Design and humanization of a murine scFv that blocks human platelet glycoprotein VI in vitro. *The FEBS journal*, 276(15), pp.4207-22. Available at: http://www.ncbi.nlm.nih.gov/pubmed/19558491 [Accessed April 16, 2012].

Myers, M.D. et al., 2006. Src-like adaptor protein regulates TCR expression on thymocytes by linking the ubiquitin ligase c-Cbl to the TCR complex. *Nature immunology*, 7(1), pp.57-66. Available at: http://www.ncbi.nlm.nih.gov/pubmed/16327786 [Accessed July 21, 2012].

Myers, M.D., Dragone, L.L. & Weiss, A., 2005. Src-like adaptor protein down-regulates T cell receptor (TCR)-CD3 expression by targeting TCRzeta for degradation. *The Journal of cell biology*, 170(2), pp.285-94. Available at: http://www.pubmedcentral.nih.gov/articlerender.fcgi?artid=2171412&tool=pmcentrez&rendertype=abstract [Accessed July 21, 2012].

Nieswandt, B et al., 2000. Expression and function of the mouse collagen receptor glycoprotein VI is strictly dependent on its association with the FcRgamma chain. *The Journal of biological chemistry*, 275(31), pp.23998-4002. Available at: http://www.ncbi.nlm.nih.gov/pubmed/10825177 [Accessed April 16, 2012].

Nieswandt, B et al., 2001. Long-term antithrombotic protection by in vivo depletion of platelet glycoprotein VI in mice. *The Journal of experimental medicine*, 193(4), pp.459-69. Available at: http://www.pubmedcentral.nih.gov/articlerender.fcgi?artid=2195902&tool=pmcentrez&rendertype=abstract.

Nieswandt, B, Pleines, I & Bender, M, 2011. Platelet adhesion and activation mechanisms in arterial thrombosis and ischaemic stroke. *Journal of thrombosis and haemostasis : JTH*, 9 Suppl 1, pp.92-104. Available at: http://www.ncbi.nlm.nih.gov/pubmed/21781245 [Accessed March 15, 2012].

Nieswandt, Bernhard & Watson, Steve P, 2003. Platelet-collagen interaction: is GPVI the central receptor? *Blood*, 102(2), pp.449-61. Available at: http://www.ncbi.nlm.nih.gov/pubmed/12649139 [Accessed March 15, 2012].

Nonne, C. et al., 2005. Importance of platelet phospholipase Cgamma2 signaling in arterial thrombosis as a function of lesion severity. *Arteriosclerosis, thrombosis, and vascular biology*, 25(6), pp.1293-8. Available at: http://www.ncbi.nlm.nih.gov/pubmed/15774906 [Accessed April 16, 2012].

Nuyttens, B.P. et al., 2011. Platelet adhesion to collagen. *Thrombosis research*, 127 Suppl, pp.S26-9. Available at: http://www.ncbi.nlm.nih.gov/pubmed/21193111 [Accessed June 20, 2012].

Ollikainen, E. et al., 2004. Platelet membrane collagen receptor glycoprotein VI polymorphism is associated with coronary thrombosis and fatal myocardial infarction in middle-aged men. *Atherosclerosis*, 176(1), pp.95-9. Available at: http://www.atherosclerosis-journal.com/article/S0021-9150(04)00214-X/abstract

O'Connor, M.N. et al., 2006. Selective blockade of glycoprotein VI clustering on collagen helices. *The Journal of biological chemistry*, 281(44), pp.33505-10. Available at: http://www.ncbi.nlm.nih.gov/pubmed/16956881 [Accessed April 16, 2012].

Pandey, A, Duan, H. & Dixit, V.M., 1995. Characterization of a novel Src-like adapter protein that associates with the Eck receptor tyrosine kinase. *The Journal of biological chemistry*, 270(33), pp.19201-4. Available at: http://www.ncbi.nlm.nih.gov/pubmed/7543898 [Accessed July 25, 2012].

Pandey, Akhilesh et al., 2002. A novel Src homology 2 domain-containing molecule, Src-like adapter protein-2 (SLAP-2), which negatively regulates T cell receptor signaling. *The Journal of biological chemistry*, 277(21), pp.19131-8. Available at: http://www.ncbi.nlm.nih.gov/pubmed/11891219

Park, S.-K. & Beaven, M.A., 2010. Mechanism of upregulation of the inhibitory regulator, src-like adaptor protein (SLAP), by glucocorticoids in mast cells. *Molecular Immunology*, 46(3), pp.492-497.

Patil, S., Newman, D.K. & Newman, P.J., 2001. Platelet endothelial cell adhesion molecule-1 serves as an inhibitory receptor that modulates platelet responses to collagen. *Blood*, 97(6), pp.1727-32. Available at: http://www.ncbi.nlm.nih.gov/pubmed/11238114.

Pearce, A.C. et al., 2004. Vav1 and vav3 have critical but redundant roles in mediating platelet activation by collagen. *The Journal of biological chemistry*, 279(52), pp.53955-62.

Peyvandi, F., Garagiola, I. & Baronciani, L., 2011. Role of von Willebrand factor in the haemostasis. *Blood transfusion = Trasfusione del sangue*, 9 Suppl 2, pp.s3-8.

Polanowska-Grabowska, R., Gibbins, J.M. & Gear, A.R.L., 2003. Platelet adhesion to collagen and collagen-related peptide under flow: roles of the [alpha]2[beta]1 integrin, GPVI, and Src tyrosine kinases. *Arteriosclerosis, thrombosis, and vascular biology*, 23(10), pp.1934-40. Available at: http://www.ncbi.nlm.nih.gov/pubmed/12869350 [Accessed March 27, 2012].

Polgár, J. et al., 1997. Platelet activation and signal transduction by convulxin, a C-type lectin from Crotalus durissus terrificus (tropical rattlesnake) venom via the p62/GPVI collagen receptor. *The Journal of biological chemistry*, 272(21), pp.13576-83.

Pollitt, A.Y. et al., 2010. Phosphorylation of CLEC-2 is dependent on lipid rafts, actin polymerization, secondary mediators, and Rac. *Blood*, 115(14), pp.2938-46. Available at: http://www.ncbi.nlm.nih.gov/pubmed/20154214 [Accessed April 16, 2012].

Poole, A. et al., 1997. The Fc receptor γ-chain and the tyrosine kinase Syk are essential for activation of mouse platelets by collagen. *The EMBO journal*, 16(9), pp.2333-2341.

Quinter, P.G. et al., 2007. Glycoprotein VI agonists have distinct dependences on the lipid raft environment. *Journal of thrombosis and haemostasis : JTH*, 5(2), pp.362-8. Available at: http://www.ncbi.nlm.nih.gov/pubmed/17096705.

Quinton, T.M., 2002. Glycoprotein VI-mediated platelet fibrinogen receptor activation occurs through calcium-sensitive and PKC-sensitive pathways without a requirement for secreted ADP. *Blood*, 99(9), pp.3228-3234. Available at: http://www.bloodjournal.org/cgi/doi/10.1182/blood.V99.9.3228 [Accessed April 16, 2012].

Rabie, T. et al., 2007. Diverging signaling events control the pathway of GPVI down-regulation in vivo. *Blood*, 110(2), pp.529-35. Available at: http://www.ncbi.nlm.nih.gov/pubmed/17374738 [Accessed April 16, 2012].

Rao, N., Miyake, S., et al., 2002. Negative regulation of Lck by Cbl ubiquitin ligase. *Proceedings of the National Academy of Sciences of the United States of America*, 99(6), pp.3794-9.

Rao, N., Dodge, I. & Band, H., 2002. The Cbl family of ubiquitin ligases: critical negative regulators of tyrosine kinase signaling in the immune system. *Journal of leukocyte biology*, 71(5), pp.753-63. Available at: http://www.ncbi.nlm.nih.gov/pubmed/11994499.

Rivera, J. et al., 2009. Platelet receptors and signaling in the dynamics of thrombus formation. *Haematologica*, 94(5), pp.700-11. Available at: http://www.pubmedcentral.nih.gov/articlerender.fcgi?artid=2675683&tool=pmcentrez&rendertype=abstract [Accessed March 6, 2012].

Roche, S. et al., 1998. Src-like adaptor protein (Slap) is a negative regulator of mitogenesis. *Current biology : CB*, 8(17), pp.975-8. Available at: http://www.ncbi.nlm.nih.gov/pubmed/9742401.

Ruggeri, Zaverio M & Mendolicchio, G.L., 2007. Adhesion mechanisms in platelet function. *Circulation research*, 100(12), pp.1673-85. Available at: http://www.ncbi.nlm.nih.gov/pubmed/17585075 [Accessed May 1, 2012].

Santoro, S.A. et al., 1991. Distinct determinants on collagen support a2b1 integrin-mediated platelet adhesion and platelet activation. *Cell regulation*, 2(November), pp.905-913.

Savage, B., Almus-Jacobs, F. & Ruggeri, Z M, 1998. Specific synergy of multiple substrate-receptor interactions in platelet thrombus formation under flow. *Cell*, 94(5), pp.657-66.

Schmaier, A. a et al., 2009. Molecular priming of Lyn by GPVI enables an immune receptor to adopt a hemostatic role. *Proceedings of the National Academy of Sciences of the United States of America*, 106(50), pp.21167-72. Available at: http://www.pubmedcentral.nih.gov/articlerender.fcgi?artid=2795544&tool=pmcentrez&rendertype=abstract.

Schulte, V. et al., 2006. Two-phase antithrombotic protection after anti-glycoprotein VI treatment in mice. *Arteriosclerosis, thrombosis, and vascular biology*, 26(7), pp.1640-7.

Seizer, P. et al., 2009. EMMPRIN (CD147) is a novel receptor for platelet GPVI and mediates platelet rolling via GPVI-EMMPRIN interaction. *Thrombosis and Haemostasis*, pp.682-686. Available at: http://www.schattauer.de/index.php?id=1214&doi=10.1160/TH08-06-0368 [Accessed April 16, 2012].

Shankaran, H., Wiley, H.S. & Resat, H., 2007. Receptor downregulation and desensitization enhance the information processing ability of signalling receptors. *BMC systems biology*, 1, p.48. Available at: http://www.pubmedcentral.nih.gov/articlerender.fcgi?artid=2228318&tool=pmcentrez&rendertype=abstract [Accessed July 13, 2012].

Sigalov, a B., 2007. More on: glycoprotein VI oligomerization: a novel concept of platelet inhibition. *Journal of thrombosis and haemostasis : JTH*, 5(11), pp.2310-2. Available at: http://www.ncbi.nlm.nih.gov/pubmed/17958751.

Siljander, P. et al., 2001. Platelet Adhesion Enhances the Glycoprotein VI-Dependent Procoagulant Response : Involvement of p38 MAP Kinase and Calpain. *Arteriosclerosis, Thrombosis, and Vascular Biology*, 21(4), pp.618-627. Available at: http://atvb.ahajournals.org/cgi/doi/10.1161/01.ATV.21.4.618 [Accessed April 16, 2012].

Sirvent, a et al., 2008. The Src-like adaptor protein regulates PDGF-induced actin dorsal ruffles in a c-Cbl-dependent manner. *Oncogene*, 27(24), pp.3494-500. Available at: http://www.ncbi.nlm.nih.gov/pubmed/18193084 [Accessed July 21, 2012].

Smethurst, P. a et al., 2004. Identification of the primary collagen-binding surface on human glycoprotein VI by site-directed mutagenesis and by a blocking phage antibody. *Blood*, 103(3), pp.903-11. Available at: http://www.ncbi.nlm.nih.gov/pubmed/14504096 [Accessed August 14, 2012].

Sosinowski, T et al., 2000. Src-like adaptor protein (SLAP) is a negative regulator of T cell receptor signaling. *The Journal of experimental medicine*, 191(3), pp.463-74. Available at: http://www.pubmedcentral.nih.gov/articlerender.fcgi?artid=2195826&tool=pmcentrez&rendertype=abstract.

Sosinowski, Tomasz, Killeen, N. & Weiss, A., 2001. The Src-like Adaptor Protein Downregulates the T Cell Receptor on CD4 CD8 Thymocytes and Regulates Positive Selection. *Immunity*, 15, pp.457-466.

Stegner, D. & Nieswandt, Bernhard, 2011. Platelet receptor signaling in thrombus formation. *Journal of molecular medicine (Berlin, Germany)*, 89(2), pp.109-21. Available at: http://www.ncbi.nlm.nih.gov/pubmed/21058007 [Accessed March 13, 2012].

Stephens, G. et al., 2005. Platelet activation induces metalloproteinase-dependent GP VI cleavage to down-regulate platelet reactivity to collagen. *Blood*, 105(1), pp.186-91. Available at: http://www.ncbi.nlm.nih.gov/pubmed/15339851 [Accessed July 25, 2012].

Sugihara, S. et al., 2010. Roles of Src-like adaptor protein 2 (SLAP-2) in GPVI-mediated platelet activation SLAP-2 and GPVI signaling. *Thrombosis research*, 126(4), pp.e276-

85. Available at: http://www.ncbi.nlm.nih.gov/pubmed/20828795 [Accessed April 17, 2012].

Sugiyama, T. et al., 1987. A novel platelet aggregating factor found in a patient with defective collagen-induced platelet aggregation and autoimmune thrombocytopenia. *Blood*, 69, pp.1712-1720.

Suzuki-Inoue, K. et al., 2002. Association of Fyn and Lyn with the proline-rich domain of glycoprotein VI regulates intracellular signaling. *The Journal of biological chemistry*, 277(24), pp.21561-6. Available at: http://www.ncbi.nlm.nih.gov/pubmed/11943772 [Accessed April 2, 2012].

Suzuki-Inoue, K. et al., 2004. Glycoproteins VI and Ib-IX-V stimulate tyrosine phosphorylation of tyrosine kinase Syk and phospholipase Cgamma2 at distinct sites. *The Biochemical journal*, 378(Pt 3), pp.1023-9. Available at: http://www.pubmedcentral.nih.gov/articlerender.fcgi?artid=1224016&tool=pmcentrez&rendertype=abstract.

Swaminathan, G., Feshchenko, E. a & Tsygankov, a Y., 2007. c-Cbl-facilitated cytoskeletal effects in v-Abl-transformed fibroblasts are regulated by membrane association of c-Cbl. *Oncogene*, 26(28), pp.4095-105. Available at: http://www.ncbi.nlm.nih.gov/pubmed/17237826 [Accessed July 21, 2012].

Takayama, Hiroshi et al., 2008. A novel antiplatelet antibody therapy that induces cAMP-dependent endocytosis of the GPVI / Fc receptor γ-chain complex. *Journal of Clinical Investigation*, 118(5), p.1785.

Tandon, N.N. et al., 1989. Isolation and characterization of platelet glycoprotein IV (CD36). *The Journal of biological chemistry*, 264(13), pp.7570-5. Available at: http://www.ncbi.nlm.nih.gov/pubmed/2468669.

Tang, J. et al., 1999. SLAP, a dimeric adapter protein, plays a functional role in T cell receptor signaling. *Proceedings of the National Academy of Sciences of the United States of America*, 96(17), pp.9775-80. Available at: http://www.pubmedcentral.nih.gov/articlerender.fcgi?artid=22286&tool=pmcentrez&rendertype=abstract.

Thien, C.B.F. & Langdon, W.Y., 2005. c-Cbl and Cbl-b ubiquitin ligases: substrate diversity and the negative regulation of signalling responses. *The Biochemical journal*, 391(Pt 2), pp.153-66. Available at: http://www.pubmedcentral.nih.gov/articlerender.fcgi?artid=1276912&tool=pmcentrez&rendertype=abstract [Accessed August 19, 2012].

Tomlinson, M.G. et al., 2007. Collagen promotes sustained glycoprotein VI signaling in platelets and cell lines. *Journal of thrombosis and haemostasis : JTH*, 5(11), pp.2274-83. Available at: http://www.ncbi.nlm.nih.gov/pubmed/17764536.

Trifiro, E. et al., 2009. The low-frequency isoform of platelet glycoprotein VIb attenuates ligand-mediated signal transduction but not receptor expression or ligand binding. *Blood*, 114(9), pp.1893-9. Available at:

http://www.pubmedcentral.nih.gov/articlerender.fcgi?artid=2738573&tool=pmcentrez&rendertype=abstract [Accessed April 16, 2012].

Unkeless, J.C. & Jin, J., 1997. Inhibitory receptors, ITIM sequences and phosphatases. *Current Opinion in Immunology*, 9(3), pp.338-343. Available at: http://dx.doi.org/10.1016/S0952-7915(97)80079-9 [Accessed August 18, 2012].

Varga-Szabo, D., Pleines, Irina & Nieswandt, Bernhard, 2008. Cell adhesion mechanisms in platelets. *Arteriosclerosis, thrombosis, and vascular biology*, 28(3), pp.403-12. Available at: http://www.ncbi.nlm.nih.gov/pubmed/18174460 [Accessed March 15, 2012].

Walker, A. et al., 2009. Single domain antibodies against the collagen signalling receptor glycoprotein VI are inhibitors of collagen induced thrombus formation. *Platelets*, 20(4), pp.268-76. Available at: http://www.ncbi.nlm.nih.gov/pubmed/19459133 [Accessed April 16, 2012].

Watson, S P et al., 2005. GPVI and integrin aIIbb3 signaling in platelets. *Journal of Thrombosis and Haemostasis*, 3, pp.1752-1762.

Watson, Steve P & Gibbins, J., 1998. Collagen receptor signalling in platelets : extending the role of the ITAM. *Immunology today*, 5699(6), pp.260-264.

Wijeyewickrema, L.C. et al., 2007. Snake venom metalloproteinases , crotarhagin and alborhagin , induce ectodomain shedding of the platelet collagen receptor , glycoprotein VI. *Platelets and Blood Cells*, 98, pp.1285-1290.

Wonerow, P. et al., 2002. Differential role of glycolipid-enriched membrane domains in glycoprotein VI- and integrin-mediated phospholipase Cγ2 regulation in platelets. *Journal of Biochemistry*, 765, pp.755-765.

Wong, C. et al., 2009. CEACAM1 negatively regulates platelet-collagen interactions and thrombus growth in vitro and in vivo. *Blood*, 113(8), pp.1818-28. Available at: http://bloodjournal.hematologylibrary.org/cgi/content/abstract/113/8/1818

Zhang, W., Trible, R.P. & Samelson, L.E., 1998. LAT palmitoylation: its essential role in membrane microdomain targeting and tyrosine phosphorylation during T cell activation. *Immunity*, 9(2), pp.239-46. Available at: http://www.ncbi.nlm.nih.gov/pubmed/9729044